การศึกษาสมรรถนะของเซลล์เชื้อเพลิงชนิดเยื่อแลกเปลี่ยนโปรตอนอุณหภูมิสูง ร่วมกับกระบวนการรีฟอร์มมิงกลีเซอรอล

นางสาวสุธิดา อรรถยานันทน์

วิทยานิพนธ์นี้เป็นส่วนหนึ่งของการศึกษาตามหลักสูตรปริญญาวิศวกรรมศาสตรดุษฎีบัณฑิต
สาขาวิชาวิศวกรรมเคมี ภาควิชาวิศวกรรมเคมี
คณะวิศวกรรมศาสตร์ จุฬาลงกรณ์มหาวิทยาลัย
ปีการศึกษา 2554

STUDY ON PERFORMANCE OF HIGH TEMPERATURE PROTON EXCHANGE MEMBRANE FUEL CELL INTEGRATED WITH GLYCEROL REFORMING PROCESSES

Miss Suthida Authayanun

A Dissertation Submitted in Partial Fulfillment of the Requirements
for the Degree of Doctor of Engineering Program in Chemical Engineering
Department of Chemical Engineering
Faculty of Engineering
Chulalongkorn University
Academic Year 2011

Thesis Title	STUDY ON PERFORMANCE OF HIGH TEMPERATURE PROTON EXCHANGE MEMBRANE FUEL CELL INTEGRATED WITH GLYCEROL REFORMING PROCESSES
By	Miss Suthida Authayanun
Field of Study	Chemical Engineering
Thesis Advisor	Assistant Professor Amornchai Arpornwichanop, D.Eng.

Accepted by the Faculty of Engineering, Chulalongkorn University in Partial Fulfillment of the Requirements for the Doctoral Degree

…….Dean of the Faculty of Engineering
(Associate Professor Boonsom Lerdhirunwong, Dr.Ing.)

THESIS COMMITTEE

…….Chairman
(Associate Professor Tharathon Mongkhonsi, Ph.D.)

……..……Thesis advisor
(Assistant Professor Amornchai Arpornwichanop, D.Eng.)

…….Examiner
(Assistant Professor Soorathep Kheawhom, Ph.D.)

…….Examiner
(Apinan Soottitantawat, D.Eng.)

…….External examiner
(Assistant Professor Wanwilai Kraipech Evans, Ph.D.)

สุธิดา อรรถยานันทน์ : การศึกษาสมรรถนะของเซลล์เชื้อเพลิงชนิดเยื่อแลกเปลี่ยนโปรตอนอุณหภูมิสูงร่วมกับกระบวนการรีฟอร์มมิงกลีเซอรอล (STUDY ON PERFORMANCE OF HIGH TEMPERATURE PROTON EXCHANGE MEMBRANE FUEL CELL INTEGRATED WITH GLYCEROL REFORMING PROCESSES) อ.ที่ปรึกษาวิทยานิพนธ์หลัก: ผศ.ดร.อมรชัย อาภรณ์วิชานพ, 215 หน้า.

งานวิจัยนี้นำเสนอการศึกษาเกี่ยวกับกระบวนการรีฟอร์มมิงกลีเซอรอลร่วมกับเซลล์เชื้อเพลิงชนิดเยื่อแลกเปลี่ยนโปรตอนอุณหภูมิสูง ในส่วนแรกคือ การศึกษาเกี่ยวกับการนำกลีเซอรอลบริสุทธิ์และกลีเซอรอลดิบจากกระบวนการผลิตไบโอดีเซลมาใช้ในการผลิตไฮโดรเจนผ่านกระบวนการรีฟอร์มมิงด้วยไอน้ำและกระบวนการรีฟอร์มมิงแบบออโตเทอร์มัล ซึ่งพบว่าการเพิ่มอุณหภูมิและอัตราส่วนเชิงโมลของไอน้ำต่อเชื้อเพลิงทำให้ผลิตไฮโดรเจนได้มากขึ้น ส่วนการเพิ่มอัตราส่วนเชิงโมลของออกซิเจนต่อเชื้อเพลิงในกรณีของกระบวนการรีฟอร์มมิงแบบออโตเทอร์มัลจะทำให้สัดส่วนของไฮโดรเจนที่ได้ในผลิตภัณฑ์ทั้งหมดมีค่าลดลง และเมื่อสัดส่วนของกลีเซอรอลต่อเมทานอลในกลีเซอรอลดิบมีค่าเพิ่มขึ้นจะทำให้ปริมาณของไฮโดรเจนที่ผลิตได้มีค่าเพิ่มขึ้น ในขณะที่สภาวะที่เหมาะสมของกระบวนการรีฟอร์มมิงแบบออโตเทอร์มัล ในสภาวะที่ไม่ต้องใช้ความร้อนจากภายนอกได้ศึกษาในงานวิจัยนี้เช่นเดียวกัน นอกจากนี้พบว่าการป้อนก๊าซที่ได้จากกระบวนการรีฟอร์มมิงกลีเซอรอลด้วยไอน้ำเข้าสู่เซลล์เชื้อเพลิงชนิดเยื่อแลกเปลี่ยนโปรตอนอุณหภูมิสูงโดยตรง จำเป็นต้องลดอุณหภูมิ และเพิ่มอัตราส่วนเชิงโมลของไอน้ำต่อกลีเซอรอลในกระบวนการรีฟอร์มมิง เพื่อเพิ่มปริมาณไฮโดรเจนและลดปริมาณคาร์บอนมอนนอกไซด์ให้น้อยกว่าข้อจำกัดของเซลล์เชื้อเพลิงชนิดนี้ อย่างไรก็ตามการเพิ่มปริมาณไอน้ำที่ใช้ในกระบวนการรีฟอร์มมิงทำให้ พลังงานที่ต้องใช้ในระบบมากขึ้นด้วย ดังนั้นในงานนี้จึงได้มีการศึกษาขอบเขตในการดำเนินการที่เหมาะสมที่ทำให้ได้สัดส่วนของก๊าซผลิตภัณฑ์ที่ต้องการและใช้พลังงานน้อยที่สุด ในส่วนต่อไปคือ การศึกษาประสิทธิภาพ ของระบบรีฟอร์มมิงกลีเซอรอลร่วมกับเซลล์เชื้อเพลิงชนิดเยื่อแลกเปลี่ยนโปรตอนอุณหภูมิสูงซึ่งพบว่า การเพิ่มสัดส่วนการใช้เชื้อเพลิงที่ด้านแอโนดของเซลล์ และอัตราส่วนเชิงโมลของไอน้ำต่อคาร์บอนในกระบวนการรีฟอร์มมิง จะทำให้การเกิดการเป็นพิษของคาร์บอนมอนนอกไซด์ที่ตัวเร่งปฏิกิริยาที่ด้านแอโนดของเซลล์ลดลงและสมรรถนะของเซลล์เพิ่มขึ้น นอกจากนี้ยังพบว่าปริมาณของคาร์บอนมอนนอกไซด์ มีผลกระทบต่อสมรรถนะของเซลล์อย่างมากที่ความหนาแน่นกระแสมีค่าสูง และที่อุณหภูมิของเซลล์มีค่าต่ำ โดยสภาวะที่ให้ความหนาแน่นกระแสไฟฟ้าสูงสุดที่ประสิทธิภาพที่ต้องการ ได้ถูกนำเสนอในงานนี้ จากนั้นได้ออกแบบและศึกษาประสิทธิภาพของระบบรีฟอร์มมิงกลีเซอรอลร่วมกับเซลล์เชื้อเพลิงชนิดเยื่อแลกเปลี่ยนโปรตอนอุณหภูมิสูงเพื่อใช้ในบ้านเรือน โดยมีการเปรียบเทียบกับระบบของเซลล์เชื้อเพลิงชนิดเยื่อแลกเปลี่ยนโปรตอนอุณหภูมิต่ำ ซึ่งพบว่า การเพิ่มเครื่องปฏิกรณ์วอเตอร์แก๊สชิฟเพื่อกำจัดคาร์บอนมอนนอกไซด์และเพิ่มปริมาณไฮโดรเจนในก๊าซที่ได้จากกระบวนการรีฟอร์มมิง ก่อนที่จะป้อนเข้าสู่เซลล์เชื้อเพลิงชนิดเยื่อแลกเปลี่ยนโปรตอนอุณหภูมิสูง ให้ประสิทธิภาพของระบบสูงสุด

ภาควิชา.....วิศวกรรมเคมี..... ลายมือชื่อนิสิต…….....

สาขาวิชา.....วิศวกรรมเคมี..... ลายมือชื่อ อ.ที่ปรึกษาวิทยานิพนธ์หลัก.....

ปีการศึกษา.....2554……

5071824921 : MAJOR CHEMICAL ENGINEERING
KEYWORDS : HIGH TEMPERATURE PROTON EXCHANGE MEMBRANE FUEL CELL/ GLYCEROL REFORMING / THEORETICAL ANALYSIS

SUTHIDA AUTHAYANUN: STUDY ON PERFORMANCE OF HIGH TEMPERATURE PROTON EXCHANGE MEMBRANE FUEL CELL INTEGRATED WITH GLYCEROL REFORMING PROCESSES. ADVISOR: ASST. PROF. AMORNCHAI ARPORNWICHANOP, 215 pp.

This research concentrates on the performance analysis of a high-temperature proton exchange membrane fuel cell (HT-PEMFC) integrated with a glycerol reforming process. Firstly, the thermodynamic analysis of steam and autothermal reforming of pure glycerol and crude glycerol derived from a biodiesel production process is investigated as a basis of the development of a hydrogen production process from a renewable resource. The simulation results of both the glycerol steam and autothermal reforming show that under isothermal condition, increases in operating temperature and steam to crude glycerol increase hydrogen yield, whereas increasing oxygen to crude glycerol ratios causes a reduction of hydrogen concentration. An increase in the ratio of glycerol to methanol in crude glycerol can increase the amount of hydrogen produced. In addition, an optimal operating condition of glycerol autothermal reforming at a thermo-neutral condition that no external heat to sustain the reformer operation is required, is investigated. When considering the steam reforming of glycerol, it is found that to maintain the CO content of the reformate gas at a desired range for HT-PEMFC, the steam reformer can be operated at lower temperatures; however, a high steam to glycerol ratio is required. This requirement results in an increase in the energy consumption for steam generation. To determine the optimal conditions of glycerol steam reforming for HT-PEMFC, both the product composition and energy requirement are taken into consideration. The operational boundary of the glycerol steam reformer is also explored. Secondly, the efficiency and output power density of an integrated HT-PEMFC system and glycerol reformer is studied by using thermodynamic analysis and pseudo 2D model of HT-PEMFC. The theoretical analysis shows that increase in the anode stoichiometric ratio and steam to carbon (S/C) operation of reformer reduce CO poisoning effect at cell's anode and therefore leads to enhanced cell performance. In addition, the optimum gas composition and flow rate is very dependent on cell operating current density and temperature. High S/C is essential when operating the HT-PEMFC at high current densities where CO has considerable impact on its performance. Optimal conditions that provide the maximum power density at a given efficiency are reported. Considering design of HT-PEMFC system for stationary application, the HT-PEMFC system with a water gas shift reactor in the glycerol processor shows the highest overall system efficiency compared to that without the water gas shift reactor and low-temperature proton exchange membrane fuel cell (LT-PEMFC) system.

Department: …...Chemical Engineering… Student's Signature……...…….

Field of Study: …Chemical Engineering… Advisor's Signature…….....

Academic Year: ..…….2011……..

ACKNOWLEDGEMENTS

During the five years of my doctoral study at Chulalongkorn University, I would first like to express my sincere gratitude to my advisor, Assistant Professor Amornchai Arpornwichanop, for giving me the opportunity to pursue a Doctoral Degree in Chemical Engineering. His support and encouragement in both technical and moral points of view have inspired and motivated me to choose my own way through the research presented in this dissertation. It has been my great opportunity and experience to work with him.

I am also grateful to my thesis committee member, Associate Professor Tharathon Mongkhonsi, Assistant Professor Soorathep Kheawhom, Dr. Apinan Soottitantawat and Assistant Professor Wanwilai Kraipech Evans for their valuable comments and suggestions. Furthermore, I would like to thank the Office of the Higher Education Commission, Thailand for their grant support under the program "Strategic Scholarships for Frontier Research Network for the Joint Ph.D. Program Thai Doctoral Degree" for this research. Support from the Thailand Research Fund, the Graduate School of Chulalongkorn University,(Conference Grant for Ph.D. Student) and the Computational Process Engineering Research Group, the Special Task Force for Activating Research (STAR), Chulalongkorn University Centenary Academic Development Project is also gratefully acknowledged.

My gratitude goes to Professor Keith Scott who gives me an opportunity to spend a period of six months in his research group at Newcastle University, UK, to undertake the research in the field of fuel cell. His idea and suggestion are of great benefit to my research area. Special thanks to Dr. Mohamed Mamlouk for his help to accomplish my work and all of my friends for their assistance during my visit to UK. I would also like to thank Dr. Yaneeporn Patcharavorchot, Dang, Anon, Lida, Narissara and all members of the Control and Systems Engineering Research Center for their friendship and encouragement. Most of all, I would like to express the highest gratitude to my family, who are always beside and support me during my study without condition.

CONTENTS

PAGE

CHAPTER PAGE

CHAPTER PAGE

CHAPTER PAGE

CHAPTER PAGE

CHAPTER PAGE

LIST OF TABLES

PAGE

LIST OF FIGURES

FIGURE PAGE

FIGURE PAGE

FIGURE PAGE

FIGURE PAGE

FIGURE PAGE

FIGURE PAGE

NOMENCLATURES

ATR	Autothermal reforming
APR	Aqueous phase reforming
C_{dissolve}	Equilibrium concentration [mole cm^{-3}]
C_{Pt}	Concentration on the catalyst surface [mole cm^{-3}]
$C_{\text{Pt}}^{\text{ref}}$	Reference concentration on the catalyst surface [mole cm^{-3}]
D_{ij}^{eff}	Binary diffusion coefficient [m^2 s^{-1}]
$D_{\text{H}_2}^{\text{H}_3\text{PO}_4}$	Diffusion coefficient of hydrogen in phosphoric acid [cm^2 s^{-1}]
$D_{\text{O}_2}^{\text{H}_3\text{PO}_4}$	Diffusion coefficient of oxygen in phosphoric acid [cm^2 s^{-1}]
E_c	Activation energy [J $mole^{-1}$ K^{-1}]
E_{cell}	Cell voltage [V]
E_r	Reversible cell potential [V]
F	Faraday constant [C mol^{-1}]
G	Gibb free energy [J mol^{-1}]
GDL	Gas diffusion layer
HT-PEMFC	High temperature proton exchange membrane fuel cell
HOR	Hydrogen oxidation reaction
K_m	Proton conductivity of LT-PEMFC [S cm^{-1}]
L_c	Catalyst loading [mg cm^{-2}]

LHV	Lower heating value [kJ mol^{-1}]
LT-PEMFC	Low temperature proton exchange membrane fuel cell
M	Molar flow rate [mol/s]
MPL	Micro porous layer
N	Molar flux [mol s^{-1} m^{-2}]
P	Pressure [atm]
P_{FC}	Power density [W m^{-2}]
$P_{\text{parasitic}}$	Power used in Auxiliary unit [W]
POX	Partial oxidation
PROX	Preferential oxidation
Q	Heat flow [J s^{-1}]
R	Gas constant [J $mol^{-1}K^{-1}$]
RH	Relative humidity
$S_{\text{Pt}-\text{anode}}$	Real platinum surface area
SR	Steam reforming
SCW	Super critical water reforming
T	Cell temperature [K]
T_{ref}	Reference cell temperature [K]
X	Mole fraction
a_c	Catalyst surface area [m^2 g^{-1}]

h	Channel height [m]
i	Current density [A m^{-2}]
i_0	Exchange current density [A m^{-2}]
i_0^{ref}	Reference exchange current density [A m^{-2}]
l_m	Membrane thickness [m]
x	Channel length [m]

Greek letters

δ	Average film thickness [cm]
α	Transfer coefficient
γ	Reaction order
θ_{CO}	CO coverage
θ_H	H_2 coverage
σ_m	Proton conductivity [S cm^{-1}]
η_{ohmic}	Ohmic loss [V]
η_{act}	Activation loss [V]
η_{FC}	Fuel cell efficiency
η_{FP}	Fuel processing efficiency
η_{sys}	System efficiency
$\eta_{sys,co}$	Cogeneration system efficiency

Subscripts and Superscripts

CH_4	Methane
CO_2	Carbon dioxide
CO	Carbon monoxide
H_2	Hydrogen
H_2O	Water
N_2	Nitrogen
O_2	Oxygen
a	Anode
c	Cathode
i, *j*	Components “*i*" and “*j*”
in	Inlet stream
m	Membrane
out	Outlet stream

CHAPTER I

INTRODUCTION

1.1 Background and motivation

An increase in power demand with an awareness of environmental problem stirs a need for efficient and clean generation of electrical energy. Traditionally, a conventional combustion process of petroleum-derived fuel, which is a limited resource, is applied to power generation. However, this process has low efficiency and releases green house gas that is a major cause of global warming. A fuel cell is a promising source of electricity generation, due to its high efficiency and environmental friendliness. Typically, a fuel cell generates electricity via an electrochemical reaction and produces only water and heat as by-products when hydrogen is used as fuel. As fuel cell provides high energy efficiency and low pollutant emission, it is considered to be the promising power source for the future.

Hydrogen is considered an important energy carrier for the future since it can be used in fuel cells to generate electricity through electrochemical reactions without a release of pollution gases. Typically, most hydrogen is produced from natural gas containing methane as a major component. Since natural gas is a limited and nonrenewable resource, it is necessary to find new sustainable feedstock for producing hydrogen. In a long term, renewable energy sources such as biomass and bio-ethanol will become the most important source for production of hydrogen (Giunta et al., 2007; Yu et al., 2009; Toonssen et al., 2009).

Glycerol is another promising alternative fuel for hydrogen production as it is a by-product from the production of biodiesel, which uses vegetable oils or fats as feedstock. Presently, the consumption of biodiesel for transportation has increased, resulting in an increased amount of glycerol generated (Guo et al., 2012). Glycerol as the principal by-product of this process is also highly generated; every 9 kg of

biodiesel, glycerol is produced about 1 kg (Byrd et al., 2008). However, it contains a lot of impurities and its composition depends on type of feedstock and biodiesel production process used. This make crude glycerol from biodiesel process be low price. Besides, the purification process of glycerol is high operating cost and uneconomic. Alternatively, the use of glycerol from biodiesel as raw material for hydrogen production process is a potential method (Luo et al., 2008; Hirai et al., 2005; Dauenhauer et al., 2006). While many researchers have been focused on pure glycerol reforming process, the thermodynamic analysis of hydrogen production from crude glycerol derived from biodiesel production process has not been reported yet. To develop hydrogen production process from renewable resource, reforming of crude glycerol from biodiesel production process should be investigated.

In general, fuel reforming processes for hydrogen production can be classified into three common methods, namely steam reforming, partial oxidation, and autothermal reforming which combines steam reforming and partial oxidation. Steam reforming shows the highest hydrogen production whereas partial oxidation and autothermal reforming is advantageous process to reduce energy input. However, the required heat input due to endothermic reactions is considered as a major drawback of steam reforming. Ahmed and Krumpelt (2001) explained that steam reforming is well suited for long periods of steady state operation while partial oxidation and autothermal reforming processes are more attractive for the rapid start and dynamic response needed in automotive applications. Rabenstein and Hacker (2008) concluded that coke formation is limited when temperature, steam to ethanol ratio and oxygen to ethanol ratio increase. The coke is formed during ethanol reforming in the following order: partial oxidation > steam reforming > autothermal reforming. In addition, they discussed that steam reforming is the least energy demand process. The total energy demand is of the order partial oxidation > autothermal reforming > steam reforming. All of the literature review shows that autothermal and steam reforming are desirable process for fuel cell, so both reforming processes should be studied in details for hydrogen production from glycerol.

Among several types of fuel cell, the polymer electrolyte membrane or proton exchange membrane fuel cell (PEMFC) is regarded as an effective electrical generator for automobile, residential and portable applications. Due to a low temperature operation (60 to 80 ^{o}C), PEMFC can quickly start and provides a good response to change in power demand. Other advantages include low weight and volume and high power density. Normally, PEMFC uses a proton conductive polymer membrane as electrolyte. The well-known membrane material for PEMFC is Nafion^{TM}, which is made of perfluorocarbon-sulfonic acid ionomer. The protonic conductivity of a polymer membrane is strongly dependent on its water content, so fuels need to be saturated with steam before being fed to fuel cell on the anode side to keep the membrane always hydrate.

Pure hydrogen or hydrogen-rich gas from reforming process is either used as fuel in PEMFC anodes. With the limitation of hydrogen storage and supporting infrastructure, a fuel cell integrated with a fuel processor allowing hydrogen generation from hydrocarbon fuels becomes an effective solution. However, to avoid a catalyst poisoning problem, the reformate gas must be highly purified to reduce the amount of carbon monoxide (CO) to be less than 10 ppm, thereby requiring a sophisticated CO clean up unit (Zhang et al, 2006). The purification process causes this system to be large size and high operational cost. Another important problem on PEMFC operation is a water management due to its low operating temperatures and the characteristics of membrane. To avoid a dry-out condition of the polymer membrane, fuels need to be saturated with water. However, the excess water may cause flooding in the cathode gas diffusion layer which blocks the transport of oxygen to the catalyst layer, resulting in voltage and performance losses.

In order to solve the problem mentioned above, a high-temperature PEMFC (HT-PEMFC) operated at the temperature of 100-200 ^{o}C has been developed. Under a high temperature operation, the extent of CO that adsorbs on Pt catalyst in the HT-PEMFC reduces, resulting in a high tolerance of CO. Li et al. (2003) demonstrated that the HT-PEMFC can tolerate CO up to 3% at the temperature of 200 ^{o}C and generate the electricity at 0.8 A cm^{-2} with the voltage losses lower than 10 mV. Das et

al. (2009) reported that the CO poisoning problem of the PEMFC operated at high temperatures is less than at low temperatures. It was found that when the PEMFC is operated at the temperature of 180 ^{o}C or above, the reforming gas with 2–5 %CO can be used with the insignificant loss of cell performance. Due to the high CO tolerance of HT-PEMFC, it is also possible to use the reformate gas from reformers without requiring CO removal processes or with simplified purification process. This could make a design and operating conditions of the fuel processor for HT-PEMFCs differ from conventional PEMFCs. Consequently, the study of HT-PEMFC directly fueled by reformate gas is necessary to improve its efficiency. Furthermore, when the reformate gas is directly used as a fuel for HT-PEMFC, the optimal operating condition of the reformer to provide appropriate composition of reformate gas for HT-PEMFC should be considered.

In addition, the higher operating temperature of PEMFCs also increases the electrochemical reaction rates at the anode and cathode and simplifies a water management within PEMFCs. When PEMFCs are operated at the temperature above 100 ^{o}C, water only presents in the vapor phase. For this reason, the flooding problem is solved and the transport of water is easy to balance. Although the operation of PEMFC at high temperatures can eliminate the flooding problem, it leads to the dehydration of membrane and loss of membrane ionic conductivity. To solve such a difficulty, the HT-PEMFC is necessary to be operated at high pressure to keep high relative humidity and water content at high temperature condition. However, the operating pressure of Nafion is usually limited (<4 atm) and consequently it is difficult to use reformate gas with high relative humidity and the same membrane with conventional PEMFCs (Zhang et al., 2008; Yang et al., 2001). Therefore, many researchers pay attention to develop the new membrane that can operate at temperature above 100 ^{o}C and has high conductivity at low humidity. A polybenzimidazole (PBI) was reported to be used in HT-PEMFC because it can be operated at low relative humidity. However, PBI has lower proton conductivity than Nafion and thus it is doped with phosphoric acid or other dopants to increase the proton conductivity (Mamlouk et al., 2012).

The higher temperature operation of PEMFC also offers the efficient utilization of waste heat from the fuel cell to preheat fuel or to supply to reforming processes. HT-PEMFCs are therefore advantageous to be used in conjunction with a fuel reformer, compared to low-temperature PEMFCs (Jespersen et al., 2009). Jensen et al. (2007) reported that the excess heat from fuel cell can be used to vaporize methanol and water in methanol reforming process. Therefore, the performance and efficiency of a fuel processor and HT-PEMFC integrated system should be studied.

Fuel cell systems' design depends greatly on their applications and desired efficiency. In the case of LT-PEMFC, the reformate gas must be treated by water gas shift and preferential oxidation processes in order to reduce CO content below. These treatments will cause hydrogen and parasitic losses. For HT-PEMFC, its operation does not rely on water for proton transport and can be operated at dry condition and thus the system can be simplified further by the removal of humidifiers. For automotive application, weight and size of the overall system, is critical. The fast starting up is also preferred and thus the autothermal reforming is suitable for this application more than steam reforming (Sopena et al., 2007). On the other hand, stationary applications require high overall efficiency without specific weight or size restrictions (Barbir, 2005). Heat and power cogeneration is favorably suited for stationary application as an effective way to improve the overall system efficiency combined with the highly efficient steam reforming (Hubert et al., 2005). To develop the HT-PEMFC to the market place, its design system for each application should be considered.

1.2 Research objective

The objective of this research is focused on the performance analysis of a glycerol reforming process and a high temperature proton exchange membrane fuel cell (HT-PEMFC) as well as the efficiency of such an integrated system.

The scopes of this study are as follows:

- Investigate the steam and autothermal reforming of pure and crude glycerol obtained from a biodiesel production process as a basis of the development of a hydrogen production process from renewable resources.

- Investigate the operational possibility of HT-PEMFC running on the reformate gas derived from the glycerol reforming process without CO removal processes and with a water gas shift reactor. The optimal operating conditions providing suitable composition of the reformate gas for HT-PEMFC are identified.

- Analyze the performance and efficiency of HT-PEMFC running on the reformate gas from the glycerol reforming process with respect to operating and design parameters.

- Investigate the performance and efficiency of a HT-PEMFC system with different fuel processors for a stationary application and compare it performance with a LT-PEMFC system.

1.3 Dissertation overview

This dissertation is divided into ten chapters as follows:

Chapter I describes the background and motivation of this research. The research objective and dissertation overview are also presented.

Chapter II presents literature reviews on simulation and experimental studies of fuel processors and PEMFCs as well as integrated reforming process and PEM fuel cell systems.

Chapter III presents general basic concepts of fuel cells and PEMFC. Detail of HT-PEMFC which is the fuel cell type of interest in this research is also given. The fuel processing, the system integration and the auxiliary units for PEMFC systems are described.

Chapter IV explains a mathematical model of reforming process and PEMFC under isothermal condition based on appropriate mass conservation and electrochemical model.

Chapter V focuses on the use of glycerol as a renewable resource to produce hydrogen. The hydrogen production from glycerol is analyzed and compared with that from methane, in terms of carbon formation boundary, amount of consumed fuel, product distribution and energy requirement.

Chapter VI presents the thermodynamic analysis of the autothermal and steam reforming of pure and crude glycerol. Effects of operating conditions on the reforming process of glycerol are reported. In addition, the optimal conditions for crude glycerol autothermal steam reforming that maximize hydrogen production without the requirement of an external energy input are studied and the results are compared with the use of pure glycerol. The steam reforming and autothermal reforming processes of glycerol are also compared.

Chapter VII presents the theoretical study on the fuel processor of glycerol for HT-PEMFCs. The CO content of the produced reformate gas is considered. The fuel processors without CO removal processes and with a water gas shift reactor are compared. The suitable conditions for two fuel processors of glycerol that not only maximize the hydrogen yield but also provide a CO concentration that satisfies the operational constraints of HT-PEMFCs system are shown.

Chapter VIII explains the performance of a fuel processor and HT-PEMFC integrated system. A pseudo 2D model of HT-PEMFC that takes the effect of CO poisoning into account is used to analyze an efficiency of the HT-PEMFC system and power output with respect to various key operating parameters. The optimal condition of the HT-PEMFC system that provides the maximum power density at a required efficiency is presented.

Chapter IX presents the theoretical study on a HT-PEMFC system for a stationary power generation. The efficiency of the HT-PEMFC system with different fuel processors is investigated and compared with a LT-PEMFC system. The HT-

PEMFC system considered here can be divided into two cases. The first one involves the HT-PEMFC and a glycerol reformer without a CO removal process, whereas in the second one, a water gas shift reactor is included in the HT-PEMFC system to further improve its overall system efficiency.

Chapter X gives the conclusions of this dissertation and the recommendation for the future work.

CHAPTER II

LITERATURE REVIEW

This chapter presents a literature review of fuel processor and PEMFC as well as the integrated reforming process and PEM fuel cell system. First of all, the experimental and theoretical studies on the hydrogen productions from various processes, e.g. steam reforming, partial oxidation and autothermal reforming, and from glycerol are revealed. Then, model development and performance of both LT-PEMFC and HT-PEMFC are given. Finally, the performance and efficiency of PEMFC system integrated with hydrogen production processes are presented.

2.1 Glycerol reforming process

Up to now, hydrogen production process has been received much more attention to scientific topic due to its usage in fuel cell application. Typically, many thermal-chemical processes and reactant can be used to produce hydrogen as shown in Fig. 2.1. Ahmed and Krumpelt (2001) presented an overview of hydrogen production from various thermal-chemical processes. They concluded that steam reforming is suitable for long periods of steady-state operation because this process provide the highest hydrogen concentration. However, this process is strongly endothermic and reactor designs are typically limited by heat transfer. Due to exothermic nature of partial oxidation, external heat is unnecessary and it is suitable for automotive applications. In the case of autothermal reforming as the combined process of the steam reforming and partial oxidation, it is also attractive for the rapid start and dynamic response needed in automotive applications. There are many work studied reforming processes from many non renewable resources such as natural gas (methane), liquid petroleum Gas (LPG), diesel, gasoline, methanol (Perna et al., 2001; Laosiripojana et al., 2006; Lattner et al., 2004; Amphlett et al., 1998; Agrell et al., 2002; Adachi et al., 2009; Chipıtı et al., 2006; Severin et al., 2005; Castaldi et al.,

2001; Danial et al., 2001; Chein et al., 2011; Lattner et al., 2005). Due to high H/C of methane, the high hydrogen concentration is obtained from natural reforming process. Steam reforming of methane yields the best hydrogen content of all the reforming processes with 75-78 vol.% (Heinzel et al., 2002).

Apart from nonrenewable gases, diesel, gasoline and methanol are also the famous nonrenewable liquid fuel which is used to produce hydrogen (Amphlett et al., 1998; Agrell et al., 2002; Severin et al., 2005; Castaldi et al., 2007; Lattner et al., 2005). It is found that the large size molecule of diesel and gasoline is the obstacle for reforming process. The diesel and gasoline fuel reforming is complicated and requires high temperatures (Amphlett et al., 1998). On the other hand, methanol is smaller molecule and thus it is easily converted to hydrogen. Agrell et al. (2002) proposed that methanol provides a high hydrogen–carbon ratio, an absence of carbon–carbon bonds and a potentially high production capacity.

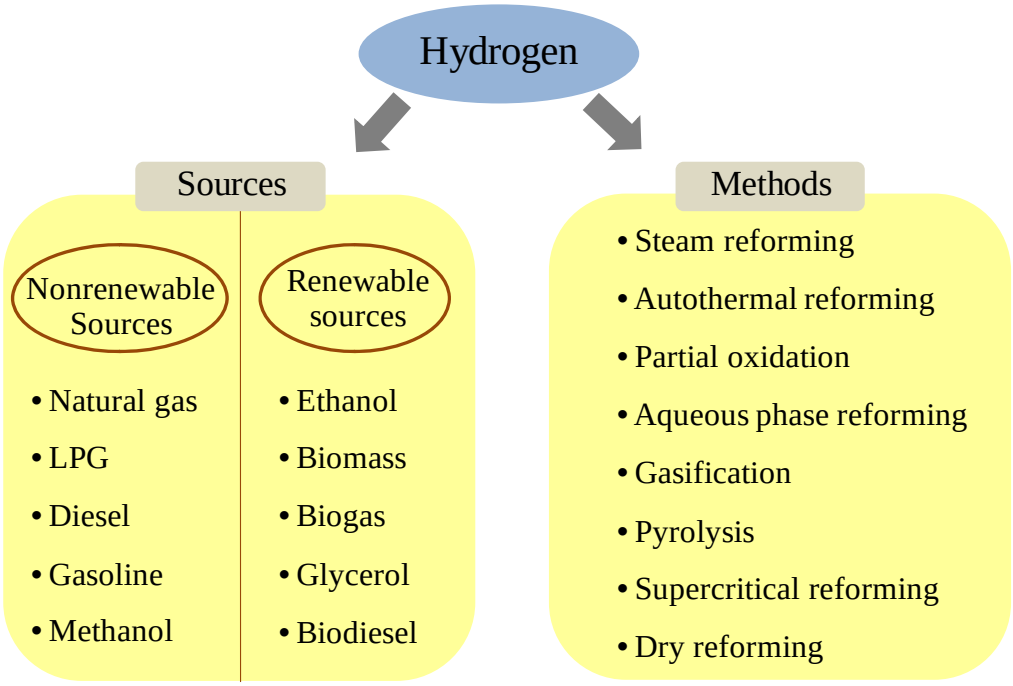

Figure 2.1 Thermal-chemical processes and fuels for hydrogen production.

Also, the renewable resources such as ethanol, biomass, bio-oil, biogas have been investigated from many researches (Martin et al., 2011; Schmersahl et al., 2005; Pandya et al., 1988). Ethanol reforming processes for hydrogen production were

studied by Ni et al. (2007). They concluded that the steam reforming of ethanol provides the highest hydrogen yield, but it requires high energy to maintain the operation of the reformer at isothermal condition. Alternatively, hydrogen can be produced by partial oxidation. However, hydrogen selectivity of ethanol partial oxidation is generally low. They mentioned that autothermal reforming can enhance hydrogen production. It not only attains self-thermally sustained operation, but also maximizes the hydrogen production. In addition, autothermal reforming is advantageous as coke formation is greatly inhibited by oxidation. Thus, long-term stable operation can be achieved. Later, Thermodynamic analysis of ethanol steam reforming, partial oxidation and autothermal reforming including the possibility of solid coke formation was also studied by Rabenstein and Hacker (2008). They concluded that coke formation is limited when temperature, steam to ethanol ratio and oxygen to ethanol ratio increase and coke is formed during ethanol reforming in the following order: partial oxidation > steam reforming > autothermal reforming.

Considering environmental and availability aspect, biomass is one of the interesting fuels for hydrogen production. Pyrolysis and gasification are the main method to produce hydrogen. Li et al. (2004) studied biomass gasification in a circulating fluidized bed and they found product gas composition and heating value depend heavily on the oxygen to carbon ratio and temperature. The gasifier should be operated at temperature of 1100-1300 K and oxygen to carbon ratio of 0.15–0.25. However, apart from main product gas, the tar and char, are byproduct which should be minimized from this process. For biomass pyrolysis process, its products are in mainly liquid form and some solid, and gaseous forms. The product composition depends on type of reactants and operating conditions (Demirbas, 2002; Demirbas and Arin, 2004). Generally, main product of this process is liquid product. It is called bio-oil and can be also used to produce hydrogen in reforming process. Vagia et al. (2008) thermodynamically analyzed the production of hydrogen via the autothermal steam reforming of selected components of aqueous bio-oil fraction. They revealed that the autothermal steam reforming offers many advantages from a technical and economic point of view, as it minimizes heat load demand in the reformer. They calculated the optimum amount of oxygen required to achieve both zero heat requirement and high

process efficiency. When the required oxygen enters the system at the reforming temperature, the autothermal steam reforming process give the hydrogen yield of about 20% lower than that by the steam reforming because part of the organic feed is consumed by a combustion reaction. Alternatively, the use of glycerol from biodiesel production process as raw material for hydrogen production is an attractive approach. Considering reforming of glycerol, various studies have relied on experiments (Dauenhauer et al., 2006; Slinn et al., 2008; Swami et al., 2006; Zhang et al., 2007; Hirai et al., 2005; Profeti et al., 2009; Pompeo et al., 2010) or simulations (Adhikari et al., 2007; Luo et al., 2007; Wang et al., 2008; Wang et al., 2009; Chen et al., 2009) to investigate the effects of key operating parameters on the various reforming processes and to identify the optimal conditions.

Glycerol aqueous phase reforming

Several reports were presented on the production of hydrogen from glycerol using a low-temperature aqueous phase reforming (Luo et al., 2007; Wen et al., 2008). Luo et al. (2007) studied the aqueous reforming of glycerol for hydrogen generation based on thermodynamic analysis. This process operate at low temperature and thus eliminating the need to vaporize water and the oxygenated hydrocarbon which reduces the energy requirements for producing hydrogen, and facilitating the WGS reaction to generate hydrogen product which contains low levels of CO in a single catalytic reformer. Also, it was found that aqueous reforming can achieve the higher hydrogen yield if methanation reaction is limited kinetically during the operation. Luo et al. (2008) also investigested glycerol aqueous phase reforming in presence of Pt and reported that the optimal operating condition is temperature of 220 $^{\circ}$C and pressure of 2.5 MPa. Lower reaction temperature seems to decrease the conversion of glycerin and higher temperature leads to more side reactions. However, the disadvantage of such a process is a drastic decrease of hydrogen content because methanation reaction favors at low temperatures. Now, many works is developed catalysts with high selectivity of hydrogen production (Manfro et al., 2011; King et al., 2010; Guo et al., 2012).

Glycerol dry reforming

Wang et al. (2009) investigated the possibility of glycerol dry reforming for hydrogen and synthesis gas production employing the total Gibbs free energy minimization method. Hydrogen yield increases with increasing temperature and CO_2 to glycerol ratios, while decreases with increasing pressure. CH_4 decreases with the increase in both temperature and carbon to glycerol ratio. In addition, they observed that the boudard reaction is predominant reaction for carbon formation and more carbon is produced in glycerol dry reforming compared with the steam reforming of glycerol.

Glycerol partial oxidation

Due to low obtained hydrogen yield and required complex temperature control system, there are few work focusing on partial oxidation process. Wang (2010) studied about glycerol partial oxidation and concluded that the operating temperature and oxygen to glycerol should be in the range of 1000-1100 K and 0.4-0.6, respectively. This is because operation at higher temperature consumes more energy while operation at lower temperature causes carbon formation. In addition, they found that the operation at > 1 atm has a negative effect on the hydrogen yield.

Glycerol supercritical reforming

Supercritical reforming process, which is presently receives much attention from a lot of research (Vlieger et al., 2012; Voll et al., 2009; Gadhe et al., 2007) is operated at critical temperature and pressure. Thus, high temperature and high pressure is required. Ortiz et al. (2011) proposed that suitable operating pressure is about 240 atm and temperature should be in the range of 750-850 C. The glycerol supercritical water gas was also studied by Byrd et al. (2008). They reported that glycerol is complete conversion to hydrogen, carbon dioxide, methane and only slight carbon monoxide content. Hydrogen yields are found to increase directly with temperature while methane formation can be reduced by operating at low residence times.

Glycerol steam reforming

Several studies concentrated on hydrogen production from glycerol steam reforming. Zhang et al. (2007) studied a glycerol steam reforming process over ceria-supported metal catalysts and found that complete glycerol conversion is at 400 - 450°C. Hirai et al. (2005) reported that steam reforming of glycerol on Ru/Y_2O_3 catalyst provided high hydrogen selectivity (≈90%) and complete conversion of glycerol at 600 °C. Also, Cui et al. (2009) revealed that at 600 °C glycerol is completely decomposed when $La_{1-x}Ce_xNiO_3$ is used as catalyst for glycerol steam reforming process.

Slinn et al. (2008) investigated steam reforming of glycerol and crude glycerol from biodiesel production. A platinum alumina catalyst was used to optimize the operating conditions. They described that the yield of by-product glycerol was on average only 70% of the yield of pure glycerol. This is because the long chain fatty acid impurities (40%) are harder to reform, and are likely to form more carbon deposition on the catalyst than pure glycerol. In addition, glycerol and crude glycerol can reach a yield of 85% at high temperature. Steam reforming of glycerol is the dominant mechanism at temperatures above 700 $^{\circ}C$, flow rates under 0.6 mole/min·kg catalyst, and the steam to carbon ratios of over 0.5. They concluded that glycerol steam reforming is a viable alternative use for glycerol and potentially a better option than purification. Later, Buffoni et al. (2009) studied glycerol steam reforming based on a nickel catalyst. Their results indicated that the operating temperature strongly influences the activity of the nickel catalyst; the minimum temperature that provides high hydrogen selectivity is 823 K. Adhikari et al. (2007) concluded from their simulation results that the optimal conditions for hydrogen production from glycerol are a temperature above 900 K, atmospheric pressure, and a steam to glycerol molar ratio of nine. Wang et al. (2008) studied steam reforming of glycerol and found that the optimal temperature and steam to glycerol molar ratio were in the range of 925-975 K and 9-12, respectively. Chen et al. (2011) reported that high temperature, low pressure, low feeding reactants to inert gas ratio and low gas flow rate are favourable for steam reforming of glycerol for hydrogen production.

Glycerol autothermal reforming

The experimental study on glycerol autothermal reforming was investigated by Swami and Abraham (2006). They concluded that the addition of oxygen enhances the reaction rate at an initial period, leading to the breakdown of glycerol. Recently, Wang et al. (2009) investigated the glycerol autothermal reforming to generate hydrogen. They suggested that the heat integration of autothermal reforming makes it more attractive and competitive. Under optimal conditions, methane production is minimized and carbon formation is thermodynamically inhibited. Dauenhauer et al. (2006) explained that glycerol is highly oxygenated with a hydroxyl group on each carbon atom and an internal carbon-to-oxygen ratio (C/O) equal to 1. This presents a challenge for gas-phase reforming with unique chemistry and a significant thermodynamic limitation for synthesis gas production relative to the reforming of alkanes. Their research was to examine the autothermal reforming of glycerol over platinum- and rhodium- based catalysts supported on alumina foams. The addition of steam maximizes selectivity to H_2 to as high as 92% near equilibrium, whereas the conversion decreased at high level of oxygen. In addition, all minor products exhibit selectivity of no more than 2% of carbon selectivity under optimum condition.

2.2 Proton exchange membrane fuel cell (PEMFC) operated on reformate gas

There are several problems occurring during operation of PEMFC, which should be overcome. The intrinsic problem of PEMFC is mainly water problem and CO poisoning problem. Pure hydrogen or hydrogen-rich gas from reforming process is either used as fuel in PEMFC anodes. With the limitation of hydrogen storage and supporting infrastructure, a fuel cell integrated with a fuel processor allowing hydrogen generation from hydrocarbon fuels becomes an effective solution.

2.2.1 Low-temperature proton exchange membrane fuel cell (LT-PEMFC)

The operating conditions, i.e. temperature, relative humidity, pressure, and flow rate have a significant effect on the cell performance. In some point of view, the influence of operating condition on PEMFC at reformate gas operation differ from pure hydrogen operation. Indeed, an increase in temperature causes reduction of theoretical cell voltage (Nernst equation). However, the actual cell voltage generally enhance with temperature because the voltage loss tend to decrease when cell temperature increase. For PEMFC operated on pure hydrogen, it is observed that its performance is improved with increasing temperatures from 65 to 75 ˚C, unchanged between 75 and 80 ˚C, and begins to decrease at 85 ˚C (Cheddie et al., 2006). The increasing cell performance at 65 to 75 ˚C is due to the fact that gas diffusivity is enhanced with temperature and thus the losses from mass transfer limitation reduce. However, an increase in cell temperature causes low relative humidity of fuel gas. This results in dehydration of membrane and thus PEMFC has poor performance when the cell temperature is increased to 85 ◦C.

Furthermore, the reformate gases obtained from fuel processing process generally contain traces of CO which strongly adsorb on the surface of Pt, occupying hydrogen oxidation reaction (HOR) sites. The performance of PEMFC fed by reformate gas typically relies on fraction of CO in feed stream, temperature and current density. Das et al. (2009) reported that effect of CO poisoning reduce at high temperature and low current density. However, the only some trace of CO can cause a significant loss in the cell and the CO content of the hydrogen feed generally must be less than 10 ppm. Minutillo et al. (2008) studied the fuel cell performance both using pure hydrogen and reformate gas produced by a natural gas reforming system. They ignored the effect of CO and reported that the increase of performance that occurs at higher temperature with pure hydrogen fueling about 20% and can occur also in the case of reformate gas fueling. The overall stack performance of the fuel cell with reformate gas fueling is lower than pure hydrogen about 8–10%.

Apart from CO effect, the effect of other gases containing reformate gas such as CO_2 on PEMFC performance is also studied by many researches (Janssen et al., 2004; Smolinka et al., 2005; Tingelof et al., 2008) . Generally, carbon dioxide contaminate in reformate gas around 20-25% depending on type of reactant and operating condition (Bruijn et al., 2002; Smolinka et al., 2005). Hedstrom et al. (2009) investigated possibility of running LT-PEMFC on reformate from biogas. A 5 kW polymer electrolyte fuel stack was supplied with simulated reformate with a hydrogen content as low as 25%. The result showed that reformed biogas and other gases with high CO_2 content are, from dilution and CO poisoning perspectives, suitable for PEMFCs. There is a small poisoning effect from carbon dioxide. The stack showed stable operating conditions for all experiments performed. The efficiency of the fuel cell stack is not significantly changed when diluted fuel streams are used. In addition, Giddey et al. (2005) studied study the effect of methane, carbon dioxide and water in the hydrogen fuel mix on the cell performance. The presence of methane up to 10% was found to have negligible effect on the cell voltage as expected due to very low equilibrium content of CO formed at this fuel composition and cell operating conditions. However, the presence of CO_2 between1-2% was found to cause degradation in the cell voltage, possibly due to the reverse water gas shift reaction at this fuel composition and cell operating condition

To support reformate gas as fuel for PEMFC before hydrogen transport and storage are readily available, several technologies, i.e. oxygen bleeding, catalyst with high CO tolerance and high temperature proton exchange membrane fuel cell (HT-PEMFC) have been developed to solve CO poisoning problem (Jensen et al., 2007). However, HT-PEMFCs provide the highest CO tolerance compared to oxygen bleeding and CO tolerance catalyst approach.

2.2.2 High-temperature proton exchange membrane fuel cell (HT-PEMFC)

In case of reformate gas operation, it is found that high operating temperature can improve the PEMFC performance operated on reformate gas (Scott et al., 2007).

From a thermodynamic point of view, the adsorption of CO on the Pt surface can be reduced by increasing the temperature and/or decreasing the CO concentration (Bellows et al., 1996). Therefore, the operation of PEMFC at high temperatures can reduce CO poisoning problem and the PEMFC has high tolerance of CO. There have been many studies that have focused on HT-PEMFC. Pan et al. (2005) investigated performance of HT-PEMFC by using the reformed hydrogen directly from a simple methanol reformer without further CO removal. A significant performance loss was observed at a fuel cell temperature of 100 ◦C when the fuel was switched from pure hydrogen to the methanol reformate. In addition, they found that the performance loss reduced, when temperature increase.

Table 2.1 Summary of CO tolerance

Literature	**Temperature (°C)**	**% CO tolerance**
Li et al. (2003**)**	200	3%
Korsgaard et al. (2008)	160	2%
Das et al. (2009)	180	5%
Mamlouk and Scott (2010)	175	10%
Jiao et al. (2011)	190	10%

Table 2.1 shows the summary of CO tolerance of HT-PEMFC from many works. Li et al. (2003) demonstrated that the HT-PEMFC can tolerate CO up to 3% at the temperature of 200 ^{o}C and generate the electricity at 0.8 A/cm^2 with the voltage losses lower than 10 mV. Das et al. (2009) reported that the CO poisoning problem of the PEMFC operated at high temperatures is less than at low temperatures. It was found that when the PEMFC is operated at the temperature of 180 ^{o}C or above, the reforming gas with 2–5 %CO can be used with the insignificant loss of cell performance. Recently, Jiao et al. (2011) developed the non-isothermal model of HT-PEMFC by considering the effect of CO on the fuel cell performance. They found that CO has a drastic effect on the HT-PEMFC at 190 ^{o}C when the CO faction in the

hydrogen feed is higher than 10%. They also reported that reformate gas from methanol reformer (CO ≈ 1-2%) can be fed directly to HT-PEMFC operated at 160 ^{o}C.

In addition, it is found from the literature that reverse water gas shift reaction disappear in operational range of HT-PEMFC. Apart from dilution effect, CO_2 containing in reformate gas does not have any effect on cell performance (Jiao et al. 2011). On the other hand, some research reported that water content in hydrogen feed can reduce CO poisoning effect reduce and enhance cell performance (Modestov et al., 2010).

2.3 PEMFC model

The good understanding of PEMFC is required for optimization of its performance and efficiency. Modeling and simulation become important tools to understand and design the complex and multidisciplinary PEMFC system where electrochemical and transport processes are tightly coupled. The detail of LT-PEMFC and HT-PEMFC model development are given:

2.3.1 LT-PEMFC

The performance of a fuel cell can be expressed by the polarization curve. It is necessary for optimization of fuel cell operating points, design of the power conditioning units, design of simulators for fuel cell stack systems, and design of system controllers. Therefore, it should be noted that the accurate electrochemical model is required to study and improve the fuel cell performance.

The first model of LT-PEMFC running with Nafion was developed by Bernardi and Verbrugge (1991). This model was one-dimensional (1D), isothermal, and for water transport within the membrane. However, it is observed that it is hard to predict the water distribution and transportation in the GDL and the overestimate occurs at high current density because of the lacking liquid water transport.

In addition, Springer et al. (1991) introduced in their model an expression to account for the porosity and tortuosity of the electrode and showed much improved agreement in the mass transport limited range at high current density. The catalyst layers are treated as interfaces**.**

The oxygen transport in cathode gas diffusion layer is investigated by Tsai et al. (2006). They concluded that the concentration flux of oxygen across the GDL was primarily dominated by the thickness and porosity of GDL. The high value of GDL thickness can cause an increase in diffusion resistance at high current density and thus low cell performance.

Amphlett et al. (1995) developed the models which could be used to predict cell voltage as a function of current density. A steady-state model for the Ballard Mark IV fuel cell has been proposed that combines performance losses into parametric equations based on cell operating conditions, such as pressure and operating temperature these models are reduced in terms of dimensionality and comprehensiveness. Amphlett et al. (1996) also studied the dynamic model of a fuel cell stack by performing a global heat and mass balance analysis, and the details of electrochemical phenomena inside the cell were ignored.

Two dimensional modeling of transport phenomena in PEMFC was presented by Yi and Nguyen (1999). They studied the effects of the operating conditions and design parameters of an air cathode on the performance of the cell with an interdigitated gas distributor. Fuller and Newman (1993) developed a two-dimensional model of a membrane electrode assembly of a LT-PEMFC to study water and thermal management. This model includes water transport in the diffusion layer. In addition, Nguyen and White (1993) developed a two-dimensional model to predict the temperature distribution and membrane hydration conditions along the flow channels.

Dutta et al. (2000) developed one of the first 3D models, which included both anode and cathode regions, and the control volume approach was used to solve the governing equations. Shimpalee et al. (2000) completed a three-dimensional straight

channel model by establishing governing equations for each gas component at the inlet. They proposed that the energy equation can predict the temperature distribution in the cell and can be used to analyze thermal management of the fuel cell stack.

Um et al. (2000) also developed a three-dimensional PEM fuel cell model. The model is an isothermal single phase with focusing on the analysis of the reactant concentration distribution in a single cell. It is observed that the interdigitated flow field can enhance mass transport of oxygen and water elimination at reaction zone, thus increasing the performance as compared to convectional flow field at a high current density.

Zhou and Liu (2004) developed a three-dimensional mathematical model of LT-PEMFC operated on reformate. They studied the effect of CO poisoning as well as the effect of hydrogen dilution due to the inert gases. From the simulation results, they concluded that near the exit, though hydrogen concentration is reduced due to reaction consumption, the fast oxidation of hydrogen makes the influence of reduced hydrogen concentration negligible. The poisoning effect of CO is predominant over the effect of hydrogen concentration reduction.

2.3.2 HT-PEMFC

Compared to Nafion based LT-PEMFCs, only a few publications have developed models for PBI based HT-PEMFCs. Cheddie and Munroe (2006) presented a one dimensional mathematical model used to predict the polarization performance of a HT-PEMFC using a polybenzimidazole (PBI) membrane. The scope of interest is on a membrane electrode assembly (MEA). Mass and energy transport in gas diffusion layer and electrochemical model were analyzed while the changes of reactant composition and temperature in gas flow channels were not considered. The greatest loss in the PBI fuel cell was the activation overpotential and the second largest was the ohmic overpotential. They suggested that the conductivity of the membrane and the membrane–catalyst interface should be improved. It is noted that the membrane conductivity was kept constant in this research. Then, the analytical correlation for HT-PEMFC was presented by the same author. They commented that

this correlation is useful to expedite calculation without depending on complex computational model.

Also, a steady-state, one dimensional model of a proton exchange membrane fuel cell (PEMFC) with a PBI membrane was developed by Scott et al. (2007). However, they assumed that the cell was operated at isothermal condition. The Stefan–Maxwell equation and Darcy's law were used to model the mass transport processes. The effects of cell temperature, pressure and gas compositions, on voltages and power densities were studied. They claimed that this model give a good agreement with experimental data and can be potentially used to optimize electrode structure and electrocatalyst composition in the electrode layers.

On the other hand, there are many researches that develop a three dimensional model of HT-PEMFC to correctly predict its performance and behavior. The model describes all transport and polarization phenomena, and accounts for the effect of gas channel flow rates. Sinha et al. (2007) developed a three-dimensional, non-isothermal model to investigate the performance of PEM fuel cells using Gore-Select membrane at elevated temperature under various operating conditions. Numerical studies revealed that at 95°C operation, oxygen transport and its depletion along the flow direction play a critical role in cell performance, even under low humidity conditions.

Su et al. (2009) applied a three-dimensional, non-isothermal model with PTFE (polytetrafluoroethylene)/Nafion/silicate (PNS) membrane. Based on simulation results, the localized characteristics within the HT-PEMFC can be reasonably predicted, which include the distributions of liquid water saturation, membrane conductivity, fuel gas depletion phenomenon, temperature, current density, etc. They also claimed that the supply of fuel gas is not insufficient to meet the requirement of electrochemical reaction, resulting in the decrease in the cell power generation.

Moreover, a transient three-dimensional, single-phase and non-isothermal numerical model of polymer electrolyte membrane (PEM) fuel cell with high operating temperatures was developed by Peng et al. (2008). This model includes charge double-layer and thermal effects on output current. From the simulation result,

current is moved smoothly and there are no overshoot or undershoot with the influence of charge double-layer effect. The maximum temperature is located in cathode catalyst layer and both fuel cell average temperature and temperature deviation are increased with increasing of current load.

Bergmann et al. (2010) investigated the performance of a phosphoric acid doped PBI membrane fuel cell based on a two-dimensional fuel cell model taking into account the CO poisoning effect. Recently, Jiao et al. (2011) developed the non-isothermal model of HT-PEMFC by considering the effect of CO on the fuel cell performance. They found that CO has a drastic effect on the HT-PEMFC at 190 ^{o}C when the CO faction in the hydrogen feed is higher than 10%.

2.4 Integration of PEMFC and reforming processes

Ersoz et al. (2003) investigated the effect of the selected fuel reforming options, namely steam reforming (SR), partial oxidation (POX) and autothermal reforming (ATR) on the overall fuel cell system efficiency, which depends on the fuel processing, PEM fuel cell and auxiliary system efficiencies. Results indicate that fuel properties, fuel processing system and its operation parameters, and PEM fuel cell characteristics all affect the overall system efficiencies. Steam reforming and autothermal reforming appear as the most competitive fuel processing options in terms of fuel processing efficiencies. High PEMFC system efficiency levels can be achieved only with intensive heat integration within the PEMFC systems. Hence, heat integration system studies are of utmost importance along with the development of novel reforming catalysts, clean-up systems and PEMFC components if on-board hydrogen production is desired.

Due to the higher temperature for PEMFC the heat quality is higher and it seems obvious to try to make use of it for fuel processing. The possible utilization of the excess heat of the fuel cell is addressed by Jensen et al. (2007). The simple heat balances are calculated for systems with methanol and methane reformers in combination with a high temperature PEM fuel cell. In the methanol system at least 11.1% of the fuel energy can be saved by using the excess heat from the fuel cell for

vaporization of water and methanol if the cell is operated at temperatures between 150 and 200 °C. Similarly, in the methane system, 9.6% can be saved under equivalent conditions. However, the heat for methane reforming is significantly larger than methanol, and the temperature is far too high for a utilization of the excess heat even with a high temperature PEM fuel cell.

A fuel processor (FP) for the vehicle on-board hydrogen production to be fed to the PEMFC stack of an auxiliary power unit (APU) was investigated by Specchia et al. (2006), with its several units: the reformer for hydrogen production; the CO cleanup process; the auxiliary units for the balance of plant of the whole system (afterburner for the combustion of the hydrogen exhaust gas from the fuel cell, heat exchangers for the internal heat recoveries, water recovery radiators, air compressor, and water and fuel pumps); and the PEMFC. From the simulation results, the highest performance, in terms of efficiency, seems to belong to the SR-based APU. The electrical gross power obtainable from the PEMFC: the SR-based APU gives the higher power as compared to the ATR-based one. However, the higher SR system performance might be counterbalanced by a much higher plant complexity, which might increase cost, the impact on system controllability, and start-up time.

A novel heat-integrated fuel cell stack system with methanol reforming was presented by Wu et al (2009). Its configuration is composed of fuel processing units (FPUs), proton exchange membrane (PEM) fuel cell stack, and heat exchangers (HEXs). To ensure the heat-integrated system is compact, and to reduce its heat duty, the original circulating device for cooling the stack system is replaced with external circulating water flow. This water is used to preheat well mixed methanol and oxygen before entering reformer. This water also dominates the production of hydrogen at the exit of FPUs and influences the stack temperature. The heat exchange connections can enhance the utilization of energy of FPUs.

Jannelli et al. (2007) studied the performance of a PEM fuel cell integrated with a hydrogen generator based on steam reforming process. The performance of the fuel cell has been evaluated by both varying the feeding mode and fuel composition. The results have pointed out that the efficiency of the PEM fuel cell system is in the

range of 22–31%. However, with higher stack temperature an increase in the performance, up to 5%, can be expected. The efficiency of the integrated system becomes highly competitive with the conventional power system in the same power range.

CHAPTER III

THEORY

3.1 PEMFC

3.1.1 Basic principle of fuel cells

A fuel cell is an electrochemical device (a galvanic cell) which converts free energy of a chemical reaction into electrical energy (electricity). The fuel cell principle was discovered in 1839 by William R. Grove, a British physicist. Fuel cells have several advantages over internal combustion engines (ICE) and batteries. To generate mechanical energy, the ICE first converts fuel energy to thermal energy by combusting fuel with oxygen at high temperature. The thermal energy is then used to generate mechanical energy. Because thermal energy is involved, the efficiency of the conversion process is limited by the Carnot Cycle. Unlike ICE, fuel cells directly convert fuel energy to electrical energy and its maximum efficiency is not subjected to Carnot Cycle limitations. If hydrogen is used as fuel, the outcome of fuel cell reaction is water and heat. Therefore, fuel cells are considered to be a zero emission power generator. They do not create pollutants such as hydrocarbon or nitrogen oxide. A battery is also an electrochemical device that converts chemical energy directly to electricity. However, the reactants of battery are stored internally and when used up, the battery must be recharged or replaced whereas the reactants of the fuel cell are externally. From Table 3.1, the major types of fuel cells being developed are: proton exchange membrane fuel cells (PEMFC) for transportation power generation, direct methanol fuel cells (DMFC) for portable power generation, alkaline fuel cells (AFC) for space program for producing electricity and drinking water for astronaughts; phosphoric acid fuel cells (PAFC), molten carbonate fuel cells (MCFC) and solid oxide fuel cells (SOFC) for stationary power generation applications. In addition, fuel cell can be classified to three groups as presented in Figure 3.1.

Table 3.1 Characteristics of important fuel cells (Shah, 2007)

	PEMFC	**DMFC**	**AFC**	**PAFC**	**MCFC**	**SOFC**
Primary application	Automotive and stationary power	Portable power	Space vehicles and drinking water	Stationary power	Stationary power	Vehicle auxiliary power
Electrolyte	Polymer (plastic) membrane	Polymer (plastic) membrane	Concentrated (30-50%) KOH in H_20	Concentrated 100% phosphoric acid	Molten carbonate retained in a ceramic matrix of $LiA10_2$	Yttrium-stabilized Zirkondioxide
Operating temperature range	50-100°C	0-60°C	50-200°C	150-220°C	600-700°C	700-1000°C
Charge carrier	H^+	H^+	OH^-	H^+	$CO^=_3$	$O^=$
Prime cell components	Carbon-based	Carbon-based	Carbon-based	Graphite-based	Stainless steel	Ceramic
Catalyst	Platinum	Pt-Pt/Ru	Platinum	Platinum	Nickel	Perovskites
Primary fuel	H_2	Methanol	H_2	H_2	H_2, CO, CH_4	H_2, CO
Start-up time	Sec-min	Sec-min	-	Hours	Hours	Hours
Power density (kW/m^3)	3.8-6.5	≈0.6	≈1	0.8-1.9	1.5-2.6	0.1-1.5
Combined cycle fuel cell efficiency	50-60%	30-40% (no combined cycle)	50-60%	55%	55-65%	55-65%

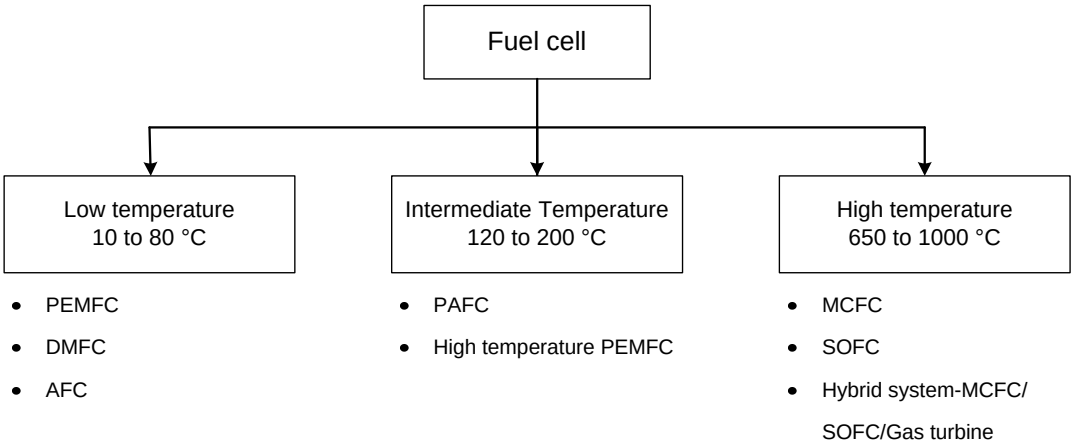

Figure 3.1 Classification of fuel cells into leading technologies (Srinivasan et al., 2006)**.**

3.1.2 Basic principle of PEMFC

As mentioned above, PEMFCs use a proton conductive polymer membrane as electrolyte. PEM stands for Polymer Electrolyte Membrane or Proton Exchange Membrane. PEMFC is the most attractive for automobile, residential and portable applications because it operates at low temperature making it start up very quickly. In addition, it also has ability to meet the changing power demands.

3.1.2.1 Components of PEMFC

Figure 3.2 displays the structure of PEMFC. The heart of a fuel cell is a polymer, proton-conductive membrane. On both sides of the membrane is placed between an anode and a cathode backing layer, or gas diffusion layer (GDL) which is a porous electrode. The electrodes must be porous because the reactant gases are fed from the back and must reach the interface between the electrodes and the membrane, where the electrochemical reactions take place in the so-called catalyst layers on the catalyst surface. The multilayer assembly of the membrane sandwiched between the two electrodes is commonly called the membrane electrode assembly or MEA. The MEA is then sandwiched between the collector/ separator or bipolar plates because

they collect and conduct electrical current and "separator" because in multicell configuration they separate the gases in the adjacent cells.

3.1.2.2 Operation of PEMFC

- Hydrogen, which is fed at anode side, splits into its primary constituents – protons and electrons. This process is made possible when the platinum is used as catalyst.

  Anode: $2H_2 \rightarrow 4H^+ + 4e^-$ (3.1)

- Protons migrate through the membrane from the anode to cathode side, while the electrons liberate through electrically conductive electrodes, and through the outside circuit where they perform useful work and return to the other side of the membrane.

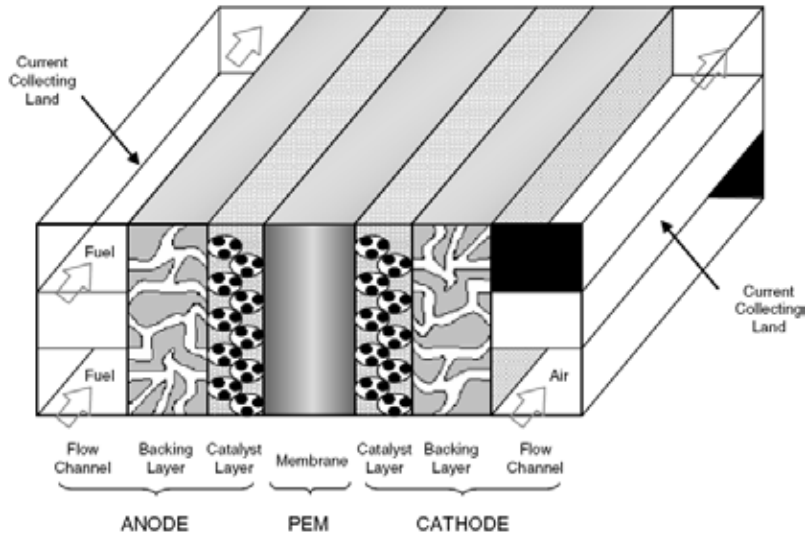

Figure 3.2 Three-dimensional schematic diagram of a PEMFC (Yang and Pitchumani, 2006).

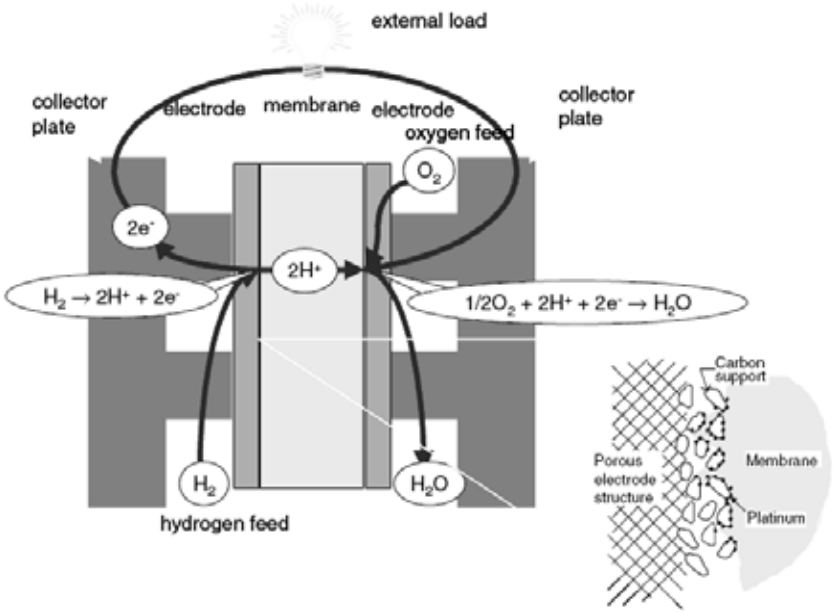

Figure 3.3 Basic operation of a PEMFC (Barbir, 2005).

- At the cathode, electrons meet with the protons from the anode side and oxygen fed on that side of the membrane. Water is produced by the electrochemical reaction, and then pushed out of the cell with an excess flow of oxygen.

Cathode: $O_2 + 4H^+ + 4e^- \rightarrow 2H_2O$ (3.2)

- Figure 3.3 shows the basic operation of a PEMFC. The net result of these simultaneous reactions, as expressed in Eq. (3.3), is current of electrons through an external circuit – direct electrical current. By products are only water and heat and thus, no pollution is released.

Overall: $2H_2 + O_2 \rightarrow 2H_2O$ (3.3)

3.1.2.3 Problem in conventional PEMFC

In spite of this large expectation of PEMFC, its commercialization has not been spread out. The reason is that the cost and the durability of PEMFC are worse than that of conventional engines competing with PEMFC (Ito, 2007). In addition, there are several problems occurring during operation of PEMFC, which should be overcome. However, the intrinsic problem of PEMFC is mainly water problem and CO poisoning problem.

Water problem

The water problem in PEMFC is caused by its low-temperature operation and by the characteristics of polymer electrolyte membrane used. The main two water problems of PEMFC are flooding occurred in gas diffusion layer (GDL) and flow channel, and drying polymer electrolyte membrane. The schematic of flooding and drying in PEMFC is presented in Figure 3.4.

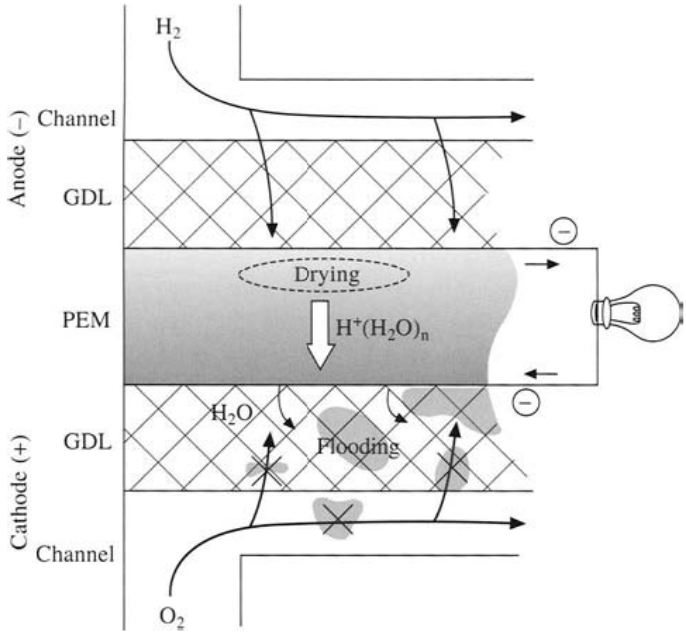

Figure 3.4 Schematic of flooding and drying in PEMFC (Ito, 2007).

The flooding is caused by the following mechanics: water or vapor generates at catalyst layer in proportion to load current, and a portion of vapor condenses in

GDL and flow channel when vapor pressure is larger than the saturated vapor pressure. If the condensation progress, flooding occurs, and then the flooding blocks the supplied gases resulting in the decrease of cell voltage and stopping electricity generation at worse. The drying is caused by the so-called electro-osmotic flow. As mentioned before, the proton conductivity mechanism of membrane electrolyte of PEMFC relies on water content and the water molecules immigrate in PEM with the proton conduction from anode to cathode resulting in decreasing water content especially near anode. Once PEM dries up, the ionic resistance increases and the cell voltage decreases. To solve water problem, the water management within the cell is studied by many researches. There are several solutions to solve flooding problem as follows (Li et al., 2008):

- Add hydrophobic material: the hydrophobic material will be added in GDL to remove water from cell easily.

- Add micro porous layer (MPL): the MPL will be placed between GDL and catalyst layer to enhance the distribution of gas from GDL to catalyst layer and the removal excess water from catalyst layer.

- Design flow field: the suitable type of flow field such as interdigitated flow field or serpentine flow field will be used instead of conventional flow field.

CO poisoning problem

The reformate gases generally contain traces of CO which strongly adsorb on the surface of Pt, occupying hydrogen oxidation reaction (HOR) sites. Trace CO dramatically reduces the activity of Pt or Pt-alloys in the anode, resulting in the deterioration of cell performance. The adsorption of CO and H_2 on the Pt surface can be described by Langmuir adsorption isotherms, as shown in Eqs. (3.4) and (3.5). The CO molecule adsorbs associatively on Pt below 500 K, whereas H_2 is dissociatively adsorbed (Zhang et al., 2006).

$$CO(g) + Pt \rightarrow Pt - CO \qquad (3.4)$$

$$H_2(g) + 2Pt \rightarrow 2Pt - H \quad (3.5)$$

Therefore, LT-PEMFCs operate at low temperatures and require hydrogen fuel with low CO content to avoid catalyst poisoning. The content of CO in the hydrogen feed for a LT-PEMFC must be less than 10-50 ppm. However, the CO contamination in hydrogen-rich reformate gas exceeds this limit. To reduce CO to the required level, it is necessary to add water gas shift (WGS) and some CO removal unit such as preferential oxidation (PROX) processes to the fuel reforming process.

3.1.3 HT-PEMFC

Although PEMFC operating at low temperature has several advantages, it has many limitations hindering its widespread commercialization for transportation and stationary application. The main problems are CO poisoning on Pt catalyst and water management both in gas diffusion layer and membrane. To solve these problems, PEMFC operated at higher temperature around 100 $^{\circ}$C has been developed. This is referred to 'High-temperature PEMFC (HT-PEMFC)'.

3.1.3.1 Advantages of high temperature operation

There are a lot of reasons for operating at high temperature as follows:

Improved CO tolerance

Higher temperature operation of fuel cells has been shown to increase the tolerance of fuel cells to CO poisoning. This increased tolerance is related to the thermodynamics of adsorption of CO and H_2 on the Pt electrocatalyst. Because hydrogen adsorption is less exothermic than CO and hydrogen adsorption requires two adsorption sites, increased temperature leads to a beneficial shift towards lower CO coverage and higher H coverage. Therefore, the operation at higher temperatures increases the ability of the fuel cell anode to perform in the presence of small amounts of CO by decreasing the coverage of CO on the catalyst surface. It also makes

PEMFC able to use hydrogen directly from a simple reformer without CO removal unit.

Simplified water management

In the conventional PEMFC operating below 100^{o}C, water produced is presented both vapor and liquid phase. When the humidification is too high, water is condensed and thus, the electrodes are flooded. This results in the restriction of oxygen transport through the porous gas diffusion electrode. On the other hand, for HT-PEMFC running at atmospheric pressure, only water vapor phase exists in PEMFC. So the transport of water in membrane, catalyst layers and diffusion layers will be easier to balance. Transport of reactants (H_2 and O_2) in the electrode layers is also expected to be enhanced, and there is no flooding problem in cathode.

Enhanced electrode reaction kinetic

The overall electrochemical kinetics of a PEMFC is determined by the slow oxygen reduction reaction (ORR). Due to the sluggish ORR kinetics, the over-potential at the cathode (ORR electrode) accounts for the major voltage loss of PEMFC and remains a major focus of PEMFC research. The reaction kinetics of hydrogen oxidation and ORR will be both enhanced at high temperature, especially for ORR.

Improved heat management

Even though PEMFC is a very efficient system, there is still 40–50% of the energy produced as heat. The produced heat in a working PEMFC stack must be removed quickly from fuel cells; otherwise the fuel cell system will overheat. For conventional PEMFC, the small temperature differences between cell and environment in the chamber environment may cause difficultly heat rejection from fuel cell reactions. For a HT-PEMFC, the waste heat can be rejected more quickly because of the larger temperature difference between the fuel cell component and the ambient surroundings. This can eliminate the requirement of sophisticated cooling system.

3.1.3.2 Limitation and recent progress of HT-PEMFC

Although HT-PEMFC has many attractive features as mentioned above, there are several major challenges.

Dehydration of membrane

Perfluorosulfonic acid (PFSA) membranes such as Nafion are the most widely used membrane for PEMFCs. In general, the proton conductivity of this membrane depends strongly upon water content. Therefore, PEMFC will have poor performance if membrane dehydrates. The water content in polymer membranes depends on the relative humidity given by the ratio of the vapor pressure to the saturation vapor pressure multiplied by 100. The saturated water vapor pressure increases exponentially with temperature. If the same gas relative humidity is kept at high operation temperature, the operating pressure will increase. The typical pressure limitation for conventional PEMFC is usually <4 atm. So at high temperature operation, it is difficult to provide wet gases with high relative humidity in a traditional fuel cell control system. To provide good performance in HT-PEMFC, polymer membranes capable of retaining high proton conductivity in anhydrous environments have been developed, in addition to possessing chemical and electrochemical stability at high temperature. Membrane developments can be classified into three groups as follows:

- Modified PFSA membranes, which incorporate hydroscopic oxides and solid inorganic proton conductors

- Sulfonated polyaromtaic polymers and composite membranes, such as polyether ether ketones (PEEK), Sulfonated aromatic polyether ether ketones (SPEEK), Sulfonated polysulfone (SPSF), and polybenzimidazole (PBI)

- Acid–base polymer membranes, such as phosphoric acid-doped PBI

In recent years, PBI membrane has been shown promise for HT-PEMFC due to its high thermal stability. Although the proton conductivity of pure PBI is very low,

after it has been doped by some acids such as phosphoric acid, high proton conductivity can be remarkable achieved even in an anhydrous state. Phosphoric acid-doped PBI (PA-PBI) membranes exhibit not only good proton conductivity and low gas permeability but also almost zero electro-osmotic drag as well as excellent oxidative and thermal stability.

Degradation of gas diffusion electrode

At elevated temperature, these may react with the carbon substrate and/or water to generate gaseous products such as CO and CO_2. This may destroy the carbon support over time, leading to a reduction in carbon content within the catalyst layer and thus, the cell life time decreases.

Mass transfer resistance

Mass transfer in fuel cell catalyst layers includes two primary parts: the diffusion of oxygen to the cathode Pt active surface and the diffusion of hydrogen to the anode Pt active surface in the catalyst layers. Temperature can significantly affect the mass transfer in a fuel cell catalyst layer. Increasing temperature can effectively increase the gas diffusivity but reduce the solubility (or gas concentration in the diffusion medium). The increased diffusivity will result in a reduced gas diffusion resistance. However, the reduced gas solubility will result in an increase in gas diffusion resistance.

3.1.4 PEMFC applications

Fuel cells can generate power from a fraction of a watt to hundreds of kilowatts. Because of this, they may be used in almost every application where local electricity generation is needed. Applications such as automobiles, buses, utility vehicles, scooters, bicycles, submarines have been already demonstrated. Fuel cells are ideal for distributed power generation, at a level of individual homes, buildings or a community, offering tremendous flexibility in power supply. In some cases both power and heat produced by a fuel cell may be utilized, resulting in very high overall efficiency. Fuel cell and fuel cell system design are not necessarily the same for each

of these applications. On the contrary, each application, besides power output, has its own specific requirements, such as efficiency, water balance, heat utilization, quick startup, long dormancy, size, weight, fuel supply, *etc* (Barbir, 2006). The summary of fuel cell market requirement for automotive and stationary application is shown in Table 3.2.

3.1.4.1 Automotive Applications

All major car manufacturers have demonstrated prototype fuel cell vehicles and announced plans for production and commercialization. The major drivers for development of automotive fuel cell technology are their efficiency, low or zero emissions, and fuel that could be produced from indigenous sources rather than being imported. The main obstacles for fuel cell commercialization in automobiles are the cost of fuel cells and the cost and availability of hydrogen.

The fuel cell may be connected to the propulsion motor in several ways, namely:

- Fuel cell is sized to provide all the power needed to run the vehicle. A battery may be present but only for startup (such as a 12V battery). This configuration is typically possible only with direct hydrogen fuel cell systems. A system with a fuel processor would not have as good dynamic response. Also, a small battery would not be sufficient to start up a system with a fuel processor.
- Fuel cell is sized to provide only the base load, but the peak power for acceleration of the vehicle is provided by the batteries or similar peaking devices (such as ultracapacitors). This may be considered as a parallel hybrid configuration since the fuel cell and the battery operate in parallel. The vehicle can be started without preheating of the fuel cell system, particularly the fuel processor, and operated as a purely battery-electric vehicle until the fuel cell system becomes operational. A battery allows for recapturing of the braking energy, resulting in a more efficient system. The disadvantages of having the battery are extra cost, weight and volume.

Table 3.2 Summary of market requirements for fuel cell systems (Barbir, 2005)

	Automotive	**Stationary (Primary Power)**	**Stationary (Backup Power)**
Power output	50-100 kW	1-10 kW & 200 kW	1-10 kW
Fuel	Reformate/H_2	Reformate	Hydrogen
Life (operational)	5000 hours	> 40000 hours	< 2000 hours
High efficiency	Critical	Critical	Critical
Instant start	Very important	Not important	Very important
Output mode	Highly variable	Variable	Constant
Operation	Intermittent	Constant	Intermittent
Preferred voltage	>300 V	> 110 V	24 V or 48 V
Heat recovery	Not needed	Very important	Not needed
Water balance	Very important	Very important	Not critical
Size and weight	Critical	Not Critical	Not critical
Extreme conditions	Critical	Not Critical	Important
Cost	< $100/kW	< $1000/kW	$1000-$3000/kW

- Fuel cell is sized only to re-charge the batteries. The batteries provide all the power needed to run the vehicle. This may be considered as serial hybrid configuration (fuel cell charges the battery and battery drives the electric motor). The same advantages and disadvantages of having a battery apply as for the parallel hybrid configuration. The fuel cell nominal power output

depends on how fast the batteries would have to be recharged. A smaller battery would have to be recharged faster and would result in a larger fuel cell.

- Fuel cell serves only as an auxiliary power unit, *i.e.* another engine is used for propulsion, but the fuel cell is used to run the entire or a part of the vehicle electrical system. This may be particularly attractive for trucks, since it would allow operation of an air-conditioning or refrigeration unit while the vehicle is not moving without the need to run the main engine.

In general, a fuel cell propulsion engine is more efficient that a comparable internal combustion engine. However, the efficiency of fuel cells vs. internal combustion engine should not be compared at their most favorable operating point. These two technologies are intrinsically different and have very different efficiency-power characteristics. The hydrogen fuel cell system efficiency in a driving schedule can be in the upper 40s and above 50%. The efficiency of a fuel cell propulsion system with an onboard fuel processor is lower than the efficiency of a hydrogen fuel cell system, but still higher than the efficiency of an internal combustion engine.

3.1.4.2 Stationary Power Applications

Although development and demonstrations of fuel cells in automobiles usually draws more attention, applications for stationary power generation offer even greater market opportunity. The drivers for both market sectors are similar – higher efficiency and lower emissions. The system design for both applications is also similar in principle. The main differences are in the choice of fuel, power conditioning, and heat rejection. There are also some differences in requirements for automotive and stationary fuel cell systems. For example, size and weight requirements are very important in automotive applications, but not so significant in stationary applications. The acceptable noise level is lower for stationary applications, especially if the unit is to be installed indoors. The fuel cell itself of course does not generate any noise, noise may be coming from air and fluid handling devices. Automobile systems are expected to have a very short start-up time (fraction of a minute), while the startup of a stationary system is not time limited, unless operated as a backup or emergency power generator. Both automotive and stationary systems are expected to survive and

operate in extreme ambient conditions, although some stationary units may be designed for indoor installation only. And finally, the automotive systems for passenger vehicles are expected to have a lifetime of 3000 to 5000 operational hours, systems for buses and trucks somewhat longer, but the stationary fuel cell power systems are expected to operate for 40000 to 800000 hours (five to ten years).

Stationary fuel cell power systems will enable the concept of distributed generation, allowing the utility companies to increase their installed capacity following the increase in demand more closely, rather than anticipating the demand in huge increments by adding gigantic power plants. Presently, obtaining the permissions and building a conventional power plant have become very difficult tasks. Fuel cells, on the other hand, do not need special permitting and may be installed virtually everywhere – inside the residential areas, even inside the residential dwellings. To the end users the fuel cells offer reliability, energy independence, “green” power, and, ultimately, lower cost of energy.

Commercialization of stationary fuel cells greatly depends on their economics, which besides the selling price includes their annual (not maximum) efficiency, capacity factor (depending on application), lifetime, maintenance, but most of all on a ratio between the prices of electricity and fuel. The economics of stationary fuel cells may be improved if the waste heat is utilized in a cogeneration manner. Some residential fuel cells are being developed to operate in a heat load following mode.

3.1.4.3 Portable Power Applications

A portable power system is a small grid-independent electric power unit ranging from a few watts to roughly one kilowatt, which serves mainly the purpose of convenience rather than being a primarily a result of environmental or energy-saving considerations. These devices may be divided into two main categories:

- battery replacements, typically well under 100 W
- portable power generators, up to 1 kW

The key feature of small fuel cells to be used as battery replacements is the running time without recharging. Obviously, by definition, the size and weight are also important. Power units with either significantly higher power densities or larger energy storage capacities than those of existing secondary batteries may find applications in portable computers, communication and transmission devices, power tools, remote meteorological or other observation systems, and in military gadgets. Besides the size of the fuel cell itself, the critical issue is the fuel and its storage. Hydrogen, although being a preferred fuel for PEM fuel cells is rarely used because of the bulkiness or weight of its storage, even in the small quantities required by those small devices. Hydrogen may be stored in room temperature metal hydride storage tanks. Some chemical hydrides offer higher energy density, however, they must be equipped with suitable reactors where hydrogen is released in a controlled chemical reaction. Most of portable fuel cells use methanol as fuel, or more precisely aqueous methanol solutions, either directly (so called direct methanol fuel cells) or via microreformers.

3.2 Fuel processing for PEMFC

Energy carriers are a convenient form of stored energy. Electricity is one type of carrier that can be produced from various sources, transported over large distances, and distributed to the end user. Hydrogen is another type of energy carrier. But because hydrogen is not readily available, it is necessary to produce it from other sources through reforming process. However, the hydrogen-rich gas obtaining from the process comprise of several components, e.g. CO, CO_2, CH_4, and H_2. Therefore, several other processes may be included to purify hydrogen enough before feeding to the PEMFCs.

3.2.1 Hydrogen production process

Although hydrogen is the most plentiful element in the universe, making up about three quarters of all matter, free hydrogen is scarce. Fuel reformer is the unit that converts hydrocarbon fuels into hydrogen and carbon monoxide or carbon

dioxide. Fuel reforming is the main step in the fuel processing train. The ideal reforming reaction in which the H in the hydrocarbons and H_2O are completely converted into H_2; the C are completely converted into CO_2; and neither CO nor any other low-carbon hydrocarbon is formed. There are several thermochemical methods to produce hydrogen from gas and liquid hydrocarbon such as steam reforming, partial oxidation, autothermal reforming, dry reforming and aqueous phase reforming as well as supercritical water reforming. They are explained individually below. Carbon formation, one of the important problems in reforming process, is also described.

3.2.1.1 Hydrogen production methods

Steam reforming (SR)

Steam reforming refers to the catalytic conversion of hydrocarbons in the presence of steam. It is widely used in industry to produce H_2 and syngas. Steam reforming is an endothermic reaction of steam with the fuel in the presence of a catalyst to produce H_2. These reformers are well suited for long periods of steady-state operation and can deliver relatively high concentrations of hydrogen. Because the process is largely endothermic, it will consume a lot of heat. Pressure, based on Le Chatelier's principle, requires the process to operate at higher temperatures to maintain the steam reforming reaction. In practice, to increase the hydrogen yield of an endothermic steam reforming reaction, high-temperature operation, low pressure and excess steam usage are required to shift the equilibrium toward the product side. Due to the high temperature operation, the CO cannot be totally converted to CO_2 by the water gas shift reaction in reformer. This is explanation that why water gas shift reactor is required to reduce CO content for PEMFC.

For steam reforming process, the reactor designs are typically limited by heat transfer, rather than by reaction kinetics. Therefore, the reactors are designed to promote heat exchange and tend to be large and heavy. This is a major drawback for the rapid start and dynamic response needed in automotive applications. However, the required external heat to maintain reactions of steam reforming may be obtained by a

combination of heat recovery, combustion of anode waste gas that contains unreacted hydrogen and methane, and/or use of primary fuel. H_2 can be produced by steam reforming of natural gas (methane), LPG, propane, and oxygenated hydrocarbons fuels (glycerol or ethylene glycol). The following chemical equation illustrates the steam reforming of oxygenated hydrocarbons:

$$C_n(H_2O)_n H_2 + (n-1)H_2O \rightarrow nCO + (2n)H_2 \quad (3.6)$$

$$nCO + nH_2O \rightarrow nCO_2 + nH_2 \quad (3.7)$$

Net reaction:

$$C_n(H_2O)_n H_2 + nH_2O \rightarrow nCO_2 + (2n+1)H_2 \quad (3.8)$$

Typically, the catalyst used for steam reforming is nickel-based catalysts. Excess water is used (normally on a 3:1 ratio to methane) to prevent carbon formation and to enhance hydrogen production. The nickel-based catalysts are sensitive to sulfur and chlorine. Caution is needed on water quality and chlorine levels given the significant mass of water that is used in steam reforming (Yang and Pitchumani, 2006).

Partial oxidation (POX)

The second option for fuel reforming is partial oxidation, which is an exothermic reaction and occurs when the feed reacts directly with air or pure oxygen at carefully balanced oxygen to fuel ratios. The major advantage of this process is to be able to reform heavy hydrocarbon without the use of catalyst. Typically, the POX reaction is carried out on an industrial basis in an empty (without catalyst) refractory-lined vessel at high temperature 2370-2730°F (1300-1500°C) and without water (Yang and Pitchumani, 2006). The heat for the reaction is supplied by oxidation of the fuel within the reactor (in-situ).

POX can be described as fuel oxidation with less than the stoichiometric amount of oxygen needed for complete fuel combustion to water and carbon dioxide. In addition to its exothermic nature make the partial oxidation suitable for

applications that require rapid start-ups and dynamic response to changes in demand. Another advantage arises from the fact that water is not a reactant in this process; therefore steam generators are not required, leading to a simpler system. However, this can also be a disadvantage since water is a source of H_2 too. Comparison of Eq. (3.8) and (3.9) shows that less H_2 is produced per mole of oxygenated hydrocarbons in partial oxidation than in steam reforming which results in lower H_2 partial pressure in the reformate stream. In addition, the hydrogen is diluted compared to steam reforming due to the high levels of nitrogen.

POX: $$C_n\left(H_2O\right)_n H_2 + \left(\frac{n}{2}\right)O_2 \rightarrow nCO_2 + \left(n+1\right)H_2 \qquad (3.9)$$

Furthermore, the non-catalytic partial oxidation has problem about the scale down and control of the reaction. Since the partial oxidation is exothermic, controls are needed to prevent the reaction temperature from increasing due off-design operation (e.g., a high oxygen ratio, x). This could cause the reactor temperature to rise quickly and potentially lead to catalyst damage or other negative side effects.

Autothermal reforming (ATR)

Autothermal reforming is a combination of partial oxidation and steam reforming. In order to achieve the desired conversion and product selectivity, an appropriate catalyst is essential. Most of catalysts used for ATR reactors are Ni-based. ATR is widely used in the fuel cell systems for automotive application. In autothermal reformer, the fuel is mixed with steam and substoichiometric amounts of oxygen or air where the ratios of oxygen to carbon (O/C) and steam to carbon (S/C) are properly adjusted so that the partial combustion supplies the necessary heat for endothermic steam reforming. Increasing oxygen to crude glycerol molar ratio decreases an external heat requirement. As a result, it is possible to operate the autothermal reformer without supplying external heat input. This condition is referred as to a thermoneutral condition. The heat integration of autothermal reforming makes it more attractive and competitive.

In order to operate the fuel processor in a steady condition, the ATR must be controlled in a thermally neutral or under slightly exothermic condition. Thus, it is important to study the design parameters of the processor, such as fed oxygen to carbon ratio, hydrogen yield, and efficiency to keep the reaction enthalpy $\Delta H \leq 0$.

ATR: $$C_n(H_2O)_n H_2 + \frac{n}{2}H_2O + \frac{n}{4}O_2 \rightarrow nCO_2 + \left(\frac{3}{2}n + 1\right)H_2 \qquad (3.10)$$

Another advantage of ATR is that the ATR reaction is more selective to CO_2 than CO, which will cause a CO poisoning problem in fuel cell operation, especially a low-temperature fuel cell like a proton exchange membrane fuel cell (PEMFC).

Aqueous phase reforming (APR)

This process is developed by Cortright et al. (2002). The hydrocarbon reactant of the process reacts with water in liquid form. This process has been studied for methanol, polyols, and sugar with C:O ratio of 1:1 in the molecules and the oxygenated hydrocarbons that have high value of equilibrium constant (Eq.(3.11)) at low temperature. The aqueous phase reforming process operates at low temperature. This result in the APR process can lead to low levels of CO (100 ppm) in a single-step catalytic process, because the reforming of oxygenated hydrocarbons and the water-gas shift reaction are both thermodynamically favorable at the same low temperatures. In addition, this process is energy saving because the vaporization of reactant is not required.

APR: $$C_n(H_2O)_n H_2(g) + nH_2O(l) \rightarrow nCO_2(g) + (2n+1)H_2(g) \qquad (3.11)$$

However, the disadvantage of such a process is a drastic decrease of hydrogen content because methanation and Fischer-Tropsch reaction favors at low temperatures. The hydrogen selectivity is dependent on the type of metal catalyst, the nature support, the feed molecules, and the reaction condition. The low acidity of both the catalyst support and feed solution favors hydrogen selectivity. In addition, it deceases with increasing carbon atom in the feed molecules. Platinum is usually used in aqueous phase reforming because it provides much higher hydrogen selectivity

than Nickel. However, the lower conversion is observed and thus catalysts providing high selectivity of hydrogen production and conversion should be further developed.

Super critical water reforming (SCW)

Supercritical water reforming process is operated at critical temperature and pressure. SCW has properties entirely different from those of liquid water or steam. The dielectric constant of SCW is much lower, and the number of hydrogen bonds is much lower and their strength is weaker. In supercritical state, water has been found like a dense gas and has solvation properties resembling that of non-polar fluids (Byrd et al., 2008). This in turn leads to an increase of solubility of hydrocarbons and light gases in supercritical water and so the reacting system maybe assumed to be a single homogeneous fluid when it reaches equilibrium.

In addition, the density of SCW is higher than that of steam resulting in a higher space time yield, and higher thermal conductivity and specific heat, which are helpful in carrying out the endothermic reforming reactions. Transport properties, too, are unique in that SCW has both low viscosity and high diffusivity. The formation of char and tar is also minimized because of the solubility of hydrocarbons in SCW. Importantly, hydrogen produced from SCW reforming is produced at high pressure, which can be stored directly, thus avoiding large expenses associated with compression.

3.2.1.2 Hydrogen production problem: Carbon formation

Carbon formation is a significant problem in fuel reforming processes because it causes deactivation of the catalyst. Many studies have proposed various methods to prevent the formation of carbon during the reforming process, including variations in the operating conditions, the development of new catalysts resisting on carbon, and the addition of oxygen and other promoters to inhibit carbon formation (Pedernera et al., 2005; Parmar et al., 2009; Laosiripojana et al., 2005; Medrano et al., 2008; Parizotto et al., 2007). The main potential reactions for the formation of carbon are shown as follows:

Boudouard: $2CO \leftrightarrow CO_2 + C$ (3.12)

Methane cracking: $CH_4 \leftrightarrow 2H_2 + C$ (3.13)

CO reduction: $CO + H_2 \leftrightarrow H_2O + C$ (3.14)

These reactions are in equilibrium and the carbon formation via Eq. (3.13) and (3.14) becomes less favored when the temperature increases. However, coke-formation in Eq. (3.12) is more pronounced at high temperature. The molar triangular diagram of carbon–hydrogen–oxygen equilibrium phase for reforming system is show in Figure 3.5. It is found that to avoid carbon formation, additional oxygen or hydrogen is needed to shift the equilibrium point to shaded section below the carbon decomposition boundary (dashed line), where carbon is present as CO,CO_2 and CH_4. Ideally, oxygenated hydrocarbon with C/O ratio of 1 does not require additional oxygen to break it down to CO and H_2.

3.2.2 Hydrogen purification processes

Due to low temperature operation and require hydrogen fuel with low CO content to avoid catalyst poisoning of PEMFC, it is necessary to add WGS reactor to the fuel processing process in order to reduce CO and enhance hydrogen content at the same time. However, the effluent gas of the WGS process still has a CO level that exceeds the acceptable level for conventional PEMFC. Therefore, the reformate gas is treated by further CO removal process, e.g. preferential oxidation, methanation and membrane separation, to reduce the concentration of CO to a satisfactory level. The descriptions of hydrogen purification process are explained below:

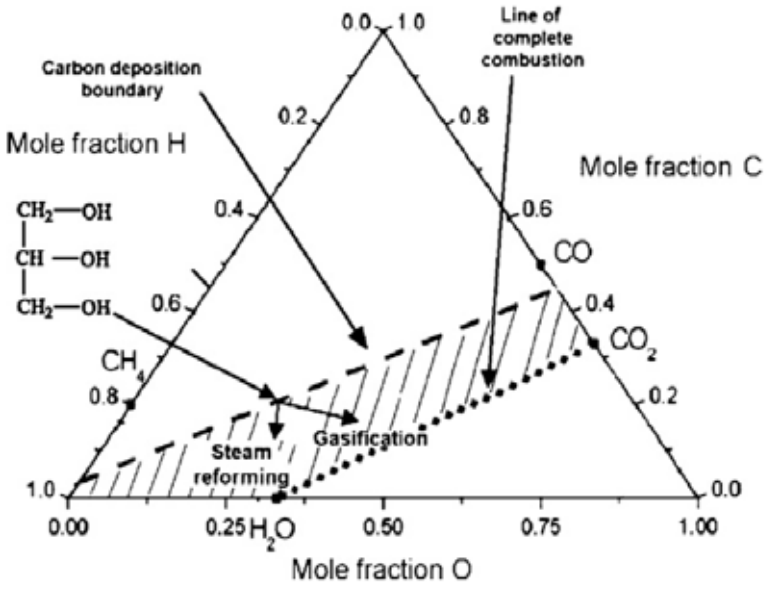

Figure 3.5 Molar triangular diagram of carbon–hydrogen–oxygen equilibrium phase (Slinn et al., 2008).

3.2.2.1 Water gas shift reaction

The CO concentration in the reformate gas varies with the reforming type and feedstock used. While high-temperature fuel cells (MCFC and SOFC) are capable of processing CH_4 and CO in the anode by internal reforming, a substantial amount of CO is considered to be poisonous in the low-temperature fuel cells (PEMFC and PAFC). At low temperatures and high concentrations, the Pt in the anode-catalyst in fuel cells preferentially adsorbs CO, consequently blocking access of H_2 to the catalytic sites and resulting in significant decreased performance of the fuel cell stack. A WGS reaction, in a separate stage(s), is the primary means for reducing the CO concentration in the fuel gas. Through WGS, the CO formed from reforming reactions further reacts with excess steam to form carbon dioxide and H_2. Thus, the H_2 yield is increased, and poisonous CO is decreased. As mentioned in the reforming section, the WGS reaction is:

$$CO + H_2O \leftrightarrow CO_2 + H_2 \qquad (3.15)$$

WGS is a reversible and exothermic reaction. Therefore, whereas the hydrogen yield from reforming is increased at higher temperatures, WGS conversion is limited at high temperatures by thermodynamic equilibrium. Consequently, the WSGR should be run at temperatures much lower than that of the reformers.

3.2.2.2 Carbon monoxide removal

PEMFC anode catalyst is comprised of Pt and its alloys and operates under low temperature. Especially at concentrations greater than 10 ppm, CO strongly adsorbs onto Pt preventing the H_2 adsorption, therefore deactivating the catalyst and reducing the fuel cell efficiency. It is very difficult for the water-gas shift reactors to reach such low CO concentration. Further CO removal is achieved by one of the following three methods.

3.2.2.3 Preferential oxidation

The term preferential oxidation (PROX) refers to selective oxidation of CO (Eq. (3.16)) over H_2 (Eq. (3.17)) in spite of the high concentration of H_2 in the stream:

$$CO + \frac{1}{2}O_2 \Leftrightarrow CO_2 \qquad (3.16)$$

$$H_2 + \frac{1}{2}O_2 \Leftrightarrow H_2O \qquad (3.17)$$

PROX process is operated to reduce the concentration of CO to a satisfactory level of PEMFC. However, the oxygen fed into the PROX process not only reacts with CO (Eq. (12)) but also consumes hydrogen, as described by Eq. (3.17). The selectivity of CO oxidation in the PROX process is about 0.4-0.9 and is dependent on the catalyst and operating parameters (Ahluwalia et al., 2005; Cipiti et al., 2009; Marino et al., 2005). It should be noted that when the effluent gas of the WGS process contains more CO, a higher amount of oxygen must be fed to the PROX process, resulting in a greater hydrogen loss due to the oxidation of hydrogen (Eq. (3.17)).

3.2.2.4 Methanation

The methanation reaction is the reverse of the steam reforming of methane:

$$CO + 3H_2 \Leftrightarrow CH_4 + H_2O \quad (3.18)$$

Obviously, this process is a convenience approach to eliminate CO as no extra reactant has to be added to the fuel stream, hence reducing the system complexity. In addition, there is no concern for formation of an explosive mixture, as is the case in PROX. The major disadvantage of the methanation process is H_2 consumption, especially if the CO concentration is as high as a few percent.

3.2.2.5 Membrane separation

A mature technology for H_2 purification is permeation through metal membranes, namely palladium. The membrane is only permeable to H_2 allowing separation of H_2 from the other fuel constituents. This method not only removes the poisonous CO but also eliminates other inert gases such CO_2, N_2, and other trace impurities causing an increase of the H_2 partial pressure in the anode feed. However, the disadvantages of this method are the cost of the noble-metal membrane, its durability. Also, the required high differential pressure across the membrane result in high parasitic loss from this process.

3.3 PEMFC system integration

Generally, the fuel for PEM fuel cells is hydrogen. Hydrogen is the lightest and most abundant element in the universe; however, on Earth it is not present in its molecular form, but in many chemical compounds, such as water or hydrocarbons. Hydrogen is therefore not an energy source but a synthetic fuel that must be produced. Typically, the design of PEMFC system depends on the available or chosen fuel. Pure hydrogen or hydrogen-rich gas from reforming process is either used as fuel in PEMFC anodes. The PEMFC system of hydrogen-rich gas operation will be more complicate than pure hydrogen operation because the fuel processing will be added to the system for producing hydrogen to supply to PEMFC. For pure hydrogen

operation, hydrogen may be produced elsewhere and then stored as a part of the system. Therefore, the system consists of only, storage tank, fuel cell and some auxiliary unit.

3.3.1 Pure hydrogen operation

For fuel cell systems, hydrogen may be produced elsewhere and then stored as a part of the system. The most common way of storing hydrogen is in high-pressure cylinders. Another option is to store hydrogen in a Liquid form. Hydrogen is Liquid at 20.3 K. This is a common way to store relatively large quantities of hydrogen. Smaller tanks for use in automobiles have been developed and demonstrated by BMW. They can reach storage efficiency of 14.2% hydrogen by weight and require about 22 liters to store 1 kg of hydrogen. These tanks must be specially constructed and heavily insulated to minimize hydrogen boil-off. A relatively simple evaporator is sufficient to produce gaseous hydrogen needed for fuel cell applications. Yet another way of storing hydrogen is in metal hydrides. Some metals (such as various alloys of magnesium, titanium, iron, manganese, nickel, chromium, and others) form metal hydrides when exposed to hydrogen. Hydrogen atoms are packed inside the metal lattice structure, and because of that, higher storage densities may be achieved than with compressed hydrogen (1kg hydrogen can be stored in 35-50 liters). The problem with this storage is that the metals are intrinsically heavy; storage efficiency of 1.0% to 1.4% hydrogen by weight can be achieved. Higher storage efficiencies have been reported with some metal hydrides, but those are typically high-temperature metal hydrides (above 100°C) and thus not practical with low-temperature PEM fuel cells. To release hydrogen from metal hydrides, heat is required. Waste heat from the fuel cell, in both water cooled and air-cooled systems, is sufficient to release hydrogen from low temperature metal hydrides. Because hydrogen is stored in basically solid form, this is considered one of the safest hydrogen storage methods. Several chemical ways of storing hydrogen have been proposed and some practically demonstrated, such as hydrazine, ammonia, methanol, ethanol, lithium hydride, sodium hydride, sodium borohydride, lithium borohydride, diborane, calcium hydride, and so forth. Although attractive because most of them are in liquid form and offer relatively high

hydrogen storage efficiencies (up to 21% by weight for diborane), they require some kind of a reactor to release hydrogen. In addition, some of them are toxic and some can cause severe corrosion problems.

Once hydrogen is released from the storage tank, the simplest way to supply hydrogen to a fuel cell is in the dead-end mode (Figure 3.6 (a)). Such a system would only require a preset pressure regulator to reduce the pressure from the stack to the fuel cell operating pressure. The long-term operation in a dead-end mode may be possible only with extremely pure gases, both hydrogen and oxygen. Any impurities present in hydrogen will eventually accumulate in the fuel cell anode. This also includes water vapor that may remain (when the back diffusion is higher than the electroosmotic drag), which may be the case with very thin membranes and when operating at low current densities. In addition, inerts and impurities may diffuse from the air side until an equilibrium concentration is established. To eliminate this accumulation of inerts and impurities, purging of the hydrogen compartment may be required (Figure 3.6 (b)). This may be programmed either as a function of cell voltage or as a function of time. If purging of hydrogen is not possible or preferred because of safety, mass balance, or system efficiency reasons, excess hydrogen may be flown through the stack ($S > 1$) and unused hydrogen returned to the inlet, either by a passive (ejector) or an active (pump or compressor) device (Figure 3.7).

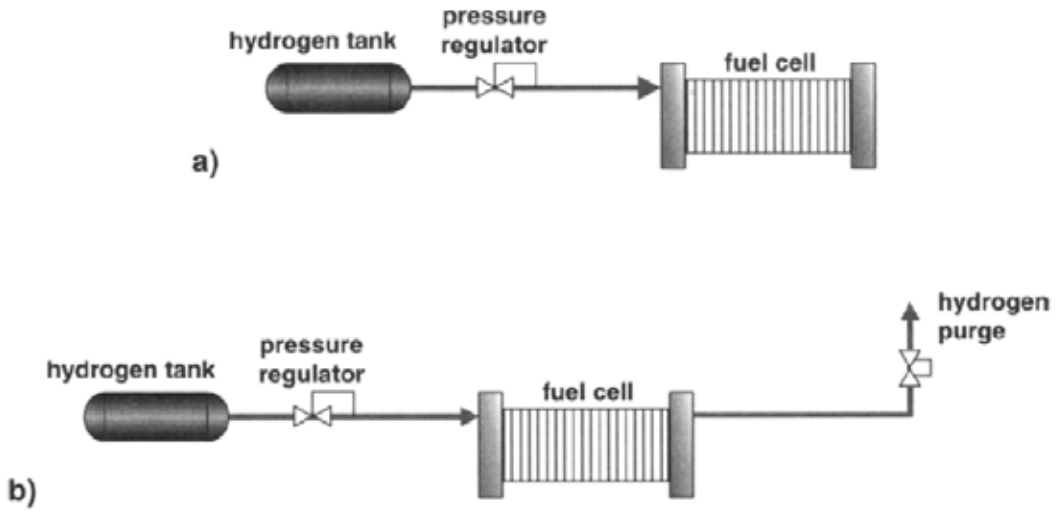

Figure 3.6 Hydrogen supply: a) dead-end; b) dead-end with intermittent purging (Barbir, 2006).

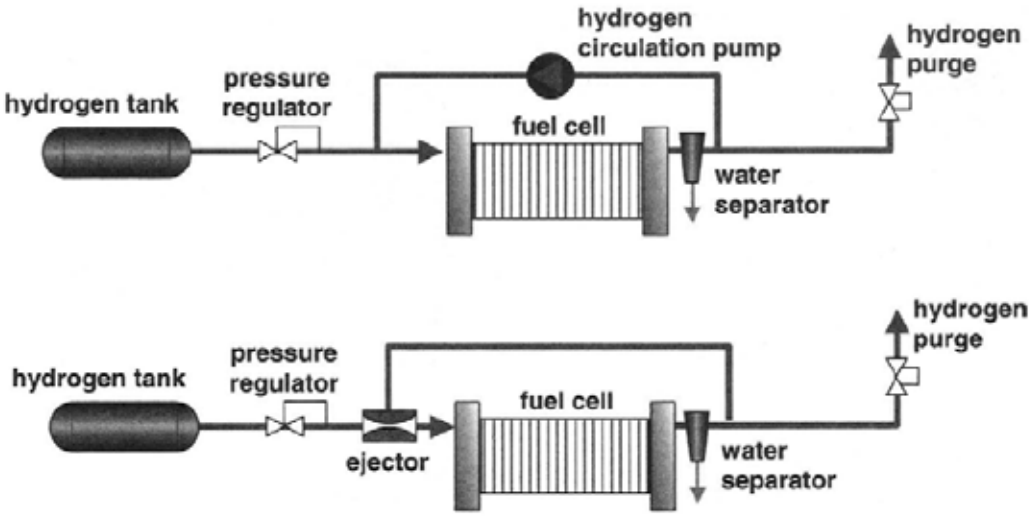

Figure 3.7 Closed-loop hydrogen supply system with pump (above) and ejector (below) (Barbir, 2006).

The systems with hydrogen storage are typically much simpler and more efficient, but hydrogen storage requires a lot of space even when hydrogen is compressed to very high pressures or even liquefied (Barbir, 2005).

3.3.2 Reformate gas operation

With the limitation of hydrogen storage and supporting infrastructure, a fuel cell integrated with a fuel processor allowing hydrogen generation from hydrocarbon fuels becomes an effective solution. Consequently, the fuel processor needs to be fully integrated with the fuel cell system. It not only provides fuel to the fuel cell, and uses the heat from the fuel cell exhaust gases, but it also shares air, water, coolant, and control subsystems. Figure 3.8 represents conventional PEMFC system. The reformate coming out of the fuel processor is hot and oversaturated with water. This eliminates the need for anode humidifier, but it requires a cooler to bring the anode gas to the fuel cell operating temperature. Condensed water is separated before entering the fuel cell stack. However, the humidification is unnecessary for both anode and cathode site of HT-PEMFC because this fuel cell can be operated at dry condition.

Furthermore, the fuel processor and the fuel cell typically operate at the same pressure, so they may share the same air supply. It is important to distribute the air flow to where it is needed, namely, fuel cell stack and fuel processor reactor (including preferential oxidation reactors in case of conventional PEMFC system). Water is needed by the fuel processor to generate steam for the fuel processor and shift reactors, and by the fuel cell for humidification of the cathode inlet. Typically, high-pressure water is required for both steam generation and injection in the humidifier. Fuel cell systems, regardless of application, may be designed to operate without need for makeup water. Water enters the system with ambient air and leaves the system with exhaust. Water is created as a product in the fuel cell, in the tail gas burner, and small quantities are produced in the preferential oxidation (as a result of unwanted hydrogen oxidation). At the same time, water is consumed in the fuel processor (both in steam reforming and in gas shift reactions).

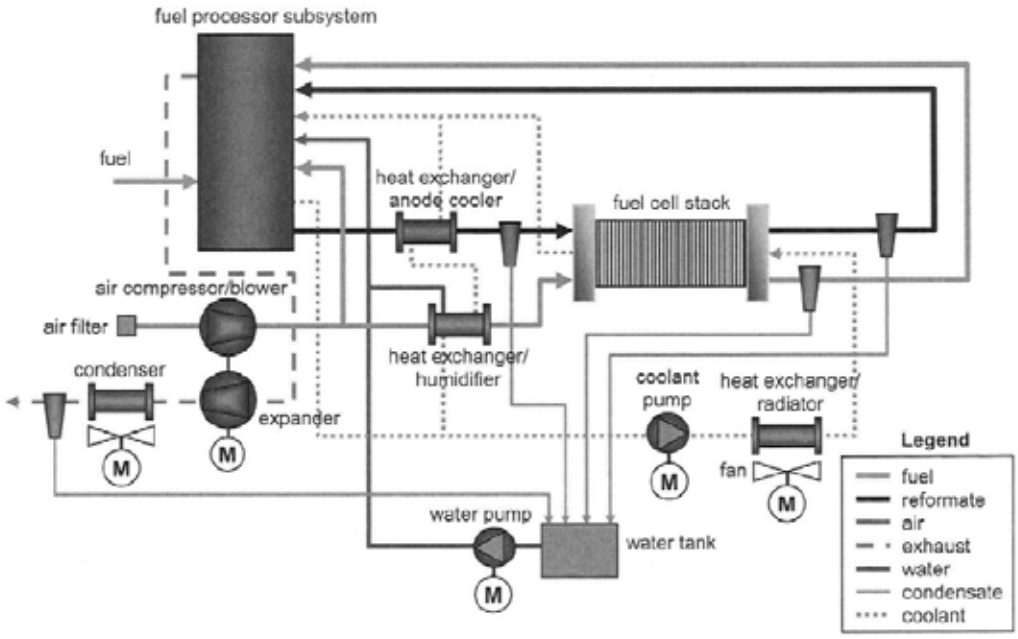

Figure 3.8 A complete PEMFC system integrated with fuel processor (Barbir, 2005).

As mentioned before, most fuel processor for PEMFC consists of a reforming reactor, one or two water shift reactors and CO purification unit. Moreover, the system also comprises the auxiliary equipment such as pumps, compressors, heaters, coolers, heat exchangers and pipes. Intensive heat integration between the PEMFC and fuel processor is necessary to achieve acceptable net efficiency. In general, a design task for fuel processor integrated with PEMFC systems depends on their applications and desired efficiency.

To develop the fuel cell to the market place, its design for each application should be considered. For automotive application, it requires the low weight and size of the overall system. The fast starting up is also preferred and thus the autothermal reforming is suitable for this application more than steam reforming (Sopena et al., 2007). At the same time, the high efficiency is needed for stationary application but the weight and size is not specified for this application. Therefore, the cogeneration system of heat and power with other process is effective way to improve the system efficiency. Because of a sharp increase of the anodic contribution of cell activation overvoltage when there is a lack of hydrogen near the membrane, a stack fed with reformate gas cannot use H_2 at 100%. As it can reach 100% with pure hydrogen, 80–

85% with reformate from steam reforming, it seems that it is not higher than 70% with a reformate gas from autothermal reforming. Therefore, the steam reforming is mostly chosen for stationary application (Hubert et al., 2006).

3.4 Auxiliary units

Apart from reformer, purification unit and fuel cell, the supporting equipment is one of the important units, which makes the integrated system work efficiently. Both fuel processor and fuel cell need water, air and thermal management to deliver the gases and control the reactors with proper temperature, humidity, flow rate and pressure. The main auxiliary in terms of power consumption is the air compressor. Then, a device to humidify and preheat this inlet air is necessary. The fuel processor and the fuel cell sub-systems interact strongly, not only in the direction from fuel processor to fuel cell, but also in the other way, like anode off-gas (sent to the burner), water produced by the cells (sent to the reaction chamber) and cooling circuit which crosses the two subsystems. Typically, auxiliary units for fuel processor/PEMFC integrated system comprise of fuel supply and heat transfer units which are explained as follows:

3.4.1 Fuel supply units

To supply reactant to fuel processor and fuel cell, the compressor and pump is needed for the integrated system. Compressors are used to compress air or oxygen for fuel cell and reformer (in case of autothermal reforming). Also, the other gas such as hydrogen, reformate gas, and reactant gas for reformer need compressor to increase pressure at desired level. However, for low temperature system, the reactant and oxidant gases are supplied by fans or blowers. On the other hand, the pump is the unit that is used to deliver liquid reactant to reactor and is important factor in the system efficiency. It should be noted that the fuel supply units is driven by electric motor, which requires power from the fuel cell or other sources to run. For the LT-PEMFC, the reactant fed to the cell need to be saturated with water due to nature of the membrane electrolyte required water for proton conducting mechanism. Therefore,

the humidification unit is necessary to prevent the cell from dehydration. The gas can be humidified by bubbling the gas through water, water or steam injection, flash evaporation, or through a water/heat exchanger device. Commercial humidifiers usually use heating coils and warm water spray to bring the gas to the desired temperature and humidity. In addition, the condenser is needed to condense and save the water in the exhaust to maintain a neutral water balance in the system.

3.4.2 Heat management units

Due to the different temperature of each unit of the fuel processor and PEMFC, the heat exchanger to recovery waste heat from hot gas is necessary in order to obtain the highest possible overall efficiency. For example, the reformate gas coming out of the fuel processor is hot and oversaturated with water. This eliminates the need for anode humidifier but it requires to be cooled before being fed to fuel cell. Therefore, the heat exchanger is the equipment to transfer these heats to preheat and vaporize the reactant of reformer. In addition, the burner unit is needed to supply heat to the reformer to keep the temperature of reformer at desired level in the case of steam reforming. However, it is unnecessary for partial oxidation and autothermal reforming but the cooling system is required to control temperature of reactor.

CHAPTER IV

MATHEMATICAL MODEL

A mathematical model is essential tool in the design and optimization of PEMFC system. In this research, the thermodynamic model by using direct minimization of Gibb free energy is applied for glycerol reforming process. The mass transport in flow channel and gas diffusion model and electrochemical model of PEMFC is also described.

4.1 Fuel processor model: Thermodynamic analysis

4.1.1 Reforming process model

The thermodynamic analysis is used to study the effect of operating parameter and find optimal condition of glycerol reforming process in this work because of the lack of kinetic rate data of this process. The equilibrium conversion of a reaction provides a goal by which to measure improvements in a process. At equilibrium, the total Gibbs free energy of a close reactive system at constant temperature and pressure decreases during reaction proceeding and the equilibrium condition is reached when the total Gibbs free energy attains its minimum value. From thermodynamic analysis point of view, the composition of reaction products from a reformer at thermodynamic equilibrium condition can be calculated in two ways, namely stoichiometric and non-stoichiometric thermodynamic approaches. In the former, a set of stoichiometrically independent reactions typically chosen from a set of possible reactions is first specified and then the equilibrium composition of each substance is computed from the reaction equilibrium constants at the fixed temperature and pressure. In the latter approach, for a given set of substances, the equilibrium composition is directly determined by solving the minimization problem of the Gibbs free energy.

Here, the method of the direct minimization of Gibbs free energy was used to predict equilibrium composition since a selection of the possible set of reactions is not necessary (Smith et al., 2005). The total Gibbs free energy of a close reactive system at constant temperature and pressure decreases during reaction proceeding and the equilibrium condition is reached when the total Gibbs free energy attains its minimum value. Therefore, the equilibrium composition can be determined by solving the minimization problem as given below (Smith et al., 20005):

$$\min_{n_i} (G^t)_{T,P} = \sum_{i=1}^{C} n_i \overline{G}_i = \sum_{i=1}^{C} n_i \left(G_i^\circ + RT \ln \frac{\overline{f}_i}{f_i^\circ} \right) \tag{4.1}$$

where C is the total number of components in the reaction system, n_i is a amount of each gaseous component. Resulting from the conservation of atomic species, n_i have to satisfy the element balance in Eq. (2).

$$\sum_i n_i a_{ik} - A_k = 0 \qquad (k = 1, 2, ..., w) \tag{4.2}$$

where a_{ik} is the number of atoms of element k in component i, b_k is the total number of atoms of element k in the reaction mixture, and M is the total number of elements.

The problem is to find the set of n_i which minimizes G_t for specified T and P, subjected to the constant of the material balances. To solve optimization problem Lagrange's undetermined method is applied and its procedure is shown as follows:

1) The Lagrange multiplier (λ_k), one for each element, by multiplying each element balance by its λ_k.

$$\lambda_k \left(\sum_i n_i a_{ik} - A_k \right) = 0 \tag{4.3}$$

These equations are summed over k, giving:

$$\sum_k \lambda_k \left(\sum_i n_i a_{ik} - A_k \right) = 0 \tag{4.4}$$

Then a new function F is formed by addition of this last sum to G^t.

$$F = G^t + \sum_k \lambda_k \left(\sum_i n_i a_{ik} - A_k \right) \tag{4.5}$$

This new function is identical with G^t, because the summation term is zero. However, the partial derivatives of F and G^t with respect to n_i are different, because the function F incorporates the constraints of the material balances.

2) The minimum value F (and G^t) occurs when all of the partial derivatives $\left(\partial F / \partial n_i\right)_{T,P,n_i}$ are zero.

$$\left(\frac{\partial F}{\partial n_i} \right)_{T,P,n_i} = \left(\frac{\partial G^t}{\partial n_i} \right)_{T,P,n_i} + \sum_k \lambda_k a_{ik} = 0 \tag{4.6}$$

From Eq. (4.1), the first term on the right of Eq. (4.6) can be written:

$$G_i^\circ + RT \ln \frac{\bar{f}_i}{f_i^\circ} + \sum_k \lambda_k a_{ik} = 0 \tag{4.7}$$

For the ideal gas operation, the Eq. (4.7) becomes:

$$G_i^\circ + RT \ln \frac{y_i P}{P^\circ} + \sum_k \lambda_k a_{ik} = 0$$

or

$$\frac{\Delta G_{f_i}^\circ}{RT} + \ln \frac{P}{P_0} + \ln\left(y_i\right) + \sum_k \frac{\lambda_k a_{ik}}{RT} = 0 \qquad \left(i = 1,\ 2,...,N\right) \tag{4.8}$$

Eq. (4.8) represents the N equilibrium equations for each chemical species, and Eq. (4.2) represents w material balance for each element. The unknowns in these equations are the n_i's (note that $y_i = n_i / \sum_i n_i$), of which there are N, and the λ_k's, of which there are w–a total of N+w unknowns. Thus, the number of equations is sufficient for the determination of all unknowns.

For glycerol steam reforming process, the six equilibrium equations for six species are:

$C_3H_8O_3$: $$\ln\frac{P}{P_0}+\frac{\Delta G^{\circ}_{C_3H_8O_3}}{RT}+\ln y_{C_3H_8O_3}+\frac{\lambda_C a_{C_3H_8O_3,C}}{RT}+\frac{\lambda_O a_{C_3H_8O_3,O}}{RT}+\frac{\lambda_H a_{C_3H_8O_3,H}}{RT}=0 \quad (4.9)$$

CH_4: $$\ln\frac{P}{P_0}+\frac{\Delta G^{\circ}_{CH_4}}{RT}+\ln y_{CH_4}+\frac{\lambda_C a_{CH_4,C}}{RT}+\frac{\lambda_H a_{CH_4,H}}{RT}=0 \quad (4.10)$$

CO_2: $$\ln\frac{P}{P_0}+\frac{\Delta G^{\circ}_{CO_2}}{RT}+\ln y_{CO_2}+\frac{\lambda_C a_{CO_2,C}}{RT}+\frac{\lambda_O a_{CO_2,O}}{RT}=0 \quad (4.11)$$

CO: $$\ln\frac{P}{P_0}+\frac{\Delta G^{\circ}_{CO}}{RT}+\ln y_{CO}+\frac{\lambda_C a_{CO,C}}{RT}+\frac{\lambda_O a_{CO,O}}{RT}=0 \quad (4.12)$$

H_2O: $$\ln\frac{P}{P_0}+\frac{\Delta G^{\circ}_{H_2O}}{RT}+\ln y_{H_2O}+\frac{\lambda_O a_{H_2O,O}}{RT}+\frac{\lambda_H a_{H_2O,H}}{RT}=0 \quad (4.13)$$

H_2: $$\ln\frac{P}{P_0}+\frac{\Delta G^{\circ}_{H_2}}{RT}+\ln y_{H_2}+\frac{\lambda_H a_{H_2,H}}{RT}=0 \quad (4.14)$$

The three atom balance equations and the equation for $\sum_i y = 1$ are:

C: $$A_{\mathrm{C}} / n_{\mathrm{total,g}} - (y_{\mathrm{C_3H_8O_3}} a_{\mathrm{C_3H_8O_3,C}} + y_{\mathrm{CH_4}} a_{\mathrm{CH_4,C}} + y_{\mathrm{CO_2}} a_{\mathrm{CO_2,C}} + y_{\mathrm{CO}} a_{\mathrm{CO,C}}) = 0 \quad (4.15)$$

H: $$A_{\mathrm{H}} / n_{\mathrm{total,g}} - (y_{\mathrm{C_3H_8O_3}} a_{\mathrm{C_3H_8O_3,H}} + y_{\mathrm{CH_4}} a_{\mathrm{CH_4,H}} + y_{\mathrm{H_2}} a_{\mathrm{H_2,H}} + y_{\mathrm{H_2O}} a_{\mathrm{H_2O,H}}) = 0 \quad (4.16)$$

O: $$A_{\mathrm{O}} / n_{\mathrm{total}}, g - (y_{\mathrm{C_3H_8O_3}} a_{\mathrm{C_3H_8O_3,O}} + y_{\mathrm{CO_2}} a_{\mathrm{CO_2,O}} + y_{\mathrm{CO}} a_{\mathrm{CO,O}} + y_{\mathrm{H_2O}} a_{\mathrm{H_2O,O}}) = 0 \quad (4.17)$$

$$1 - y_{\mathrm{C_3H_8O_3}} - y_{\mathrm{CH_4}} - y_{\mathrm{CO}} - y_{\mathrm{CO_2}} - y_{\mathrm{H_2}} - y_{\mathrm{H_2O}} = 0 \quad (4.18)$$

For glycerol autothermal reforming process, the equilibrium equation for oxygen in Eq. (4.19) is added in the system.

O_2: $$\ln \frac{P}{P_0} + \frac{\Delta G^{\circ}_{\mathrm{O_2}}}{RT} + \ln y_{\mathrm{O_2}} + \frac{\lambda_{\mathrm{O}} a_{\mathrm{O_2,O}}}{RT} = 0 \quad (4.19)$$

Also, the atom balance equation of oxygen and equation for $\sum_i y = 1$ in Eq. (4.17) and Eq. (4.18) are changed to Eq. (4.20) and Eq. (4.21).

O: $$A_{\mathrm{O}} / n_{\mathrm{total,g}} - (y_{\mathrm{C_3H_8O_3}} a_{\mathrm{C_3H_8O_3,O}} + y_{\mathrm{CO_2}} a_{\mathrm{CO_2,O}} + y_{\mathrm{CO}} a_{\mathrm{CO,O}} + y_{\mathrm{H_2O}} a_{\mathrm{H_2O,O}} + y_{\mathrm{O_2}} a_{\mathrm{O_2,O}}) = 0 \quad (4.20)$$

$$1 - y_{\mathrm{C_3H_8O_3}} - y_{\mathrm{CH_4}} - y_{\mathrm{CO}} - y_{\mathrm{CO_2}} - y_{\mathrm{H_2}} - y_{\mathrm{H_2O}} - y_{\mathrm{O_2}} = 0 \quad (4.21)$$

In the case of considering the carbon formation, the equilibrium equation for solid carbon in Eq. (4.22) is added in the system.

C: $$\frac{\lambda_{\mathrm{C}} a_{\mathrm{C,C}}}{RT} = 0 \tag{4.22}$$

Also, the atom balance equation of carbon in Eq. (4.17) is changed to Eq. (4.23) to include the carbon atom of solid carbon.

C: $$A_{\mathrm{C}} / n_{\mathrm{total,g}} - (y_{\mathrm{C_3H_8O_3}} a_{\mathrm{C_3H_8O_3,C}} + y_{\mathrm{CH_4}} a_{\mathrm{CH_4,C}} + y_{\mathrm{CO_2}} a_{\mathrm{CO_2,C}} + y_{\mathrm{CO}} a_{\mathrm{CO,C}} + (n_{\mathrm{C}} / n_{\mathrm{total,g}}) a_{\mathrm{C,C}}) = 0 \tag{4.23}$$

4.1.2 Fuel processor efficiency

The efficiency of a fuel processing process (η_{FP}) can be determined by the following expression:

$$\eta_{FP} = \frac{LHV_{H_2} \cdot \left(\dot{m}_{H_2}\right)}{LHV_{fuel} \cdot \left(\dot{m}_{fuel}\right) + \text{external heat required}} \tag{4.24}$$

where $\dot{m}_{H_2}$ is the molar flow rate of H_2 and $\dot{m}_{fuel}$ is the molar flow rate of fuel used for producing hydrogen. The external heat used to maintain the glycerol reformer at isothermal condition and to preheat reactant is determined from difference between overall heat required for glycerol steam reforming process and recovery heat from hot reformate gas.

4.2 PEMFC model

The PEMFC model considered here consists of mass transport in flow channel and gas diffusion layer as well as electrochemical model. The mass transport in the flow channel is taken account to investigate CO poisoning effect along the direction of channel length while the mass transport in gas diffusion layer and thin film electrolyte considers only the diffusion flux direction. The model schematic of HT-PEMFC is shown in Figure 4.1. The following assumptions are made in the development of the model.

- Steady state and isothermal operation
- Only gas phases present
- Ideal gas mixtures
- Zero gas permeability through membrane
- Catalyst layer treated as interface
- Pressure drop is negligible
- The operating voltage is constant along the cell coordinate

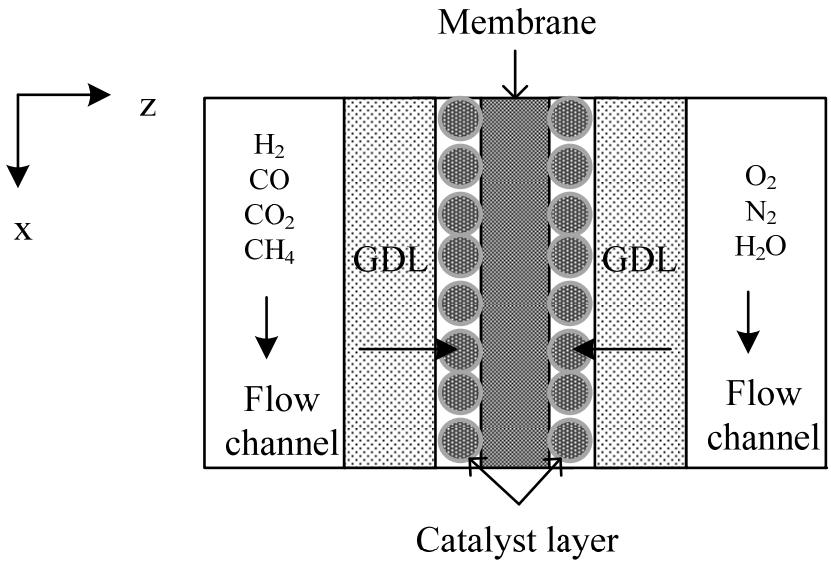

Figure 4.1 Schematic diagram of HT-PEMFC.

4.2.1Flow channel

In the flow channel, the molar flow of each gas will be changed by the electrochemical reactions as given in Eqs. (4.25)-(4.27). At the anode side, the hydrogen molar flow decreases when the reactions take place. This generally causes an increase in the CO mole fraction and therefore, the CO poisoning effect on the PEMFC performance is more pronounced, especially at the end of the flow channel. For HT-PEMFC, the specie balance in flow channel is shown as following equation:

At anode

$$\frac{dM_{H_2}}{dx} = -h\left(\frac{i}{2F}\right) \tag{4.25}$$

At cathode

$$\frac{dM_{O_2}}{dx} = -h\left(\frac{i}{4F}\right) \tag{4.26}$$

$$\frac{dM_{H_2O}}{dx} = h\left(\frac{i}{2F}\right) \tag{4.27}$$

For LT-PEMFC, transport properties of the electrolyte for Nafion membranes are considered and the water vapor flux transport across the membrane by electro-osmosis drag force (n_d) and back diffusion ($D_{w,mem}$) will be added in the model and flow channel model is describe as follows:

At anode

$$\frac{dM_{H_2}}{dx} = -h\left(\frac{i}{2F}\right) \tag{4.28}$$

$$\frac{dM_{H_2O,a}}{dx} = h\left(-n_d\frac{i}{F} + D_{w,mem}\frac{\left(C_{H_2O,a} - C_{H_2O,c}\right)}{\delta}\right) \tag{4.29}$$

At cathode

$$\frac{dM_{O_2}}{dx} = -h\left(\frac{i}{4F}\right) \tag{4.30}$$

$$\frac{dM_{H_2O,c}}{dx} = h\left(\frac{i}{2F} + n_d\frac{i}{F} - D_{w,mem}\frac{\left(C_{H_2O,a} - C_{H_2O,c}\right)}{\delta}\right) \tag{4.31}$$

In the case of LT-PEMFC, n_d is electro-osmosis drag force and $D_{w,mem}$ is back diffusion. These two parameters can be calculated from the following equation (Springer et al., 1991):

$$n_d = \begin{cases} 0.0049 + 2.02a_{anode} - 4.53a_{anode}^2 + 4.09a_{anode}^3 & for\ a_{anode} \le 1 \\ 1.59 + 0.159(a_{anode} - 1) & for\ a_{anode} > 1 \end{cases} \tag{4.32}$$

$$D_{w,mem} = n_d\, 5.5\times10^{-11}\exp\left[2416\left(\frac{1}{303} - \frac{1}{T}\right)\right] \tag{4.33}$$

$$a_{anode} = \frac{x_{H_2O,a}P}{P_{sat}} \tag{4.34}$$

The set of ordinary differential equations explaining the distribution of gaseous components along the flow channel of PEMFC is used to calculate the mole fraction of reactants at the flow channel/gas diffusion layer interface.

4.2.2 Diffusion layer

To reach catalyst surface, the reactant gas from anode and cathode flow channel need to diffuse through gas diffusion layer and film electrolyte layer. The model used to represent gas transport is shown as follows:

4.2.2.1 Gas diffusion layer

Diffusion of multi-component gas streams through the porous carbon electrode like gas diffusion layer (GDL) can be described using the Stefan-Maxwell equation:

$$\frac{dX_i}{dz} = \frac{RT}{P} \sum \frac{X_i N_j - X_j N_i}{D_{ij}^{eff}} \tag{4.35}$$

In the case of reformate gas operation, the components at the anode consist of H_2, CO, CO_2, H_2O and CH_4 while the cathode components compose of O_2, N_2 and H_2O.

At anode:

CO_2:

$$\frac{dX_{CO_2}}{dz} = \frac{RT}{P} X_{CO_2} \left(\frac{N_{H_2,g}}{D_{H_2,CO_2}^{eff}} \right) \tag{4.36}$$

H_2O:

$$\frac{dX_{H_2O}}{dz} = \frac{RT}{P} X_{H_2O} \left(\frac{N_{H_2,g}}{D_{H_2,H_2O}^{eff}} \right) \tag{4.37}$$

CO:

$$\frac{dX_{\mathrm{CO}}}{dz} = \frac{RT}{P} X_{\mathrm{CO}} \left(\frac{N_{\mathrm{H_2,g}}}{D^{eff}_{\mathrm{H_2,CO}}} \right) \tag{4.38}$$

CH_4:

$$\frac{dX_{\mathrm{CH_4}}}{dz} = \frac{RT}{P} X_{\mathrm{CH_4}} \left(\frac{N_{\mathrm{H_2,g}}}{D^{eff}_{\mathrm{H_2,CH_4}}} \right) \tag{4.39}$$

H_2:

$$X_{\mathrm{H_2}} = 1 - X_{\mathrm{CO_2}} - X_{\mathrm{H_2O}} - X_{\mathrm{CO}} - X_{\mathrm{CH_4}} \tag{4.40}$$

At cathode:

N_2:

$$\frac{dX_{\mathrm{N_2}}}{dz} = \frac{RT}{P} X_{\mathrm{N_2}} \left(\frac{N_{\mathrm{O_2}}}{D^{eff}_{\mathrm{N_2,O_2}}} + \frac{N_{\mathrm{H_2O,g}}}{D^{eff}_{\mathrm{N_2,H_2O}}} \right) \tag{4.41}$$

H_2O:

$$\frac{dX_{\mathrm{H_2O}}}{dz} = \frac{RT}{P} \left[X_{\mathrm{H_2O}} \left(\frac{N_{\mathrm{O_2}}}{D^{eff}_{\mathrm{O_2,H_2O}}} \right) - N_{\mathrm{H_2O}} \left(\frac{X_{\mathrm{O_2}}}{D^{eff}_{\mathrm{O_2,H_2O}}} + \frac{X_{\mathrm{N_2}}}{D^{eff}_{\mathrm{N_2,H_2O}}} \right) \right] \tag{4.42}$$

O_2:

$$X_{\mathrm{O_2}} = 1 - X_{\mathrm{N_2}} - X_{\mathrm{H_2O}} \tag{4.43}$$

where D^{eff}_{ij} is calculated by using the Slattery-Bird correlation (Slattery et al., 1958) and corrected to account for the porosity/tortuosity effects using the Bruggeman correlation (Scott et al., 2007).

$$D_{ij}^{eff} = \frac{a}{P}\left(\frac{T}{\sqrt{T_{c,i}T_{c,j}}}\right)^{b}\left(P_{c,i}P_{c,j}\right)^{1/3}\left(T_{c,i}T_{c,j}\right)^{5/12}\left(\frac{1}{M_i}+\frac{1}{M_j}\right)^{1/2}\varepsilon^{\tau} \qquad (4.44)$$

where T_c and P_c are the gas critical temperature and pressure, respectively. M is the as molecular weight. ε and τ is the porosity and the tortuosity. a is 0.0002745 for di-atomic gases and 0.000364 for water vapor and b is 1.832 for di-atomic gases and 2.334 for water vapor.

The molar flux of each component at anode and cathode side of HT-PEMFC and LT-PEMFC are shown in Table 4.1 and 4.2, respectively.

Table 4.1 Molar flux of each component at anode

HT-PEMFC	**LT-PEMFC**
$N_{\mathrm{CO_2},g} = 0$	$N_{\mathrm{CO_2},g} = 0$
$N_{\mathrm{CO_2},g} = 0$	$N_{\mathrm{CO_2},g} = 0$
$N_{\mathrm{H_2,g}} = \frac{i}{2F}$	$N_{\mathrm{H_2,g}} = \frac{i}{2F}$
$N_{\mathrm{CH_4},g} = 0$	$N_{\mathrm{CH_4},g} = 0$
$N_{\mathrm{H_2O},g} = 0$	$N_{\mathrm{H_2O,g}} = -n_D\frac{i}{F} + D_w\frac{\left(C_{\mathrm{H_2O,a}} - C_{\mathrm{H_2O,c}}\right)}{\delta}$

Table 4.2 Molar flux of each component at cathode

HT-PEMFC	**LT-PEMFC**
$N_{\mathrm{O_2,g}} = \frac{i}{4F}$	$N_{\mathrm{O_2,g}} = \frac{i}{4F}$
$N_{\mathrm{H_2O},g} = \frac{-j}{2F}$	$N_{\mathrm{H_2O,g}} = \frac{-i}{2F} + n_D\frac{i}{F} - D_w\frac{\left(C_{\mathrm{H_2O,a}} - C_{\mathrm{H_2O,c}}\right)}{\delta}$
$N_{\mathrm{N_2},g} = 0$	$N_{\mathrm{N_2},g} = 0$

4.2.2.1 Film electrolyte layer

In this research, the PBI doped phosphoric acid membrane is used as electrolyte for HT-PEMFC whereas electrolyte of LT-PEMFC is Nafion. To find H_2 and O_2 concentrations at the catalyst intersurface, Fick's law for diffusion is applied (Eqs. (4.45)-(4.46)). Reactant gases need to diffuse through electrolyte film layer covering before arriving at the catalyst active surface (Mamlouk et al., 2011).

$$\frac{N_{\mathrm{O_2}}}{S_{\mathrm{Pt-cathode}}} = \frac{-D_{O_2}\left(C_{\mathrm{O_2-pt}} - C_{\mathrm{O_2(dissolve)}}\right)}{\delta_{\mathrm{cathode}}} \tag{4.45}$$

$$\frac{N_{\mathrm{H_2}}}{S_{\mathrm{Pt-anode}}} = \frac{-D_{\mathrm{H_2}}\left(C_{\mathrm{H_2-pt}} - C_{\mathrm{H_2(dissolve)}}\right)}{\delta_{\mathrm{anode}}} \tag{4.46}$$

where N is the molar flux, C_{Pt} is the reactant concentration on the catalyst surface, C_{dissolve} is the equilibrium reactant concentration in the acid film at the studied temperature. S_{Pt} is the real platinum surface area and δ is the film thickness.

The concentration of H_2 and O_2 dissolving at film electrolyte layer boundary can be calculated from their solubility ($C_{\mathrm{i}}^{\mathrm{dissolved}}$) as follows:

$$C_{\mathrm{H_2(dissolve)}} = C_{\mathrm{H_2}}^{\mathrm{dissolved}} \cdot X_{\mathrm{H_2}} \cdot P \tag{4.47}$$

$$C_{\mathrm{O_2(dissolve)}} = C_{\mathrm{O_2}}^{\mathrm{dissolved}} \cdot X_{\mathrm{O_2}} \cdot P \tag{4.48}$$

where $X_{\mathrm{H_2}}$ and $X_{\mathrm{O_2}}$ are the mole fraction of H_2 and O_2 at GDL/electrolyte film interface.

It is noted that the solubility ($C_{\mathrm{i}}^{\mathrm{dissolved}}$) and diffusion coefficient (D_{i}) can be calculated from the correlation reported by Mamlouk et al. (2011) and shown in Appendix A.

4.2.3 Electrochemical model

4.2.3.1 Actual cell voltage

Typically, the fuel cell performance is represented by the relation of a fuel cell voltage and current density. Actual cell potentials or operating voltage of fuel cell (E_{cell}) is always smaller than the reversible cell potential (E_r) due to irreversible losses. The proportion of these losses is shown in polarization curve (Figure 4.2). E_{cell} can be calculated by subtracting E_r, the maximum voltage that can be achieved by a fuel cell at specific operating condition, by various voltage losses.

$$E_{\text{cell}} = E_r - \eta_{\text{act,a}} - \eta_{\text{act,c}} - \eta_{\text{ohmic}} \tag{4.49}$$

where $\eta_{\text{act,a}}$ is the activation loss at the anode, $\eta_{\text{act,c}}$ is the activation loss at the cathode and η_{ohmic} is the ohmic loss.

The reversible cell potential is described by Nernst equation (Eq. (4.50)):

$$E_r = -\left(\frac{\Delta H_T}{nF} - \frac{T\Delta S_T}{nF}\right) + \frac{RT}{nF}\ln\left[\frac{(RT)^{1.5} C_{\text{H}_2-\text{Pt}} C_{\text{O}_2-\text{Pt}}^{0.5}}{a_{\text{H}_2\text{O}}}\right] \tag{4.50}$$

where $a_{\text{H}_2\text{O}}$ is the water activity defined by the ratio of water partial pressure to its saturation pressure ($P_{H_2O}^{sat}$) which is given in Eq. (2). $C_{\text{H}_2-\text{Pt}}$ and $C_{\text{O}_2-\text{Pt}}$ are the hydrogen and oxygen concentration at the catalyst surface.

$$P_{H_2O}^{sat} = \begin{pmatrix} 142.07682T^4 - 171026.12676T^3 + 78013638.11584T^2 \\ -15953375633.8471T + 1231888491801.45 \end{pmatrix} * 10^{-10} \tag{4.51}$$

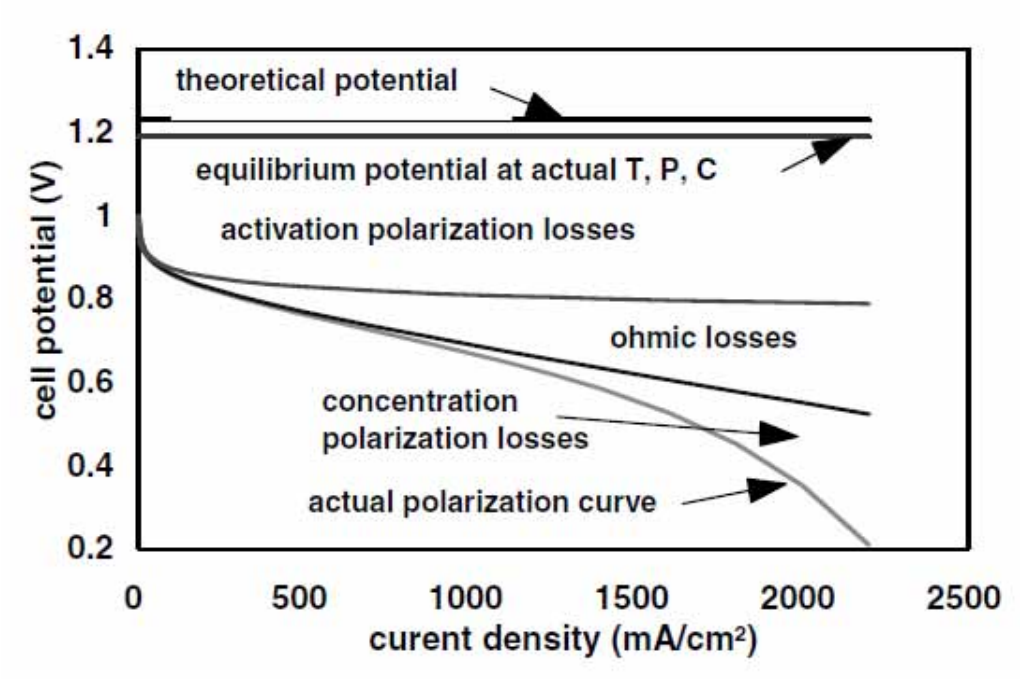

Figure 4.2 Various voltage losses and resulting polarization curve of fuel cell (Barbir, 2005).

4.2.3.2 Voltage losses

As mentioned before, there are some voltage losses occurring in fuel cell during the electrochemical reaction. Voltage losses in an operational fuel cell are described as follows:

Activation losses

Some voltage difference from equilibrium is needed to get the electrochemical reaction going. This is called activation polarization. These losses happen at both anode and cathode; however, oxygen reduction requires much higher overpotentials, that is, it is a much slower reaction than hydrogen oxidation. Activation losses are governed by the Butler-Volmer equation:

$$i_a = i_{0,a}\left(\exp\left(\frac{-\alpha_{Rd,a}F}{RT}\left(\eta_{act,a}\right)\right) - \exp\left(\frac{-\alpha_{Ox,a}F}{RT}\left(\eta_{act,a}\right)\right)\right) \qquad (4.52)$$

$$i_c = i_{0,c}\left(\exp\left(\frac{-\alpha_{Rd,c} F}{RT}\left(\eta_{act,c}\right)\right) - \exp\left(\frac{-\alpha_{Ox,c} F}{RT}\left(\eta_{act,c}\right)\right)\right) \tag{4.53}$$

where i is current density and α is transfer coefficient. i_0 is exchange current density which can be calculated from Eq. (4.54).

$$i_0 = i_0^{ref} a_c L_c \left(\frac{C_{Pt}}{C_{Pt}^{ref}} \right)^{\gamma} \exp\left[-\frac{E_c}{RT}\left(1 - \frac{T}{T_{ref}}\right)\right] \tag{4.54}$$

i_0^{ref} is the exchange current density measured at a reference temperature (T_{ref}) and reference dissolved reactant concentration (C_{Pt}^{ref}). C_{Pt} is the reactant concentration on the catalyst surface calculated from Eq. (4.45) for oxygen and Eq. (4.46) for hydrogen. a_c is the catalyst specific accessible electrochemical surface area. L_c is the catalyst loading is the pressure coefficient or the reaction order. E_c is the activation energy.

Assuming $\alpha_{Rd} = \alpha_{Ox} = \alpha$, the hyperbolic sine function can be substituted in Eq. (4.55) yielding the following relationship.

$$\eta_{\text{act}} = \frac{RT}{\alpha F} \sinh^{-1}\left(\frac{i}{2i_0} \right) \tag{4.55}$$

If the fuel used at the anode is a reformate gas from the fuel processor section, the effect of CO poisoning is included in the anode activation loss model of both the HT-PEMFC and LT-PEMFC. The CO poisoning model of LT-PEMFC, which is proposed by Bhatia et al. (2004), is used in this work. The anode activation loss of LT-PEMFC can be calculated by Eq. (4.56).

$$\eta_{\text{act,a}} = \frac{RT}{\alpha F} \sinh^{-1}\left(\frac{i}{2k_{\text{eh}}\theta_{\text{H}}} \right) \tag{4.56}$$

where θ_H is the hydrogen coverage which can be calculated from Eq. (4.57) and (4.58).

$$k_{fh} x_{H_2} P\left(1-\theta_H-\theta_{CO}\right)-b_{fh} k_{fh} \theta_H - i = 0 \quad (4.57)$$

$$k_{fc} x_{CO} P\left(1-\theta_H-\theta_{CO}\right)-b_{fc} k_{fc} \theta_{CO} = 0 \quad (4.58)$$

For HT-PEMFC, the exchange current density of hydrogen oxidation in the presence of CO is i_0^{CO} instead of i_0 (for pure hydrogen). The i_0^{CO} can be calculated from CO coverage (θ_{CO}) assuming the bridge model of CO adsorption on Pt and the anode activation loss of HT-PEMFC is represented by Eq. (4.59).

$$\eta_{act,a} = \frac{RT}{\alpha F} \sinh^{-1}\left(\frac{i}{2i_0\left(1-\theta_{CO}\right)^2}\right) \quad (4.59)$$

The CO coverage in Eq. (4.60) is developed from experimental data reported by Li et al. (2003) to explain a CO poisoning effect on HT-PEMFC in case of the reformate gas containing high CO content (3-10%) and can be described as follows:

$$\theta_{CO} = a * \ln\frac{[CO]}{[H_2]} + b * \ln(i) * \ln\frac{[CO]}{[H_2]} + c \quad (4.60)$$

$$a = -0.00012784 * T^2 + 0.11717499 * T - 26.62908873$$

$$b = 0.0001416 * T^2 - 0.12813608 * T + 28.852463626$$

$$c = -0.00034886 * T^2 + 0.31596903 * T - 70.11693333$$

The CO poisoning model for HT-PEMFC was validated against experimental data (Li et al., 2003) at different fractions of CO in hydrogen-rich gas and operating temperatures as shown in Figure 4.3. In their experiment, the anode fuel is dry hydrogen containing CO while pure oxygen is fed at the cathode side. The membrane thickness and catalyst loading is 65 μm and 0.5 mg cm^{-2}, respectively. It can be seen from Figure 4.3, the model prediction is in agreement with experimental data. From other experimental results, the CO_2 containing in hydrogen feed has the same provides the same performance with nitrogen at the same level of concentration and thus CO_2 is considered to have only the dilution effect on HT-PEMFC in this work

(Li et al., 2003). In addition, the voltage loss from methane is very low (< 50 mV at high current density of 1.5 A cm^{-2}) and thus it has a small effect on anode kinetic (Sustersic et al., 1980).

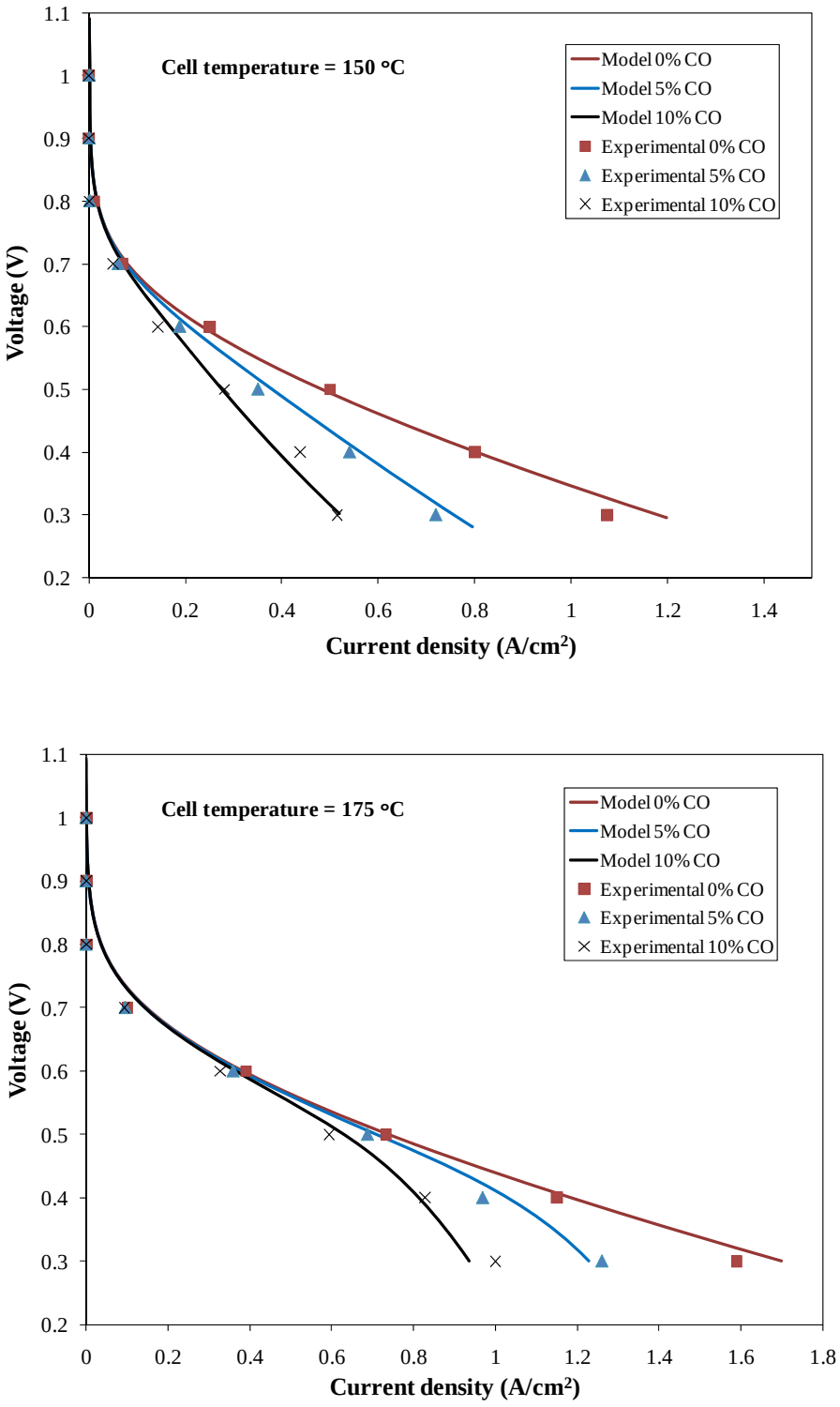

Figure 4.3 Validation of model and experimental (Li et al., 2003) at different %CO.

Ohmic loss

Ohmic losses occur because of resistance to the flow of ions in the electrolyte and resistance to the flow of electrons through the electrically conductive fuel cell components.

$$\eta_{\text{ohmic}} = iR \tag{4.61}$$

where R is total cell internal resistance (which includes ionic, electronic, and contact resistance, $\Omega\,\text{cm}^2$)

The considered ohmic losses are resistance of ions in the electrolyte through membrane (R_{mem}). For LT-PEMFC, ohmic loss is described as follows (Springer et al., 1991):

$$\eta_{\text{ohmic}} = R_{\text{mem}} i = \left(\frac{K_{\text{mem}}}{l_{\text{m}}} \right) i \tag{4.62}$$

The proton conductivity (K_{mem}) are correlated with the water content of the membrane (λ) in Eq. (4.63). λ can be calculated from Eq. (4.64) and is a function of the water activity (a) which is represented in Eq. (4.65).

$$K_{mem} = (0.5139\lambda - 0.326) \exp\left[1268 \left(\frac{1}{303} - \frac{1}{T} \right) \right] \times 100 \tag{4.63}$$

$$\lambda = \begin{cases} 0.043 + 17.81a - 39.85a^2 + 36.0a^3 & for\ 0 < a \le 1 \\ 14 + 1.4(a-1) & for\ 1 < a \le 3 \end{cases} \tag{4.64}$$

$$a = \frac{x_{H_2O} P}{P_{\text{sat}}} \tag{4.65}$$

For HT-PEMFC, ohmic loss is described as follows:

$$\eta_{\text{ohmic}} = R_{\text{mem}} i = \left(\frac{\sigma_{\text{m}}}{l_{\text{m}}} \right) i \tag{4.66}$$

The proton conductivity as a function of temperature and relative humidity obtained from Mamlouk et al. (2011) is represented in Eq.(4.67)-(4.69).

$$\sigma_m = \frac{A}{T}\exp\left(\frac{-B}{R(T)}\right) \tag{4.67}$$

$$A = \exp\left(\left(k_1^a RH^3\right) + \left(k_2^a RH^2\right) + \left(k_3^a RH\right) + k_0^a\right) \tag{4.68}$$

$$B = \left(k_1^b RH^3\right) + \left(k_2^b RH^2\right) + \left(k_3^b RH\right) + k_0^b \tag{4.69}$$

where *RH* is the relative humidity at given temperature. The values of constants k^a and k^b are given in the Appendix A.

4.2.4 Power and efficiency of fuel cell

The power output of the fuel cell (P_{FC}) can be calculated from the current density (i) and E_{cell} as follows:

$$P_{\text{FC}} = i \cdot A \cdot n \cdot E_{\text{cell}} \tag{4.70}$$

where A is the cell active area and n is the number of cells.

The fuel cell efficiency, defined as a ratio between the electricity produced and hydrogen consumed.

$$\eta = \frac{W_{\text{el}}}{W_{\text{H}_2}} \tag{4.71}$$

Electricity produced is simply a product between voltage and current.

$$W_{\text{el}} = E_{\text{cell}} \cdot I \tag{4.72}$$

where I is the current (A) and V is the cell voltage (V). Hydrogen consumed is directly proportional to current:

$$N_{H_2} = \frac{I}{nF} \tag{4.73}$$

$$W_{H_2} = \Delta H \frac{I}{nF} \tag{4.74}$$

where W_{H_2} is the energy value of hydrogen consumed (W) and ΔH is the hydrogen's higher heating value (286 kJ/mol).

By combining Equations (4.70) through (4.74), the fuel cell efficiency is simply directly proportional to cell potential:

$$\eta = \frac{V}{1.482} \tag{4.75}$$

where 1.482 is the thermoneutral potential corresponding to hydrogen's higher heating value. Sometimes, the efficiency is expressed in terms of the lower heating value (LHV):

$$\eta_{LHV} = \frac{V}{1.254} \tag{4.76}$$

If hydrogen is supplied to the cell in excess of that required for the reaction stoichiometry, this excess will leave the fuel cell unused. In case of pure hydrogen, this excess may be recirculated back into the stack so it does not change the fuel cell efficiency (not accounting for the power needed for hydrogen recirculation pump), but if hydrogen is not pure (such as in reformate gas feed) unused hydrogen leaves the fuel cell and does not participate in the electrochemical reaction. The fuel cell efficiency is then:

$$\eta = \frac{V}{1.482}\eta_{fu} = \frac{V}{1.482} \times \frac{1}{S} \tag{4.77}$$

where η_{fu} is fuel utilization and S is the stoichiometric ratio, *i.e.*, the ratio between the amount of hydrogen actually supplied to the fuel cell and that consumed in the electrochemical reaction.

$$S_{H_2} = \frac{\text{mole of } H_2 \text{ supplied}}{\text{mole of } H_2 \text{ consumed}} = \frac{\dot{N}_{H_2,\text{sup}}}{\dot{N}_{H_2,cons}} = \frac{\dot{N}_{H_2,\text{sup}}}{i/2F} \tag{4.78}$$

$$S_{O_2} = \frac{\text{mole of } O_2 \text{ supplied}}{\text{mole of } O_2 \text{ consumed}} = \frac{\dot{N}_{O_2,\text{sup}}}{\dot{N}_{O_2,cons}} = \frac{\dot{N}_{O_2,\text{sup}}}{i/4F} \tag{4.79}$$

4.3 Auxiliary units

To supply fuel for fuel processor and PEMFC, a pump and a compressor are used as auxiliary units. Therefore, the required power from a pump and a compressor is taken into account for calculating the system efficiency.

The power needed for compressor of air and pump from pressure P_1 to P_2 are shown in Eq.(4.80) and (4.81).

$$W_{\text{comp}} = \frac{\dot{m}_{\text{airin}} \cdot C_{\text{p}} \cdot T}{\eta_{\text{comp}}} \left[\left(\frac{P_2}{P_1} \right)^{\frac{k-1}{k}} - 1 \right] \tag{4.80}$$

$$W_{\text{pump}} = \frac{\dot{m}_{\text{liq}} \cdot (P_2 - P_1)}{\eta_{\text{pump}} \cdot \rho_{\text{liq}}} \tag{4.81}$$

where $\dot{m}$ is mass flow rate, C_p is specific heat, T is temperature before compression, k is ratio of specific heat (for diatomic gases k = 1.4), ρ is density and η is efficiency.

Furthermore, the heat management in the integrated systems is carried out by using a heat exchanger and a burner. The heat from product streams of the reformer and the anode and cathode off gases are recovered by using the heat exchanger. The amount of energy recovered from the heat exchanger is calculated from the enthalpy change between the inlet and outlet of hot and cold streams as follows:

The heat recovery from heat exchanger is calculated from enthalpy change between inlet and outlet of hot and cold stream as follows:

$$Q_{\text{hot}} = Q_{\text{cold}} \tag{4.82}$$

$$Q_{\text{hot}} = \sum M_{\text{in,hot}} H_{\text{in,hot}}(T) - \sum M_{\text{out,hot}} H_{\text{out,hot}}(T) \quad (4.83)$$

$$Q_{\text{cold}} = \sum M_{\text{in,cold}} H_{\text{in,cold}}(T) - \sum M_{\text{out,cold}} H_{\text{out,cold}}(T) \quad (4.84)$$

where M is molar flow rate and H is the enthalpy.

The total heat recovered from hot stream is not actual value because there are some heat losses occurring in heat exchanger. Therefore, the heat exchanger efficiency at 0.85 will be added to consider heat loss in the model.

To keep cell temperature at desired level, water is used as a cooling medium to remove the excess heat from PEMFC. The heat recovery from the release heat from the fuel cell can be calculated by Eq. (4.85).

$$Q_{\text{FC}} = m_{\text{a,in}} H_{\text{a,in}} + m_{\text{c,in}} H_{\text{c,in}} - m_{\text{a,out}} H_{\text{a,out}} - m_{\text{c,out}} H_{\text{c,out}} - P_{\text{FC}} \quad (4.85)$$

For the LT-PEMFC system, a humidifier is needed to produce a humidified air for the cathode and the amount of heat required for this unit is determined by:

$$Q_{\text{hum}} = m_{\text{air,out}} H_{\text{air,out}} - m_{\text{air,in}} H_{\text{air,in}} - m_{\text{H}_2\text{O,in}} H_{\text{H}_2\text{O,in}} \quad (4.86)$$

4.4 System efficiency

Considering the heat integration of PEMFC and reforming processes in this study, the required energy for the reforming process is partially supplied by the heat recovered from the anode and cathode off gases. The system efficiency is calculated by Eq. (4.87).

$$\eta_{\text{sys}} = \frac{P_{\text{FC}} - P_{\text{parasitic}}}{\dot{m}_{\text{glycerol}} \cdot LHV_{\text{glycerol}} + Q_{\text{ref}} - Q_{\text{rec}}} \quad (4.87)$$

where $\dot{m}_{\text{glycerol}}$ is the molar flow rate of glycerol used for producing hydrogen. LHV_{glycerol} is the lower heating value of glycerol. Q_{ref} is the energy required for the steam reforming process accounting for the heat of vaporization, specific heat to heat

up the reactants to the desired temperature and the heat needed for maintaining the reformer at an isothermal operation level. Q_{rec} is the recovered heat from the anode and cathode off gases as well as from the high temperature product gas of the glycerol reformer. $P_{\text{parasitic}}$ is the required power used in auxiliary units, namely compressor and pump. When the heat integration is not considered, the recovered heat (Q_{rec}) accounts for only the heat that recovered from the high temperature product gas of the reformer.

For the power and heat cogeneration of the PEMFC system, both the electrical and thermal output are included in the calculation of the cogeneration system efficiency, as defined by Eq. (4.88). The thermal output is the heat released from the fuel cell, which is used for a boiler heating system.

$$\eta_{\text{sys,co}} = \frac{P_{\text{FC}} - P_{\text{parasitic}} + Q_{\text{thermal}}}{\dot{m}_{\text{glycerol}} \cdot LHV_{\text{glycerol}} + Q_{\text{ref}} - Q_{\text{rec}}} \tag{4.88}$$

CHAPTER V

GLYCEROL: AN ALTERNATIVE FUEL

FOR HYDROGEN PRODUCTION

5.1 Introduction

Increasing energy demand and environmental awareness stimulate a number of researchers to explore alternative fuels which are environmental friendly and readily available. Biodiesel is a promising alternative fuel because it can be produced from renewable resources such as vegetable oils or fats. While the production of biodiesel increases, glycerol as a major by-product is also highly generated about 10%wt (Silva et al., 2009). Generally, crude glycerol always contains impurities and thus this make crude glycerol from biodiesel production process be low price. Its composition depends on type of feedstock and biodiesel production process as well as separation process of biodiesel and glycerol. Figure 5.1 represents price of pure and crude glycerol at Europe. We can see that selling price of both pure and crude glycerol tend to diminish. Therefore, many works attempt to find useful application of glycerol and find the methods that transform glycerol to new valuable product. In addition, the growing up of biodiesel production for many years ago cause quantity of crude glycerol increase over marketing demand (Fernand et al., 2007). The utilization of glycerol not only reduces waste but also decreases cost of biodiesel production process. Crude glycerol from biodiesel production process can be used in several ways and we can classified in main two approach, namely purification of crude glycerol before using in any application and direct use of crude glycerol to produce a valuable product such as hydrogen, ethanol, 1,3-Propandiol and Docosahexenoic acid (DHA).

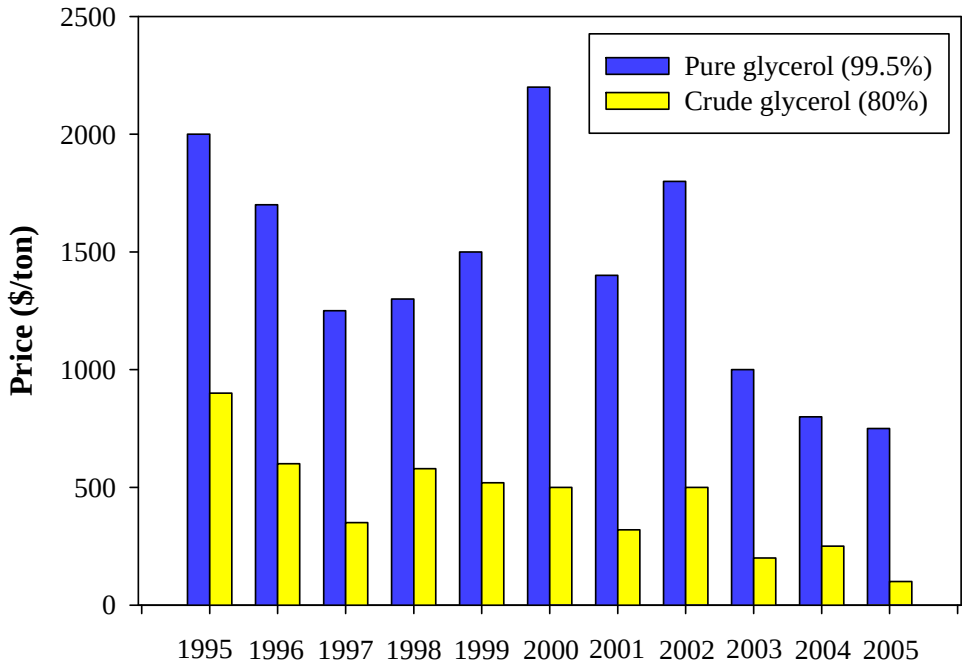

Figure 5.1 Cost of pure and crude glycerol at Europe (Singhabhandhu and Tezuka, 2010).

Currently, most hydrogen is produced from reforming processes of natural gas and the ratio of hydrogen production around the world from each reactant is shown in Figure 5.2. Although natural gas is a cost-effective feedstock, it is also a limited and nonrenewable resource (Halabi et al., 2008; Levent et al., 2003). It is necessary to find new feedstock for producing hydrogen. In the long term, renewable energy sources such as biomass, biodiesel and bio-ethanol will become the most important source for the production of hydrogen because it consumes CO_2 in life cycle making it environmentally friendly and has ability to produce hydrogen as same as natural gas (Douvartzides et al., 2004; Vagia et al, 2007) . Therefore, the use of glycerol from biodiesel as raw material for hydrogen production process is a potential method not only to exploit waste from biodiesel production process but also to develop hydrogen production from renewable source (Dauenhauer et al., 2006; Hirai et al., 2005; Slinn et al., 2008; Valliyappan et al., 2008). In this study, glycerol as a representative of renewable resource is compared with methane in order to find differences and advantages of each fuel in term of carbon formation boundary, amount of consumed

fuel and product distribution. The steam reforming process is chosen as hydrogen production process and a thermodynamic analysis is performed by using HYSYS simulator.

5.2 Glycerol property

Glycerol or glycerin ($C_3H_8O_3$) is polyhydric alcohol which has three hydroxyl groups in its molecule. In addition, it is non-toxic liquid substance that has high viscosity and high solubility in water and alcohol as well as sweet taste but it is insolubility in hydrocarbon. The outer carbon atom of glycerol is higher reactivity than the center carbon atom in neutral and base condition. At room temperature, glycerol can immediately adsorb water and easily oxidize (Othmer, 1997). The physical property of glycerol is also presented in Table 5.1. Furthermore, glycerol is a famous material that is used in many industries such as cosmetic, pharmaceutical, chemical and food. Glycerol can be produced from many processes such as propene production process, soup process, sugar fermentation process and biodiesel production process etc.

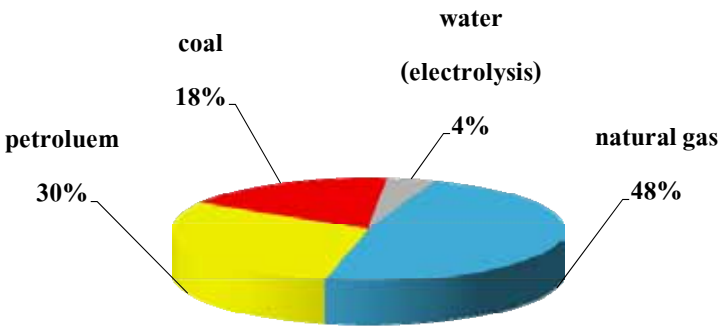

Figure 5.2 Ratio of worldwide hydrogen production from different resources (Yang and Pitchumani, 2006).

Table 5.1 Physical property of glycerol (Barbara et al., 1994)

Property	Value
Molecular weight	92.09
Melting point	18 °C
Boiling point (101.3 kPa)	290 °C
Density (20 °C)	1.261 g/cm^3
Dynamic viscosity (20 °C)	1.410
Surface tension (20 °C)	63.4 mN/m
Heat of formation	669 kJ/mol
Heat of combustion	1662 kJ/mol
Heat of vaporization (55 °C)	88.2 kJ/mol
Heat of vaporization (195 °C)	76.1 kJ/mol
Heat of fusion (18 °C)	18.3 kJ/mol
Heat of solution (infinite dilution)	5.8 kJ/mol
Heat capacity (26 °C)	2.41 kJ/ kg·K
Thermal conductivity (0 °C)	0.29 W/m·K
Diffusion coefficient of water into glycerol (20 °C)	1.336 x 10^{-11} m^2/s
Specific electrical conductivity (20 °C)	0.1 μs /cm
Relative dielectric constant (25 °C)	42.48
Flash point	177 °C
Fire point	204 °C
Autoignition temperature	429 °C

Glycerol obtaining from transesterification of vegetable oil or waste cooking oil always contains impurities. It is brown color, high pH and low density and viscosity. The purity of glycerol depends on type of feedstock and biodiesel production process as well as separation process of biodiesel and glycerol. Apart from glycerol, crude glycerol consists of unreacted methanol, fatty acid, catalyst, and water as well as some trace of vitamin and pigment that contain in vegetable oil. It should be noted that methanol and water containing in crude glycerol can be used as reactant in hydrogen production process. Table 5.2 shows composition of glycerol that containing in crude glycerol from several oils used as reactant in transesterification process. Furthermore, the different production and separation processes of biodiesel also make crude glycerol have different compositions of impurities.

Table 5.2 Composition of glycerol and other components in crude glycerol from different types of oil (Thompson et al., 2006)

Type of oil	Glycerol (%wt)
IdaGold	62.9
PacGold	62.9
Rapeseed	65.7
Canola	67.8
Soy	67.8
Crambe	62.5
Waste vegetable oil	76.6

5.3 Application of crude glycerol

Crude glycerol from biodiesel production process can be used in several ways and we can classified in main two approach, namely purification of crude glycerol before using in any application and direct use of crude glycerol without removal of other impurities. For purification of crude glycerol, the several units need to be added in glycerol purification process and the sophistication of glycerol purification process depends on %purity of glycerol. If high purity is required, glycerol purification process is highly complicated. The purified glycerol can be utilized as reactant in cosmetic, pharmaceutical, chemical and food industries. The general purification process of glycerol has procedure as follows:

- Neutralization unit: crude glycerol will be added with acid to eliminate base catalyst (NaOH or KOH) from biodiesel production process.
- Evaporation unit: unreacted methanol will be evaporated in this unit.
- Distillation unit: glycerol will be distillated from other components

However, sophistication of glycerol purification process depends on %purity of glycerol. If high purity is required, glycerol purification process is highly complicated. The sophistication of glycerol purification process also indicates operating cost of system. Some work concluded that glycerol purification process has high operating cost and uneconomic (Yoon et al., 2010). At the same time, some of researchers have continuously studied about this process (Hajek et al., 2010). On the other hand, many works have continuously found out the application of crude glycerol as shown in Figure2. The investigated approach of directly converting crude glycerol to be high value product is described as follows:

- 1,3-Propandiol : To produce 1,3-Propandiol, crude glycerol is supplied for fermentation process by using bacteria. 1,3-Propandiol can be utilized as monomer in production of polyester such as polytrimethylene terephthalate (PTT) and polyethylene terephthalate (PET).

- Docosahexenoic acid (DHA): DHA is unsaturated fatty acid which is several benefit for human in term of anti-cancer and anti-cardiovascular. Crude glycerol is used as food for algae for producing DHA.

- Ethanol: Crude glycerol is fermented by using enzyme as catalyst to produce ethanol. It can be used in various applications such as beverage industry, fuel cell and gasohol etc.

- Hydrogen: Hydrogen production from crude glycerol was studied in many ways that are reforming process, gasification and fermentation. Hydrogen obtaining will be supplied in chemical industry and fuel cell application.

Using glycerol from biodiesel as raw material for hydrogen production process is one of the attractive application of crude glycerol and it is the way to support hydrogen production from renewable resource. Several reports were presented on the production of hydrogen from glycerol using thermal-chemical processes e.g. steam reforming, autothermal reforming, partial oxidation, supercritical water reforming and aqueous-phase reforming. Further, the reaction pathway to produce hydrogen is shown in Figure 5.3.

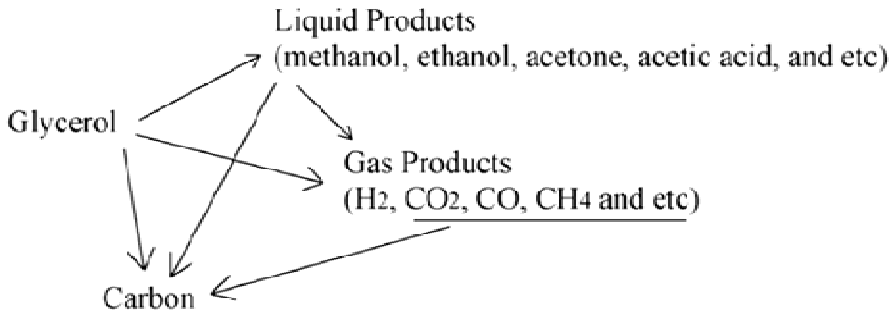

Figure 5.3 Possible reaction pathways of glycerol reforming to hydrogen (Luo et al., 2011).

5.4 Description of hydrogen production process

The hydrogen production process considered in this research is steam reforming process and the heat requirement for the system are heat to vaporize and preheat reactant, and heat to maintain reactor at reaction temperature. The illustration of steam reforming process is shown in Figure 5.4.

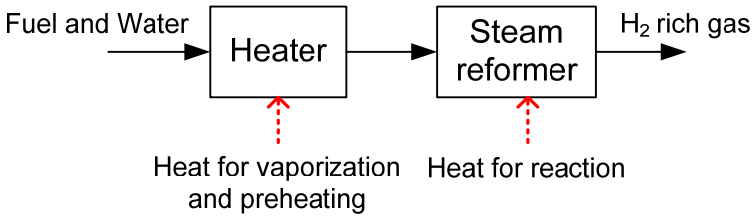

Figure 5.4 The illustration of steam reforming process.

In the case of using glycerol and methane for hydrogen production, the overall steam reforming reactions is represented by Eq. (5.1) and Eq. (5.2), respectively. For a water gas shift (WGS) unit, the reaction occurred is given in Eq. (5.3).

$$C_3H_8O_3 + 3H_2O \leftrightarrow 3CO_2 + 7H_2 \quad (5.1)$$

$$CH_4 + 2H_2O \leftrightarrow 3H_2 + CO_2 \quad (5.2)$$

$$CO + H_2O \leftrightarrow CO_2 + H_2 \quad (5.3)$$

$$CO + 3H_2 \leftrightarrow CH_4 + H_2O \quad (5.4)$$

$$2CO \leftrightarrow CO_2 + C \quad (5.5)$$

$$CH_4 \leftrightarrow 2H_2 + C \quad (5.6)$$

$$CO + H_2 \leftrightarrow H_2O + C \quad (5.7)$$

The possible side reactions of the steam reforming are water gas shift (Eq. (5.3)), methanation reactions (Eq. (5.4)) and carbon formation (Eqs. (5.5)-(5.7)), and thus the gaseous components appeared in the steam reforming system are $C_3H_8O_3$,

CH_4, H_2, CO, CO_2, C and H_2O. The equilibrium composition of the reformate gas obtained from the steam reforming of glycerol is calculated from the direct minimization of Gibbs free energy as given below:

$$\min_{n_i} (G^t)_{T,P} = \sum_{i=1}^{C} n_i \overline{G}_i = \sum_{i=1}^{C} n_i \left(G_i^{\circ} + RT \ln \frac{\overline{f}_i}{f_i^{\circ}} \right) \tag{5.8}$$

where C is the total number of components in the reaction system, n_i is a amount of each gaseous component. Resulting from the conservation of atomic species, n_i have to satisfy the following relation:

$$\sum_{i=1}^{C} a_{ji} n_i = b_j, \quad \text{for } 1 \le j \le M \tag{5.9}$$

where a_{ji} is the number of atoms of element j in component i, b_j is the total number of atoms of element j in the reaction mixture, and M is the total number of elements.The detail of this method is provided in Chapter IV.

The prediction results were compared with the experiment data reported by Profeti et al. (Profeti et al., 2009).It was observed from Figure 5.5 that the product distribution obtained from the HYSYS simulator and the experimental data were in agreement.

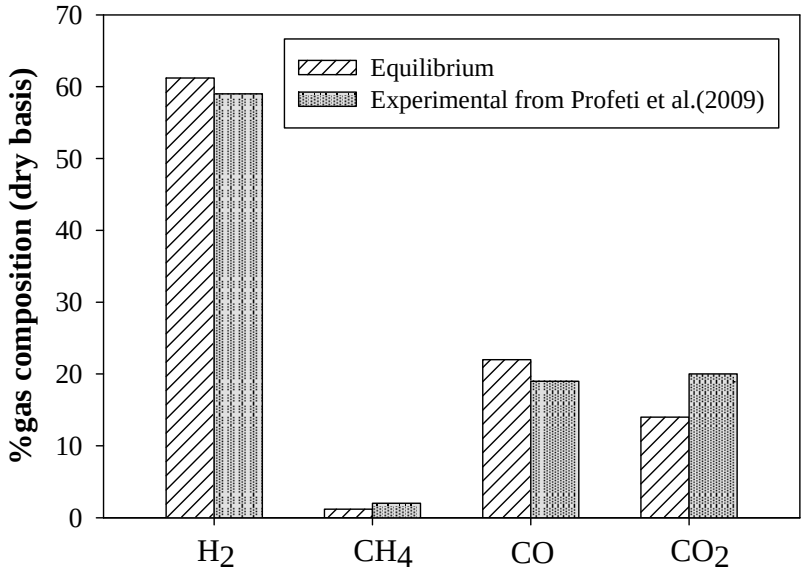

Figure 5.5 Validation of glycerol steam reforming process (steam to crude glycerol ratio = 3 and T = 950 K).

5.5 Results and discussion

In this study, glycerol is used as a green and renewable fuel for hydrogen production via a steam reforming process. This work will compare between methane and glycerol in order to explore difference and advantage of each fuel in term of carbon formation, amount of consumed fuel and product distribution. Carbon formation is a significant problem in a reforming process and thus many studies have proposed various methods to prevent the formation of carbon during the reforming process, including variations in the operating conditions, the development of new catalysts resisting on carbon, and the addition of oxygen and other promoters to inhibit carbon formation (Pedernera et al., 2007; Parmar et al., 2009; Laosiripojana et al., 2005; Medrano et a., 2008; Parizotto et al., 2007). The simple method to avoid carbon formation is the selection of suitable operating condition, e.g. temperature and steam to carbon (S/C) ratio feed ratio. For glycerol, oxygen containing in its molecule cause possibility of carbon formation lower than hydrocarbon without oxygen in molecule (Slinn et al., 2008). Figure 5.6 shows the boundary of carbon formation

when glycerol and methane are reformed to hydrogen. The region above the boundary line is the area where the formation of carbon is possible. The results show that at a lower reforming temperature, glycerol requires more steam than methane to inhibit the formation of carbon; however, the opposite trend is observed when the steam reformer is operated under high temperatures (T_R > 730 K).

Next, the performance of the steam reformer for hydrogen production from glycerol is evaluated and compared with methane. Figure 5.7 shows that at the same hydrogen production rate, the amount of glycerol fed to the steam reformer is lower than that of methane. This can be explained by a higher hydrogen atom in the glycerol molecule. When the steam reformer is operated at a higher temperature, an amount of glycerol or methane fed to the reformer is less required. For the glycerol steam reforming, the optimal operating temperature (providing maximum hydrogen content) is 950 K, whereas it is 1000 K for the methane steam reforming. It is also found that the amount of CO produced from the glycerol reforming is higher than that from methane, especially at high temperatures. However, under the optimal operating temperature, the content of CO produced from the steam reforming of glycerol and methane is approximately the same. In general, CO has a direct impact on the activity of Pt catalyst in PEMFC. For a low-temperature PEMFC operated at a temperature range of 60-80 ^{o}C, a purification unit such as a preferential oxidation process, is further needed to remove CO from the reformate gas. If the reformate gas has a higher fraction of CO, the loss of hydrogen through the oxidation reaction of hydrogen in the preferential oxidation process may be occurred. Therefore, the CO content has an indirect effect on the amount of hydrogen containing in the reformate gas.

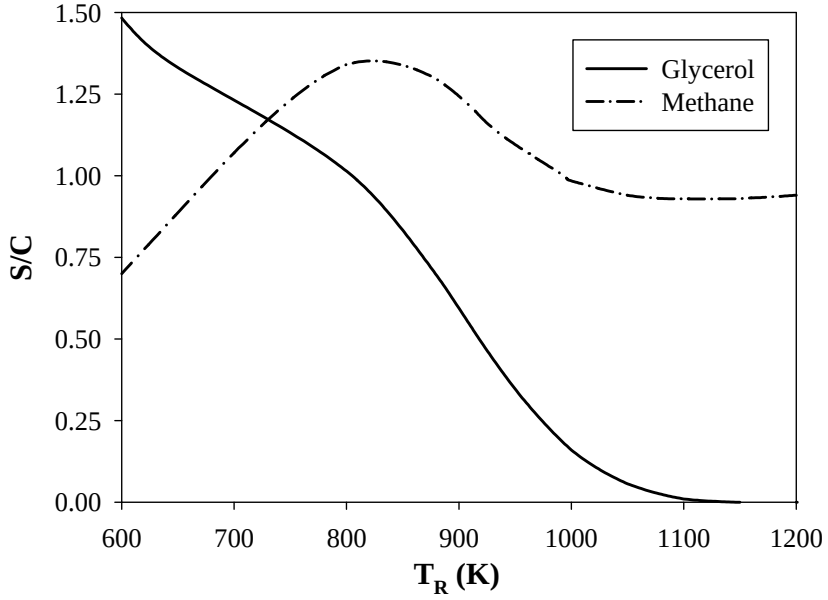

Figure 5.6 Carbon formation boundaries of glycerol and methane.

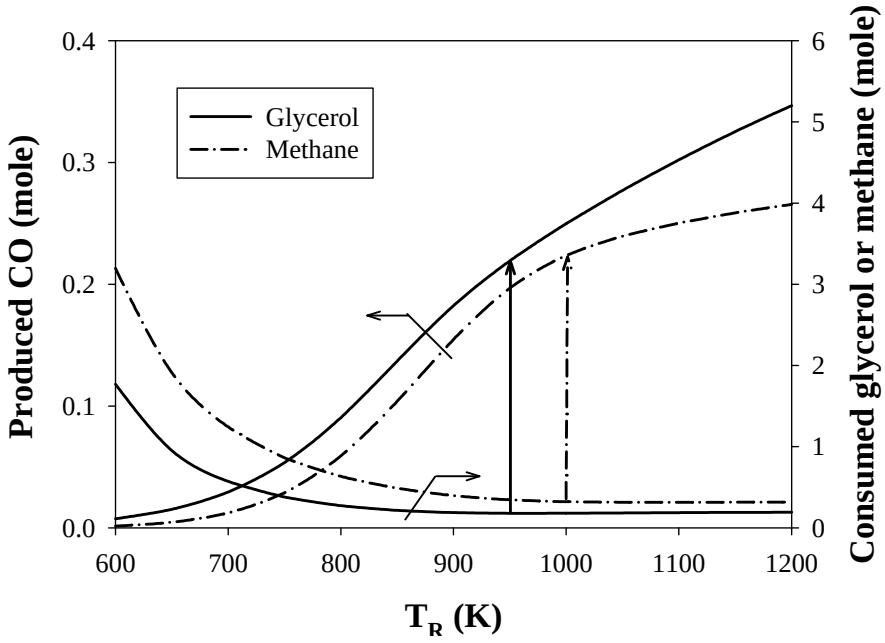

Figure 5.7 Fuel consumption and CO generation for 1 mole H_2 production (S/C = 2).

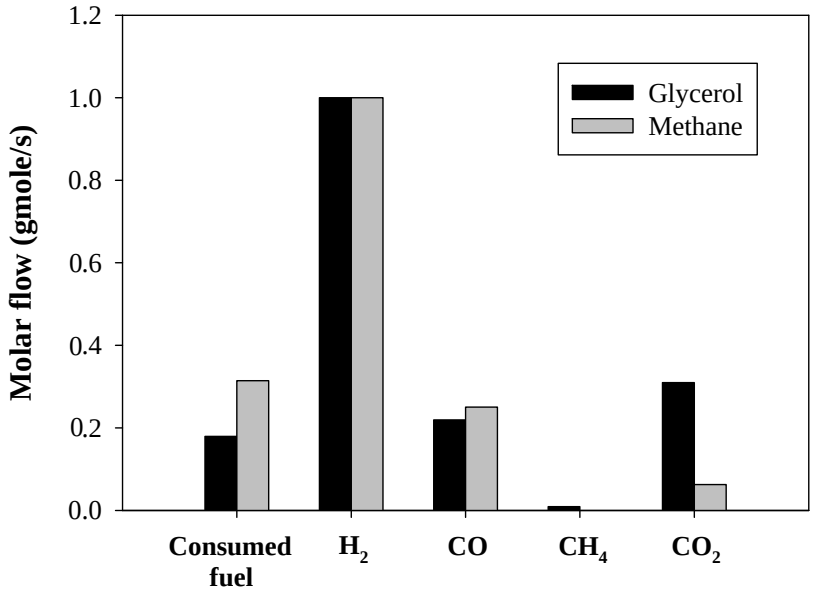

Figure 5.8 Product distribution of glycerol and methane steam reforming at optimal conditions.

Figure 5.8 shows the comparison of glycerol and methane steam reforming processes in terms of the product distribution and the fuel consumption when the steam reformer is operated at the steam-to-carbon ration of 2 and optimal operating temperature. The result indicates that the consumption of glycerol is less than that of methane at the same level of hydrogen production. It is noted that the amount of CO_2 generated should also be taken into consideration because it decreases the fraction of hydrogen in the reformate gas.

Table 5.3 Total net energy of glycerol and methane reforming process

	Glycerol	Methane
Condition		
T_R (K)	950	1000
S/C	2	2
Energy (kW)		
Latent heat		
- Glycerol	15.37	-
- Water	43.86	25.65
Sensible heat	118.48	64.32
Required heat for reformer	35.70	68.56
Total heat requirement	213.41	158.53

The total energy requirement for operation of the steam reformer running on glycerol and methane is investigated and the results are shown in Table 5.3. The energy required for the steam reforming process accounts for the heat of vaporization, the sensible heat to heat up reactants to the desired temperature and the heat needed for maintaining the reformer at an isothermal operation. It is observed that the glycerol processor requires a higher external energy for hydrogen production. The main energy consumption of glycerol reformer is heat to vaporize and preheat reactant.

From the simulation results mentioned above, glycerol shows the potential of fuel for hydrogen production in terms of low possibility to carbon formation and high hydrogen yield as well as it is the renewable resource. Consequently, it becomes the competitive fuel when compared with methane. In addition, the use of glycerol to produce a high-value added product could reduce a biodiesel production cost.

5.6 Conclusions

In this study, glycerol as a representative of renewable resource is compared with methane in term of carbon formation boundary, amount of consumed fuel, product distribution and energy requirement. Because a glycerol molecule have high oxygen atom, the possibility to carbon formation from the steam reforming of glycerol is less than that of methane. The consumption of glycerol to produce hydrogen is lower than methane at the same hydrogen production rate. When comparing with methane, the reforming of glycerol generates more CO_2 that will decrease the fraction of hydrogen in the reformate gas and requires a higher energy to vaporize and preheat reactants.

CHAPTER VI

GLYCEROL REFORMING PROCESS

6.1 Introduction

As mentioned earlier, biodiesel is a promising alternative fuel because it can be produced from renewable resources such as vegetable oils or fats. While the production of biodiesel increases, glycerol as a major by-product is also highly generated. Generally, crude glycerol always contains impurities and its composition depends on type of feedstock and biodiesel production process as well as separation process of biodiesel and glycerol. This makes crude glycerol from biodiesel production process be low price and the purification process of crude glycerol requires high operating cost and is uneconomic. Valliyappan et al. (2008) reported that crude glycerol consists of mostly glycerol (60 wt.%) and methanol (31 wt.%) and slightly water and KOH. At present, a number of researches have been being explored to find useful applications for glycerol, especially in cosmetic, pharmaceutical, and food industries. Producing hydrogen from glycerol is also a promising alternative option (Adhikari et al., 2009; Byrd et al., 2008; Chen et al., 2009; Dou at al., 2009). Alternatively, the use of glycerol from biodiesel production process as raw material for hydrogen production is an attractive approach (Dauenhauer et al., 2006; Hirai et al., 2005; Slinn et al., 2006; Valliyappan et al., 2009).

There are several thermochemical methods to produce hydrogen from gas and liquid hydrocarbon such as steam reforming, partial oxidation, autothermal reforming, dry reforming and aqueous phase reforming as well as supercritical water reforming. For a low-temperature aqueous phase reforming (Luo et al., 2007; Luo et al., 2007; Wen et al., 2008), the disadvantage of such a process is a drastic decrease of hydrogen content because methanation reaction favors at low temperatures. Thus, catalysts with high selectivity of hydrogen production should be further developed. On the other hand, steam reforming shows the highest hydrogen production whereas partial

oxidation and autothermal reforming is advantageous process to reduce energy input. However, the required heat input due to endothermic reactions is considered as a major drawback of steam reforming. Ahmed and Krumpelt (2001) explained that steam reforming is well suited for long periods of steady state operation while partial oxidation and autothermal reforming processes are more attractive for the rapid start and dynamic response needed in automotive applications. Rabenstein and Hacker (2008) concluded that coke formation is limited when temperature, steam to ethanol ratio and oxygen to ethanol ratio increase. The coke is formed during ethanol reforming in the following order: partial oxidation > steam reforming > autothermal reforming. In addition, they discussed that steam reforming is the least energy demand process. The total energy demand is of the order partial oxidation > autothermal reforming > steam reforming. All of the literature review shows that autothermal and steam reforming are desirable process for fuel cell, so both reforming processes should be studied in detail for hydrogen production from glycerol. Furthermore, while many researchers have been focused on pure glycerol reforming process (Swami, and Abraham, 2006; Wang et al., 2009; Adhikari et al., 2007; Iriondo et al., 2008), the detailed analysis of the synthesis of hydrogen from crude glycerol is limited. Since crude glycerol contains unreacted methanol from biodiesel production process, an understanding of the characteristics of crude glycerol reforming process is necessary.

Therefore, in this study, a thermodynamic analysis of autothermal and steam reforming of both pure and crude glycerol is investigated as a basic tool of process development for hydrogen production from a renewable resource. The direct minimization of the Gibbs free energy is used to compute the equilibrium composition of synthesis gas. Effects of operating condition, i.e., temperature, steam to crude glycerol ratio, and oxygen to crude glycerol ratio is investigated. Also, effects of operating condition on the reforming of crude glycerol at various methanol to glycerol ratios are reported. In addition, optimal conditions for crude glycerol autothermal steam reforming that maximize hydrogen production at no external energy input are studied and the results are compared with the use of pure glycerol. Finally, the glycerol steam reforming and glycerol autothermal reforming process are compared.

6.2 Methodology

The thermodynamic analysis of pure and crude glycerol reforming process was performed by using commercial software HYSYS to study the effect of key operating parameters such as reformer temperature, steam to glycerol ratio and oxygen to glycerol ratio on hydrogen production under the atmospheric pressure. These parameters are defined as follows:

$$\text{Steam to glycerol ratio} = \frac{\text{molar flow rate of steam}}{\text{molar flow rate of glycerol}} \tag{6.1}$$

$$\text{Oxygen to glycerol ratio} = \frac{\text{molar flow rate of oxygen}}{\text{molar flow rate of glycerol}} \tag{6.2}$$

In general, crude glycerol obtained from the production of biodiesel constitutes various kinds of impurities such as methanol, soap, catalyst, and organic matter, depending on raw materials and process technologies applied. However, the main compositions of crude glycerol are glycerol and methanol (Valliyappan et al., 2008), which were considered in this study as a fuel for hydrogen production. Therefore, the fraction of glycerol in crude glycerol was varied to investigate its effect on hydrogen production. The standard conditions of the steam and autothermal reforming and their operational ranges examined in this study are shown in Table 6.1.

Table 6.1 Operating conditions for reforming of glycerol

Parameters	Standard condition	Operational range
Reformer temperature (K)	1000	600-1200
Pressure (atm)	1	-
Steam to glycerol ratio	3	1-9
Oxygen to glycerol ratio	0.6	0.1-0.8
% glycerol in crude glycerol	100	40-100

Table 6.2 Possible reactions of glycerol reforming process

Possible reaction	Steam reforming		Autothermal reforming	
	pure glycerol	crude glycerol	pure glycerol	crude glycerol
$C_3H_8O_3 + 3H_2O \leftrightarrow 7H_2 + 3CO_2$ (1)	/	/	/	/
$CH_3OH + H_2O \leftrightarrow 3H_2 + CO_2$ (2)	-	/	-	/
$C_3H_8O_3 + \frac{3}{2}O_2 \leftrightarrow 3CO_2 + 4H_2$ (3)	-	-	/	/
$CH_3OH + \frac{1}{2}O_2 \leftrightarrow CO_2 + 2H_2$ (4)	-	-	-	/
$CO + H_2O \leftrightarrow CO_2 + H_2$ (5)	/	/	/	/
$CO + 3H_2 \leftrightarrow CH_4 + H_2O$ (6)	/	/	/	/
$CO_2 + CH_4 \leftrightarrow 2H_2 + 2CO$ (7)	/	/	/	/

The equilibrium compositions of synthesis gas obtained from the reformer were determined by solving the minimization problem of the Gibbs free energy. The equation of state used in the calculation was based on the Peng-Robinson Stryjek-Vera (PRSV) method. From the set of the reactions, the components involved the steam reforming system are $C_3H_8O_3$, H_2O, CO, CO_2, H_2, CH_4, and CH_3OH (in case of crude glycerol). For autothermal reforming system, O_2 will be added to set of component. During reaction proceeding, the total Gibbs free energy decreases and the equilibrium condition is reached when the total Gibbs free energy (G^t) attains its minimum value. Therefore, the equilibrium composition can be determined by solving the minimization problem as follows:

$$\min_{n_i}\left(G^t\right)_{T,P} = \min_{n_i}(\sum_{i=1}^{C} n_i \bar{G}_i) = \min_{n_i}\left[\sum_{i=1}^{C} n_i \left(G_i^\circ + RT\ln\frac{\bar{f}_i}{f_i^\circ}\right)\right] \tag{6.3}$$

where G_i° is the Gibb free energy of species at standard condition, C is the total number of components in the reaction system, n_i is an amount of each gaseous component. According to the conservation of atomic species, n_i have to satisfy the following relation:

$$\sum_{i=1}^{C} a_{ji} n_i = b_j, \quad \text{for } 1 \le j \le M \tag{6.4}$$

where a_{ji} is the number of atoms of element j in component i, b_j is the total number of atoms of element j in the reaction mixture and M is the total number of elements.

The possible reaction which can occur in glycerol steam and autothermal reforming are shown in Table 6.2. These compose of steam reforming (Eq. (1)-(2)) and oxidation (Eq. (3)-(4)) as major reactions, and water gas shift (Eq. (5)), methanation (Eq. (6)), dry reforming (Eq. (7)) as side reactions. It is noted that in this study, the products of glycerol reforming are predicted based on a thermodynamic analysis without considering the effects of catalyst used. There are a number of researches concerning about the synthesis and study of catalysts for glycerol reforming (Adhikari et al., 2007; Iriondo et al., 2008; Zhang et al., 2007). In this work, the system of reforming process is represented in Figure 6.1. The heat requirement for the system is heat of vaporization, heat for preheating, heat to maintain reformer whereas some heat can be recovered from hat reformate gas before being fed to water gas shift reactor. The total energy used is calculated from Eq. (6.5).

$$\text{Total energy}\,(\mathrm{E}_{\text{total}}) = \mathrm{E}_{\text{preheating}} + \mathrm{E}_{\text{reforming}} - \mathrm{E}_{\text{cooling}} \tag{6.5}$$

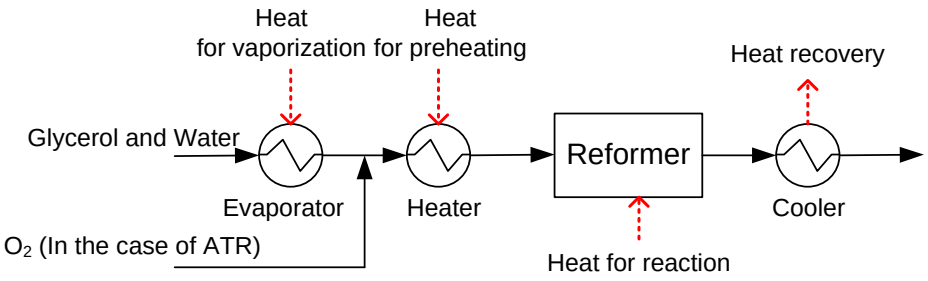

Figure 6.1 The heat requirement for the reforming system.

6.3 Results and discussion

The effect of operating parameter on product composition of pure glycerol steam reforming and autothermal reforming is presented in this work. In addition, the fraction of glycerol in crude glycerol was varied to investigate its effect on hydrogen production and the results were also compared with the use of pure glycerol. Depending on types of feedstock and technologies, the mole fraction of glycerol in crude glycerol is varied in range of 40-80% (Onwudili et al., 2010; Dou et al., 2009; Hazimah et al., 2003) to investigate its impact on hydrogen production. The prediction results were compared with the experiment data reported by Profeti et al. (Profeti et al., 2009) and the product distribution obtained from the HYSYS simulator and the experimental data were in agreement.

6.3.1 Glycerol steam reforming

In this section, the performance of a steam reforming of glycerol for hydrogen production is thermodynamically analyzed under atmospheric pressure. A mixture of glycerol and methanol, major components in crude glycerol, at different ratios was used to investigate its effect on the steam reforming process.

6.3.1.1 Effect of temperature and steam to glycerol ratio

Figure 6.2 shows the effect of operating temperature on the product composition. It is found that increasing the reforming temperature increases the molar flow of H_2 and CO but decreases CH_4 and CO_2. An increase in CO is because the reverse reaction of water gas shift is favored while the methanation is unfavored at

high temperatures. These effects result in the reduction of CO_2 and CH_4. It is noted that the conversion of glycerol is completed at all operating temperatures. The effect of the molar ratio of steam to glycerol on the production of hydrogen is also shown in Figure 6.2. Increasing the amount of steam in the feed stream can shift the chemical equilibrium toward the product side and causes an increase in the molar flow of hydrogen produced. However, the change in CO and CH_4 shows a decrease trend when feed steam is increased since more steam promotes the water gas shift and suppresses the methanation. It is noted that although the operation of the steam reformer at high steam to glycerol ratio maximizes H_2 yield and minimizes CO content, a large amount of the unreacted steam can dilute the concentration of H_2 in the product stream.

(a)

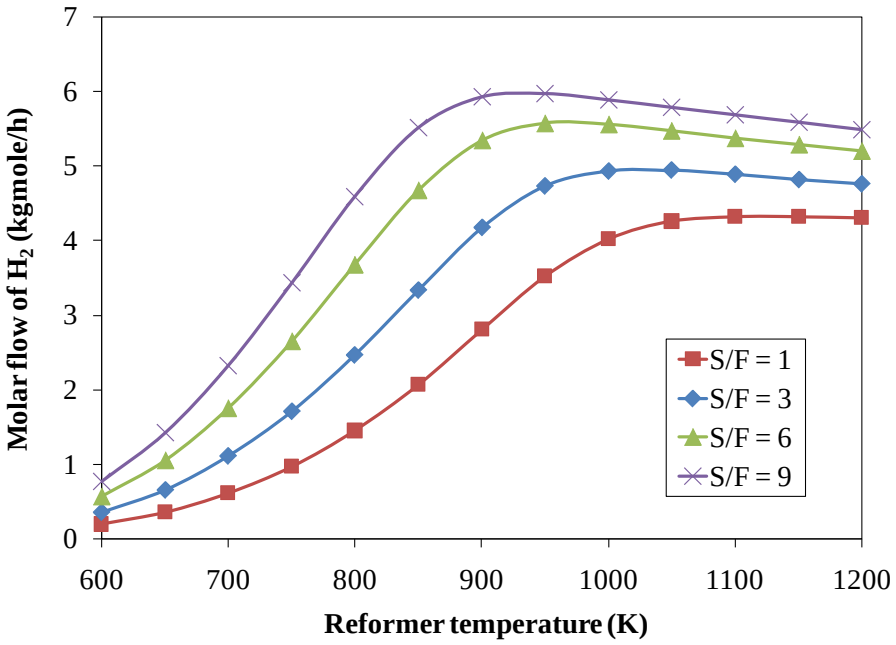

(b)

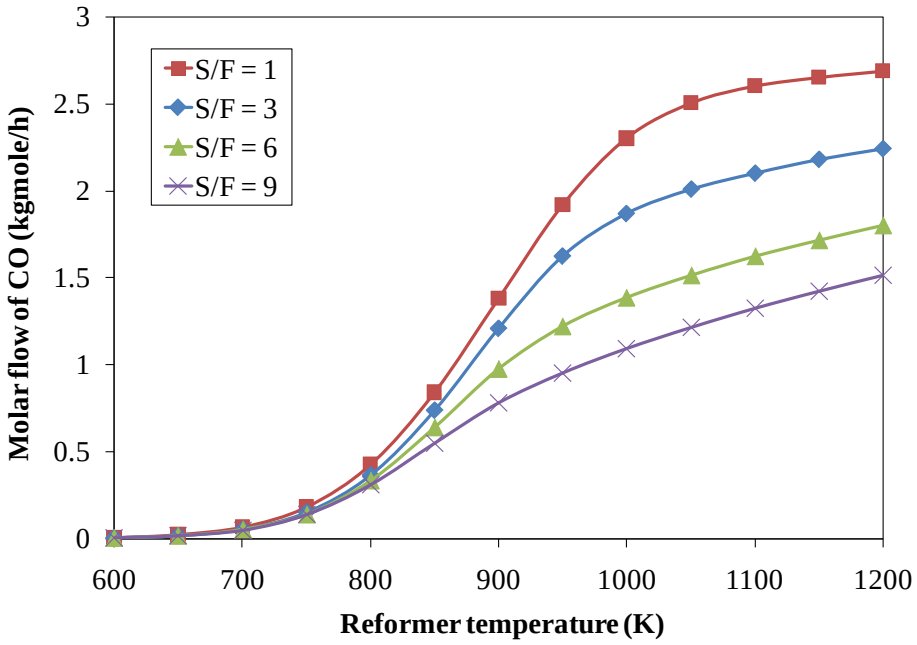
Molar flow of CO (kgmole/h)
Reformer temperature (K)
S/F = 1
S/F = 3
S/F = 6
S/F = 9
0
0.5
1
1.5
2
2.5
3
600
700
800
900
1000
1100
1200

(c)

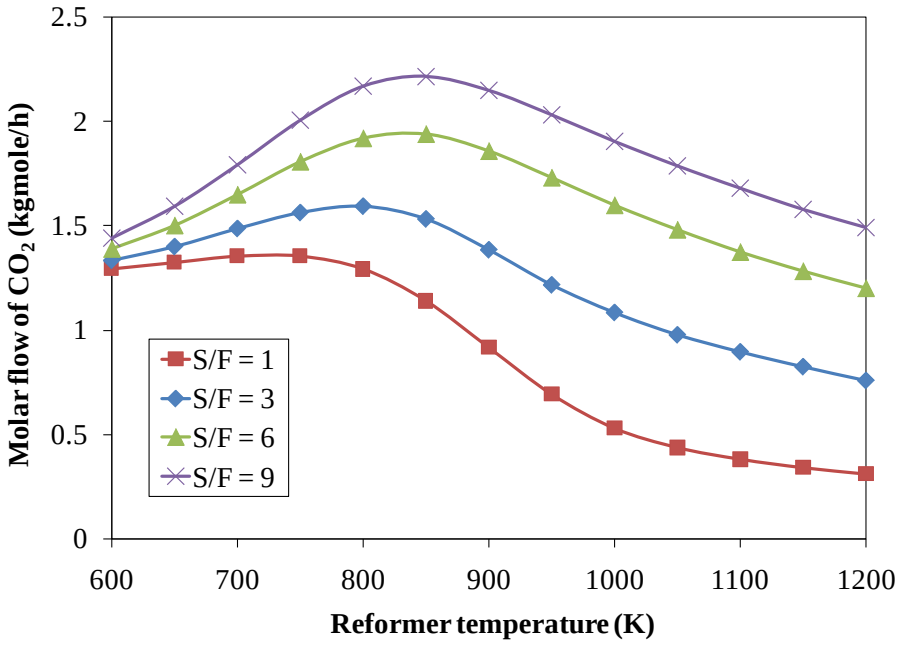
Molar flow of CO_2 (kgmole/h)
Reformer temperature (K)
S/F = 1
S/F = 3
S/F = 6
S/F = 9
0
0.5
1
1.5
2
2.5
600
700
800
900
1000
1100
1200

(d)

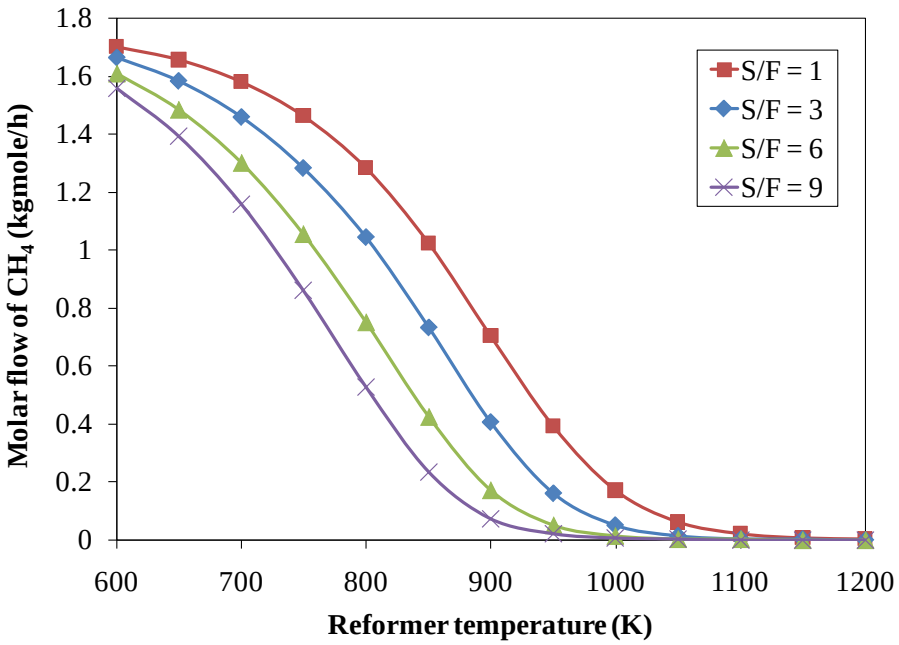

Figure 6.2 Product distribution of pure glycerol reforming: (a) H_2, (b) CO, (c) CO_2 and (d) CH_4.

6.3.1.2 Effect of methanol contaminating in crude glycerol

This section is intended to explore the effect of methanol contaminating in crude glycerol for steam reforming process. The fraction of glycerol in crude glycerol considered here is varied from 40 to 100% when the crude glycerol consists of only glycerol and methanol. The results from Figure 6.3(a) show that the amount of CO, CO_2 and H_2 increases with increasing the fraction of glycerol in crude glycerol. This is because the more H_2 and CO can be produced from glycerol steam reforming than methanol steam reforming (see Eq. (1)-(2)). At the same time, the higher remaining water is observed at lower glycerol content in crude glycerol because the methanol required water to produce H_2 lower than glycerol. However, it should be noted that the hydrogen fraction and CO_2 fraction (dry basis) decline but CO fraction increases with respect to the fraction of glycerol in crude glycerol (see Figure 6.3(b)).

(a)

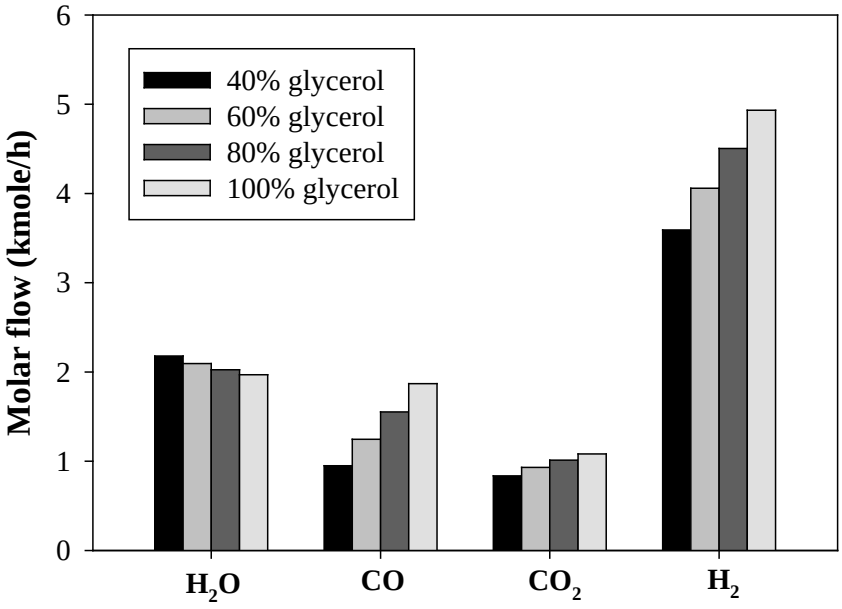

(b)

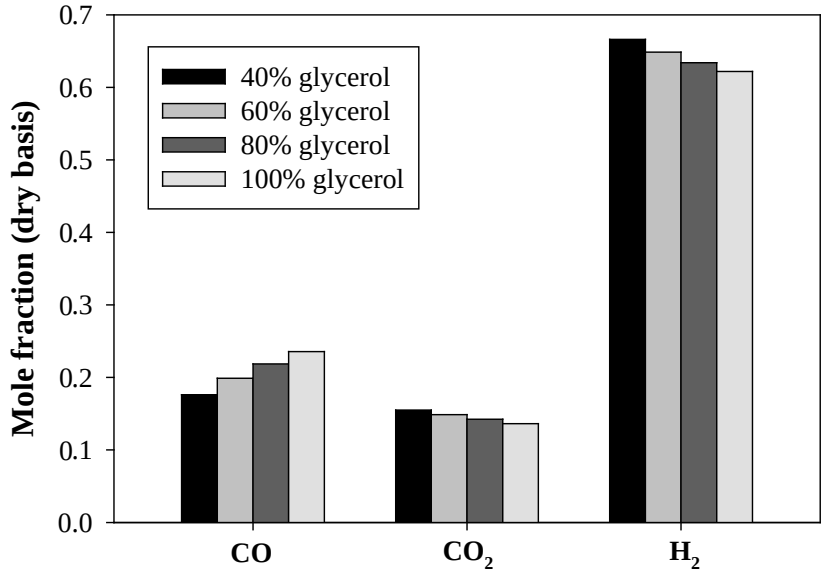

Figure 6.3 Product distribution of glycerol reforming process at standard condition: (a) Molar flow rate and (b) Mole fraction.

6.3.2 Glycerol autothermal reforming

For autothermal reforming, equilibrium compositions of reforming gas obtained were determined as a function of temperature, steam to crude glycerol ratio, and oxygen to crude glycerol ratio. An optimal operating condition of glycerol autothermal reforming at a thermoneutral condition that no external heat to sustain the reformer operation is required, was investigated. At the standard condition, the equilibrium product distribution of crude and pure glycerol autothermal reforming including water is reported in Table 6.3. It is observed that the amount of CO, CO_2, CH_4 and H_2 increases with increasing the fraction of glycerol in crude glycerol whereas H_2O is more produced at lower glycerol content in crude glycerol. Table 6.3 also presents the product compositions in dry basis.

Table 6.3 Product distribution at standard condition

%	Molar flow rate (kgmole/h)					Mole fraction (dry basis)			
glycerol	H_2	CO	CO_2	CH_4	H_2O	H_2	CO	CO_2	CH_4
100	4.202	1.527	1.455	0.018	2.762	0.583	0.212	0.202	0.002
80	3.727	1.228	1.361	0.011	2.850	0.589	0.194	0.215	0.002
60	3.231	0.943	1.251	0.007	2.956	0.595	0.174	0.230	0.001
40	2.709	0.678	1.119	0.003	3.084	0.601	0.150	0.248	0.001

6.3.2.1 Effect of operating temperature

Figure 6.4(a) shows the mole fraction and molar flow profile of hydrogen as a function of temperatures at different crude glycerol compositions. Raising the operating temperatures increases both the molar fraction and the molar flow of hydrogen. A similar trend is also observed when other fuels such as methane, methanol, and ethanol are utilized for hydrogen production (Seo et al., 2002; Faungnawakij et al., 2006; Liu et al., 2008). At equilibrium condition, crude glycerol is completely consumed in all the temperature ranges considered. This implies that an

increase in hydrogen is due to the increased reverse methanation reaction; the reduction of methane is also observed. The results also indicate that when comparing to case of using pure glycerol (100% glycerol), the concentration of hydrogen obtained from crude glycerol reforming is lower. This can be explained by the presence of methanol contained in crude glycerol; hydrogen produced from the steam reforming and oxidation of methanol is less than that obtained from glycerol (Eqs. (3)-(4)). Therefore, the amount of hydrogen decreases when methanol containing in crude glycerol increases.

Figure 6.4(b) illustrates an increased CO concentration at high temperature operation. This results from the reverse water gas shift which is the endothermic reaction and favored at high temperatures. Further, the methanation is also less pronounced due to its exothermicity. It is observed that at the specified operating temperature, the autothermal reforming of glycerol with less methanol generates a higher CO concentration. It is noted here that an increase in reforming temperatures has an advantage to achieve high hydrogen concentration, which would enhance fuel cell performance; however, more CO formation will cause a CO poisoning problem in fuel cell operation, especially a low-temperature fuel cell like a proton exchange membrane fuel cell (PEMFC). For this case, additional purification processes such as water gas shift reaction, preferential oxidation or membrane separation process should be added in the fuel processing process to reduce CO content to acceptable level. In addition, the developments of CO tolerant catalyst, air bleeding technique, and high temperature proton exchange membrane would be alternative options to overcome the CO poisoning problem in PEMFC.

(a)

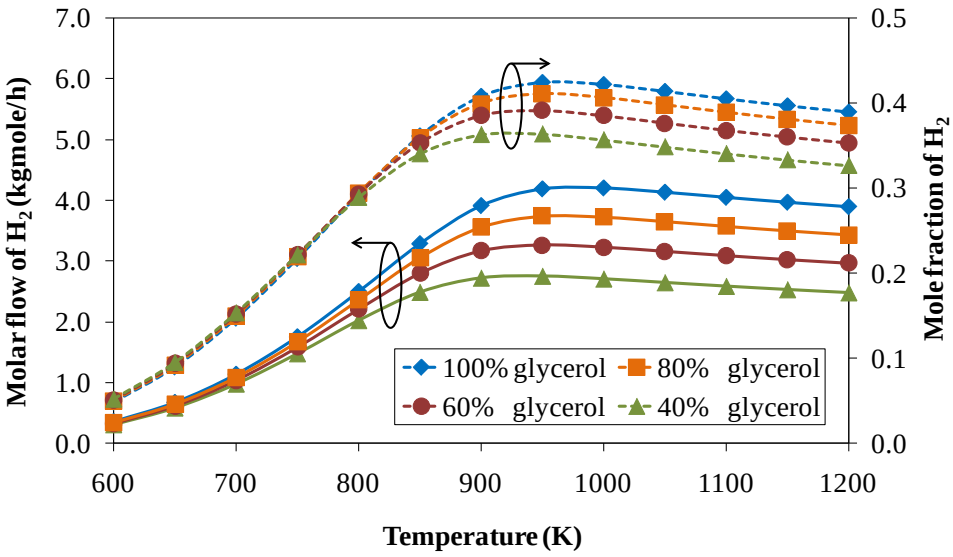

(b)

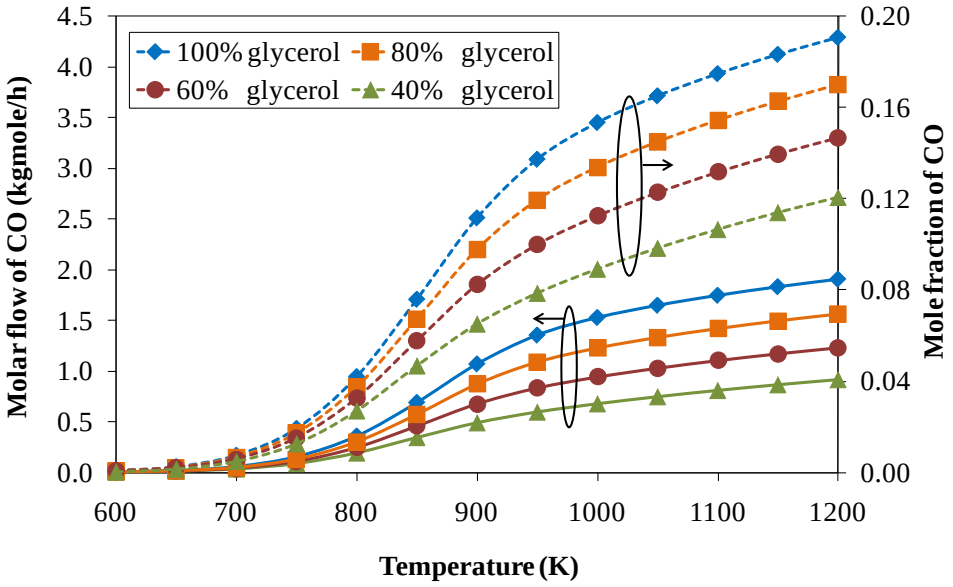

Figure 6.4 Effect of operating temperature on equilibrium compositions and molar flow rate of reforming gas: (a) H_2 and (b) CO (steam to crude glycerol ratio = 3 and oxygen to crude glycerol ratio = 0.6).

6.3.2.2 Effect of steam to crude glycerol ratio

A steam to crude glycerol ratio is a critical parameter to design the production and purification processes of hydrogen used for fuel cells. Typically, an excess steam is used to overcome the equilibrium limitation of steam reforming reaction, enhancing the extent of hydrogen produced (Ashrafi et al., 2008). From the simulation results (Figure 6.5(a)), although the flow rate of hydrogen increases with increasing steam to crude glycerol ratio, the fraction of hydrogen in the reforming product stream shows an opposite trend because the unreacted steam dilutes hydrogen product. If the reforming gas with dilute hydrogen concentration is directly fed to fuel cells, its electrical performance would diminish and thus a hydrogen separation process is needed. Figure 6.5(b) shows the effect of the steam to crude glycerol ratio on the fraction and molar flow of CO in the reforming gas. The change in CO concentration shows a decreased trend when feed steam is increased since more steam promotes the water gas shift reaction. Similar results are observed when using crude glycerol with different methanol contents. An increase of methanol fraction in crude glycerol makes the concentration of hydrogen and CO decrease.

(a)

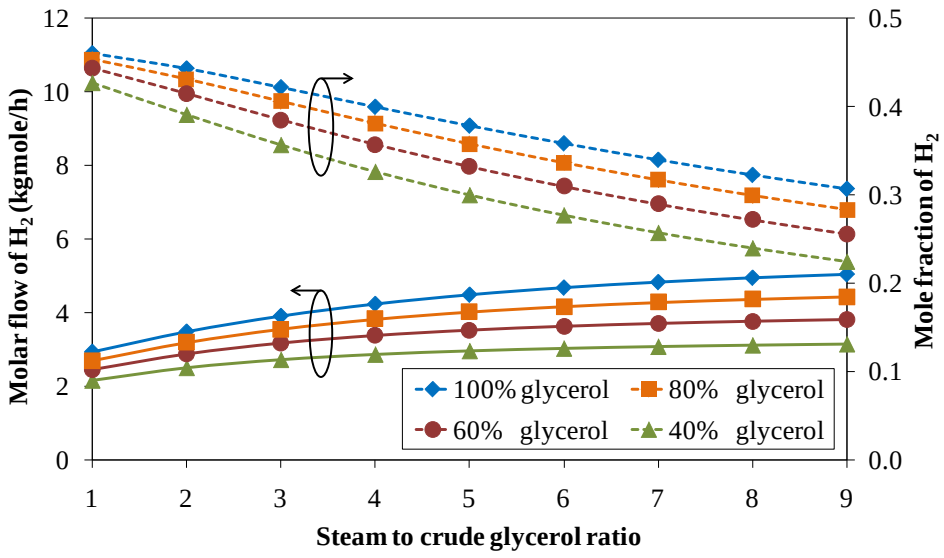

(b)

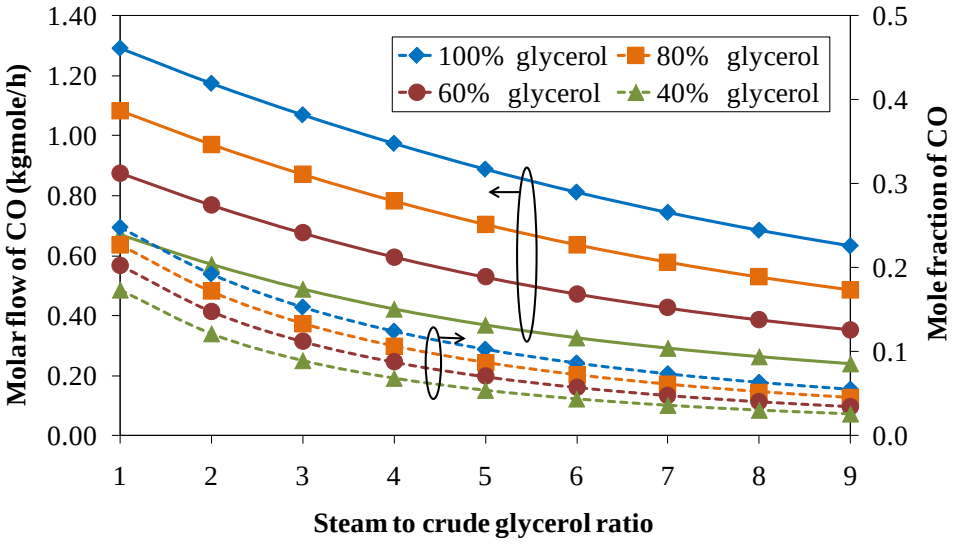

Figure 6.5 Effect of steam to crude glycerol ratio on equilibrium compositions and molar flow rate of reforming gas: (a) H_2 and (b) CO (oxygen to crude glycerol ratio = 0.6 and T = 1000 K).

6.3.2.3 Effect of oxygen to crude glycerol ratio

Figure 6.6(a) and 6.6(b) show that increasing oxygen to crude glycerol not only reduces the fraction of hydrogen but also decreases CO in the reforming gas. The increased amount of oxygen favors the oxidation reaction and suppresses the steam reforming, resulting in the depleted fraction of hydrogen. The content of CO is reduced since the increased oxidation causes more unreacted feed steam and thus the water gas shift reaction is more pronounced. When the ratio of glycerol in crude glycerol increases, both the mole fractions of hydrogen and CO in the reforming gas also increase. From the simulation results, no oxygen exists in the reforming gas at all operating conditions. This indicates that oxygen reacts with glycerol via the oxidation reaction and then the remaining glycerol reacts with steam in the reforming reaction. In general, the addition of oxygen to the reformer is an important factor having the direct impact on a heat requirement to sustain the process. In an autothermal reforming, the system can be operated without requiring an external heat input by adjusting oxygen feed. To maximize hydrogen concentration at no external energy

input, an optimal condition for operating the autothermal reformer should be determined.

(a)

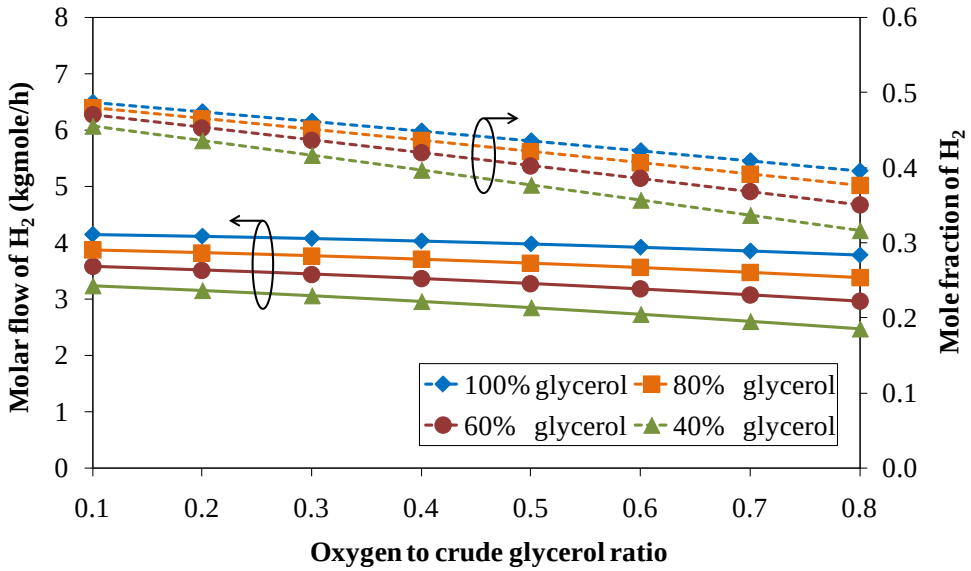

(b)

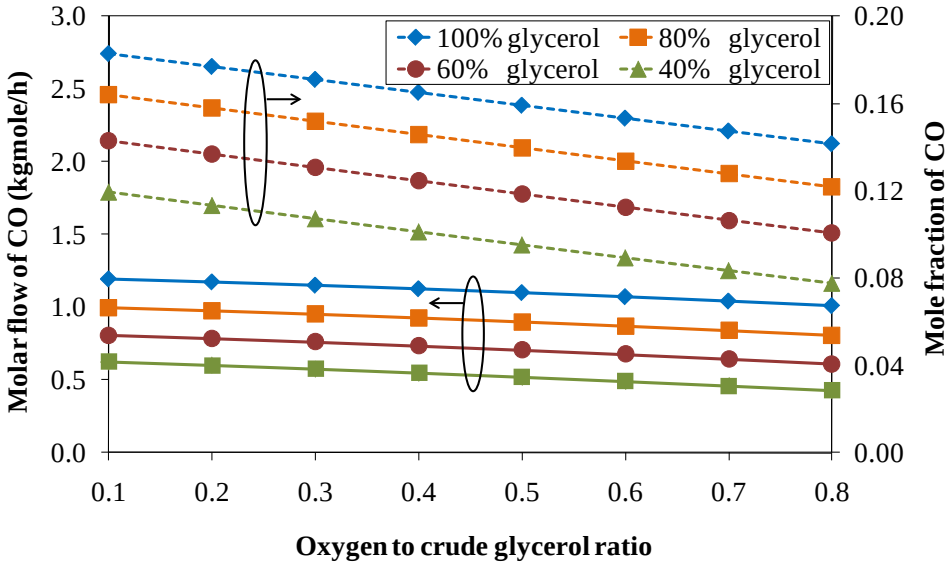

Figure 6.6 Effect of oxygen to crude glycerol ratio on equilibrium compositions and molar flow rate of reforming gas: (a) H_2 and (b) CO (steam to crude glycerol ratio = 3 and T = 1000 K).

6.3.2.4 Thermoneutral condition

In an autothermal steam reforming process, oxygen supplies the necessary heat via oxidation reaction for endothermic steam reforming; increasing oxygen to crude glycerol molar ratio decreases an external heat requirement. As a result, it is possible to operate the autothermal reformer without supplying external heat input by controlling oxygen feed ratio. This condition is referred as to a thermoneutral condition. The operating temperature at which the external heat flow equals to zero is also known as an adiabatic temperature. Figure 6.7 shows the relation of adiabatic temperature and oxygen to pure glycerol ratio at different steam to pure glycerol (S/F) ratios when the inlet temperature is fixed at 550 K. The adiabatic temperature increases with increasing the extent of oxygen. In contrast, the adiabatic temperature decreases when the steam to pure glycerol ratio increases. Similar trend is observed when crude glycerol is used. These results imply that the net energy required from the reactions enlarges when the excess steam is fed to the autothermal process.

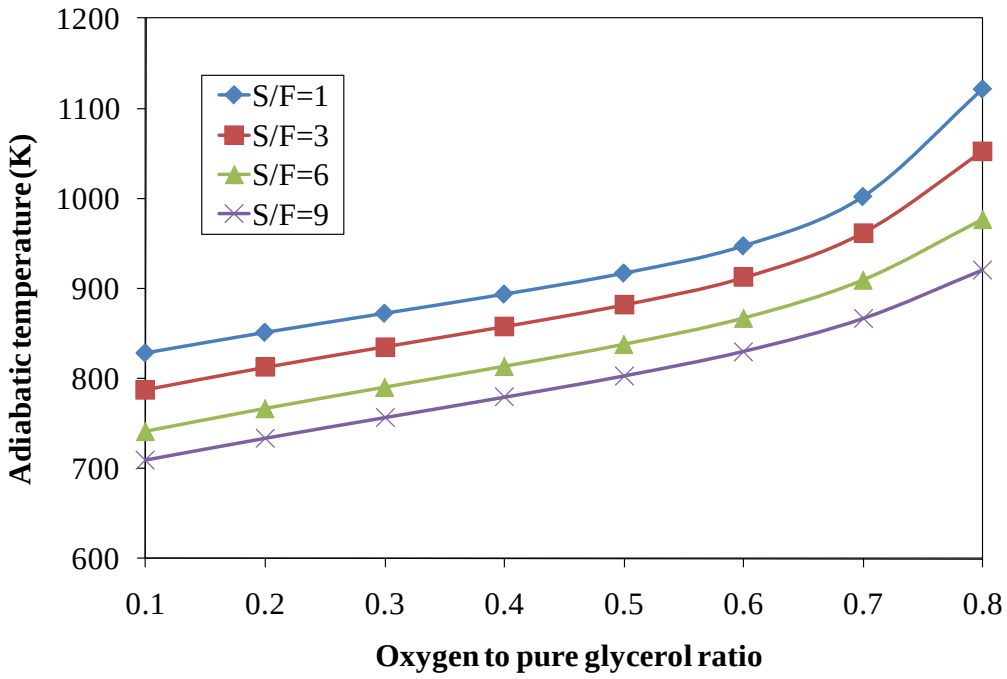

Figure 6.7 Relation of oxygen to pure glycerol ratio and adiabatic temperature at different steam to pure glycerol ratios.

Apart from the operating temperatures, steam to glycerol ratio, and oxygen to glycerol ratio, an inlet feed temperature is one of the most key parameters for achieving the thermoneutral condition of the autothermal process. Figure 6.8 shows the effect of feed inlet temperatures on the fraction of hydrogen and CO in the reforming product stream and on the oxygen to pure glycerol ratio required to achieve the thermoneutral condition when the autothermal reformer is operated at the temperature of 1000 K and the steam to glycerol ratio of 3. Increasing the inlet feed temperature causes a reduction of the amount of oxygen needed to maintain heat for the autothermal reformer at the desired reformer temperature. The reduced oxygen results in the increased hydrogen concentration in the product stream as the glycerol consumed by the oxidation reaction diminishes and thus more glycerol can react with steam via steam reforming that provides a higher hydrogen product. However, an increase in the inlet feed temperature also make more CO produced.

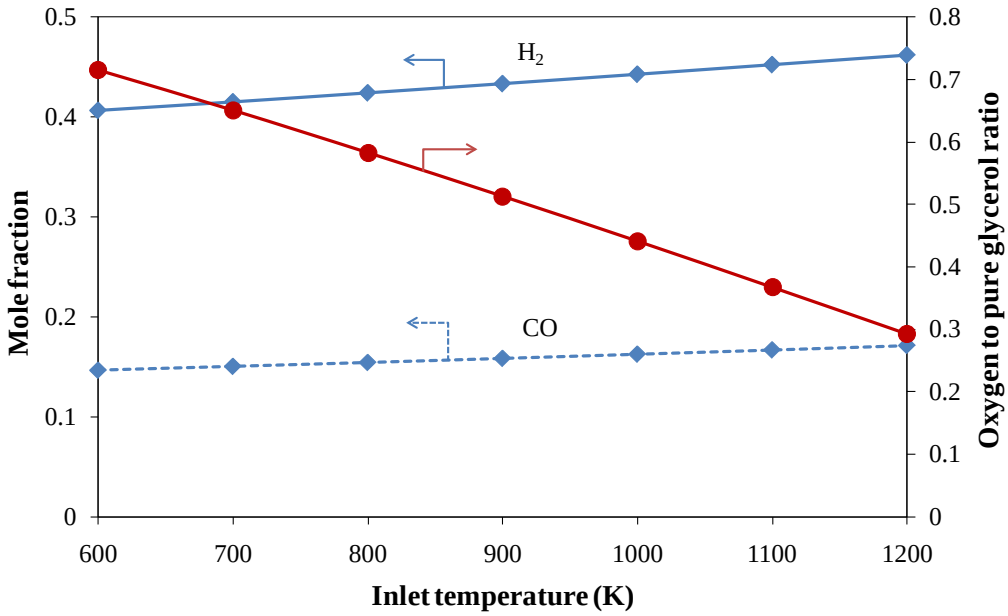

Figure 6.8 Effect of inlet feed temperature on product fraction and oxygen to pure glycerol ratio (steam to glycerol ratio = 3 and T = 1000 K).

Figure 6.9 demonstrates the amount of hydrogen produced from the autothermal reforming of pure and crude glycerol as a function of the oxygen to glycerol and the steam to glycerol ratios under the thermoneutral condition. At the thermoneutral condition, the performance of the autothermal reformer in term of hydrogen production is enhanced when the oxygen to crude glycerol ratio increases. This result shows an opposite trend when the autothermal reformer is operated at an isothermal condition. For thermoneutral operation, oxygen affects not only the oxidation reaction but also the reformer temperature. When increasing the oxygen to glycerol ratio, the oxidation is more pronounced and at the same time, the temperature of the autothermal reformer is also elevated until its optimal condition where hydrogen content reaches the maximum value. Considering the condition at which hydrogen is maximum produced, the oxygen required for the autothermal reforming of pure glycerol is higher than that of crude glycerol. It can be concluded that pure glycerol reforming requires more heat to maintain the reformer than crude glycerol reforming. Figure 6 also shows that at the thermoneutral condition, an increase in the steam to crude glycerol ratio improves the production of hydrogen and the hydrogen produced from pure glycerol is still more than that from crude glycerol.

(a)

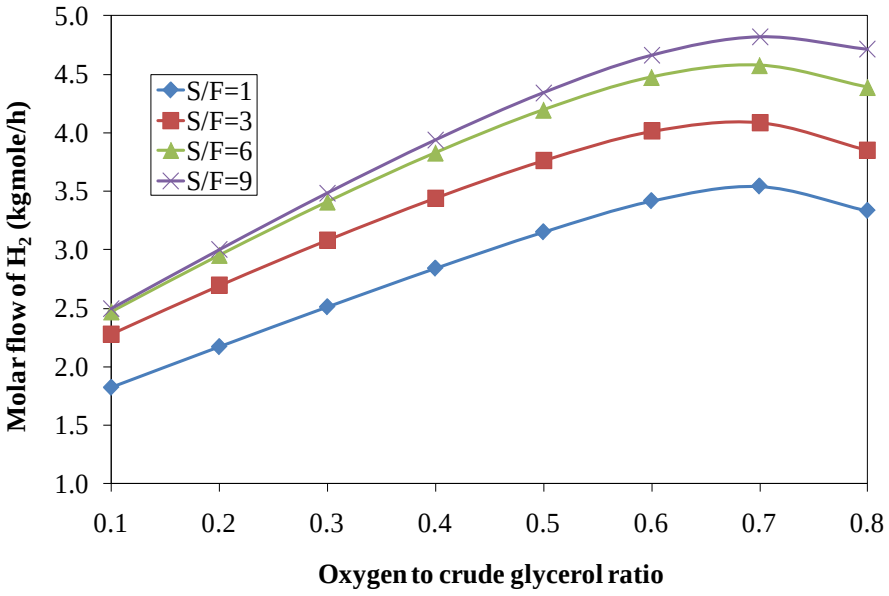

(b)

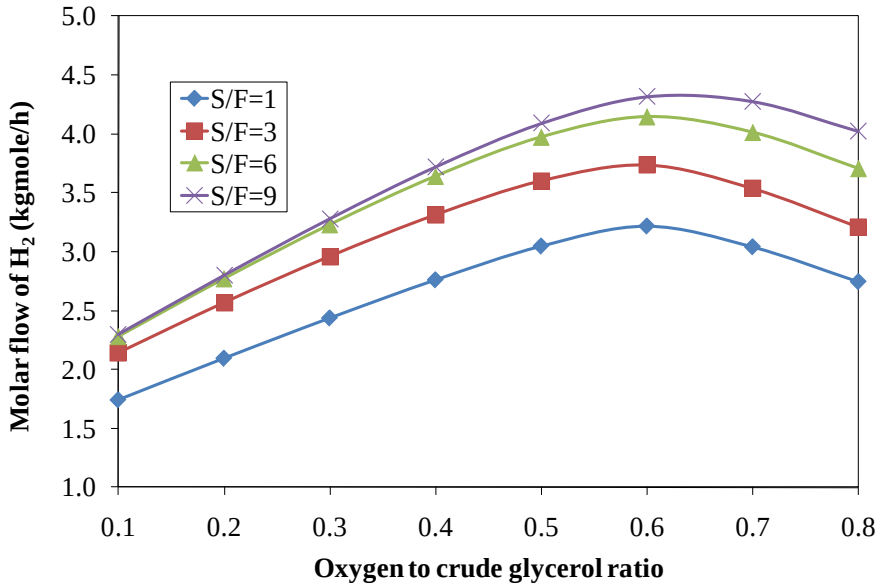
5.0
4.5
4.0
3.5
3.0
2.5
2.0
1.5
1.0
S/F=1
S/F=3
S/F=6
S/F=9
Molar flow of H2 (kgmole/h)
0.1
0.2
0.3
0.4
0.5
0.6
0.7
0.8
Oxygen to crude glycerol ratio

(c)

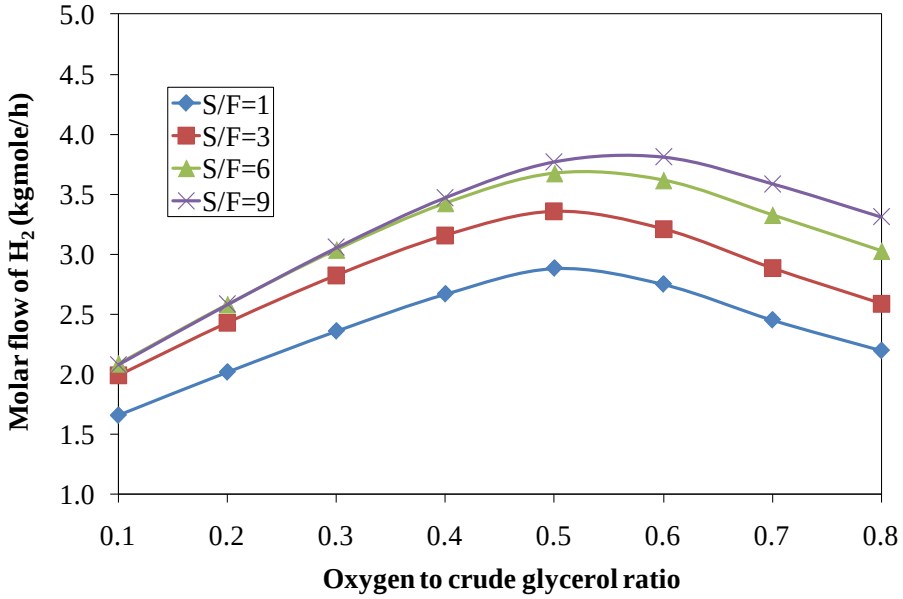
5.0
4.5
4.0
3.5
3.0
2.5
2.0
1.5
1.0
S/F=1
S/F=3
S/F=6
S/F=9
Molar flow of H2 (kgmole/h)
0.1
0.2
0.3
0.4
0.5
0.6
0.7
0.8
Oxygen to crude glycerol ratio

(d)

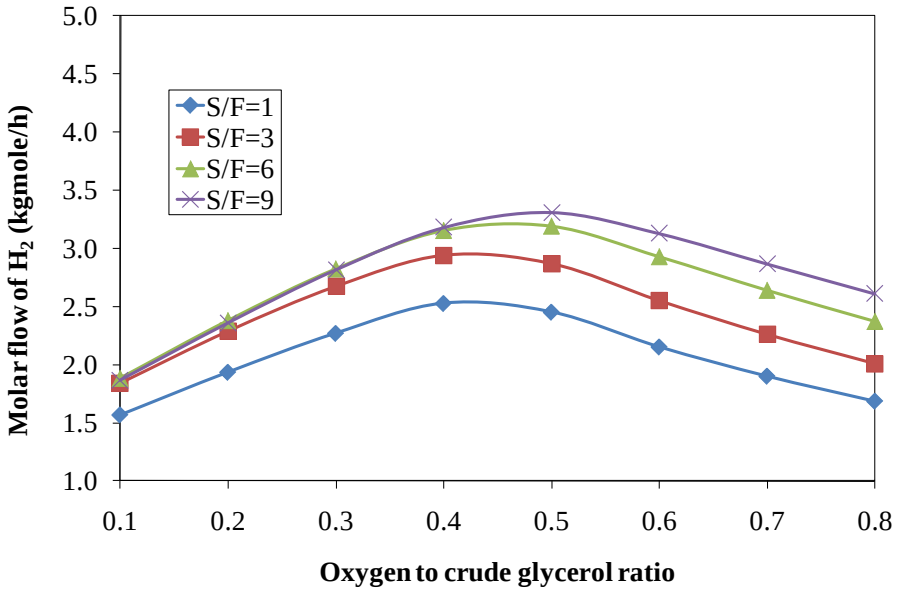

Figure 6.9 Molar flow of H_2 from pure and crude glycerol autothermal reforming process at thermoneutral condition: (a) pure glycerol, (b) 80% glycerol, (c) 60% glycerol, and (d) 40% glycerol.

Table 6.4 shows the optimal operating conditions of crude glycerol autothermal reforming process at the thermoneutral condition and the amount of hydrogen produced. The suitable ratio of oxygen to crude glycerol to achieve an optimum hydrogen yield is around 0.4-0.7 depending on the fraction of glycerol containing in crude glycerol. The corresponding adiabatic temperatures are in the range of 850-1000 K.

Table 6.4 Optimal operating condition of crude glycerol autothermal reforming at thermoneutral condition

Glycerol content (%)	Steam to crude glycerol ratio	Oxygen to crude glycerol ratio	Adiabatic temperature (K)	Molar flow of H_2 (kgmole/h)	Mole fraction of H_2	
					wet basis	dry basis
100	1	0.7	1002	3.543	0.447	0.542
	3	0.7	962	4.089	0.412	0.577
	6	0.7	910	4.576	0.355	0.604
	9	0.7	867	4.820	0.304	0.616
80	1	0.6	987	3.219	0.453	0.553
	3	0.6	943	3.734	0.410	0.589
	6	0.6	888	4.147	0.344	0.615
	9	0.6	844	4.317	0.287	0.624
60	1	0.5	969	2.881	0.459	0.567
	3	0.5	922	3.355	0.401	0.604
	6	0.5	864	3.677	0.327	0.626
	9	0.55	842	3.834	0.268	0.635
40	1	0.4	950	2.527	0.464	0.584
	3	0.4	896	2.940	0.395	0.620
	6	0.45	863	3.227	0.307	0.642
	9	0.5	842	3.311	0.244	0.648

6.3.3 Comparison between glycerol steam reforming and autothermal reforming

The performance of glycerol steam reforming and autothermal reforming (at adiabatic condition) is compared and shown in Figure 6.10. It is observed that the adiabatic condition of autothermal reforming occur firstly at reformer temperature of 750 K when steam to glycerol ratio and inlet feed temperature are 3 and 550 K, respectively. At this condition, there is no oxygen added to the system. As mentioned before, the reformer temperature will increase with increasing oxygen/glycerol ratio. From Figure 6.10, it shows that product distribution of steam and autothermal reforming is the similar trend. However, the hydrogen content obtaining from steam reforming is higher than autothermal reforming at reformer temperature > 850 K. At below this temperature, the equal hydrogen content is gained from both of the two processes. On the other hand, amount of CO product from autothermal reforming is lower than steam reforming because of higher remaining steam of autothermal reforming to react with CO through water gas shift reaction.

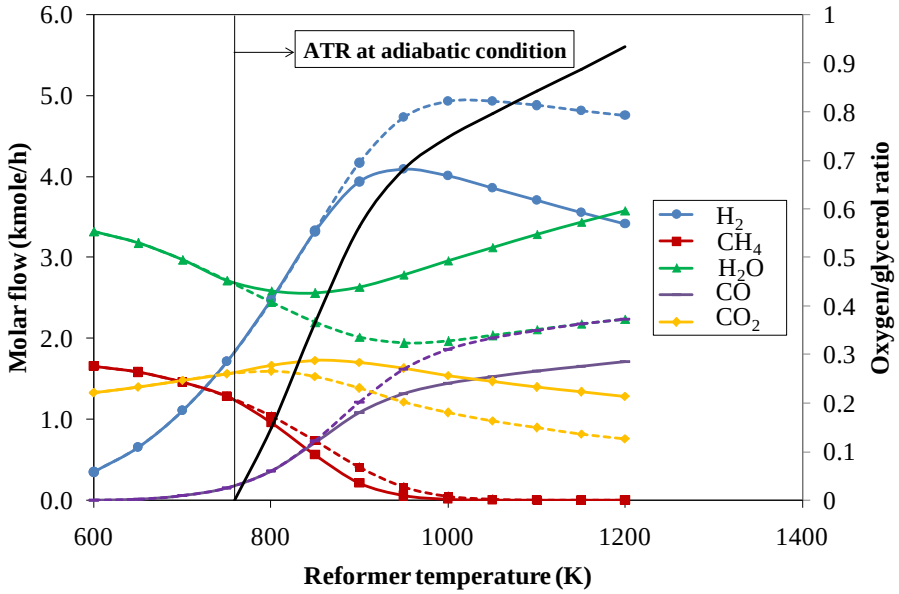

Figure 6.10 Molar flow of product gas from glycerol reforming process at different temperatures: ATR (solid line) and SR (dash line).

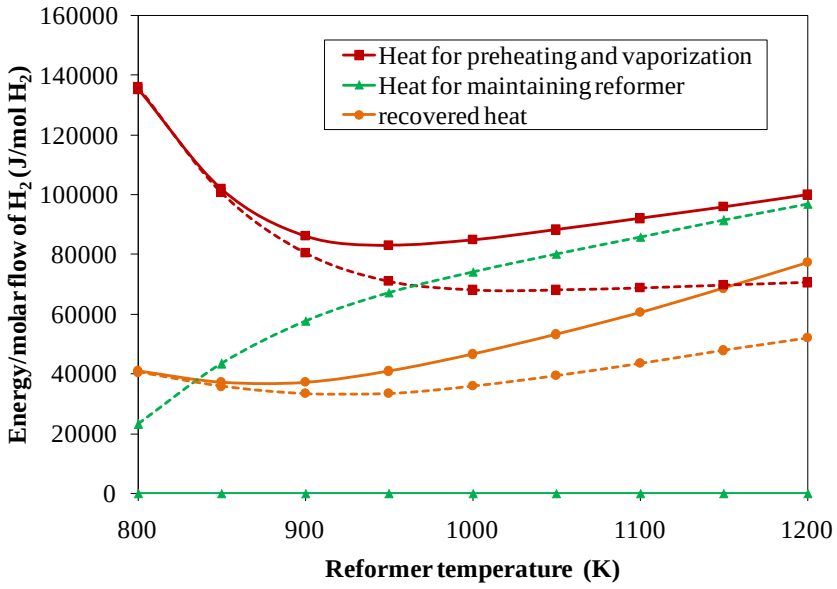

Figure 6.11 Energy requirement of glycerol reforming process: ATR (solid line) and SR (dash line).

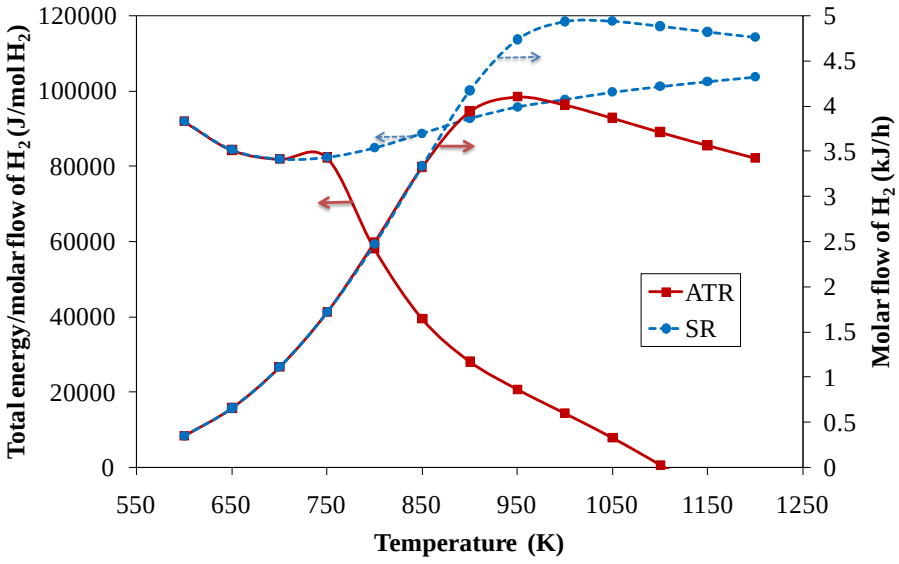

Figure 6.12 Total energy requirement of glycerol reforming process: ATR (solid line) and SR (dash line).

In this section, the required energy of glycerol autothermal and steam reforming is studied. The heat is consumed to preheat and vaporized reactant in the first step and then it is used to maintain the reformer to reaction temperature. In addition, the hot product gas is reduced temperature to 473 K because it is the operating temperature of water gas shift reactor which is need to be connect with reformer in case of PEMFC system. The heat release from hot gas is considered the recovered heat that can be used to preheat or vaporize reactant in the system. Figure 6.11 shows the required heat to produced 1 mol of hydrogen in the autothermal and steam reforming. It is found that the autothermal reforming process needs heat to preheat and vaporize reactant for producing equivalent mole of hydrogen higher than steam reforming process. This is because the steam reforming provides the high hydrogen yield. On the other hand, the heat to maintain reactor increase respect to temperature for steam reforming but it is unnecessary for autothermal reforming. The higher recovery heat can be obtained from autothermal reforming process. The total energy required of those two processes is shown in Figure 6.12. It is found that the autothermal reforming required lower energy at high reformer temperature and the heat requirement reduce with temperature. The contradiction trend is observed for steam reforming because heat requirement increase with temperature.

6.4 Conclusions

The steam and autothermal reforming of both pure and crude glycerol were investigated by thermodynamic analysis approach. Equilibrium compositions of reforming gas obtained were determined as a function of temperature, steam to crude glycerol ratio, and oxygen to crude glycerol ratio (in case of autothermal reforming). The results show that hydrogen production of steam and autothermal process enhance with increasing temperature and steam to glycerol ratio. Although adding more steam in glycerol causes an increase in hydrogen product, the fraction of hydrogen depletes due to the dilution effect of steam. For the oxygen to glycerol effect of autothermal reforming process, causes a reduction of hydrogen concentration. The results also show that CO formation, which cause a poisoning problem in low-temperature fuel cells, increases with increasing the reformer temperature but decreases with

increasing the steam to glycerol ratio. Methane dose not present in the system at high temperature operation (> 1000 K). Compared to pure glycerol, the use of crude glycerol to produce hydrogen gives lower hydrogen content but higher hydrogen fraction (dry basis). Considering the crude glycerol autothermal reforming at a thermoneutral condition where no external heat input is required, the maximum hydrogen yield can be achieved at the condition having sufficient oxygen to sustain energy for system. It is found that the appropriate oxygen to crude glycerol ratio is around 0.4-0.7 depending on the purity of crude glycerol. The amount of oxygen needed to sustain the autothermal reformer operation is higher when excess steam is applied and crude glycerol containing less methanol is used for hydrogen production. Although the hydrogen content obtained from steam reforming is higher than autothermal reforming, the energy requirement of autothermal reforming is lower compared to steam reforming. However, the selection of reforming process also depends on specification and limitation of application.

CHAPTER VII

OPTIMAL CONDITIONS OF GLYCEROL REFORMING FOR HT-PEMFC

7.1 Introduction

To date, glycerol is considered an alternative fuel for hydrogen production because it is a by-product of the production of biodiesel, which uses vegetable oils or fats as feedstock. Therefore, glycerol is a promising, renewable source of hydrogen production (Byrd et al., 2008). Typically, the main goal of hydrogen production is to maximize hydrogen yield, and thus, most of the previous investigations have identified the favourable conditions and methods to achieve this goal. It is found that low-temperature operation and a high steam to glycerol molar ratio are required to minimize CO formation (Wang et al., 2008). While high-temperature operation is preferable for hydrogen production, CO removal is desired for applications in fuel cells.

Among the different types of fuel cell, the polymer electrolyte membrane, or proton exchange membrane, fuel cell (PEMFC) is one of the most attractive fuel cells for automobile, residential and portable applications because it operates at low temperatures (allowing it to start up and shut down very quickly) and provides a high current density (Lin et al., 2007; Dawes et al., 2009). Currently, PEMFCs can be divided into two types depending on the operating temperatures, low-temperature (LT-PEMFCs) and high-temperature (HT-PEMFCs) proton exchange membrane fuel cells. LT-PEMFCs can be operated at temperatures of approximately 333-353 K and are limited to sources of high hydrogen purity. The content of CO in the hydrogen feed for a LT-PEMFC can be no greater than 10 ppm to avoid catalyst poisoning (Zhang et al., 2006). Therefore, the obtained reformate gas needs to be treated using water gas shift and preferential oxidation processes before being fed to the LT-

PEMFC. The HT-PEMFC was developed from a LT-PEMFC and operates at temperatures around 373-473 K. At higher temperatures, the extent of CO that adsorbs on Pt in a HT-PEMFC is reduced, resulting in a high tolerance for CO (Li et al., 2003). In fact, a HT-PEMFC can tolerate CO up to 2-5% at 453 K with a insignificant degradation in the cell performance (Das et al., 2009); thus, it is possible to use the reformate gas for a HT-PEMFC directly without purification processes or with only water gas shift reactor. There have been few studies that have focused on determining the optimal conditions for the glycerol reforming process of LT-PEMFC, and based on our knowledge, no research has reported the optimal conditions of reforming processes for HT-PEMFC. It should be noted that the generation of hydrogen for each type of PEMFC has different requirements and limitations. Therefore, apart from maximizing the hydrogen yield, it is necessary to take these aspects into consideration in the production of hydrogen for PEMFC applications.

In this study, a steam reforming of glycerol to generate hydrogen for HT-PEMFCs is considered by taking into account requirement for the CO content of the reformate gas. A thermodynamic analysis is performed to find suitable conditions for the glycerol steam reforming process that not only maximize the hydrogen yield but also provide a CO concentration that satisfies the operational constraints of HT-PEMFCs system. This study aims to explore the possibility of using the reformate gas directly from the glycerol steam reforming with and without CO removal process. The operational boundary of the glycerol steam reforming for HT-PEMFCs system without CO purification process is also examined. Another case, a water gas shift reactor is included in the reforming process to remove CO and enhance hydrogen concentration. The optimal conditions of the glycerol steam reforming for both HT-PEMFCs systems are examined.

7.2 Fuel processing for HT-PEMFC

From a thermodynamic point of view, the adsorption of CO on the Pt surface can be reduced by increasing the temperature and/or decreasing the CO concentration (Bellows et al., 1996). As a result of the high operating temperature (in the range of

373-473 K), HT-PEMFCs can tolerate up to 5% CO, compared to LT-PEMFCs in which the CO content of the hydrogen feed must be less than 10-50 ppm. In general, CO coverage on Pt decreases at higher temperatures; because the adsorption of CO is an exothermic process, the Pt active sites for hydrogen adsorption increase. This result means that the possibility of hydrogen adsorption, which is less exothermic than CO adsorption, increases at high temperatures. The relative activity of a Pt catalyst for hydrogen oxidation as a function of temperature at different CO concentrations and found that the oxidation of hydrogen can be promoted at high-temperature operation (Li et al., 2003). Other advantages of the high-temperature operation of PEMFCs (apart from the enhanced CO tolerance) include an increase in the electrochemical reaction rates, simplified water management, and improved heat management (Pan et al., 2005; Shao et al., 2007; Yang et al., 2001).

In order to circumvent the issue of hydrogen availability and infrastructure, a fuel cell may be integrated with a fuel processor allowing hydrogen generation from hydrocarbon fuels. The main reaction that occurs in the steam reformer is glycerol steam reforming (Eq. (7.1)), whereas the side reactions are water gas shift (Eq. (7.2)), methanation (Eq. (7.3)), and methane dry reforming (Eq. (7.4)).

$$C_3H_8O_3 + 3H_2O \leftrightarrow 7H_2 + 3CO_2 \quad (7.1)$$

$$CO + H_2O \leftrightarrow H_2 + CO_2 \quad (7.2)$$

$$CO + 3H_2 \leftrightarrow CH_4 + H_2O \quad (7.3)$$

$$CO_2 + CH_4 \leftrightarrow 2H_2 + 2CO \quad (7.4)$$

Furthermore, the main potential reactions for the formation of carbon are shown as follows:

Boudouard:

$$2CO \leftrightarrow CO_2 + C \quad (7.5)$$

Methane cracking:

$$CH_4 \leftrightarrow 2H_2 + C \tag{7.6}$$

CO reduction:

$$CO + H_2 \leftrightarrow H_2O + C \tag{7.7}$$

To avoid carbon formation, an appropriate temperature and steam to glycerol ratio should be determined. In this work, the boundaries of carbon formation during glycerol steam reforming is also presented to describe a carbon free region and a carbon formation region.

Due to the increased CO tolerance of HT-PEMFCs at high temperatures, it is possible to use the reformate gas directly from reformers without the use of CO removal processes. Generally, to increase hydrogen yield in endothermic steam reforming process, high temperature and excess steam are required. However, CO formation pronounce at high temperature so water gas shift unit may be included to maximize hydrogen content and eliminate CO before feeding to the PEMFCs. Owing to high CO tolerance of HT-PEMFCs, preferential oxidation process is unnecessary for this fuel cell. Therefore, the glycerol reforming process with and without water gas shift process are analyzed to determine optimal condition and efficiency. The studied system of the fuel processing for a HT-PEMFC is illustrated in Figure 7.1. For the system without water gas shift process, the operational boundary that provides an appropriate reformate product to supply to the HT-PEMFC is explored. The simulation results are presented while considering the constraint on CO content in the reformate gas.

a)

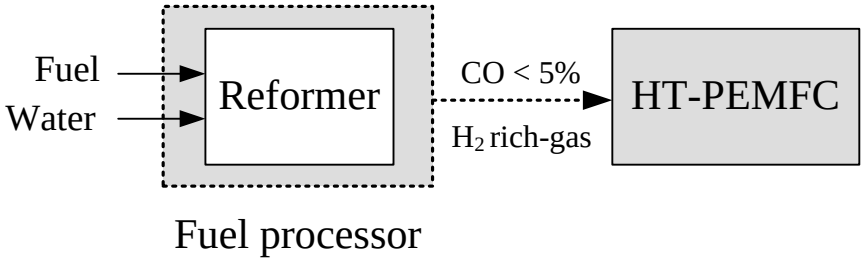

b)

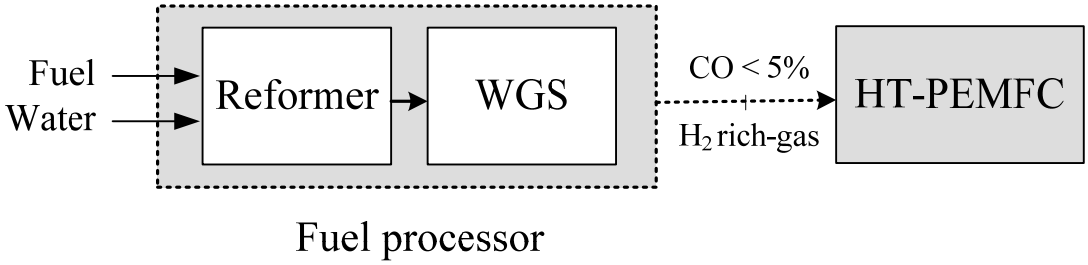

Figure 7.1 Fuel processor for HT-PEMFC: a) without water gas shift reactor and b) with water gas shift reactor.

In this work, the equilibrium composition of the reformate gas obtained from the steam reforming system of glycerol mentioned earlier was calculated using direct minimization of the Gibbs free energy. The primary components were $C_3H_8O_3$, H_2O, CO, CO_2, H_2, CH_4, and C. The other intermediate compounds of the glycerol steam reforming, such as ethane, propane, methanol and ethanol, can be neglected (Dou et al., 2010; Chen et al., 2011). As the reaction proceeds, the total Gibbs free energy (G^t) attains its minimum value. Therefore, the equilibrium composition can be determined by solving the minimization problem as follows:

$$\min_{n_i}\left(G^t\right)_{T,P} = \sum_{i=1}^{C} n_i \overline{G}_i = \sum_{i=1}^{C} n_i \left(G_i^{\circ} + RT \ln \frac{\bar{f}_i}{f_i^{\circ}} \right) + n_S G_S \qquad (7.8)$$

where G_i° is the Gibbs free energy of the species in standard conditions, C is the total number of components in the reaction system, n_i is the amount of each gaseous component, n_s is the number of carbon molecules involved in the carbon formation, and G_s is the Gibbs free energy of solid carbon.

According to the conservation of atomic species, n_i has to satisfy the following relationship:

$$\sum_{i=1}^{C} a_{ji} n_i = b_j, \quad \text{for} \, 1 \le j \le M \tag{7.9}$$

where a_{ji} is the number of atoms of element j in component i, b_j is the total number of atoms of element j in the reaction mixture, and M is the total number of elements.

The solid component is also considered for element balances in Eq. (7.9). The thermodynamic characteristics of glycerol and the other products can be obtained from HYSYS's pure component library database. The thermodynamic analysis of a steam reformer was performed by using the HYSYS simulator. Based on a Gibbs reactor module coupled with the Peng-Robinson Stryjek-Vera (PRSV) method for computing thermodynamic properties, the minimization problem of Gibbs free energy (as stated above) was solved to find the equilibrium composition of the reactive system. The prediction results were compared with the experiment data reported by Profeti et al. (2009). It was observed that the product distribution obtained from the HYSYS simulator and the experimental data were in agreement.

7.3 Results and discussion

To analyze the performance of a glycerol steam reforming process, it was assumed that the inlet temperature of the reactant feeds was 25 °C and that a steam reformer is operated under isothermal conditions. As carbon formation is one of the most critical problems that can affect the catalyst activity in reforming processes, the operating conditions of the steam reformer should be carefully selected. Figure 7.2 illustrates the effects of the steam to glycerol ratio (S/G) and the reformer temperature

on carbon formation. It indicates the boundary of carbon formation for glycerol steam reforming, which is helpful for determining feasible conditions to avoid carbon formation. It is observed that carbon formation is thermodynamically inhibited at high temperatures and high steam to glycerol ratios.

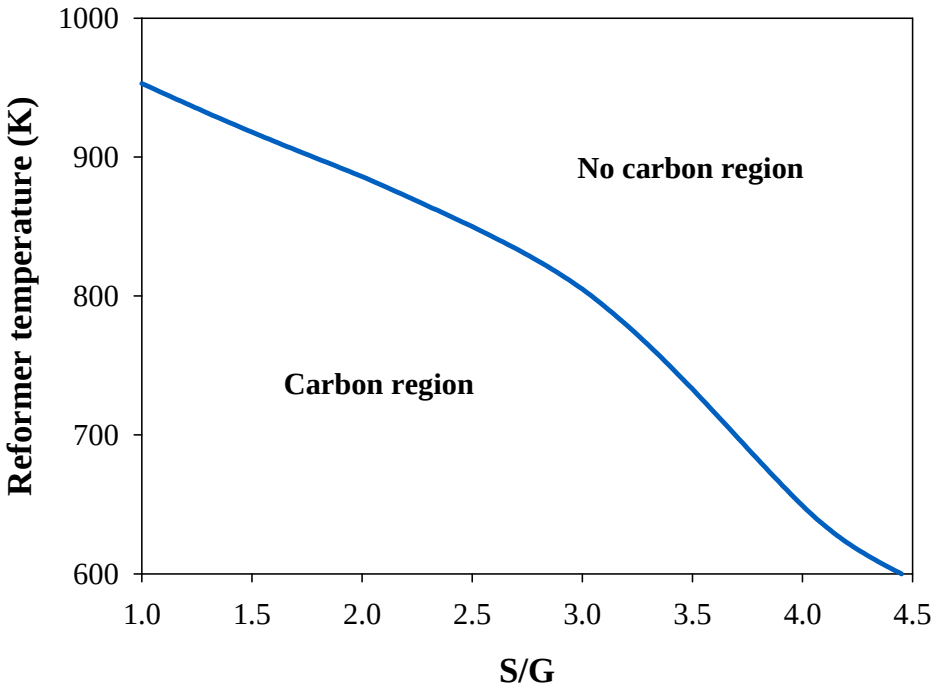

Figure 7.2 Boundary of carbon formation for a glycerol steam reformer at atmospheric pressure.

7.3.1 Glycerol reforming process for HT-PEMFCs without water gas shift reactor

As mentioned above, the high CO tolerance of HT-PEMFCs makes it possible to use the reformate gas directly from the steam reformer. This type of PEMFC can withstand CO up to 5% with no significant loss of performance. For HT-PEMFC, the concentration of CO in the reformate gas from the steam reformer was taken into consideration. To control the fraction of CO to an acceptable level, the reformer needs to operate at low temperatures and high steam to glycerol ratios. However, the low-temperature operation of the reformer causes a reduction in hydrogen content, which

has a considerable effect on the fuel cell performance. To directly use the reformate gas obtained for HT-PEMFC, this study aims at finding optimal conditions that favor hydrogen yield while avoiding CO contamination levels in the reformate gas that surpass the tolerable level of HT-PEMFC.

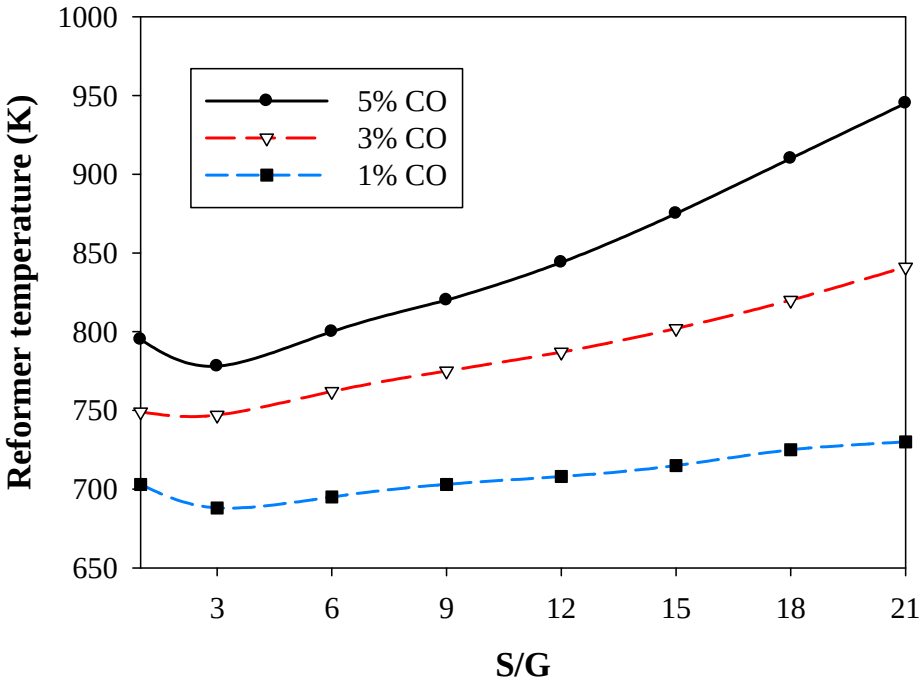

Figure 7.3 Relation of steam to glycerol molar ratio and reformer temperature at different %CO tolerances of HT-PEMFC.

Figure 7.3 shows the relationship between the steam to glycerol ratio and the reformer temperature at different %CO tolerances of the HT-PEMFC. The results reveal that the reformer can be operated at higher temperatures when the steam to glycerol ratio is increased, at all %CO tolerances considered. In addition, the operating reformer temperature also increases with an increased CO tolerance level of HT-PEMFC. Several investigations have shown that temperature has a direct effect on hydrogen yield (Faungnawakij et al., 2006; Liu et al., 2008). Therefore, the hydrogen yield increases with respect to the CO tolerance level and the steam glycerol ratio, as shown in Figure 7.4. For a 5% CO tolerance, hydrogen yield becomes constant when the steam to glycerol ratio is over 18.

Figure 7.5 shows the compositions of hydrogen, methane and CO_2 at different %CO tolerances of a HT-PEMFC when the steam to glycerol ratio is fixed at 12. The reformer temperature is adjusted according to the %CO tolerance, and the relation of the steam to glycerol ratio and the reformer temperature for each %CO tolerance is shown in Figure 7.3. The simulation results indicate that the hydrogen composition obtained from the steam reformer is higher when a high CO fraction in the reformate gas is allowed, compared to cases in which only a low CO fraction is allowed. Carbon dioxide and methane gradually decrease when increasing the content of CO in the reformate gas. Therefore, the hydrogen fraction (a key parameter affecting the fuel cell performance) is increased if the HT-PEMFC can tolerate more CO. It can be concluded from Figs. 7.4 and 7.5 that high steam to glycerol ratios and CO tolerance in the HT-PEMFC improves the performance of the reformer in terms of hydrogen content and concentration.

The extent of CO has a significant influence on the performance of the PEMFC when reformate gas is used as the reactant feed. Therefore, the appropriate reforming conditions need to be determined. Figure 7.6 shows the boundary of the operating conditions for glycerol steam reforming that generate CO levels below 5%. The region above the solid line indicates the operating conditions in which the content of CO produced is in the acceptable level for HT-PEMFCs. If the glycerol steam reformer is operated at conditions far away from the CO boundary line, the concentration of CO will decrease. However, the fraction of hydrogen, which has a direct effect on the PEMFC performance, also decreases. Figure 7.6 also indicates the boundary of carbon formation (dashed line). At conditions above this boundary line, carbon formation is thermodynamically inhibited. As a result, the optimal condition of glycerol steam reforming for a HT-PEMFC is shown in the gray region. Within this region, there is no carbon formation and the CO level contaminating the hydrogen-rich reformate gas is lower than 5%.

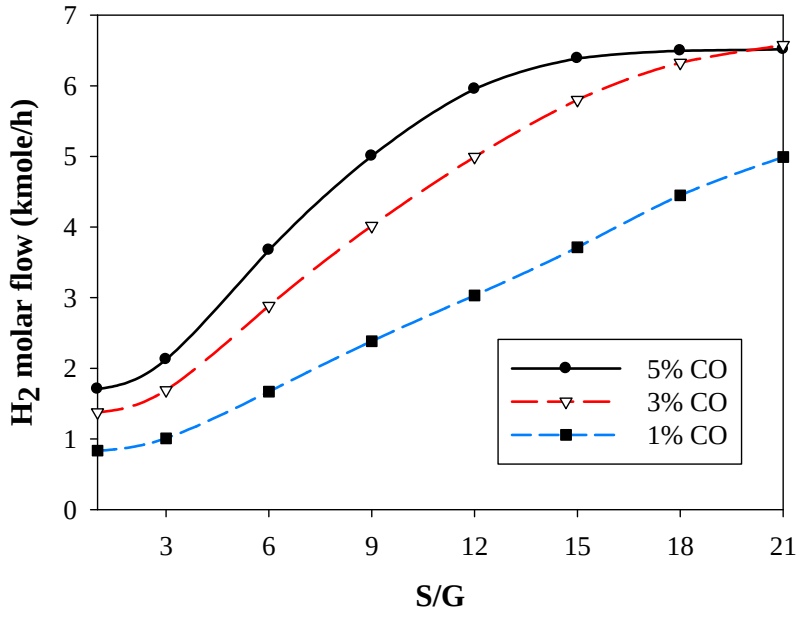

Figure 7.4 Effect of steam to glycerol molar ratio on hydrogen molar flow at different %CO tolerances of HT-PEMFC.

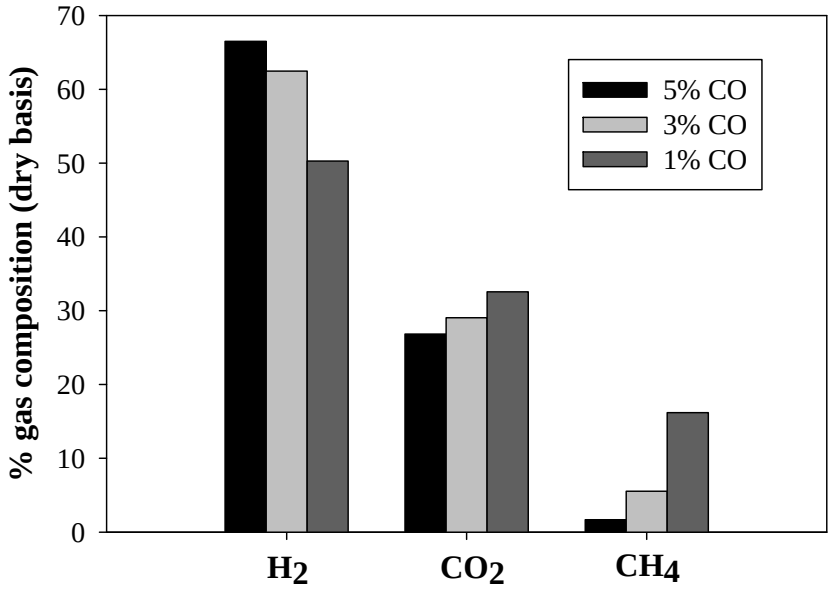

Figure 7.5 Product distributions of glycerol steam reforming (steam to glycerol ratio = 12) at different %CO tolerances of HT-PEMFC.

The extent of CO has a significant influence on the performance of the PEMFC when reformate gas is used as the reactant feed. Therefore, the appropriate reforming conditions need to be determined. Figure 7.6 shows the boundary of the operating conditions for glycerol steam reforming that generate CO levels below 5%. The region above the solid line indicates the operating conditions in which the content of CO produced is in the acceptable level for HT-PEMFCs. If the glycerol steam reformer is operated at conditions far away from the CO boundary line, the concentration of CO will decrease. However, the fraction of hydrogen, which has a direct effect on the PEMFC performance, also decreases. Figure 7.6 also indicates the boundary of carbon formation (dashed line). At conditions above this boundary line, carbon formation is thermodynamically inhibited. As a result, the optimal condition of glycerol steam reforming for a HT-PEMFC is shown in the gray region. Within this region, there is no carbon formation and the CO level contaminating the hydrogen-rich reformate gas is lower than 5%.

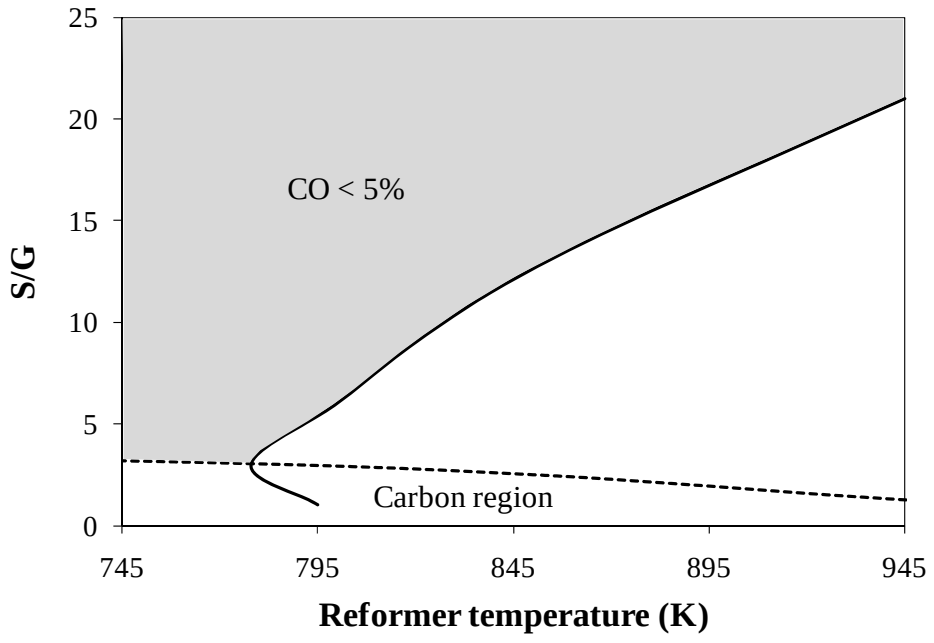

Figure 7.6 Operational boundary of glycerol steam reforming for HT-PEMFC.

Figure 7.7 shows the relation between the energy requirement for the glycerol steam reforming process and the operating temperature at different steam to glycerol ratios. Although increases in the temperature and steam to glycerol ratio enhance the hydrogen yield, the energy needed for reformer operation increases. To identify the actual optimal conditions of glycerol reforming for HT-PEMFCs, the efficiency of the reformer, taking into account the energy consumption as shown in Eq. (7.10), was used as the parameter to indicate performance.

$$\text{efficiency } (\%) = \frac{\text{LHV of hydrogen } \left(\dot{m}_{H_2}\right)}{\text{LHV of glycerol } \left(\dot{m}_{\text{glycerol}}\right) + \text{energy used for reforming process}} \times 100 \qquad (7.10)$$

where LHV is the lower heating value. It should be noted that the energy required for the steam reforming process accounts for the heat of vaporization, sensible heat to heat up the reactants to the desired temperature and the heat needed for maintaining the reformer at an isothermal operation level.

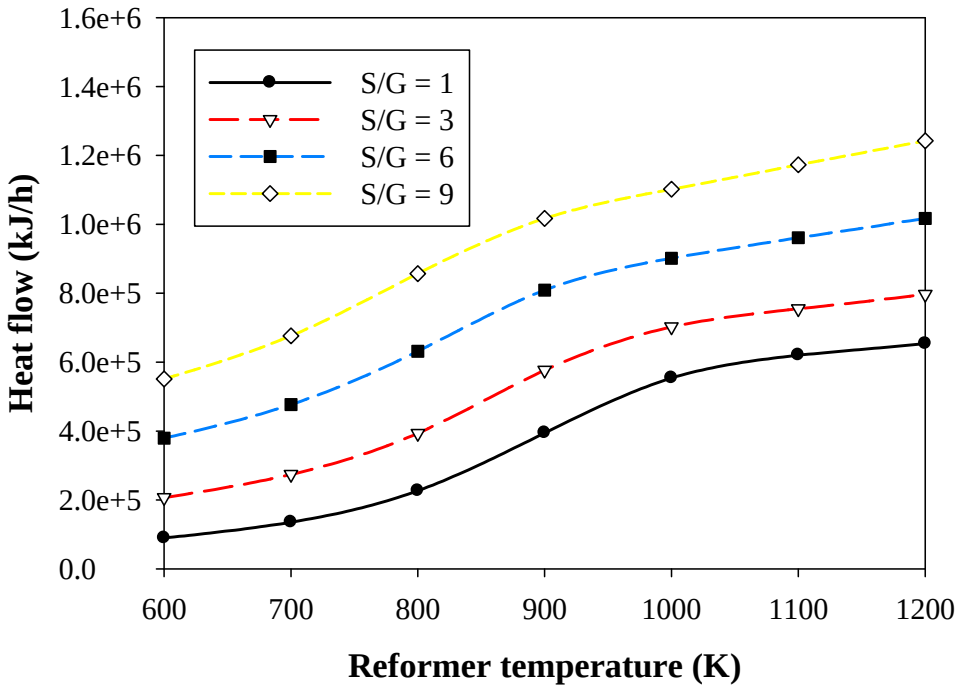

Figure 7.7 Heat flow of glycerol steam reforming at different steam to glycerol molar ratios.

Figure 7.8 indicates that the efficiency of the reformer increases as the reformate gas is allowed to contain more CO. This effect is due to increased hydrogen production. In addition, the results reveal that increasing the steam to glycerol ratio also enhances the reformer process efficiency. Apart from the increased hydrogen yield, operation at a high steam to glycerol ratio also causes the reformer to operate at a high temperature until reaching the limiting level of CO. Moreover, the external heat required for vaporization is reduced because the waste heat in the product stream can be recovered to preheat the reactant feeds. This reduction enhances the total efficiency of the reforming process. From Figure 7.8, the maximum efficiency of the reformer producing reformate gas with 5%CO is reached at a steam to glycerol ratio of 11-14. At this ratio, the operating temperature of the glycerol steam reformer is around 830-860 K (see Figure 7.3). When more steam is added, the reformer efficiency decreases because the external heat required to sustain the reformer is higher than the energy obtained from the hydrogen produced. In the case of a 1% CO tolerance, the reformer can reach its maximum efficiency if it is operated at a higher steam to glycerol molar ratio.

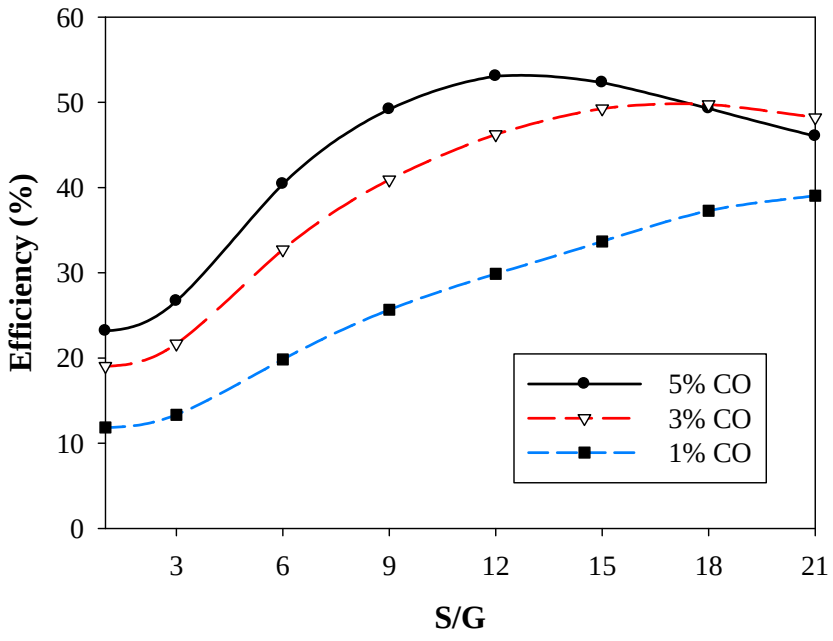

Figure 7.8 Efficiency of the glycerol steam reforming process at different %CO tolerances of HT-PEMFC.

7.3.2 Glycerol reforming process for HT-PEMFCs with water gas shift reactor

The quality of the reformate gas used in HT-PEMFCs differs from that used in LT-PEMFCs, and consequently, the optimal operating conditions of the reforming process would also be different. The sophisticate CO purification such as preferential oxidation, methanation or membrane separation can be eliminated in the fuel processor for HT-PEMFC. Therefore, glycerol reforming process comprising of reformer and water gas shift unit (GRP) is examined in this work. Water gas shift is added to the system in order to reduce CO fraction and increase hydrogen concentration. Figure 7.9 shows the amount of hydrogen obtained from the GRP operated under different temperatures (T_R) and steam to glycerol (S/G) ratios. The results indicate that the reformer temperature is the key factor to improve the hydrogen production, whereas the S/G ratio has a slight effect. When the GRP is operated under the S/G ratio of higher than 6 and the temperature of higher than 1000 K, the production of hydrogen is kept constant. It is found that the highest amount of hydrogen obtained from the GRP is very close to the maximum mole of hydrogen (7 moles) based on the reaction stoichiometry in Eq. (7.1).

Figure 7.10 shows the content of CO in the reformate gas when the reformer is operated at different temperatures and S/G ratios. It is found that at S/G > 6, the CO flowing out from the water gas shift unit in the GRP is lower than 0.5% for all operating reformer temperatures. An increase in the S/G ratio and the reformer temperature over such the conditions have an insignificant effect on the CO content. At S/G < 6, the operating temperature of the reformer affects the presence of CO; however, its concentration satisfies the desired specification of the reformate gas for HT-PEMFC. As a result, the reformate gas obtained from the GRP can be directly fed to the HT-PEMFC without further purification.

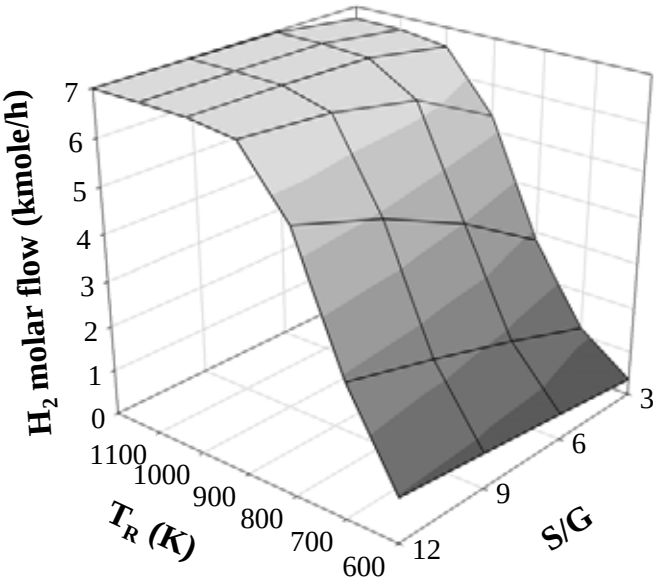

Figure 7.9 Hydrogen molar flow at different temperatures and steam to glycerol ratios.

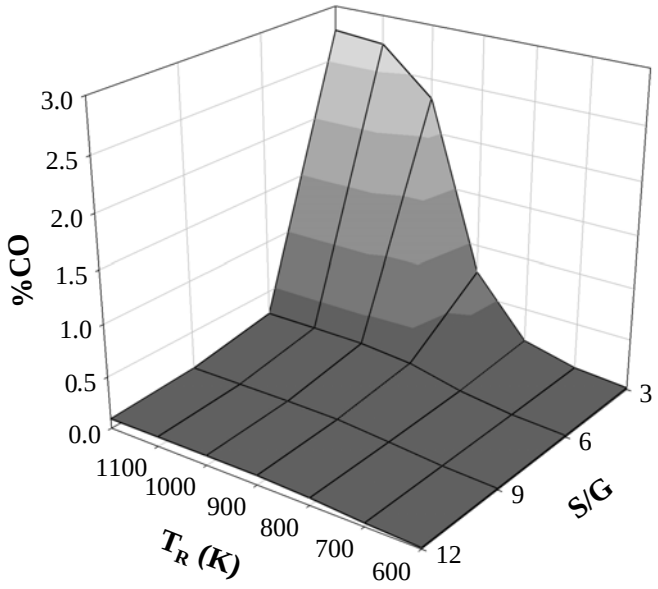

Figure 7.10 %CO in dry reformate gas at different temperatures and steam to glycerol ratios.

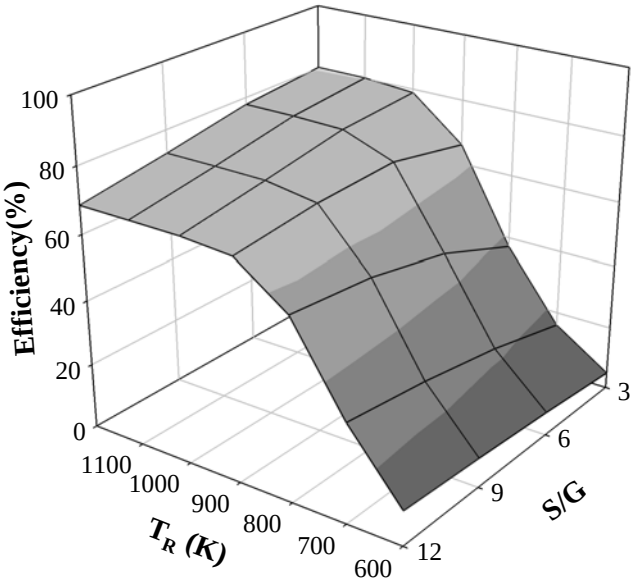

Figure 7.11 Efficiency of glycerol reforming process integrated with water gas shift reactor at different temperatures and steam to glycerol ratios.

The thermal efficiency of the GRP is demonstrated in Figure 7.11. The reformer operating temperature and S/G are the critical factor in achieving a high efficiency of the GRP. Although operation of the reformer with high S/G ratio provides more hydrogen content, it leads to a large energy consumption and thus decreases the efficiency of the GRP. The highest efficiency is about 80% at the S/G of 3-6 and the temperature of 1000-1200 K.

7.4 Conclusions

Hydrogen production from a glycerol steam reforming process without water gas shift unit for HT-PEMFCs was investigated in this study with the aim of determining the optimal hydrogen production conditions. At different %CO tolerances of HT-PEMFC, it was found that the glycerol steam reformer without water gas shift reactor can be operated at higher temperatures when a higher CO tolerance in the HT-PEMFC is allowed. An increase in the steam to glycerol ratio also enhances hydrogen production, but requires more energy. Considering the performance of the glycerol

steam reformer in terms of energy efficiency, the operation of the reformer at a steam to glycerol ratio of 11-14 produces the highest reformer efficiency when reformate gas containing 5%CO is considered. In addition, glycerol reformer integrated with water gas shift unit, which is operated at a temperature of 473 K, to maximize hydrogen yield and minimize CO for HT-PEMFC is also investigated to find optimal condition providing high efficiency. The simulation results showed that the glycerol reforming process is independent of the S/G ratio and the reformer temperature (T_R) when operated at S/G > 6 and T_R > 1000 K. The content of CO in all studied operational range satisfies the desired specification of the reformate gas for HT-PEMFC.

CHAPTER VIII

EFFICIENCY OF HT-PEMFC SYSTEM INTEGRATED WITH GLYCEROL REFORMER

8.1 Introduction

A proton exchange membrane fuel cell (PEMFC) offers one of the highest energy densities in comparison to the other type of fuel cells. Pure hydrogen or hydrogen-rich gas from reforming process is either used as fuel in PEMFC anodes. With the limitation of hydrogen storage and supporting infrastructure, a fuel cell integrated with a fuel processor allowing hydrogen generation from hydrocarbon fuels becomes an effective solution. However, the hydrogen-rich gas fed to PEMFC has to be highly purified in order to remove any traces of carbon monoxide (CO), which has a poisoning effect on the anode electro-catalyst, platinum, reducing its activity and consequently power output.

To date, a high temperature proton exchange membrane fuel cell (HT-PEMFC) operated at temperatures around 100-200 ^{o}C has been developed. At higher temperature operation, the amount of CO that adsorbs on Pt in a HT-PEMFC reduces. With elevated temperatures, the electrochemical reaction rates at the anode and cathode are increased and water management within PEMFC is also simplified (Pan et al., 2005; Yang et al., 2001). When the PEMFC is operated at the temperature above 100 $^{\circ}$C, water is only present in the vapor phase and for this reason, the flooding problem is solved and the transport of water becomes easy to balance (Shao et al., 2007). Although the operation of PEMFC at high temperatures can eliminate the flooding problem, it leads to the dehydration of membrane and loss of membrane ionic conductivity. Therefore, many researchers pay attention to develop the new membrane that can operate at temperature above 100 ^{o}C and has high conductivity at low humidity. A polybenzimidazole (PBI) was reported to be used in HT-PEMFC

because it can be operated at low relative humidity. However, PBI has lower proton conductivity than Nafion and thus it is doped with phosphoric acid or other dopants to increase the proton conductivity (Asensio et al., 2005; Li et al., 2009).

The higher temperature operation of PEMFC also offers the efficient utilization of waste heat from the fuel cell to preheat the fuel used or to supply to reforming processes. HT-PEMFCs are therefore advantageous to be used in conjunction with a fuel reformer, compared to low-temperature PEMFCs (Jespersen et al., 2009). As a consequence, the improvement of thermal management and the design of heat recovery for a HT-PEMFC system is an alternative option to enhance its efficiency. The theoretical analysis of a glycerol reformer and LT-PEMFC combined system without considering CO poisoning effect was investigated by Oliva et al. (2010). The maximum system efficiency is around 37.79% at cell pressure of 3 atm and power of 1 kW. Recently, Martin and Worner (2011) studied the efficiency of HT-PEMFC integrated with biodiesel and bioethanol reforming when the fuel cell efficiency of 40% was specified and the CO poisoning effect was not considered. They found that the system efficiency of biodiesel and bioethanol achieved were 30.2% and 30.5%, respectively.

Due to a high CO tolerance of HT-PEMFC, it is possible to directly use the reformate gas for HT-PEMFC without the requirement of complicate purification processes. In this study, the performance of a fuel processor and HT-PEMFC integrated system is examined. Glycerol, a by-product from biodiesel production, is considered a renewable fuel for hydrogen production via a steam reforming process (Martin and Worner, 2011). Since CO still has some effect on HT-PEMFC performance, a pseudo 2D model of HT-PEMFC that takes the effect of CO poisoning into account was used to analyze an efficiency of the HT-PEMFC system and power output with respect to various key operating parameters such as reformer temperature, steam to carbon ratio, fuel cell temperature and anode stoichiometric ratio. Finally, the optimal condition of the HT-PEMFC system that provides the maximum power density at a required efficiency is investigated.

8.2 A fuel processor and HT-PEMFC integrated system

The HT-PEMFC system considered here mainly consists of a glycerol steam reformer and a HT-PEMFC as shown in Figure 8.1. In general, to increase hydrogen yield in an endothermic steam reforming process, high operating temperature and excess steam are required. However, from our previous study (Authayanun et al., 2010), increasing the reformer temperature also increases the content of CO in the reformate gas obtained. With the aim to use the reformate gas directly from the glycerol steam reformer, the reformer temperature should be reduced to keep CO content in the acceptable level for HT-PEMFC. Excess steam is required to shift the equilibrium of the steam reforming reaction toward the hydrogen product side and will lead to lower CO content in the reformate gas. Although the performance losses from purification process can be eliminated from this system, the amount of energy to preheat excess steam, required to enhance hydrogen yield at low temperatures, also increases.

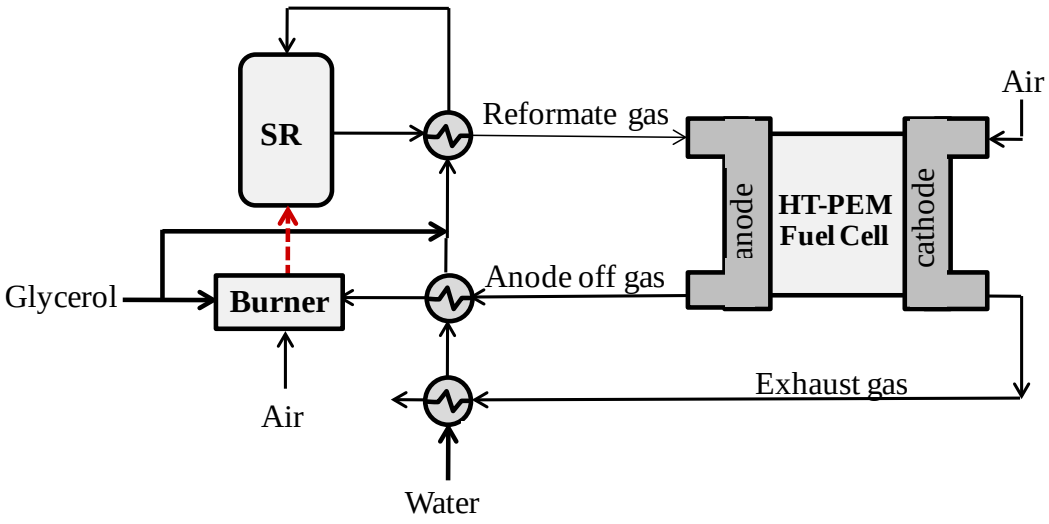

Figure 8.1 A fuel processor and HT-PEMFCs integrated system.

The improvement of thermal management within the HT-PEMFC system is an alternative option to enhance the system efficiency. To enhance efficiency of the integrated system, heat from hot reformate gas is recovered by preheating and vaporizing water and glycerol feeds. A portion of the glycerol is burnt to supply heat

to the steam reformer. Since the higher operating temperature of PEMFC offers the efficient utilization of waste heat from fuel cell, the anode off gas and the exhaust gas from the fuel cell are also used to preheat a water stream. The remaining fuel in the anode off gas is combusted in a burner in order to supply heat to the steam reformer.

8.3 Model of a HT-PEMFC system

8.3.1 Reformer

The main reaction that occurs in the steam reformer is glycerol steam reforming, whereas the side reactions are water gas shift, methanation and methane dry reforming. The equilibrium composition of the reformate gas obtained from the steam reforming system of glycerol is calculated from the direct minimization of the Gibbs free energy. Due to no coke formation occurring at all operational range of this study, the primary components consist of $C_3H_8O_3$, H_2O, CO, CO_2, H_2 and CH_4.

8.3.2 HT-PEMFC

In this study, the pseudo 2D model is applied for HT-PEMFC in which the PBI doped phosphoric acid membrane is used as an electrolyte. The mass transport in the flow channel is taken into account to investigate CO and hydrogen distributions along the flow direction while the mass transport in a gas diffusion layer and thin film electrolyte is considered only in the diffusion flux direction. As explained in Chapter IV, the following assumptions have been made: HT-PEMFC is operated at steady state and isothermal operations, ideal gas law is assumed, all gases cannot permeate through the membrane electrolyte, pressure drop is negligible and operating cell voltage is constant along the cell coordinate.

8.3.2.1 Flow channel

In the flow channel, the molar flow of each gas will be changed by the electrochemical reactions as given in Eqs. (8.1)-(8.3). At the anode side, the hydrogen molar flow decreases when the reactions take place. This generally causes an increase in the CO mole fraction and therefore, the CO poisoning effect on the HT-PEMFC performance is more pronounced, especially at the end of the flow channel.

$$\frac{dM_{H_2}}{dx} = -h\left(\frac{i}{2F}\right) \tag{8.1}$$

$$\frac{dM_{O_2}}{dx} = -h\left(\frac{i}{4F}\right) \tag{8.2}$$

$$\frac{dM_{H_2O}}{dx} = h\left(\frac{i}{2F}\right) \tag{8.3}$$

The set of ordinary differential equations explaining the distribution of gaseous components along the flow channel of HT-PEMFC is solved and used to calculate the mole fraction of reactants at the flow channel/gas diffusion layer interface.

8.3.2.2 Gas diffusion layer

The Stefan Maxwell is used to calculate the molar fraction of gaseous reactants in the gas diffusion layer (GDL) of the porous electrodes as:

$$\frac{dX_i}{dz} = \frac{RT}{P}\sum \frac{X_i N_j - X_j N_i}{D_{ij}^{eff}} \tag{8.4}$$

The components at the anode consist of H_2, CO, CO_2 and CH_4 while the cathode components compose of O_2, N_2 and H_2O. The boundary conditions are as follows:

At anode: $N_{CO_2,g} = 0$, $N_{CO_2,g} = 0$, $N_{H_2,g} = \frac{j}{2F}$, $N_{CH_4,g} = 0$, $N_{H_2O,g} = 0$

At cathode: $N_{N_2,g} = 0$, $N_{O_2,g} = \frac{j}{4F}$, $N_{H_2O,g} = \frac{-j}{2F}$

The set of equations (Eq. (8.4)) can be integrated to determine the composition of gaseous reactants at the interface between electrode and electrolyte film.

8.3.2.3 Film electrolyte model

The PBI doped phosphoric acid membrane is used as electrolyte in this model. To find H_2 and O_2 concentrations at the catalyst intersurface, Fick's law for diffusion is applied (Eqs. (8.5)-(8.6)). Reactant gases need to diffuse through electrolyte film layer covering before arriving at the catalyst active surface (Mamlouk et al., 2011).

$$\frac{N_{H_2}}{S_{Pt-anode}} = \frac{-D_{H_2}^{H_3PO_4}\left(C_{H_2-Pt} - C_{H_2(dissolve)}\right)}{\delta_{anode}} \tag{8.5}$$

$$\frac{N_{O_2}}{S_{Pt-cathode}} = \frac{-D_{O_2}^{H_3PO_4}\left(C_{O_2-Pt} - C_{O_2(dissolve)}\right)}{\delta_{cathode}} \tag{8.6}$$

The concentration of H_2 and O_2 dissolving at film electrolyte layer boundary can be calculated from their solubility ($C_i^{dissolved}$) as follows:

$$C_{H_2(dissolve)} = C_{H_2}^{dissolved} \cdot X_{H_2} \cdot P \tag{8.7}$$

$$C_{O_2(dissolve)} = C_{O_2}^{dissolved} \cdot X_{O_2} \cdot P \tag{8.8}$$

where X_{H_2} and X_{O_2} are the mole fraction of H_2 and O_2 at GDL/electrolyte film interface.

It is noted that the oxygen solubility can be calculated from the correlation reported by Mamlouk et al. (2011) whereas the hydrogen solubility is assumed to be the same value with the oxygen solubility.

8.3.2.4 Electrochemical model

Cell voltage (V_{cell}) can be calculated by starting with the cell reversible potential (E_{rev}), the maximum voltage that can be achieved by fuel cells at specific operating condition, and then subtracting by the various voltage losses as:

$$E_{\text{cell}} = E_r - \eta_{\text{act},c} - \eta_{\text{act},a} - \eta_{\text{ohmic}} \tag{8.9}$$

The reversible cell potential is described by Nernst equation in Eq. (8.10)

$$E_r = -\left(\frac{\Delta H_T}{nF} - \frac{T\Delta S_T}{nF}\right) + \frac{RT}{nF}\ln\left[\frac{(RT)^{1.5} C_{\text{H}_2-\text{Pt}} C_{\text{O}_2-\text{Pt}}^{0.5}}{a_{\text{H}_2\text{O}}}\right] \tag{8.10}$$

where $a_{\text{H}_2\text{O}} = \frac{P_{\text{H}_2\text{O}}}{P^*_{\text{H}_2\text{O}}} = \frac{RH\%}{100}$.

The activation loss is calculated from Butler Volmer equation (Eqs. (8.11)-(8.12)).

$$i_a = i_{0,a}\left(\exp\left(\frac{-\alpha_{\text{Rd},a}F}{RT}\left(\eta_{\text{act},a}\right)\right) - \exp\left(\frac{-\alpha_{\text{Ox},a}F}{RT}\left(\eta_{\text{act},a}\right)\right)\right) \tag{8.11}$$

$$i_c = i_{0,c}\left(\exp\left(\frac{-\alpha_{\text{Rd},c}F}{RT}\left(\eta_{\text{act},c}\right)\right) - \exp\left(\frac{-\alpha_{\text{Ox},c}F}{RT}\left(\eta_{\text{act},c}\right)\right)\right) \tag{8.12}$$

where $i_0 = i_0^{\text{ref}} a_c L_c \left(\frac{C_{\text{Pt}}}{C_{\text{Pt}}^{\text{ref}}}\right)^{\gamma} \exp\left[-\frac{E_c}{RT}\left(1 - \frac{T}{T_{\text{ref}}}\right)\right]$

If the fuel used at the anode is not pure hydrogen and have some CO contamination, it is necessary to take in account CO poisoning effect by using i_0^{CO} (the exchange current density of hydrogen oxidation in the presence of CO) instead of i_0 at the anode. The i_0^{CO} can be calculated from CO coverage (θ_{CO}) assuming bridge model of CO adsorption on Pt as follows:

$$i_0^{CO} = i_0 \left(1 - \theta_{CO}\right)^2 \tag{8.13}$$

The CO coverage in Eq. (16) is developed from experimental data reported by Li et al. [11] to explain a CO poisoning effect on HT-PEMFC in case of the reformate gas containing high CO content (3-10%) and can be described as follows:

$$\theta_{CO} = a \cdot \ln\frac{[CO]}{[H_2]} + b \cdot \ln(i) \cdot \ln\frac{[CO]}{[H_2]} + c \tag{8.14}$$

$$a = -0.00012784 \cdot T^2 + 0.11717499 \cdot T - 26.62908873$$

$$b = 0.0001416 \cdot T^2 - 0.12813608 \cdot T + 28.852463626$$

$$c = -0.00034886 \cdot T^2 + 0.31596903 \cdot T - 70.11693333$$

The CO poisoning model for HT-PEMFC was validated against experimental data (Li et al., 2003) at different fractions of CO in hydrogen-rich gas and operating temperatures. Due to low performance loss from CO_2 and methane, they effect on anode kinetic of HT-PEMFC can be neglected (Li et al., 2003; Sustersic et al., 1980).

The ohmic loss is caused by a resistance of ions in the electrolyte through membrane. This loss can be expressed as:

$$\eta_{ohmic} = \left(\frac{\sigma_m}{l_m}\right) i \tag{8.15}$$

The proton conductivity as a function of temperature and relative humidity obtained from Mamlouk et al. (2011) is represented by Eqs. (8.16)-(8.18).

$$\sigma_m = \frac{A}{T}\exp\left(\frac{-B}{R(T)}\right) \tag{8.16}$$

$$A = \exp\left(\left(k_1^a RH^3\right) + \left(k_2^a RH^2\right) + \left(k_3^a RH\right) + k_0^a\right) \tag{8.17}$$

$$B = \left(k_1^b RH^3\right) + \left(k_2^b RH^2\right) + \left(k_3^b RH\right) + k_0^b \tag{8.18}$$

8.3.2.5 Numerical solution of HT-PEMFC

The numerical solution of pseudo 2D model of HT-PEMFC model is shown in flow diagram in Figure 8.2. To study the performance of cell and gas distribution along the flow channel, the desired value of cell voltage (V_{cell}) and stoichiometric ratio (S) is defined and input into the program. The gas compositions at flow channel, gas diffusion layer, film electrolyte and catalyst surface are calculated and then the electrochemical model which represents relation of voltage, individual loss and current density is solved.

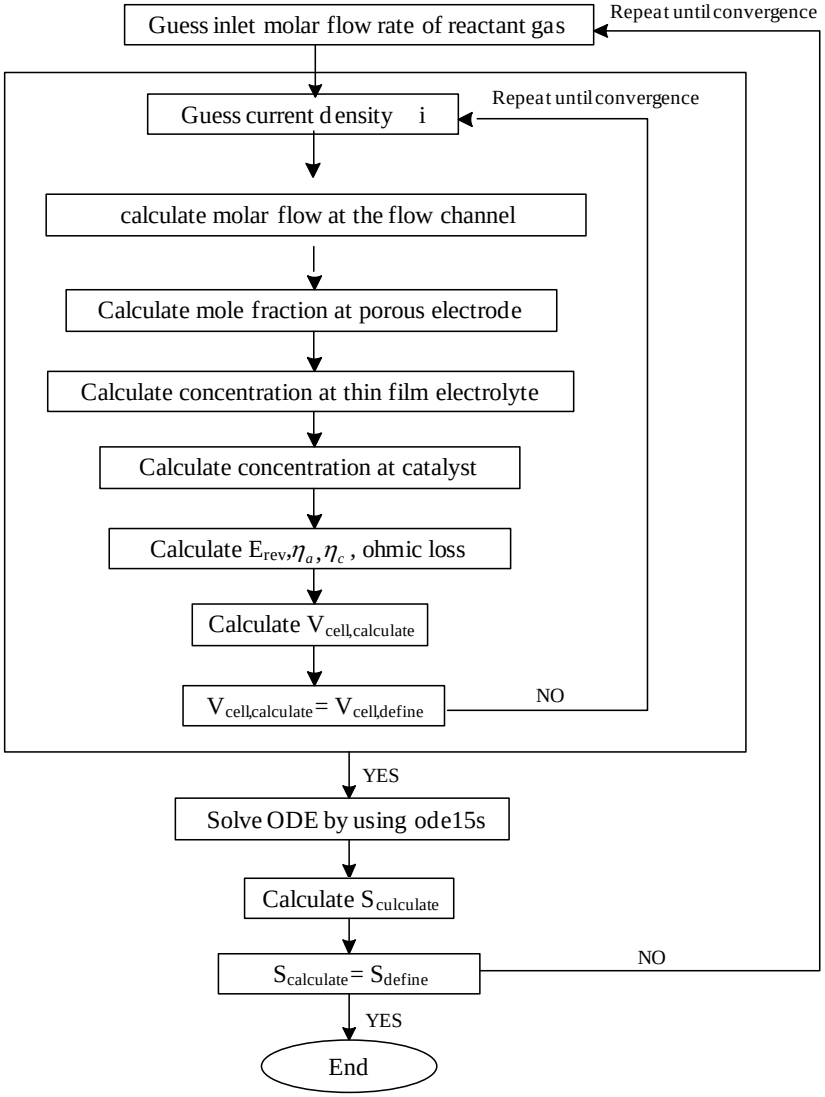

Figure 8.2 Flow diagram of numerical solution for two-dimensional analysis of HT-PEMFC.

8.3.3 Efficiency of HT-PEMFC system

To improve system efficiency, the heat from product stream of reformer, anode and cathode exhaust gases are recovered by using heat exchangers. Typically, the outlet temperature of reformer is about 800-1000 K; however, operating temperature of HT-PEMFC is 373-473 K. Therefore, the reformate gas needs to be cooled before entering the fuel cell. The heat recovery will be utilized to preheat and vaporize reactant of reformer and water. Similarly, heat from the anode and the cathode exhaust gases is also recovered to preheat reactants. Due to some heat losses occurring in the heat transfer process, the efficiency of heat exchanger is specified at 85%. Energy balance based on enthalpy changes in inlet and outlet of hot and cold streams is performed. Also, the remaining un-spent fuel in the anode exhaust gas (stoichiometic ratio > 1) is utilized by combusting in a burner in order to sustain heat for the reformer.

The efficiency of the fuel processing process (η_{FP}) can be calculated by the ratio of the heating value of hydrogen produced and the total energy used for steam reforming process as follows:

$$\eta_{FP} = \frac{LHV_{H_2} \cdot \left(M_{H_2}\right)}{LHV_{fuel} \cdot \left(M_{fuel}\right) + Q_{ref} - Q_{rec}} \times 100 \qquad (8.19)$$

where M_{H_2} is the molar flow rate of H_2 and M_{fuel} is the molar flow rate of fuel used for producing hydrogen, Q_{ref} is the energy required for the steam reforming process accounting for the heat of vaporization, sensible heat to heat up the reactants to the desired temperature and the heat needed for maintaining the reformer at an isothermal operation level and Q_{rec} is the recovered heat from anode and cathode off gas as well as high temperature product gas coming out of the glycerol reformer.

The thermal efficiency of fuel cell is evaluated by considering the electric power density and the lower heating value of H_2 (LHV_{H_2}) as:

$$\eta_{FC} = \frac{P_{FC}}{M_{\mathrm{H_2}} \cdot LHV_{\mathrm{H_2}}} \tag{8.20}$$

For a fuel processor and fuel cell integrated system, the system efficiency can be calculated as follows:

$$\eta_{sys} = \eta_{FP}\eta_{FC} \tag{8.21}$$

8.4 Results and discussion

The mathematical models of a HT-PEMFC system integrated with a glycerol steam reforming process were programmed using Matlab. The fsolve function was employed to solve the set of non-linear thermodynamic equations of the glycerol reforming process. The ordinary differential equations explaining reactant distributions along the flow channel length of the HT-PEMFC were solved by using the ODE45 function. Stefan Maxwell equation was integrated and changed from ordinary differential equation to algebraic equation, which is solved to give the gas composition at the interface between electrode and electrolyte film. The parameters used in this simulation are described in Table 8.1. Performance of the fuel cell system is analyzed with respect to key operating parameters such as reformer temperature, steam to carbon ratio (S/C), fuel cell temperature, and anode stoichiometric ratio. The cell voltage and system efficiency at different conditions are investigated.

In the case of HT-PEMFC integrated with glycerol reforming, the anode fuels not only consist of H_2 and CO but also contain some amount of CO_2 and CH_4. The composition of glycerol reformate gas varies depending on the operational condition of glycerol reforming process. This composition will have considerable effect on the HT-PEMFC performance. The hydrogen and CO fractions at different reformer temperatures and S/C ratios from glycerol reforming process are shown in Table 8.2 and Table 8.3, respectively. The hydrogen fraction increase with increasing the temperature and the S/C ratio, whereas the CO fraction decreases when the S/C ratio increases and the temperature falls. The CO fraction in the synthesis gas obtained

from of the steam reforming of glycerol in the operational range considered is about 2-9% while the hydrogen fraction is 59-68%.

Table 8.1 Model parameters used in the simulation of the HT-PEMFC system (Mamlouk et al., 2011)

Parameters	Value	Unit
Operating pressure at anode, P_a	1	atm
Operating pressure at anode, P_c	1	atm
Faraday constant, F	96485	C mol^{-1}
Gas constant, R	8.314	m
Channel height, h	0.01	m
Channel length, x	0.1	m
GDL thickness, z	0.0002	m
Membrane thickness, l_m	4×10^{-5}	m
Anode film thickness , δ_{anode}	2.5×10^{-9}	m
Cathode film thickness , $\delta_{cathode}$	1.48×10^{-9}	m
Anode reference exchange current density, $i_{0,a}^{ref}$	1440	A m^{-2}
Cathode reference exchange current density, $i_{0,c}^{ref}$	0.0004	A m^{-2}
Anode catalyst surface area, $a_{c,a}$	64	m^2 g^{-1}
Cathode catalyst surface area, $a_{c,c}$	32.25	m^2 g^{-1}

Parameters	Value	Unit
Anode catalyst loading, $L_{c,a}$	0.2	mg cm^{-2}
Cathode catalyst loading, $L_{c,c}$	0.4	mg cm^{-2}
Transfer coefficient at anode, α_a	0.5	-
Transfer coefficient at cathode, α_c	0.75	-
Reaction order, γ	1.375	-
Anode reference concentration, $c_{\text{ref},a}$	0.0002	mol cm^{-3}
Cathode reference concentration, $c_{\text{ref},c}$	0.0004	mol cm^{-3}
Anode activation energy, $E_{c,a}$	16900	J $mole^{-1}$ K^{-1}
Cathode activation energy, $E_{c,c}$	72400	J $mole^{-1}$ K^{-1}
Anode reference cell temperature, $T_{\text{ref},a}$	433.15	K
Cathode reference cell temperature, $T_{\text{ref},c}$	373.15	K
Lower heating value of glycerol , $\text{LHV}_{\text{glycerol}}$	1564.9	kJ mol^{-1}

Table 8.2 Hydrogen fraction in the synthesis gas obtained from glycerol reforming process

Reformer temperature (K)	Steam to carbon ratio (S/C)				
	3	4	5	6	7
800	0.5963	0.6305	0.6524	0.6666	0.6759
900	0.6624	0.6735	0.6797	0.6835	0.6860

Table 8.3 Carbon monoxide fraction in the synthesis gas obtained from glycerol reforming process

Reformer temperature (K)	Steam to carbon ratio (S/C)				
	3	4	5	6	7
800	0.0424	0.0360	0.0311	0.0273	0.0241
900	0.0917	0.0726	0.0597	0.0506	0.0438

The reformate gases obtained from the glycerol reformer will be fed to the HT-PEMFC after cooling (heat transfer) by reformer reactants. The H_2 and CO distribution along the flow channel at different operating condition of glycerol reforming is shown in Figures 8.3 and 8.4. Hydrogen in the anode flow channel is consumed and its molar fraction decreased and consequently, CO molar ratio will increase along the channel length, especially at the end of channel. The hydrogen and CO fraction at the anode's exhaust of HT-PEMFC is shown in Table 8.4. It was found that the CO fraction at the end of anode's flow channel can become very high up to 17% (from ca. 9% at the inlet) at high reformer temperature and low stoichiometric ratio.

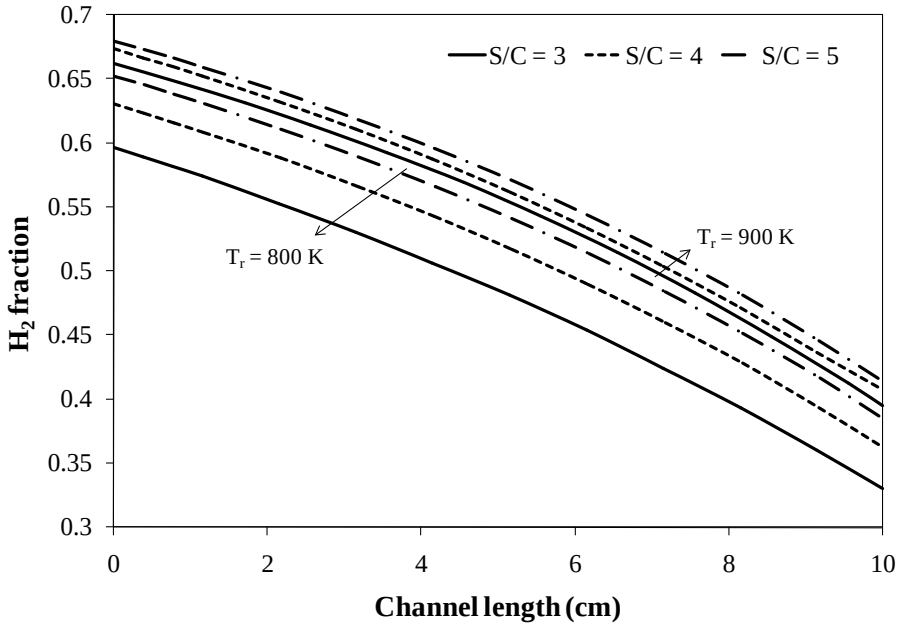

Figure 8.3 Hydrogen fraction along the channel length of HT-PEMFC at different steam to carbon ratios (S/C).

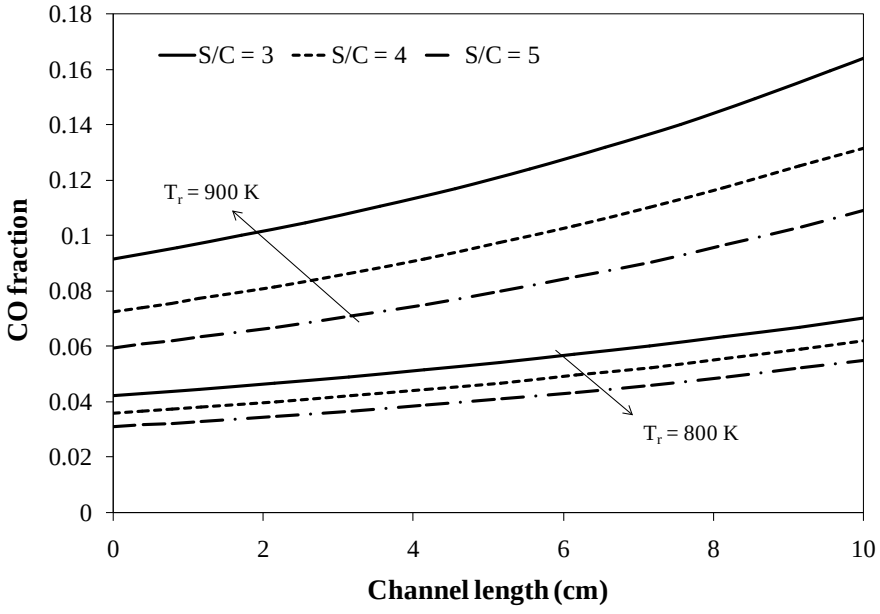

Figure 8.4 CO fraction along the channel length of HT-PEMFC at different steam to carbon ratios (S/C).

The performance of HT-PEMFC at different %CO is shown in Figure 8.5. It is found that at cell temperature of 448.15 K, the CO<5% has insignificant loss on HT-PEMFC at studied voltage range. For cell temperature of 423.15 K, the significant loss is observed at voltage less than 0.6. For the integrated system of glycerol reforming and HT-PEMFC, the performance of HT-PEMFC is evaluated by varying the H_2 and CO concentrations, which depend on reformer temperature and steam to glycerol ratio. For a cell temperature of 423.15 K and reformer temperature of 800 K (Figure 8.6(a)), it is observed that CO has a small effect on HT-PEMFC performance at low current densities. The CO poisoning effect becomes more pronouced at high current densities (above 500 A m^{-2}). However, when the reformer is operated at temperature of 900 K (Figure 8.6(b)), CO has dramatic effect on cell performance at all range of current density. This is because of the large CO fraction up to 10% in hydrogen-rich gas at this reformer operation. Similar cell performance is obtained at low current densities (typical operating condition above 0.6 V) when the cell temperature is increased to 448.15 K (Figure 8.7). This is due to the increased CO tolerance of HT-PEMFCs at high temperatures. On the other hand, the cell voltage drop still appear at high current densities when steam to carbon ratio decreases or reformer temperature increases. A minimum limit of S/C of 4 should be set for this system to stop the irreversible loss of cell performance. A S/C ratio of 3 and reformer temperature of 900 K have a strong effect on the cell polarization curve, not only when the cell is operating at 423.15 K but also at 448.15 K. This is caused by very high CO ratio of 17% at the end of anode's channel.

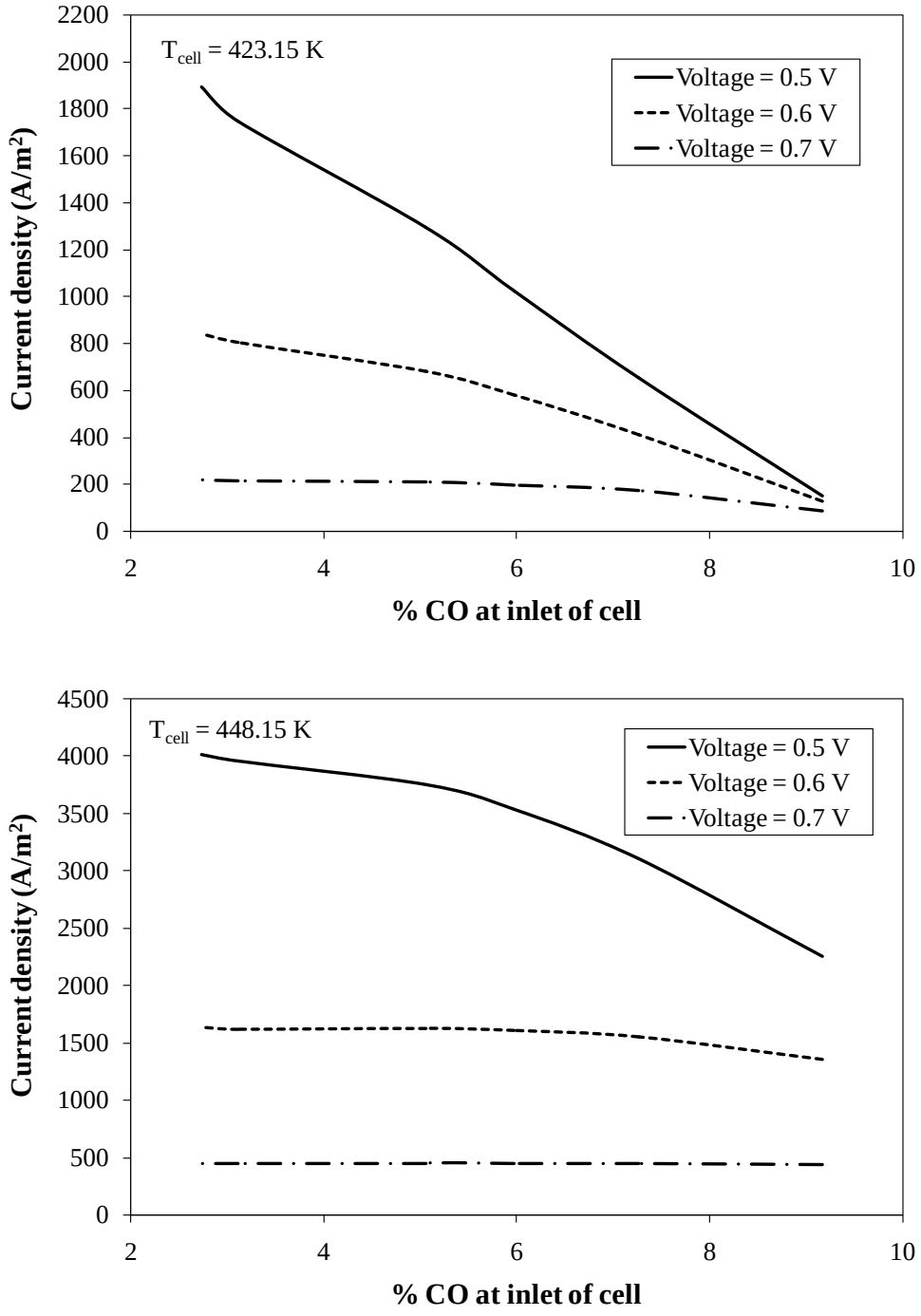

Figure 8.5 The influence of CO on the HT-PEMFC performance.

Table 8.4 Hydrogen and carbon monoxide fractions at the outlet of the HT-PEMFC

Reformer temperature (K)	S_a = 1.2				S_a = 1.3				S_a = 1.4			
	Steam to carbon ratio (S/C)				Steam to carbon ratio (S/C)				Steam to carbon ratio (S/C)			
	4	5	6	7	4	5	6	7	3	4	5	6
Hydrogen												
800	0.2215	0.2383	0.2499	0.2579	0.2826	0.3022	0.3157	0.3249	0.2968	0.3278	0.3490	0.3636
900	0.2559	0.2613	0.2647	0.2670	0.3226	0.3287	0.3326	0.3352	0.3592	0.3709	0.3774	0.3816
CO												
800	0.0759	0.0683	0.0614	0.0552	0.0699	0.0625	0.0560	0.0502	0.0738	0.0655	0.0583	0.0520
900	0.1655	0.1377	0.1175	0.1023	0.1494	0.1252	0.1066	0.0927	0.1741	0.1399	0.1161	0.0988

(a)

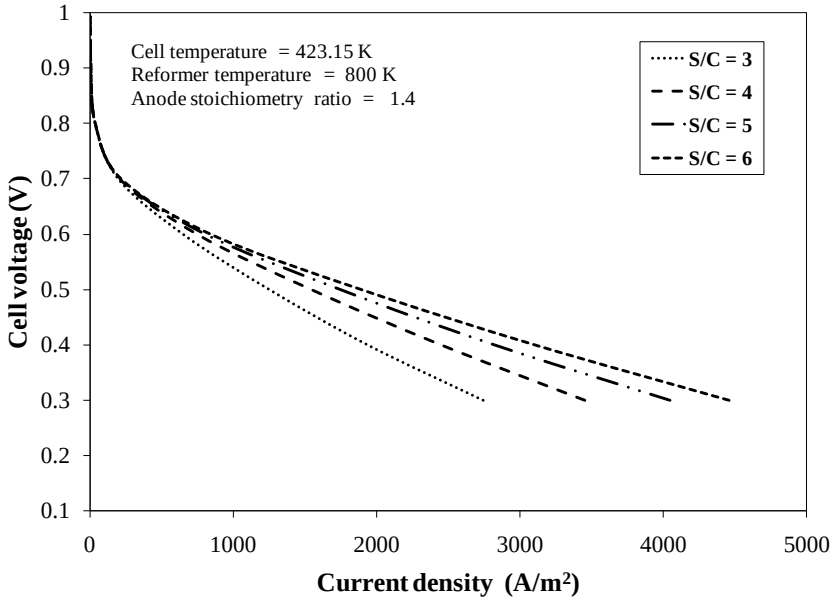

(b)

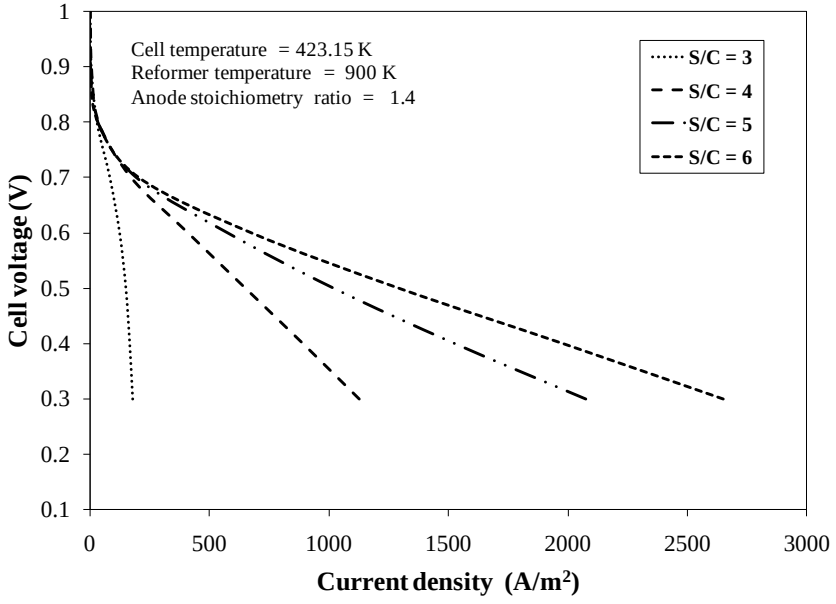

Figure 8.6 Polarization curve of HT-PEMFC at different operating steam to glycerol ratios of glycerol reforming process (HT-PEMFC temperature = 423.15 K).

(a)

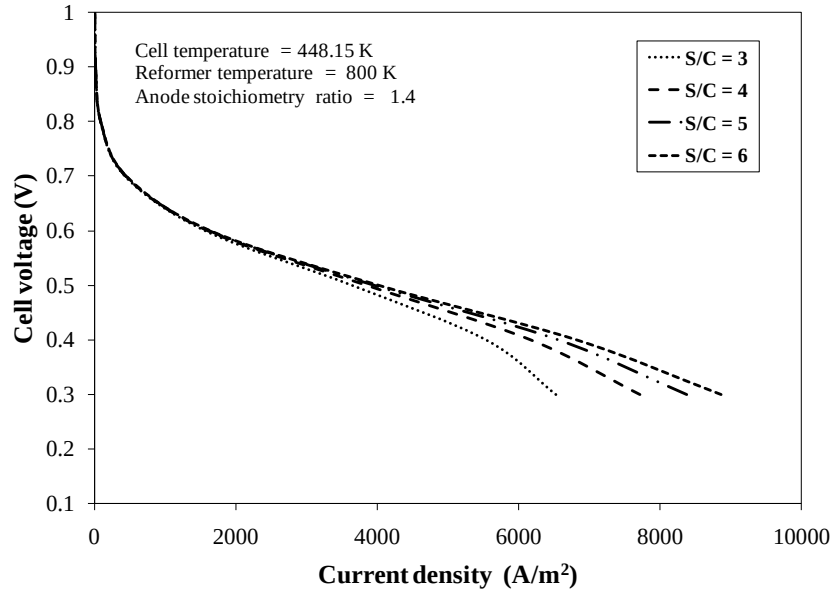

(b)

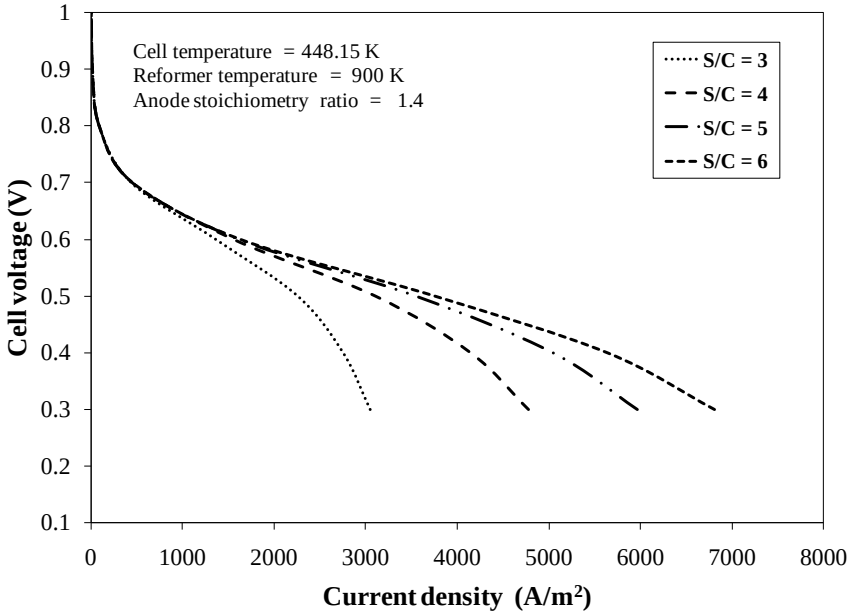

Figure 8.7 Polarization curve of HT-PEMFC at different operating steam to glycerol ratios of glycerol reforming process (HT-PEMFC temperature = 448.15 K).

The efficiency of integrated system is shown in Figure 8.8 and Figure 8.9. To enhance the overall efficiency, the heat recovery from anode and cathode exhaust gases is taken into account. At cell temperature of 423.15 and reformer temperature of 800 K (Figure 8.8(a)), the system efficiency remains similar at low current densities (up to 1000 A m^2) when the S/C ratio changed from 4 to 6. At high current densities, increasing S/C ratio provides enhancement in the overall system efficiency despite the energy loss to vaporize more steam. On the other hand, when the reformer temperature raised to 900 K, lower S/C gave higher system efficiency at low current densities (less than 500 A m^2) (Figure 8.8(b)), while high S/C operation provided higher efficiency at high current densities. The high amount of S/C required more energy to preheat and generate steam, however, higher steam content will lead to lower CO content in the anode feed leading to lower anode losses, particularly at high current densities. Therefore, an increase in S/C improves the integrated system efficiency at high current densities. For cell temperature of 448.15 K (Figure 8.9), the increase of CO tolerance at the anode led to an insignificant effect of S/C ratio in the range of 3 to 6 on system efficiency at current densities up to 4000 A m^2 when the reformer temperature was 800 K. With reformer temperature at 900 K, the low steam to carbon ratio provided higher overall system efficiency at low current densities in comparison to high S/C ratio, however, the case reverses quickly when the current density increased and CO poisoning effect became more pronounced.

(a)

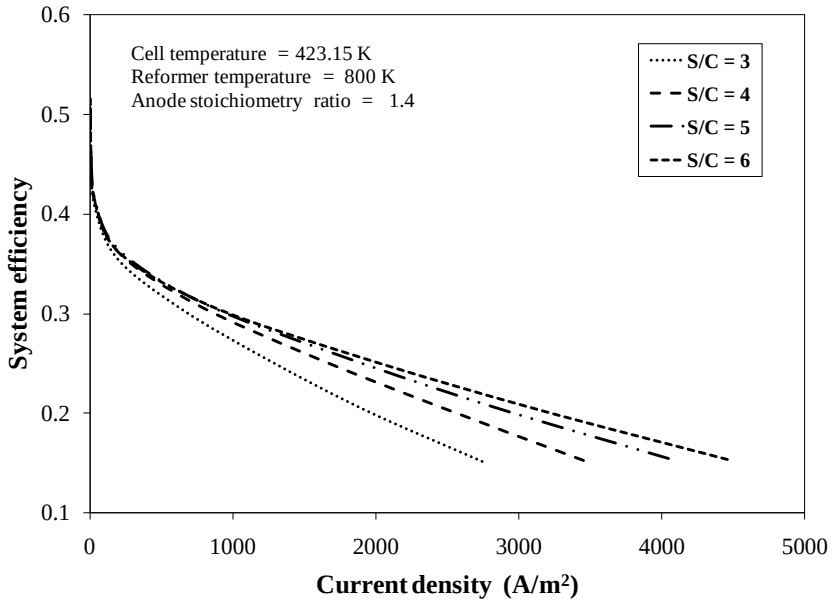

(b)

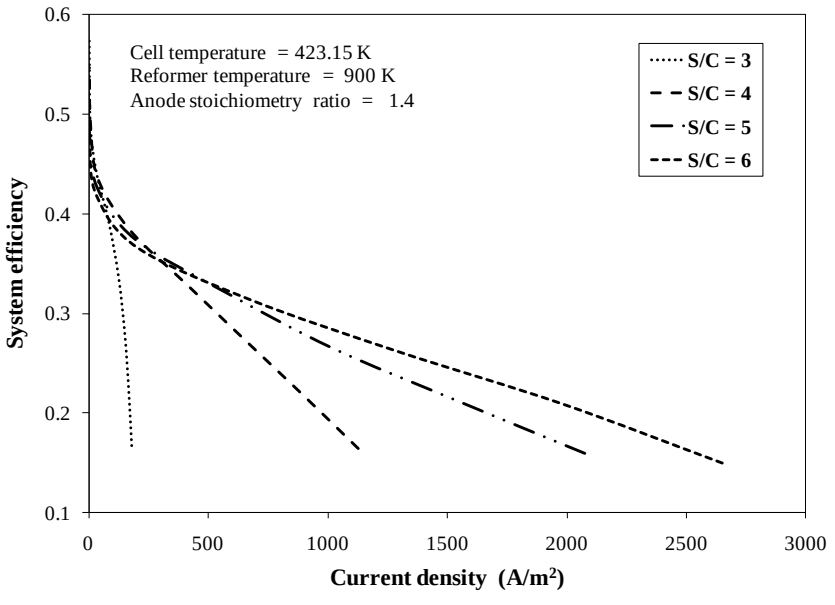

Figure 8.8 Efficiency of the fuel processor and HT-PEMFC integrated system at different operating steam to glycerol ratios of glycerol reforming process (HT-PEMFC temperature = 423.15 K).

(a)

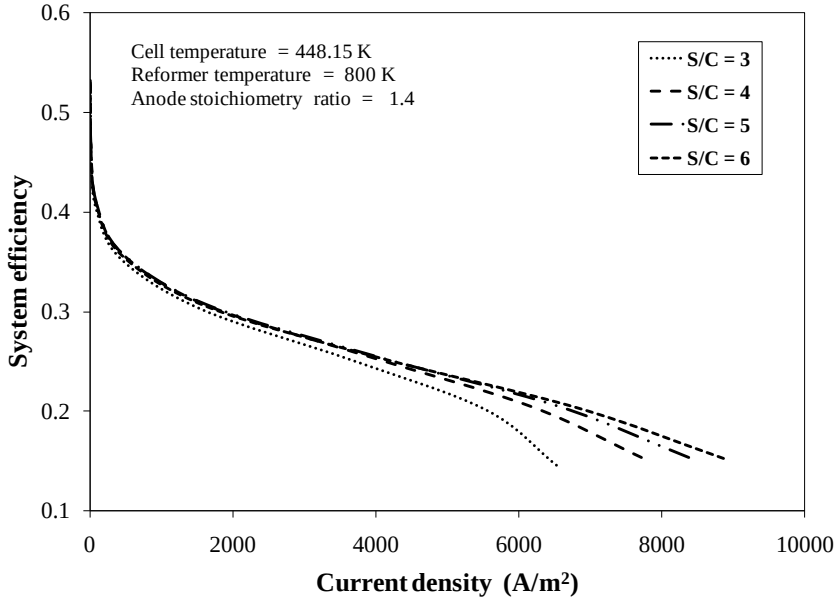

(b)

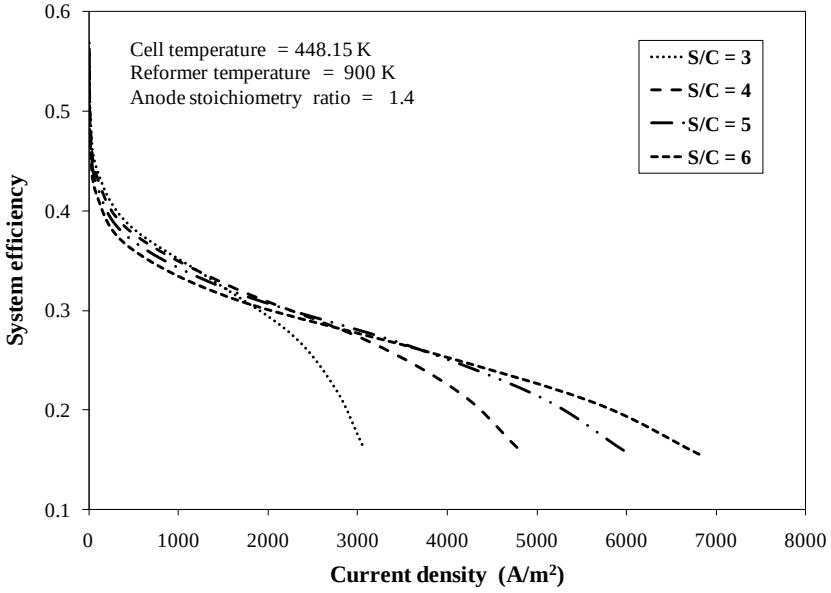

Figure 8.9 Efficiency of the fuel processor and HT-PEMFC integrated system at different operating steam to glycerol ratios of glycerol reforming process (HT-PEMFC temperature = 448.15 K).

Figs. 8.10(a)-(b) show the effect of stoichiometric ratio on cell performance and system efficiency when the reformer temperature and S/C are 900 K and 4, respectively. At low stoichiometric ratio, hydrogen will be depleted faster and the CO fraction will increase faster along the flow channel significantly increasing the CO poisoning. As expected, the cell performance declines with decreased stoichiometric ratio (Figure 8.10(a)). The low stoichiometric ratio provides higher system efficiency at low current densities (where CO impact is small), while the high stoichiometric ratio operation leads to higher system efficiency at higher current densities (see Figure 8.10(b)). However, it should be noted that the low stoichiometric ratio may provide higher efficiency over the entire current density range when using low reformer temperature (800 K) and high S/C ratio.

(a)

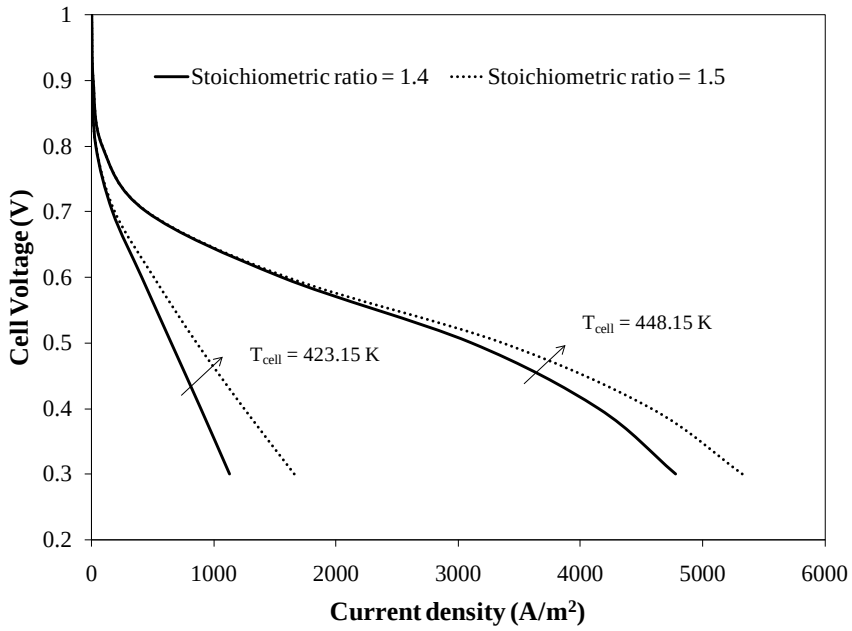

(b)

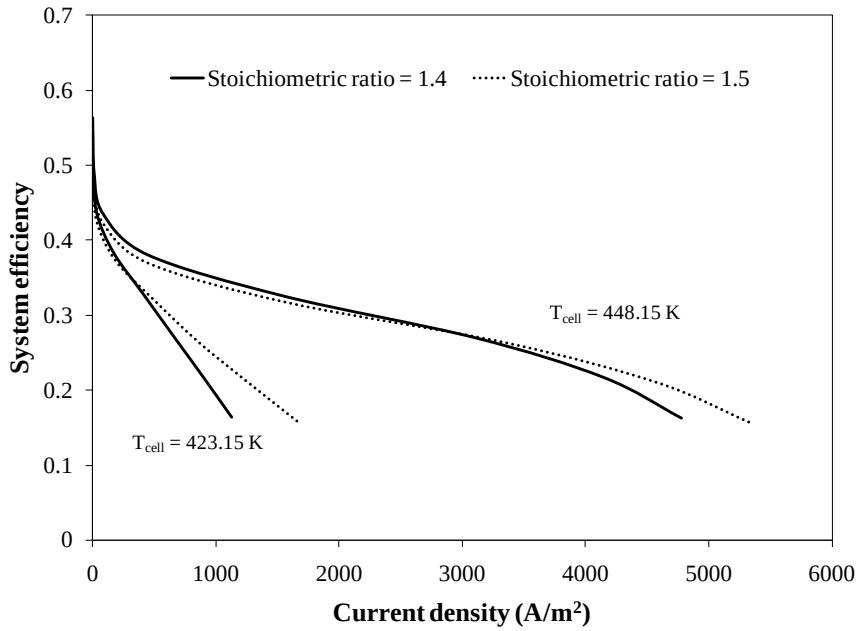

Figure 8.10 Effect of stoichiometric ratio on HT-PEMFC performance and system efficiency.

From the simulation results, the system efficiency is about 30-40% at cell voltage range of 0.55-0.75. The system efficiency achieved is in the same range when compared with the HT-PEMFC system with bioethanol and biodiesel reformers (Martin, and Worner, 2011). To find the optimal operating condition for the HT-PEMFC system integrated with glycerol reforming at a given efficiency of 35%, the power density at different reformer temperatures and S/C ratios is calculated and presented in Figure 8.11 and Figure 8.12 for cell temperatures of 423.15 and 448.15 K, respectively. It is observed that the achieved power of the system at reformer temperature of 800 K is higher than at 900 K for cell temperature of 423.15 (see Figure 8.11) because the amount of CO is over the tolerance of HT-PEMFC at this cell temperature. However, when the cell temperature increases and thus the CO tolerance of HT-PEMFC increases, the HT-PEMFC system, operated at the reformer temperature of 900 K, provides higher power density than that of 800 K (see Figure 8.12). From Figure 8.12, it is found that the conditions that provide the maximum power density are reformer temperature of 800 K, S/C ratio of 6 and anode

stoichiometric ratio of 1.2. For cell temperature of 448.15 in Figure 8.12, the maximum power density is achieved at a reformer temperature of 900 K, S/C ratio of 4 and anode stoichiometric ratio of 1.3.

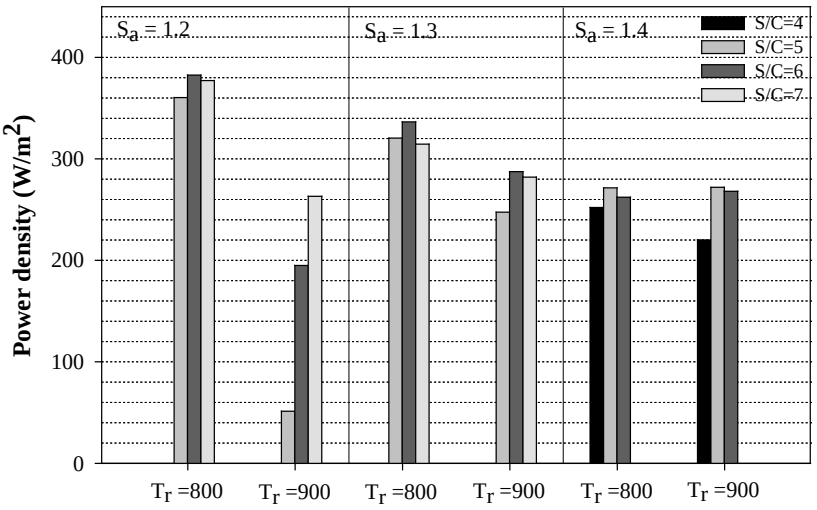

Figure 8.11 Power density of HT-PEMFC (T_{cell} = 423.15 K) at different reformer temperatures and S/C when the system efficiency is fixed at 35% and $L_{c,c}$ = 0.5.

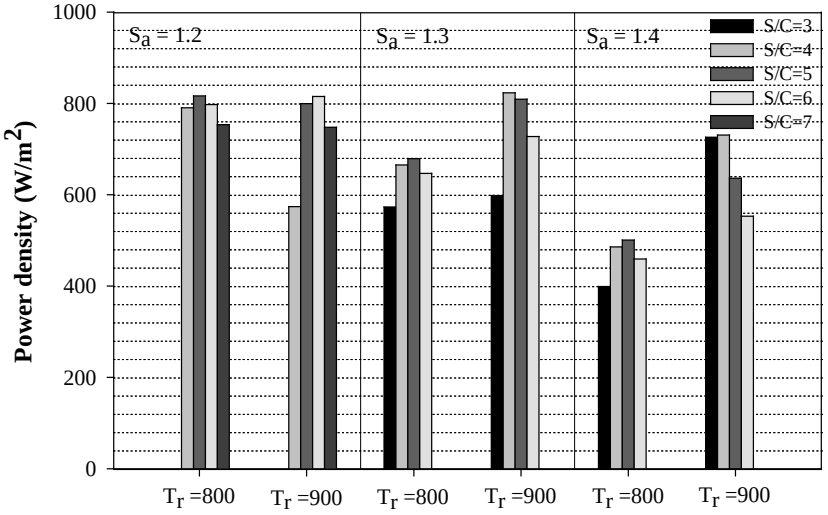

Figure 8.12 Power density of HT-PEMFC (T_{cell} = 448.15 K) at different reformer temperatures and S/C when the system efficiency is fixed at 35% and $L_{c,c}$ = 0.5.

8.5 Conclusions

The HT-PEMFC integrated with glycerol steam reforming was investigated in this study by analyzing the CO poisoning effect on system efficiency. The hydrogen and CO compositions of reformate gas obtained from the glycerol reforming were varied by changing reformer temperature (800-900 K) and steam to carbon (S/C) ratio (3-7). It was found that the CO fraction at the end of anode flow channel increases by up to 17% at a reformer temperature of 900 K and S/C ratio of 3. The cell voltage losses increased significantly at high current density when S/C ratio decreased and reformer temperature increased. In addition, the overall system efficiency was not affected greatly by S/C ratio at low current densities, however, at high current densities a higher S/C ratio proofed to be beneficial. This was due to the low effect of CO at low current densities and high energy required for additional steam at high S/C value. Although the high anode stoichiometric ratio provided higher cell performance, increased anode stoichiometry led to lower power output for a given system efficiency (35%) due to the waste of the excess hydrogen at the anode. At the system efficiency of 35%, the maximum power density was obtained at reformer temperature of 900 K, S/C ratio of 4 and anode stoichiometric ratio of 1.3 when cell temperature was operated at temperature of 448.15 K.

CHAPTER IX

DESIGN AND ANALYSIS OF HT-PEMFC SYSTEM WITH DIFFERENT FUEL PROCESSORS FOR STATIONARY APPLICATIONS

9.1 Introduction

In general, a conventional PEMFC, which is operated at temperatures below 100 ^{o}C, has a flooding problem especially at dry operating condition and requires pure hydrogen fuel with low CO content to avoid catalyst poisoning. To overcome some limitations of the low-temperature PEMFC (LT-PEMFC), a high-temperature PEMFC (HT-PEMFC) has been developed. Due to a lower CO coverage on the surface of a platinum catalyst at a operating temperature of the HT-PEMFC, it is possible to use directly the reformate gas from a fuel processor with simple purification processes (Das et al., 2009). In the case of LT-PEMFC, the reformate gas obtained needs to be treated by water gas shift and preferential oxidation processes. Another advantage of HT-PEMFC is that it can be operated at dry condition and thus the humidifier is unnecessary for this fuel cell. As a result, the HT-PEMFC system is less complicate than the LT-PEMFC system. In addition, there are no hydrogen and parasitic loss from preferential oxidation processes in the case of HT-PEMFC. However, the complexity of the integrated system depends on the fuel used and the requirement of each application as well (Lindstrom et al., 2009).

At present, a reformate gas derived from fuel processors is the preferred fuel for PEMFC operation before hydrogen transport and storage are readily available. In general, a design task for fuel cell systems depends on their applications and desired efficiency. To develop the fuel cell to the market place, its design for each application should be considered. For automotive application, it requires the low weight and size

of the overall system. The fast starting up is also preferred and thus the autothermal reforming is suitable for this application more than steam reforming (Sopena et al., 2007). At the same time, the high efficiency is needed for stationary application but the weight and size is not specified for this application (Barbir et al., 2005). Therefore, the cogeneration system of heat and power with other process is effective way to improve the system efficiency. Furthermore, the steam reforming is mostly chosen for stationary applications because it provides high efficiency (Hubert et al., 2006).

This study focuses on the development of a HT-PEMFC system for a stationary power generation. Glycerol is considered a potential feedstock for producing hydrogen. The efficiency of the HT-PEMFC system with different fuel processors is investigated and compared with a LT-PEMFC system. The HT-PEMFC system considered here can be divided into two cases. The first one involves the HT-PEMFC and a glycerol reformer without a CO removal process, whereas in the second one, a water gas shift reactor is included in the HT-PEMFC system to further improve its overall system efficiency. To examine the performance of LT-PEMFC and HT-PEMFC system, pure hydrogen and reformate gas from glycerol fuel processor are used as fuel and the effect of CO poisoning is also incorporated in the simulation model of PEMFCs. Also, the efficiency of LT-PEMFC and HT-PEMFC system with different fuel processors for stationary application is investigated and compared. The integrated system is studied in the term of combined heat and power (CHP) for stationary application. The waste heat generated during fuel cell operation is utilized in producing steam to use in the household.

9.2 PEMFC system for stationary applications

A fuel steam reforming (SR) is regarded as a suitable process to produce hydrogen in the stationary application of fuel cells because it provides high hydrogen yield (Hubert et al., 2006). In addition, for this fuel cell application, size and weight of the system seem to be not a critical issue. However, the heat integration of a fuel processor and a fuel cell is preferred to enhance the overall efficiency of stationary power systems. As shown in Figure 9.1 (a)-(c), the unreacted hydrogen and oxygen from the anode and cathode sides of HT-PEMFC and LT-PEMFC are sent to a burner to supply heat for a glycerol steam reforming.

Due to a high CO tolerance of HT-PEMFCs, it is possible to use the reformate gas obtained directly from the glycerol reformer without the requirement of CO removal processes. This process system is presented in Figure 9.1(a). Generally, to increase hydrogen yield in endothermic steam reforming processes, high reforming temperature and excess steam feed are required. However, the content of CO increases with increasing the reforming temperatures. With the aim at direct use of the reformate gas, the operating temperature of the steam reformer needs to be reduced to satisfy the operational constrain of the HT-PEMFC, while excess steam is still required to shift the equilibrium of the steam reforming reaction toward the product side. However, this causes the higher requirement of energy to preheat excess steam, which is necessary to enhance the hydrogen yield at the low-temperature operation of the reformer. To improve the HT-PEMFC performance, the fuel processing subsystem, i.e., a water gas shift reactor (WGS), is added to the steam reformer (Figure 9.1(b)) to maximize the hydrogen content and eliminate CO before being fed to the HT-PEMFC. It should be noted that a large size of the water gas shift reactor is the main problem of PEMFC systems for automotive applications, but not for stationary applications (Zalc et al., 2002).

For LT-PEMFCs, they are operated at low temperatures and requires the reformate fuel with less CO to avoid catalyst poisoning. The content of CO in a hydrogen feed for LT-PEMFC is limited to be less than 10 ppm. Therefore, both water gas shift and preferential oxidation (PROX) processes are added to the fuel reforming process for the LT-PEMFC system. Typically, the fuel processing system for LT-PEMFCs is demonstrated in Figure 9.1(c). In the WGS reactor, CO is reduced and at the same time, more hydrogen is also generated. Nonetheless, the reformate gas obtained from this process still has CO exceeding the acceptable level of LT-PEMFC. Therefore, the reformate gas should be further treated by the PROX reactor to reduce the concentration of CO to a satisfactory level. However, the oxidation reaction occurred in this process is the cause of hydrogen loss and parasitic loss from a compressor for feeding air to the reactor.

(a)

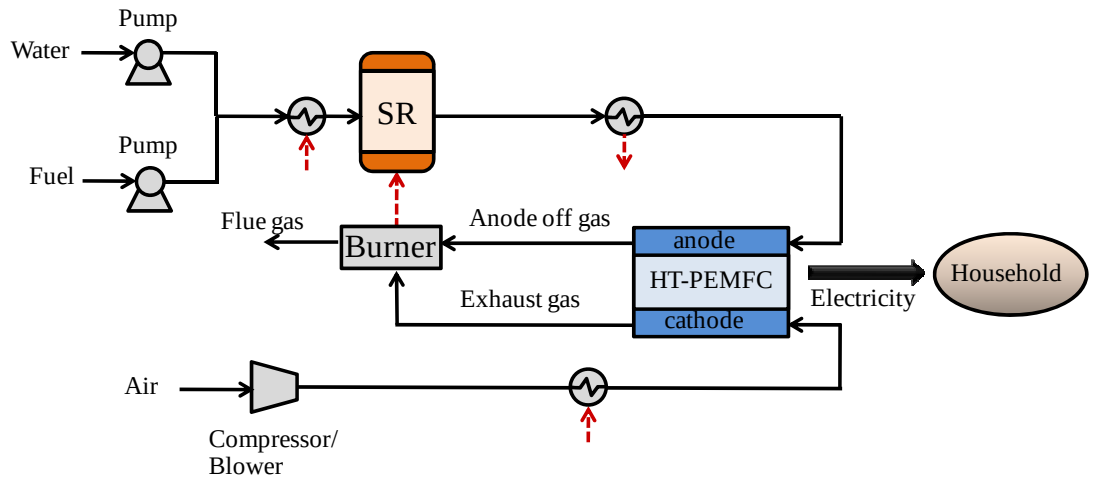

(b)

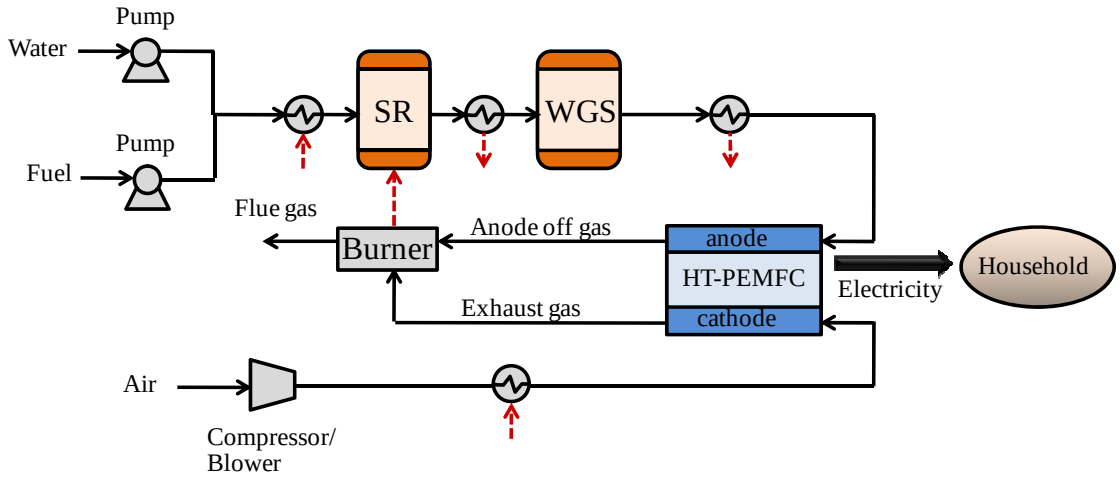

(c)

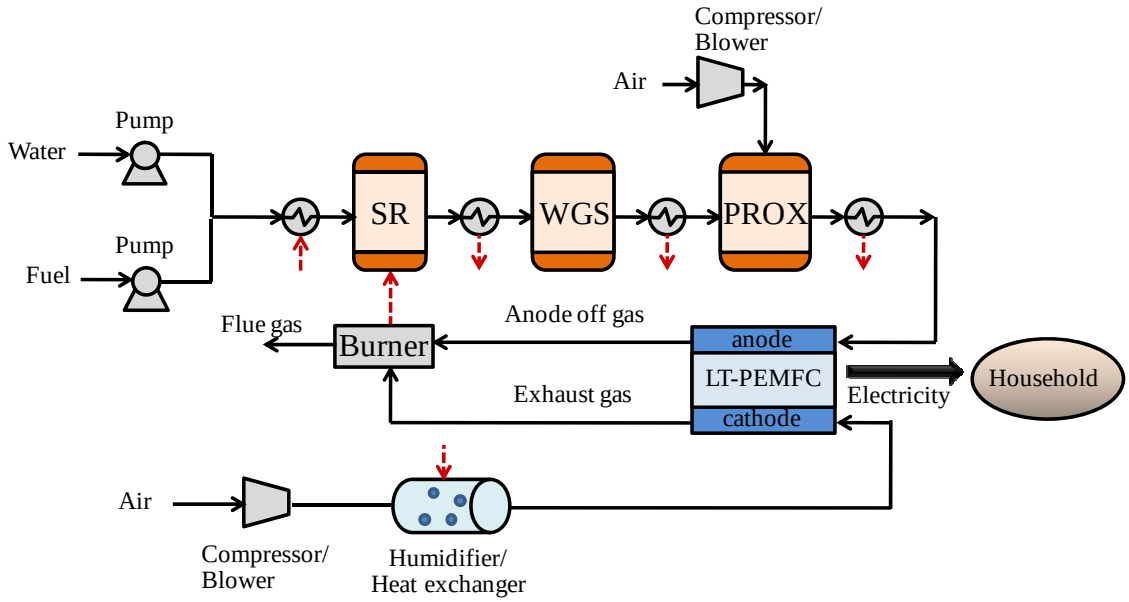

Figure 9.1 PEMFC system integrated with a fuel processing process for stationary application: (a) HT-PEMFC with only a steam reformer (case 1), (b) HT-PEMFC with a steam reformer and a water gas shift reactor (case 2) and (c) LT-PEMFC with a steam reformer, a water gas shift reactor and a preferential oxidation reactor (case 3).

Apart from the CO purification process, the main difference between the LT-PEMFC and HT-PEMFC systems involves the use of a humidifier unit. Due to the fact that HT-PEMFC can be operated at dry condition, the humidification is unnecessary for this type of PEMFC, but the reactant feed needs to be humidified in the case of LT-PEMFC to prevent drying out of a Nafion membrane. However, the humidifier can be removed from the anode side of LT-PEMFC when operated by using the reformate gas because the reformate gas from the reforming process is saturated with water.

The designed condition of PEMFC investigated in this study is shown in Table 9.1. The target power output of both LT-PEMFC and HT-PEMFC system for stationary applications are about 3 kW. The main purpose is to produce electricity for small household. For heat management of PEMFC stack, the cell temperature is typically controlled by water cooling. Due to the low quality of heat recovered from released heat from the fuel cell, the obtained hot water is considered to be used for boiler heating system in a small household combined heat and power system.

Table 9.1 The designed condition of PEMFC for stationary application

	Stationary application (household)
• Power output	3 kW
• Heat integration between fuel cell and fuel processing	Included
• Water recovery	Included
• Type of reforming process	SR
• Cogeneration system	Included

9.3 Description of system modeling

In this study, the thermodynamic model of a reforming process and the electrochemical model of PEMFCs are employed to investigate the performance and efficiency of combined glycerol fuel processor and PEMFC systems.

9.3.1 Fuel processing

The equilibrium composition of a reformate gas obtained from the steam reforming of glycerol is calculated from the direct minimization of Gibbs free energy. The external heat used to maintain the glycerol reformer at isothermal condition is determined by considering the enthalpy change between reactants and products of the reformer when inlet and outlet temperatures are equal to the reforming temperature. The WGS reactor is also modelled as an equilibrium reactor and its operating temperature is specified at 473.15 K (Chen et al., 2008). The reaction occurring in the WGS reactor involves a water gas shift reaction. For PROX process, the conversion reactor is chosen to model this reactor. It is operated at the oxygen to CO ratio of 1.5 and temperature of 423.15 K. The CO conversion is fixed at 95% (Hu et al., 2010) and the remaining oxygen will react with hydrogen. In addition, the sequentially two stages of the PROX reactor are applied, for this work, to reduce the CO concentration lower than 10 ppm in case of the LT-PEMFC system.

9.3.2 PEMFC

The basic relation of voltage and current density for PEMFC is described in Eq. (9.1). The cell voltage (E_{cell}) can be calculated by subtracting the reversible cell potential (E_r), the maximum voltage that can be achieved by a fuel cell at specific operating condition, by various voltage losses.

$$E_{\text{cell}} = E_r - \eta_{\text{act,a}} - \eta_{\text{act,c}} - \eta_{\text{ohmic}} \tag{9.1}$$

where $\eta_{act,a}$ is the activation loss at the anode, $\eta_{act,c}$ is the activation loss at the cathode and η_{ohmic} is ohmic loss. For LT-PEMFC, the electrochemical model is validated with the experimental data (Yan et al., 2006) and the model parameter which is used to calculate activation loss at the cathode is presented and compared with LT-PEMFC in Table 9.2. The detail of voltage loss model used in this study can find in Table 9.3. Due to the fact that the fuel used at the anode is reformate gas, CO poisoning effect is included in the model of both HT-PEMFC and LT-PEMFC. The concentration of hydrogen and oxygen at catalyst surface is determined from Stefan Maxwell equation Fick's law is used to represent diffusion model of the reactant in gas diffusion layer and film electrolyte (Mamlouk et al., 2011).

Due to the fact that the fuel used at the anode is a reformate gas from the fuel processor section, the effect of CO poisoning is included in the anode activation loss model of both the HT-PEMFC and LT-PEMFC. The CO poisoning model of LT-PEMFC, which is proposed by Bhatia et al.(2004), is used in this work. For HT-PEMFC, the CO poisoning model is developed from experimental data reported by Li et al. (2003) to explain a CO poisoning effect on HT-PEMFC in case of the reformate gas containing high CO content (3-10%). The detail model of HT-PEMFC and LT-PEMFC including CO poisoning model can be found in Chapter IV (Mathematical model).

The power output of fuel cell (P_{FC}) can be calculated from current density (i) and E_{cell} as follows:

$$P_{FC} = i \cdot A \cdot n \cdot E_{cell} \tag{9.2}$$

where A is cell active area and n is the number of cell.

9.3.3 Auxiliary units

To supply fuel for fuel processor and PEMFC, pump and compressor are used as auxiliary unit. Therefore, the required power from pump and compressor is taken into account for calculating the system efficiency when the efficiency of pump and compressor are specified at 0.7. Furthermore, the heat management in the integrated systems is carried out by using heat exchanger and burner. The heat from product streams of the reformer and the anode and cathode off gases are recovered by using the heat exchanger. The recovered heat will be utilized to preheat and vaporize water for the glycerol reformer. An amount of energy recovered from the heat exchanger is calculated from the enthalpy change between the inlet and outlet of hot and cold streams. To keep cell temperature at desired level, water is used as a cooling medium to remove excess heat from PEMFC. The heated water is considered the valuable product to use in boiler heating system for cogeneration system. The heat recovery from cell can be calculated in Eq. (9.3).

$$Q_{\text{thermal}} = m_{\text{a,in}} H_{\text{a,in}} + m_{\text{c,in}} H_{\text{c,in}} - m_{\text{a,out}} H_{\text{a,out}} - m_{\text{c,out}} H_{\text{c,out}} - P_{\text{FC}} \qquad (9.3)$$

For LT-PEMFC system, the humidifier is needed to provide humid air for cathode side and the calculation of heat required for this unit is described in Eq. (9.4).

$$Q_{\text{hum}} = m_{\text{air,out}} H_{\text{air,out}} - m_{\text{air,in}} H_{\text{air,in}} - m_{\text{H}_2\text{O,in}} H_{\text{H}_2\text{O,in}} \qquad (9.4)$$

9.3.4 System efficiency

Considering heat integration between PEMFC and reforming process, a required energy for the reforming process is partially supplied by the heat recovered from the anode and cathode off gases. The system efficiency is calculated by Eq. (9.5).

$$\eta_{\text{sys}} = \frac{P_{\text{FC}} - P_{\text{parasitic}}}{\dot{m}_{\text{glycerol}} \cdot LHV_{\text{glycerol}} + Q_{\text{ref}} - Q_{\text{rec}}} \qquad (9.5)$$

where $\dot{m}_{\text{glycerol}}$ is the molar flow rate of glycerol used for producing hydrogen. LHV_{glycerol} is lower heating value of glycerol. Q_{ref} is energy required for the steam reforming process accounts for the heat of vaporization, sensible heat to heat up the reactants to the desired temperature and the heat needed for maintaining the reformer at an isothermal operation level. Q_{rec} is the recovered heat from anode and cathode off gas as well as high temperature product gas coming out of the glycerol reformer. $P_{\text{parasitic}}$ is the required power used in auxiliary units, namely compressor and pump. Without the integration, recovered heat term (Q_{rec}) is only the heat recovery from high temperature product gas coming out of the glycerol reformer.

For cogeneration system, both electrical and thermal output is considered in calculation of cogeneration system efficiency which is shown in Eq. (9.6). The thermal output is the released heat from cell which is used for boiler heating system.

$$\eta_{\text{sys,co}} = \frac{P_{\text{FC}} - P_{\text{parasitic}} + Q_{\text{thermal}}}{\dot{m}_{\text{glycerol}} \cdot LHV_{\text{glycerol}} + Q_{\text{ref}} - Q_{\text{rec}}} \tag{9.6}$$

Furthermore, due to the fact that the fuel processor consumes water, while the fuel cell produces some, the water balance between recovered water from the fuel cell exhaust gas and the required water of reforming process is calculated in this work.

9.4 Results and discussion

9.4.1 HT-PEMFC and LT-PEMFC performances

9.4.1.1 Pure hydrogen operation

Figure 9.2 shows the performance of HT-PEMFC and LT-PEMFC running on pure hydrogen and air. Under the atmospheric pressure operation, the simulation results show that the LT-PEMFC has a higher performance, compared with the HT-PEMFC at current densities lower than 6000 A m^{-2}. Low oxygen permeability and strong phosphate adsorption (phosphoric acid is required for HT-PEMFCs operation)

are the main reasons for the observed slower oxygen reduction kinetics in HT-PEMFCs cathodes even at the higher operating temperature.

However, the performance of the HT-PEMFC improves significantly and becomes comparable to that of LT-PEMFC when the fuel cell pressure is increased to 3 atm. Increasing the operating pressure causes in higher hydrogen and oxygen partial pressure resulting in enhanced kinetics and mass transport. The increase in pressure has larger impact on the HT-PEMFCs in comparison to the LT-PEMFCs due to the lower permeability of oxygen in phosphoric acid in comparison to that in Nafion.

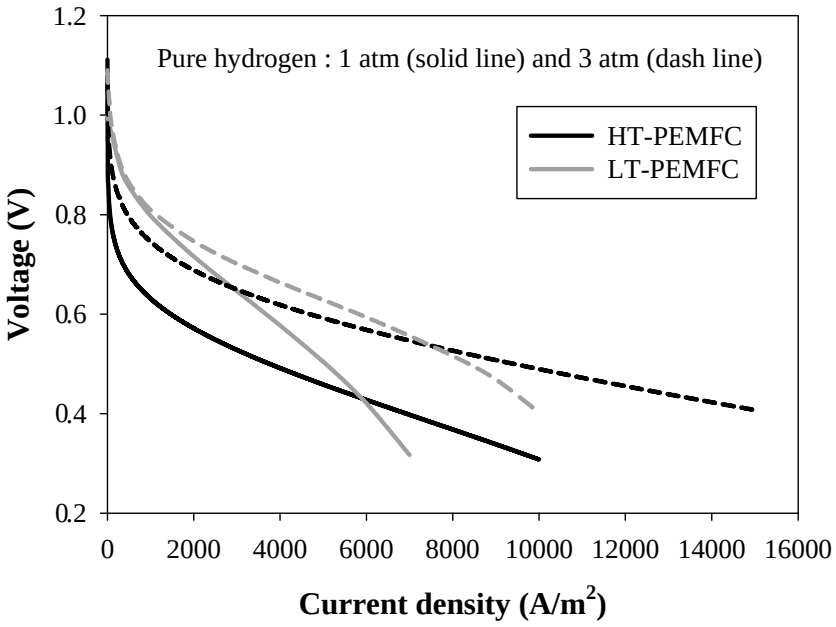

Figure 9.2 The Polarization curve of HT-PEMFC and LT-PEMFC at pure hydrogen operation.

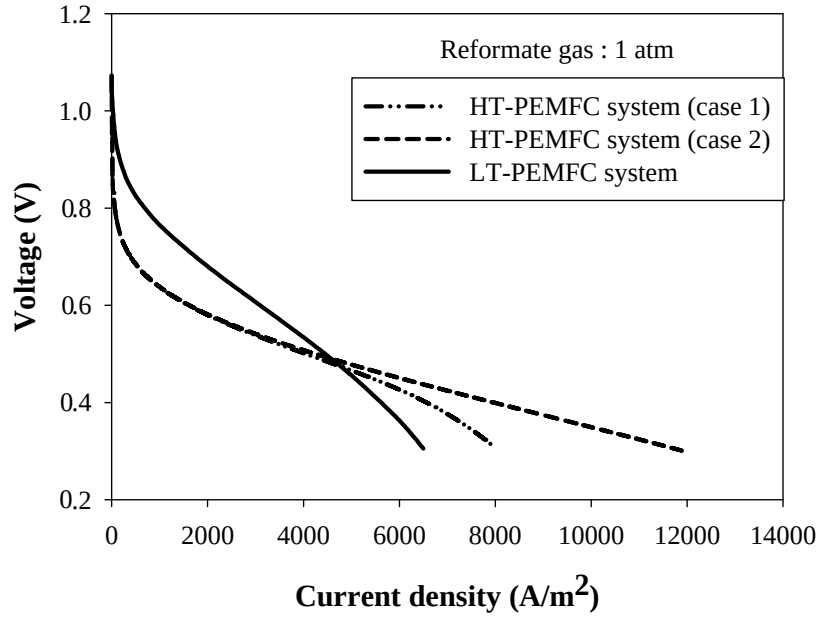

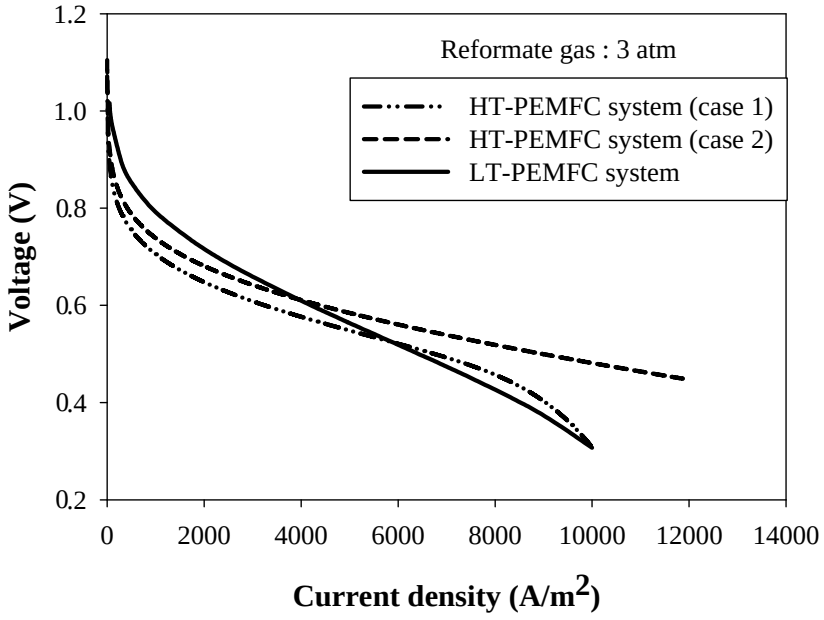

Figure 9.3 The Polarization curve of HT-PEMFC and LT-PEMFC at reformate operation.

9.4.1.2 Reformate gas operation

A reformate gas that is derived from the glycerol steam reforming process contains H_2, CO, CO_2, CH_4, H_2O and some trace of N_2 (in case of applying a PROX unit in the glycerol processor). The operating condition of the glycerol processor is chosen by considering the operational constraints (i.e., CO contamination) of HT-PEMFCs and LT-PEMFCs (see Table 9.4). The corresponding hydrogen fraction from the glycerol processor is given in Table 9.4 for both HT-PEMFC and LT-PEMFC systems. The CO fraction coming from PROX in the glycerol processor at a desired condition is lower than 10 ppm in case of LT-PEMFC system. For HT-PEMFC system without the WGS reactor (case 1), the optimal condition of the reformer providing the highest system efficiency is used in this study when CO fraction is about 7%. Considering the HT-PEMFC system including the WGS reactor (case 2), the CO fraction in the synthesis gas obtained from the WGS reactor operated under the defined reformer and WGS reactor conditions is lower than 0.1%. The resulting hydrogen fraction in the anode feed can be classified as follows: HT-PEMFC (case 2) > HT-PEMFC (case 1) > LT-PEMFC (Table 9.4).

From the simulation result in Figure 9.3, it can be seen that when operated at 1 atm, the HT-PEMFC system without a WGS reactor (case 1) has the same performance as that with the WGS reactor (case 2) at a low current density operation. However, the performance of the HT-PEMFC without a WGS reactor decreases sharply at high current densities because of poisoning effect of the increased CO concentration in reformate gas towards the end of the anode channels at high current densities (hydrogen is consumed). For LT-PEMFC system, superior performance is obtained at current densities up to 5000 A m^{-2} beyond which the cell performance drops sharply. At high pressure (3 atm) operation, the HT-PEMFC with a WGS reactor shows the highest performance among the studied systems at high current density above 4000 A m^{-2}, whereas LT-PEMFC system shows superior performance at lower current densities known as the kinetic region (see Figure 9.3). The limited performance of LT-PEMFC system at high current densities results from CO poisoning effect on anode and oxygen starvation at the cathode caused by flooding and low oxygen partial pressure (humidified air).

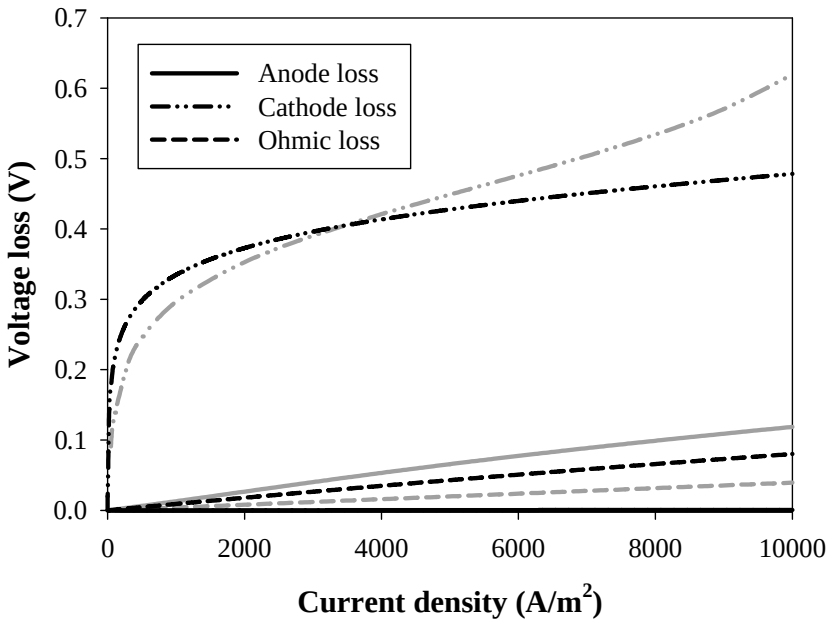

Figure 9.4 Voltage loss at reformate operation and cell pressure of 3 atm: HT-PEMFC system (case2) (black line) and LT-PEMFC (gray line).

Figure 9.4 shows the individual voltage loss in HT-PEMFC and LT-PEMFC operated on the reformate gas. As expected the CO poisoning problem is more pronounced in LT-PEMFC than HT-PEMFC resulting in larger anode over-potentials of LT-PEMFC in comparison to that of HT-PEMFC. The ohmic loss in HT-PEMFC, on the other hand, is marginally greater than that in LT-PEMFCs as Nafion exhibits higher ionic conductivities at fully humidified conditions. The cathode activation loss in LT-PEMFCs is smaller than that of HT-PEMFCs. This is explained earlier due to the higher exchange current density at Nafion/Pt interface in comparison to that of H_3PO_4/Pt. As cathode current density increases, mass transport limitation in LT-PEMFCs becomes pronounced at current densities as low as 4000 A m^{-2} when operated with air. The decrease of oxygen partial pressure due to cathode stream humidification, cathode flooding and slower oxygen diffusion in the gaseous phase in comparison to HT-PEMFCs (higher operating temperature) is the main reason for the observed limitation. These behaviors explain why the performance of HT-PEMFC surpasses that of LT-PEMFC at high current density (> 4000 A m^{-2}).

Table 9.2 Parameter of cathode activation loss at base case operation

Parameters	**HT-PEMFC**	**LT-PEMFC**
Cell operating pressure at anode, P (atm)	3	3
Cathode reference exchange current density, $i_{0,c}^{\text{ref}}$ (A m^{-2})	0.0004	4.2×10^{-4}
Anode catalyst surface area, $a_{c,a}$ (m^2 g^{-1})	64	54
Cathode catalyst loading, $L_{c,c}$ (mg $cm^{-2)}$	0.4	0.4
Transfer coefficient at cathode, α_c	0.75	0.45
Reaction order, γ	1.375	1.3
Cathode reference concentration, $c_{\text{ref},c}$ (mol cm^{-3})	0.0004	2.03×10^{-7}
Cathode activation energy, $E_{c,c}$ (J $mole^{-1}$ K^{-1})	72400	66000
Cathode reference cell temperature, $T_{\text{ref},c}$ (K)	373.15	298.15

Table 9.3 The individual loss model used in the HT-PEMFC and LT-PEMFC model (Spriner et al., 1991; Bhatia et al., 2004; Mamlouk et al., 2011)

Parameters	HT-PEMFC	LT-PEMFC
Anode activation loss	$\eta_{\text{act,a}} = \frac{RT}{\alpha F}\sinh^{-1}\left(\frac{i}{2i_0\left(1-\theta_{\text{CO}}\right)^2}\right)$	$\eta_{\text{act,a}} = \frac{RT}{\alpha F}\sinh^{-1}\left(\frac{i}{2k_{\text{eh}}\theta_{\text{H}}}\right)$
Cathode activation loss	$\eta_{\text{act,c}} = \frac{RT}{\alpha F}\sinh^{-1}\left(\frac{i}{2i_0}\right)$	$\eta_{\text{act,c}} = \frac{RT}{\alpha F}\sinh^{-1}\left(\frac{i}{2i_0}\right)$
Ohmic loss	$\sigma_m = \frac{A}{T}\exp\left(\frac{-B}{R(T)}\right)$ $\eta_{\text{ohmic}} = \left(\frac{\sigma_m}{l_m}\right)i$	$K_{mem} = (0.5139\lambda - 0.326)\exp\left[1268\left(\frac{1}{303}-\frac{1}{T}\right)\right]\times 100$ $\eta_{\text{ohmic}} = \left(\frac{K_{\text{mem}}}{l_{\text{m}}}\right)i$

Table 9.4 Supplied hydrogen mole fraction at each unit of HT-PEMFC and LT-PEMFC system at operating pressure of 3 atm

System	S/C	Reformer Temperature (K)	Cell temperature (K)	Glycerol steam reforming (wet basis)	WGS (wet basis)	PROX (wet basis)	Humidifier/ Heat exchanger
HT-PEMFC : case 1	4	900	448.15	0.3014	-	-	0.6513 (RH= 0)
HT-PEMFC : case 2	2	1000	448.15	0.4135	0.5164	-	0.6882 (RH= 0)
LT-PEMFC	2	1000	353.15	0.4135	0.5164	0.5076	0.5704 (RH= 1)

9.4.2 Comparison of HT-PEMFC and LT-PEMFC system efficiency

To compare the efficiency of HT-PEMFC and LT-PEMFC systems for small stationary application, the power output target is specified at 3 kW and the PEMFC systems is operated at pressure of 3 atm. The efficiency of LT-PEMFC and HT-PEMFC system is investigated at the same power output (3 kW) and voltage (0.65 V). The parameters used for efficiency analysis in this work are shown in Table 9.5. The main purpose of examining LT-PEMFC and HT-PEMFC for small household electricity generation is to determine the system that will achieve the maximum possible overall efficiency. In order to improve the system efficiency, the cogeneration system of heat and power should also be considered. The system efficiency of individual integrated PEMFC system at full and partial loads (50%, 1.5 kW) is shown in Table 9.6. It is found that the highest system efficiency is obtained when using HT-PEMFC system with WGS reactor (case 2) followed closely by LT-PEMFCs. While the HT-PEMFC system without the WGS reactor (case 1) provides the lowest system efficiency among the studied systems. Without WGS, a higher steam to carbon ratio is required to reduce the fraction of CO in the reformate gas and thus, high energy is required to generate steam for this system. In addition, in the HT-PEMFC system (case 1), the reformate gas obtained from the glycerol processor contains a lower hydrogen fraction and a higher CO fraction, compared to the HT-PEMFC system with WGS (case 2). Additionally, the high CO fraction results in a large anode activation loss (case 1). When the system is operated at partial load condition (1.5 kW), higher efficiency is achieved (from 33 to 37.5% for HT-PEMFC case 2) however on the expense of lower power output (50%). In addition, the water balance of all the systems shows a positive value even at the half load condition. This means water recovered from the PEMFC system is sufficient and exceeds the required amount for reformer and humidifier operation (for LT-PEMFC system).

The system efficiency with and without heat integration between PEMFC and reforming process ($\eta_{sys,int}$ and $\eta_{sys,no\ int}$) as well as cogeneration system efficiency ($\eta_{sys,co}$) of individual integrated system are shown in Figure 9.5. It is found that the PEMFC system without heat integration between PEMFC and the reforming process

provides low overall efficiency around 20-25%. However, the system efficiency increases to 28-33% when heat recovered from anode and cathode exhaust gas is used to maintain the endothermic reforming process. The results show that this integrated system provides higher efficiency than conventional electrical generator like gas turbine. The efficiency (based on lower heating value) of glycerol combustion engine is around 19- 29% depending on operation condition of gas turbine. In addition, the system efficiency increases further to 50-60% (cogeneration system efficiency) when released heat during the electrochemical reaction is utilized to heat up water for household usage. The released heat from cell and molar flow of produced hot water (50 ◦C) are shown in Table 9.7.

Table 9.5 The parameter used for efficiency analysis of HT-PEMFC and LT-PEMFC

Parameters	Value	Unit
System pressure	3	atm
Active area	250	cm^2
Number of cell		
• HT-PEMFC (case 1)	115	-
• HT-PEMFC (case 2)	81	-
• LT-PEMFC	71	-
Cell temperature		
• HT-PEMFC	175	◦C
• LT-PEMFC	80	◦C
Anode stoichiometry	1.25	-
Cathode stoichiometry	2	-

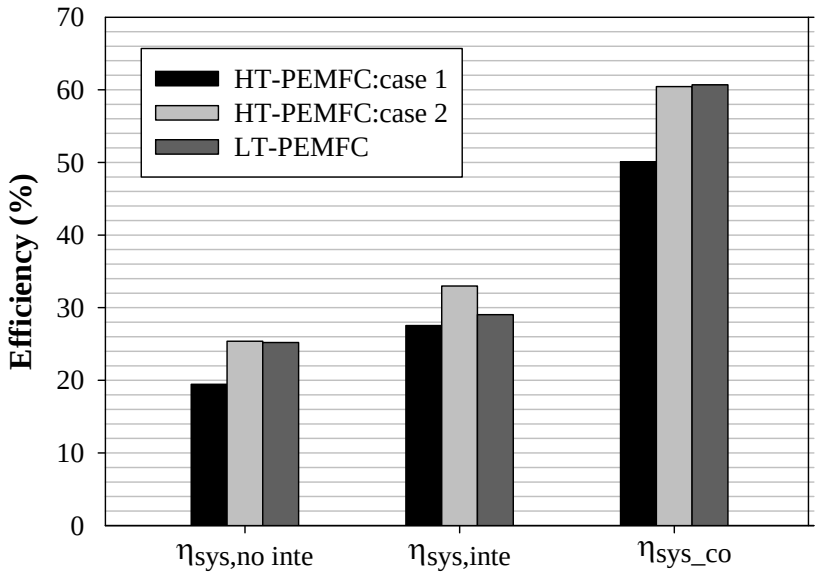

Figure 9.5 The system efficiency with and without heat integration between PEMFC and reforming process ($\eta_{sys,int}$ and $\eta_{sys,no\ int}$) as well as cogeneration system efficiency ($\eta_{sys,co}$) of HT-PEMFC and LT-PEMFC.

Table 9.6 System efficiency and water balance of designed system

Parameters	Full load	Partial load
Power (kW)	3	1.5
System efficiency (%)		
• HT-PEMFC system (case1)	27.55	30.96
• HT-PEMFC system (case2)	32.98	37.48
• LT-PEMFC system	29.03	35.30
Water balance (mole/s)		
• HT-PEMFC system (case1)	0.0074	0.0033
• HT-PEMFC system (case2)	0.0076	0.0033
• LT-PEMFC system	0.0097	0.0040

Table 9.7 The released heat from cell and produced hot water (50 °C) molar flow rate of each system.

System	Released heat from electrochemical reaction (J/s)	Molar flow rate (mol/s) of hot water (50°C)
HT-PEMFC system (case1)	3126	1.6618
HT-PEMFC system (case2)	3080	1.6376
LT-PEMFC system	3297	1.7530

9.5 Conclusions

The system efficiency of HT-PEMFC systems with different fuel processors for a small 3 kW stationary application is investigated and compared with a LT-PEMFC system. The HT-PEMFC system integrates a glycerol reformer with and without a CO removal process using a water gas shift reactor. The HT-PEMFC system with the water gas shift reactor provides higher performance than the LT-PEMFC system when using a reformate gas from a glycerol and the fuel cell is operated at current density higher 6000 A m^{-2} or cell voltage < 0.67 V.. Considering the system efficiency, it is found that HT-PEMFC system with water gas shift reactor shows the highest value, followed by the LT-PEMFC system and the HT-PEMFC system without the water gas shift reactor. The highest efficiency obtained from HT-PEMFC system is approximately 32% and 36% at full load and partial load conditions, respectively. Furthermore, the efficiency can be increased up to 60% in case of HT-PEMFC system with the water gas shift reactor when the heat generated in the fuel cell is used to produce hot water for cogeneration system (household usage).

CHAPTER X

CONCLUSION AND RECOMMENDATION

This work studies on the performance of HT-PEMFC and glycerol reforming as well as the integrated system. Thermodynamic analysis of steam and autothermal reforming of glycerol from biodiesel production process are investigated as a basis of development of a hydrogen production process from renewable resource. Equilibrium compositions and thermal efficiency is determined as a function of temperature, preheat temperature, glycerol to steam molar ratio, and glycerol to oxygen ratio, and to find out an optimal operating condition providing suitable composition of reformate gas for HT-PEMFC. Moreover, a steady-state and isothermal model of HT-PEMFC fed by a reformate gas from glycerol reforming process is developed. The flow channel, diffusion and electrochemical model are performed in Matlab to study the effect of fuel utilization, inlet temperature and inlet gas composition on the current density distribution and efficiency. The performance and efficiency of the HT-PEMFC system with different fuel processors for stationary application are investigated and compared with a LT-PEMFC system.

10.1 Conclusion

It is found that the glycerol is a promising fuel source for hydrogen production. In comparison with methane, glycerol shows a better performance in terms of high hydrogen production and low possibility to carbon formation. However, the content of CO_2 in the reformate gas and the energy required for the glycerol processor should be concerned. Equilibrium compositions of glycerol steam and autothermal reforming gas obtained were determined as a function of temperature, steam to glycerol ratio, and oxygen to glycerol ratio (in the case of autothermal reforming). The results showed that at isothermal condition, raising operating temperature and steam to glycerol increases hydrogen yield, whereas increasing and oxygen to glycerol ratios causes a reduction of hydrogen concentration. However,

high temperature operation also promotes CO formation which would hinder the performance of low-temperature fuel cells. The steam to crude glycerol ratio is a key factor to reduce the extent of CO but a dilution effect of steam should be considered if reforming gas is fed to fuel cells. An increase in the ratio of glycerol to methanol in crude glycerol can increase the amount of hydrogen produced. Considering the crude glycerol autothermal reforming at a thermoneutral condition where no external heat input is required, the maximum hydrogen yield can be achieved at the condition having sufficient oxygen to sustain energy for system. The suitable oxygen to glycerol ratio is around 0.4-0.7 depending on the purity of crude glycerol. The amount of oxygen needed to sustain the autothermal reformer operation is higher when excess steam is applied and crude glycerol containing less methanol is used for hydrogen production.

To directly use reformate gas from glycerol reforming for HT-PEMFC, it is necessary to keep the CO content of the reformate gas within a desired range. The steam reformer should be operated at lower temperatures; however, a high steam to glycerol ratio is required. This requirement results in the increasing of the energy consumption for steam generation. To determine the optimal conditions of glycerol steam reforming for HT-PEMFC, both the hydrogen yield and energy requirements were taken into consideration. The operational boundary of the glycerol steam reformer is presented and the operation of the reformer at a steam to glycerol ratio of 11-14 produces the highest reformer efficiency when reformate gas containing 5%CO is considered. For glycerol reformer integrated with water gas shift unit, the reformer temperature and S/C have an insignificant effect on hydrogen yield and efficiency at S/C > 2 and T > 1000 K whereas CO content is lower than limitation of HT-PEMFCs at all operational range.

Furthermore, the efficiency and output power density of an integrated HT-PEMFC system and glycerol reformer is studied. The effects of reformer temperature, steam to carbon ratio (S/C), fuel cell temperature, and anode stoichiometric ratio were examined. An increase in anode stoichiometric ratio will reduce CO poisoning effect at cell’s anode but cause lower fuel utilization towards energy generation. High S/C operation requires large amount of the energy available, however, it will increase

anode tolerance to CO poisoning and therefore will lead to enhanced cell performance. Consequently, the optimum gas composition and flow rate is very dependent on cell operating current density and temperature. For example, at low current densities, similar efficiencies were obtained for all the S/C ratio studied range at cell temperature of 423.15 K, however, at cell temperature of 448.15 K, low S/C ratio provided higher efficiency in comparison to high S/C ratio. High S/C is essential when operating the cells at high current densities where CO has considerable impact on cell performance. Optimal conditions that provide maximum power density at a given efficiency are reported.

The performance and efficiency of a HT-PEMFC system integrated with a glycerol steam reformer with and without a water gas shift reactor for stationary application is carried out and compared with a LT-PEMFC system. The HT-PEMFC system shows good performance over the LT-PEMFC system when operated under a low current density condition (lower than 6000 A m^{-2}). The high concentration of CO is the major problem for operation of the HT-PEMFC system without the water gas shift reactor at high current density, whereas the LT-PEMFC suffers from the CO poisoning effect and the low oxygen concentration. Considering the system efficiency the power and heat generation are taken into account, the HT-PEMFC system with the water gas shift reactor in the glycerol processor shows the highest overall system efficiency (approximately 60%).

In conclusion, to apply a HT-PEMFC system for stationary application, the steam reforming process is appropriate for use in hydrogen production. The optimal conditions that provide high hydrogen yield and acceptable CO concentration for the HT-PEMFC system without a WGS reactor is the reformer temperature of 900 K, S/C ratio of 4 and anode stoichiometric ratio of 1.3 when the HT-PEMFC is operated at temperature of 448.15 K. However, the highest system efficiency can be achieved when the WGS reaction is included in the HT-PEMFC system and the glycerol steam reformer is operated at the S/C of 1-2 and the temperature of 1000-1200 K.

10.2 Recommendation

1) In this study, the reformate gas is fed to HT-PEMFC at dry condition. However, it is found from the literature that water content in hydrogen feed can enhance CO tolerance of HT-PEMFC because the water gas shift reaction can occur at operational temperature range of HT-PEMFC and thus CO content reduces. Therefore, the effect of water content on HT-PEMFC performance at reformate gas operation should be study in detail to find out the alternative option to improve cell performance.

2) In general, a design task for fuel cell systems depends on their applications and desired efficiency. In this study, the design and analysis of HT-PEMFC system for stationary application has already investigated. However, the design fuel processor for automotive application, which is not studied yet, should be examined. In addition, the future work should focus on economic analysis of HT-PEMFC system for each application.

REFERENCES

Adachi, H., Ahmed, S., Lee, S.H.D., Papadias, D,, Ahluwalia, R.K., Bendert, J.C., et al. A natural-gas fuel processor for a residential fuel cell system. Journal of Power Sources 188 (2009): 244-255.

Adhikari, S., Fernando, S., Gwaltney, S.R., To, S.D., Bricka, R.M., Steele, P.H. and Haryanto, A., A thermodynamic analysis of hydrogen production by steam reforming of glycerol. International Journal of Hydrogen Energy 32 (2007): 2875-2880.

Adhikari, S., Fernando, S., Haryanto, A., Production of hydrogen by steam reforming of glycerin over alumina supported metal catalysts. Catalysis Today 129 (2007): 355–364.

Adhikari, S., Fernando, S.D., Haryanto, A., Hydrogen production from glycerol: An update. Energy Conversion and Management 50 (2009): 2600–2604.

Agrell, J., Birgersson, H., Boutonnet, M., Steam reforming of methanol over a $Cu/ZnO/Al_2O_3$ catalyst: a kinetic analysis and strategies for suppression of CO formation. Journal of Power Sources 106 (2002): 249–257.

Ahluwalia, R.K., Zhang, Q., Chmielewski, D.J., Lauzze, K.C. and Inbody, M.A., Performance of CO preferential oxidation reactor with noble-metal catalyst coated on ceramic monolith for on-board fuel processing applications. Catalysis Today 99 (2005): 271–283.

Ahmed, S., and Krumpelt, M., Hydrogen from hydrocarbon for fuel cells. International Journal of Hydrogen Energy 26 (2001): 291–301.

Amphlett, J.C., Baumert, R.M., Mann, R.F. Peppley, B.A. Roberge, P.R., Performance modeling of the Ballard Mark IV solid polymer electrolyte fuel cell. Journal of Electrochemical Society 142 (1995): 1–15.

Amphlett, J.C., Mann, R.F., Peppley, B.A., Roberge, P.R., Rodrigues, A., A model predicting transient responses of proton exchange membrane fuel cells. Journal of Power Sources 61 (1996): 183–188.

Amphlett, J.C., Mann, R.F., Peppley, B.A., Roberge, P.R., Rodrigues, A., Salvador, J.P., Simulation of a 250 kW diesel fuel processor/PEM fuel cell system. Journal of Power Sources 71 (1998): 179–184.

Asensio, J.A., Gomez-Romero, P., Recent Developments on Proton Conducting Poly(2,5-benzimidazole) (ABPBI) Membranes for High Temperature Polymer Electrolyte Membrane Fuel Cell. Fuel Cells 5 (2005): 336-343.

Ashrafi, M., Proll, T., Pfeifer, C., and Hofbauer, H., Experimental Study of Model Biogas Catalytic Steam Reforming: 1. Thermodynamic Optimization. Energy & Fuel 22 (2008): 4182–4189.

Authayanun, S., Arpornwichanop, A., Paengjuntuek, W. and Assabumrungrat, S., Thermodynamic Study of Hydrogen Production from Crude Glycerol Autothermal Reforming for Fuel Cell Applications. International Journal of Hydrogen Energy, 35(2010): 6617-6623.

Barbara, E., et. al., Ullmann's Encyclopedia of Industrial Chemistry. Germamy. 1994 Vol.A112.

Barbir, F., PEM fuel cells: theory and practice. Elsevier, London, 2005.

Barbir, F., PEM Fuel Cells, Fuel cell Technology. Springer, London, 2006.

Bellows, R.J., Marucchi-Soos, E.P., and Buckley, D.T., Analysis of Reaction Kinetics for Carbon Monoxide and Carbon Dioxide on Polycrystalline Platinum Relative to Fuel Cell Operation. Industrial & Engineering Chemistry Research 35 (1996): 1235-1242.

Bergmann, A., Gerteisen, D., Kurz, T., Modelling of CO Poisoning and its Dynamics in HTPEM Fuel Cells. Fuel Cells 10 (2010): 278-287.

Bernardi, D.M., Verbrugge, M.W., Mathematical model of a gas diffusion electrode bonded to a polymer electrolyte. American Institute of Chemical Engineers Journal 37 (1991): 1151–1163.

Bhatia, K.K., Wang, C.Y., Transient carbon monoxide poisoning of a polymer electrolyte fuel cell operating on diluted hydrogen feed. Electrochimica Acta 34 (2004): 2333-2341.

Bruijn, F.A., Papageorgopoulos, D.C., Sitters, E.F., Janssen, G.J.M., The influence of carbon dioxide on PEM fuel cell anodes. Journal of Power Sources 110 (2002) 117–124.

Buffoni, I.N., Pompeo, F., Santori, G.F., Nichio, N.N. Nickel catalysts applied in steam reforming of glycerol for hydrogen production. Catalysis Communications 10 (2009): 1656–1660.

Byrd, A.J., Pant, K.K., Gupta, R.B., Hydrogen production from glycerol by reforming in supercritical water over Ru/Al_2O_3 catalyst. Fuel 87 (2008): 2956–2960.

Castaldi, M.J., Barrai, F., An investigation into water and thermal balance for a liquid fueled fuel processor. Catalysis Today 129 (2007): 397-406.

Chein, R.Y., Chen, Y.C., Lin, Y.S., Chung, J.N., Experimental study on the hydrogen production of integrated methanol-steam reforming reactors for PEM fuel cells. International Journal of Thermal Sciences 50 (2011): 1253-1262.

Cheddie, D., and Munroe, N., Mathematical model of a PEMFC using a PBI membrane. Energy Conversion and Management 47 (2006): 1490–150.

Chen, H., Ding, Y., Cong, N.T., Dou, B., Dupont, V., Ghadiri, M., Williams, P.T., A comparative study on hydrogen production from steam-glycerol reforming: thermodynamics and experimental. Renewable Energy 36 (2011): 779-788

Chen H., Zhang, T., Dou, B., Dupont, V., Williams, P., Ghadiri, M., Ding, Y. Thermodynamic analyses of adsorption-enhanced steam reforming of glycerol for hydrogen production. International Journal of Hydrogen Energy 34 (2009): 7208–7222.

Chen, W.H., Hsieh, T.C., Jiang, T.L., An experimental study on carbon monoxide conversion and hydrogen generation from water gas shift reaction. Energy Conversion and Management 49 (2008): 2801–2808.

Chipit, F., Recupero, V., Pino, L., Vita, A., Lagana, M., Experimental analysis of a 2 kWe LPG-based fuel processor for polymer electrolyte fuel cells. Journal of Power Sources 157 (2006): 914-920.

Chi, Z., Pyle, D., Wen, Z., Frear, C., Chen, S. A laboratory study of producing docosahexaenoic acid from biodiesel-waste glycerol by microalgal fermentation. Process Biochemistry 42 (2007): 1537–1545.

Cipiti, F., Recupero, V., Design of a CO preferential oxidation reactor for PEFC systems: A modelling approach. Chemical Engineering Journal 146 (2009): 128–135.

Cortright, R.D., Davda, R.R., Dumesic, J.A., Hydrogen from catalytic reforming of biomass-derived hydrocarbons in liquid water. Nature 418 (2002): 964–967.

Cui, Y., Galvita, V., Rihko-Struckmann, L., Lorenz, H., Sundmacher, K., Steam reforming of glycerol: The experimental activity of $La_{1-x}Ce_xNiO_3$ catalyst in comparison to the thermodynamic reaction equilibrium. Applied Catalysis B: Environmental 90 (2009): 29–37.

Danial, D.E., Kumar, R., Ahluwalia, R.K., Krumpelt, M., Fuel processors for automotive fuel cell systems: a parametric analysis. Journal of Power Sources 102 (2001): 1-15.

Das, S.K., Reis, A., and Berry, K.J., Experimental evaluation of CO poisoning on the performance of a high temperature proton exchange membrane fuel cell. Journal of Power Sources 193 (2009): 691-698.

Dauenhauer, P.J., Salge, J.R. and Schmidt, L.D., Renewable hydrogen by autothermal steam reforming of volatile carbohydrates. Journal of Catalysis 244 (2006): 238–247.

Dawes, J.E., Hanspal, N.S., Family., O.A, Turan, A. Three-dimensional CFD modelling of PEM fuel cells: An investigation into the effects of water flooding. Chemical Engineering Science 64 (2009): 2781–2794.

Demirbas A. Yields of hydrogen-rich gaseous products via pyrolysis from selected biomass samples. Fuel 80 (2001): 1885–1891.

Demirbas A, Arin G. Hydrogen from Biomass via Pyrolysis: Relationships between Yield of Hydrogen and Temperature. Energy Sources 26 (2004): 1061-1069.

Dou, B., Dupont, V., Rickett, G., Blakeman, N., Williams, P.T., Chen, H., Ding, Y., Ghadiri, M., Hydrogen production by sorption-enhanced steam reforming of glycerol. Bioresource Technology 100 (2009): 3540–3547.

Dou, B., Dupont, V., Williams, P.T., Chen, H., Ding, Y., Thermogravimetric kinetics of crude glycerol. Bioresource Technology 100 (2009): 2613–2620.

Dou, B., Rickett, G.L., Dupont, V., Williams, P.T., Chen, H., Ding, Y., Ghadiri, M. Steam reforming of crude glycerol with in situ CO_2 sorption . Bioresource Technology 101 (2010): 2436-2442.

Douvartzides, S.L., Coutelieris, F.A., Demin, A.K., and Tsiakaras, P.E., Electricity from ethanol fed SOFCs: the expectations for sustainable development and technological benefits. International Journal of Hydrogen Energy 29 (2004): 375-379.

Dutta, S., Shimpalee, S., Van Zee, J.W., Three-dimensional numerical simulation of straight channel PEM fuel cells. Journal of Applied Electrochemistry 30 (2000): 135–146.

Ersoz, A., Olgun, H., Ozdogan, S., Gungor, C., Akgun, F., and Tırıs, M., Autothermal reforming as a hydrocarbon fuel processing option for PEM fuel cell. Journal of Power Sources 118 (2003): 384–392.

Faungnawakij, K., Kikuchi, R., Eguchi, K., Thermodynamic evaluation of methanol steam reforming for hydrogen production. Journal of Power Sources 161 (2006): 87–94.

Fernand, S., Adhikari, S., Kota, K., Bandi, R., Glycerol based automotive fuels from future biorefineries. Fuel 86 (2007): 2806–2809.

Fuller, T., and Newman, J., Water and thermal management in solid-polymerelectrolyte fuel cells. Journal of Electrochemical Society 140 (1993): 1218-1225.

Gadhe, J.B., Gupta, R.B., Hydrogen production by methanol reforming in supercriticalwater: Catalysis by in-situ-generated copper nanoparticles. International Journal of Hydrogen Energy 32 (2007): 2374 – 2381.

Giddey, S., Ciacchi, F., T., and Badwal, S., P., S., Fuel Quality and Operational Issues for Polymer Electrolyte Membrane (PEM) Fuel Cells. Ionics 11 (2005): 1-10.

Giunta, P., Mosquera, C., Amadeo, N., Laborde, M., Simulation of a hydrogen production and purification system for a PEM fuel-cell using bioethanol as raw material. Journal of Power Sources 164 (2007): 336–343.

Guo, Y., Azmat, M.U., Liu, X., Wang, Y., Lu, G., Effect of support's basic properties on hydrogen production in aqueous-phase reforming of glycerol and correlation between WGS and APR. Applied Energy 92 (2012): 218–223.

Guo, Y., Liu, X., Azmat, M.U., Xu, W., Ren, J., Wang, Y., Lu, G., Hydrogen production by aqueous-phase reforming of glycerol over Ni-B catalysts**.** International Journal of Hydrogen Energy 37 (2012): 227-234**.**

Hajek, M., Skopal, F., Treatment of glycerol phase formed by biodiesel production. Bioresource Technology 101 (2010): 3242–3245.

Halabi, M.H., de Croon, M.H.J.M., van der Schaaf, J., Cobden, P.D., Schouten, J.C. Modeling and analysis of autothermal reforming of methane to hydrogen in a fixed bed reformer. Chemical Engineering Journal 137 (2008): 568–578.

Hazimah, A.H., Ooi, T.L., Salmiah, A., Recovery of glycerol and diglycerol from glycerol pitch. Journal of Oil Palm Research 15 (2003): 1–5.

Hirai, T., Ikenaga, N., Miyake, T., and Suzuki, T., Production of Hydrogen by Steam Reforming of Glycerin on Ruthenium Catalyst. Energy & Fuels 19 (2005): 1761-1762.

Hedstrom, L., Tingelof, T., Alvfors, P., and Lindbergh, G., Experimental results from a 5 kW PEM fuel cell stack operated on simulated reformate from highly diluted hydrocarbon fuels: Efficiency, dilution, fuel utilisation, CO poisoning and design criteria. International Journal of Hydrogen Energy 34 (2009): 1508-1514.

Heinzel, A., Vogel, B., Hubner, P., Reforming of natural gas-hydrogen generation for small scale stationary fuel cell system. Journal of Power Source 105 (2002): 202-207.

Hirai, T., Ikenaga, N., Miyake, T., and Suzuki, T., Production of Hydrogen by Steam Reforming of Glycerin on Ruthenium Catalyst. Energy & Fuels 19 (2005): 1761-1762.

Hu, J.E., Pearlman, J.B., Jackson, G.S., Tesluk, C.J., Evaluating the impact of enhanced anode CO tolerance on performance of proton-exchange-membrane

fuel cell systems fueled by liquid hydrocarbons. Journal of Power Sources 195 (2010): 1926–1935.

Hubert, C.E., Achard, P., Metkemeijer, R., Study of a small heat and power PEM fuel cell system generator. Journal of Power Sources 156 (2006): 64–70.

Iriondo, A., Barrio, V.L., Cambra, V.L., Arias, P.L., Guemez, M.B., Navarro, R.M., Sanchez-Sanchez, M. C., Fierro, J. L. G., Hydrogen Production from Glycerol Over Nickel Catalysts Supported on Al_2O_3 Modified by Mg, Zr, Ce or La. Topics in Catalysis 49 (2008): 46–58.

Ito, K., Water Problem in PEMFC. Recent Trends in Fuel Cell Science and Technology, Springer and Anamaya Publishers, New Delhi, 2007.

Ito, T., Nakashimada, Y., Senba, K., Matsui, T., Nishio, N. Hydrogen and ethanol production from glycerol-containing wastes discharged after biodiesel manufacturing process. Journal of Bioscience and Bioengineering 100 (2005): 260–265.

Jannelli, E., Minutillo, M., Galloni, E., Performance of a Polymer Electrolyte Membrane Fuel Cell System Fueled With Hydrogen Generated by a Fuel Processor. Journal of Fuel Cell Science and Technology 4 (2007): 435-440.

Jespersen, J.L., Schaltz, E., Kaer, S.K., Electrochemical characterization of a polybenzimidazole-based high temperature proton exchange membrane unit cell. Journal of Power Sources 191 (2009): 289-296.

Janssen, G.J.M., Modelling study of CO_2 poisoning on PEMFC anodes. Journal of Power Sources 136 (2004) 45–54.

Jensen, J.O., Li, Q., Pan, C., Vestbo, A.P., Mortensen, K., Petersen, H.N., Sorensen, C.L., Clausen, T.N., Schramm, J., and Bjerrum, N.J., High temperature PEMFC and the possible utilization of the excess heat for fuel processing. International Journal of Hydrogen Energy 32 (2007): 1567 – 1571.

Jiao, K., Alaefour, I.E., Li, X., Three-dimensional non-isothermal modeling of carbon monoxide poisoning in high temperature proton exchange membrane fuel cells with phosphoric acid doped polybenzimidazole membranes. Fuel 90 (2011): 568–582.

Korsgaard, A.R., Nielsen, M.P., Kær, S.K., Part one: A novel model of HTPEM-based micro-combined heat and power fuel cell system. International Journal of Hydrogen Energy 33 (2008): 1909-1920.

King, D.L., Zhang, L., Xia, G., Karim, A.M., Heldebrant, D.J., Wang, X., Peterson, T., Wang, Y**.,** Aqueous phase reforming of glycerol for hydrogen production over Pt–Re supported on carbon. Applied Catalysis B: Environmental 99 (2010): 206–213.

Laosiripojana, N., Assabumrungrat S., Hydrogen production from steam and autothermal reforming of LPG over high surface area ceria. Journal of Power Sources 158 (2006): 1348-1357.

Laosiripojana, N., Sutthisripok, W., Assabumrungrat, S., Synthesis gas production from dry reforming of methane over CeO_2 doped Ni/Al_2O_3: Influence of the doping ceria on the resistance toward carbon formation. Chemical Engineering Journal 112 (2005): 13–22.

Lattner, J.R., Harold, M.P., Comparison of conventional and membrane reactor fuel processors for hydrocarbon-based PEM fuel cell systems. International Journal of Hydrogen energy 29 (2004): 393 – 417.

Lattner, J.R., Harold, M.P., Comparison of methanol-based fuel processors for PEM fuel cell systems. Applied Catalysis B: Environmental 56 (2005): 149–169.

Levent, M., Gunn D.J., El-Bousi, M.A. Production of hydrogen-rich gases from steam reforming of methane in an automatic catalytic microreactor. International Journal of Hydrogen Energy 28 (2003): 945 – 959.

Li, H., Tang, Y., Wang, Z., Shi, Z., Wu, S., Song, D., Zhang, J., Fatih, K., Zhang J., Wang, H., Liu, Z., Abouatallah, R., Mazza, A., Review of Water Flooding Issues in Proton Exchange Membrane Fuel Cell. Journal of Power Sources 178 (2008): 103-117.

Li, Q., He, R., Gao, J.A., Jensen, J.O., and Bjerrum, N.J., The CO Poisoning Effect in PEMFCs Operational at Temperatures up to 200˚C. Journal of the Electrochemical Society 150 (2003): A1599-A1605.

Li, Q., Jensen, J.O., Savinell, R.F., and Bjerrum, N.J., High temperature proton exchange membranes based on polybenzimidazoles for fuel cells. Progress in Polymer Science 34 (2009): 449-477.

Li, X.T., Grace, J.R., Lim, C.J., Watkinson, A.P., Chen, H.P., Kim, J.R., Biomass gasification in a circulating fluidized bed. Biomass and Bioenergy 26 (2004): 171 – 193**.**

Lin,Y., Lin,C., Chen,Y., Yin, K., Yang, C. An analytical study of the PEM fuel cell with axial convection in the gas channel. International Journal of Hydrogen Energy 32 (2007): 4477–4488.

Lindstrom, B., Karlsson,J.A.J., Ekdunge, P., De Verdier, L., Haggendal, B., Dawody, J., Nilsson, M., Pettersson, L.J., Diesel fuel reformer for automotive fuel cell applications. International Journal of Hydrogen Energy 34 (2009): 3367 – 3381.

Liu, S., Zhang, K., Fang, L., and Li, Y., Thermodynamic Analysis of Hydrogen Production from Oxidative Steam Reforming of Ethanol. Energy & Fuel 22 (2008): 1365–1370.

Luo, N., Cao, F., Zhao, X., Xiao, T. and Fang, D. Thermodynamic analysis of aqueous-reforming of polylols for hydrogen generation. Fuel 86 (2007): 1727–1736.

Luo, N., Zhao, X., Cao, F., Xiao, T. and Fang, D. Thermodynamic Study on Hydrogen Generation from Different Glycerol Reforming Processes. Energy & Fuels 21 (2007): 3505–3512.

Luo, N., Fu, X., Cao, F., Xiao, T, Edwards, P.P., Glycerol aqueous phase reforming for hydrogen generation over Pt catalyst – Effect of catalyst composition and reaction conditions. Fuel 87 (2008): 3483–3489**.**

Luo, N., Wang, J., Xiao, T., Cao, F., Fang, D., Influence of nitrogen on the catalytic behavior of Pt/γ-Al2O3 catalyst in glycerol reforming process. Catalysis Today 166 (2011): 123-128.

Mamlouk, M., Scott, K., The effect of electrode parameters on performance of a phosphoric acid-doped PBI membrane fuel cell. International Journal of Hydrogen Energy 35 (2010): 784 – 793.

Mamlouk, M., Sousa, T., Scott, K., A High Temperature Polymer Electrolyte Membrane Fuel Cell Model for Reformate Gas. International Journal of Electrochemistry 2011 (2011): 1-18.

Manfro, R. L., Costa, A.F., Ribeiro, N.F.P., Souza, M.M.V.M., Hydrogen production by aqueous-phase reforming of glycerol over nickel catalysts supported on CeO_2. Fuel Processing Technology 92 (2011): 330–335**.**

Marino, F., Descorme, C., Duprez, D., Supported base metal catalysts for the preferential oxidation of carbon monoxide in the presence of excess hydrogen (PROX). Applied Catalysis B: Environmental 58 (2005): 175–183.

Martin, S., Worner, A., On-board reforming of biodiesel and bioethanol for high temperature PEM fuel cells: Comparison of autothermal reforming and steam reforming. Journal of Power Sources 196 (2011): 3163–3171.

Medrano, J.A., Oliva, M., Ruiz, J., Garcia, L., Arauzo, J. Catalytic steam reforming of acetic acid in a fluidized bed reactor with oxygen addition. International Journal of Hydrogen Energy 33 (2008): 4387–4396.

Minutillo, M., Jannelli, E., and Tunzio, F., Experimental Results of a PEM System Operated on Hydrogen and Reformate. Journal of Fuel Cell Science and Technology 5 (2008).

Modestov, A.D., Tarasevich, M.R., Filimonov, V.Y., Davydova, E.S., CO tolerance and CO oxidation at Pt and Pt–Ru anode catalysts in fuel cell with polybenzimidazole–H_3PO_4 membrane. Electrochim Acta 55 (2010) 6073–6080.

Ni, M., Leung, D., and Leung, M., A review on reforming bio-ethanol for hydrogen production. International Journal of Hydrogen Energy 32 (2007): 3238 – 3247.

Nguyen, T., and White, R., A water and heat management model for protonexchange-membrane fuel cells. Journal of Electrochemical Society 140 (1993): 2178-2186.

Oliva, D.G., Francesconi, J.A., Mussati, M.C., Aguirre, P.A., Energy efficiency analysis of an integrated glycerin processor for PEM fuel cells: Comparison with an ethanol-based system. International Journal of Hydrogen Energy 35 (2010): 709–724.

Onwudili, J.A. and Williams, P.T., Hydrothermal reforming of bio-diesel plant waste: Products distribution and characterization. Fuel 89 (2010): 501–509.

Ortiz, F.J.G., Ollero, P., Serrera, A., Sanz, A., Thermodynamic study of supercritical reforming. International Journal of Hydrogen Energy 36 (2011): 8994-9013.

Othmer, K. Encyclopedia of Chemical Technology. John Wiley&Sons. New York. 1997 vol.12.

Pan, C., He, R., Li, Q., Jensen, J., O., Bjerrum, J., N., Hjulmand, H., A., Jensen, A., B., Integration of high temperature PEM fuel cells with a methanol reformer. Journal of Power Sources 145 (2005): 392–398.

Pandya, J.D., Ghosh, K.K., Rastogi, S.K., A PHOSPHORIC ACID FUEL CELL COUPLED WITH BIOGAS. Energy 13 (1988): 383-388.

Parizotto, N.V., Rocha, K.O., Damyanova, S., Passos, F.B., Zanchet, D., Marques, C.M.P., Bueno, J.M.C., Alumina-supported Ni catalysts modified with silver for the steam reforming of methane: Effect of Ag on the control of coke formation. Applied Catalysis A: General 330 (2007): 12–22.

Parmar, R.D., Kundu, A., Karan, K. Thermodynamic analysis of diesel reforming process: Mapping of carbon formation boundary and representative independent reactions. Journal of Power Sources 194 (2009): 1007–1020.

Peng, J., Shin, J.Y., and Song, T.W., Transient response of high temperature PEM fuel cell. Journal of Power Sources 179 (2008): 220–231.

Perna, A., Cicconardi, S.P., Cozzolino, R., Performance evaluation of a fuel processing system based on membrane reactors technology integrated with a PEMFC stack. International Journal of Hydrogen energy 36 (2001): 9906-9915.

Pedernera, M.N., Pina, J., Borio, D.O., Kinetic evaluation of carbon formation in a membrane reactor for methane reforming. Chemical Engineering Journal 134 (2007): 138–144.

Pompeo, F., Santori G., Nichio, N.N. Hydrogen and/or syngas from steam reforming of glycerol. Study of platinum catalysts. International Journal of Hydrogen Energy 35 (2010): 8912–8920.

Profeti, L.P.R., Ticianelli, E.A., Assaf E.M. Production of hydrogen via steam reforming of biofuels on $Ni/CeO_2–Al_2O_3$ catalysts promoted by noble metals. International Journal of Hydrogen Energy 34 (2009): 5049 – 5060.

Rabenstein, G., Hacker, V., Hydrogen for fuel cells from ethanol by steam-reforming, partial-oxidation and combined auto-thermal reforming: A thermodynamic analysis. Journal of Power Sources 185 (2008): 1293–1304.

Sabourin-Provost, G., Hallenbeck, P.C. High yield conversion of a crude glycerol fraction from biodiesel production to hydrogen by photofermentation. Bioresource Technology 100 (2009): 3513–3517.

Schmersahl, R., and Scholz, V., Testing a PEM Fuel Cell System with Biogas Fuel. Agricultural Engineering International: the CIGR Ejournal 7 (2005): 1-12.

Scott, K., Pilditch, S., and Mamlouk, M., Modelling and experimental validation of a high temperature polymer electrolyte fuel cell. Journal of Applied Electrochemistry 37 (2007): 1245–1259.

Seo, Y., S., Shirley, A., Kolaczkowski, S., T., Evaluation of thermodynamically favourable operating conditions for production of hydrogen in three different reforming technologies. Journal of Power Sources 108 (2002): 213–225.

Severin, C., Pischinger, S., Ogrzelwalla, J., Compact gasoline fuel processor for passenger vehicle APU. Journal of Power Sources 145 (2005): 675-682.

Shah, R., Recent Trends in Fuel Cell Science and Technology. Introduction to Fuel Cell, Springer, New York, 2007.

Shimpalee, S., and Dutta, S., Numerical prediction of temperature distribution in PEM fuel cells. Numerical Heat Transfer 38 (2000): 111-128.

Shao, Y., Yin, G., Wang, Z., and Gao, Y., Proton exchange membrane fuel cell from low temperature to high temperature: Material challenges. Journal of Power Sources 167 (2007): 235–242.

Silva, G.P., Mack, M., and Contiero, J., Glycerol: A promising and abundant carbon source for industrial microbiology. Biotechnology Advances 27 (2009): 30-39.

Singhabhandhu, A., Tezuka, T., A perspective on incorporation of glycerin purification process in biodiesel plants using waste cooking oil as feedstock. Energy 35 (2010): 2493-2504.

Sinha, P.K., Wang, C.Y., and Beuscher, U, Transport Phenomena in Elevated Temperature PEM Fuel Cells. Journal of Electrochemical Society 154 (2007): B106-B116.

Slattery, J.C. and Bird, R.B., Calculation of the Diffusion Coefficient of Dilute Gases and of the Self-diffusion Coefficient of Dense Gases. American Institute of Chemical Engineers Journal 4 (1958): 137-142.

Slinn, M., Kendall, K., Mallon, C., and Andrews, J., Steam reforming of biodiesel by-product to make renewable hydrogen. Bioresource Technology 99 (2008): 5851-5858.

Smith, J.M., Van Ness, H.C. and Abbott, M.M., Introduction to Chemical Engineering Thermodynamics. McGraw-HILL International Edition, 2005.

Smolinka, T., Heinen, M., Chen, Y.X., Jusys, Z., Lehnert, W., Behm, R.J., CO_2 reduction on Pt electrocatalysts and its impact on H_2 oxidation in CO_2 containing fuel cell feed gas – A combined in situ infrared spectroscopy, mass spectrometry and fuel cell performance study. Electrochimica Acta 50 (2005): 5189–5199.

Sopena, D., Melgara, A., Briceno, Y., Navarrob, R.M., Alvarez-Galvan, M.C., Rosa, F., Diesel fuel processor for hydrogen production for 5 kW fuel cell application. International Journal of Hydrogen Energy 32 (2007): 1429 – 1436.

Specchia, S., Cutillo, A., Saracco, G., and Specchia V., Concept Study on ATR and SR Fuel Processors for Liquid Hydrocarbons. Industrial & Engineering Chemistry Research 4 (2006): 5298-5307.

Springer, T.E., Zawodzinski, T.A., Gottesfeld,S. Polymer electrolyte fuel cell model. Journal of Electrochemical Society. 138 (1991): 2334–2342.

Srinivasan, S., Krishnan, L., and Marozzi, C., Fuel Cells. Springer, US, 2006.

Swami, S.M., Abraham M.A., Integrated catalytic process for conversion of biomass to hydrogen. Energy & Fuels 20 (2006): 2616-2622.

Su, A., Ferng, Y.M., and Shih, J.C., Experimentally and numerically investigating cell performance and localized characteristics for a high-temperature proton exchange membrane fuel cell. Applied Thermal Engineering 29 (2009): 3409-3417.

Sustersic, M. G., Cordova, R., Triaca, W. E., and Arvia, A. J., Electrosorption of methane and its potentiodynamic electrooxidation on platinized platinum. Journal of the Electrochemical Society 127 (1980): 1242–1248.

Thompson, J.C., He, B.B., CHARACTERIZATION OF CRUDE GLYCEROL FROM BIODIESEL PRODUCTION FROM MULTIPLE FEEDSTOCKS. Applied Engineering in Agriculture 22 (2006): 261-265.

Tingelof, T., Hedstrom, L., Holmstrom, N., Alvfors, P., Lindbergh, G., The influence of CO2, CO and air bleed on the current distribution of a polymer electrolyte fuel cell. International Journal of Hydrogen Energy 33 (2008): 2064 – 2072.

Toonssen, R., Woudstra, N, Verkooijen, A.H.M., Decentralized generation of electricity from biomass with proton exchange membrane fuel cell. Journal of Power Sources 194 (2009): 456–466.

Tsai, C.R., Chena, F., Ruoa, A.C., Chang, M.H., Chu, M.S., Soong, C.Y. , Yan, W.M., and Cheng, C.H., An analytical solution for transport of oxygen in cathode gas diffusion layer of PEMFC. Journal of Power Sources 160 (2006): 50-56.

Um, S., Wang, C.Y., Three-dimensional analysis of transport and reaction in proton exchange membrane fuel cells, Proceeding of ASME IMECE, Orlando, (2000): 19.

Vagia, E.C., Lemonidou, A.A., Thermodynamic analysis of hydrogen production via autothermal steam reforming of selected components of aqueous bio-oil fraction. International Journal of Hydrogen Energy 33 (2008): 2489 – 2500.

Valliyappan, T., Bakhshi, N.N., and Dalai**,** A.K., Pyrolysis of glycerol for the production of hydrogen or syngas. Bioresource Technology 99 (2008): 4476-4483.

Valliyappan, T., Ferdous, D., Bakhshi, N., N., and Dalai, A., K., Production of Hydrogen and Syngas via Steam Gasification of Glycerol in a Fixed-Bed Reactor. Topic in Catalysis 49 (2008): 59-67.

Vlieger, D.J.M., Chakinala, A.G., Lefferts, L., Kersten, S.R.A., Seshan, K., Brilman, D.W.F., Hydrogen from ethylene glycol by supercritical water reforming using noble and base metal catalysts. Applied Catalysis B: Environmental 111– 112 (2012): 536–544.

Voll, F.A.P., Rossi, C.C.R.S., Silva, C., Guirardello, R., Souza, R.O.M.A., Cabral. V.F., Cardozo-Filho, L., Thermodynamic analysis of supercritical water gasification of methanol, ethanol, glycerol, glucose and cellulose. International Journal of Hydrogen Energy 34 (2009): 9737-9744.

Wu, W., Pai, C., Control of a heat-integrated proton exchange membrane fuel cell system with methanol reforming. Journal of Power Sources 194 (2009): 920-930.

Wang, H., Wang, X., Li, M., Wang, M., Li, S., Wang, S., and Ma, X., Thermodynamic analysis of hydrogen production from glycerol autothermal reforming. International Journal of Hydrogen Energy 34 (2009): 5683–5690.

Wang, K, Hawley, M.C., DeAthos, S.J. Conversion of glycerol to 1,3-propanediol via selective dehydroxylation. Industrial & Engineering Chemistry Research 42 (2003): 2913–2923.

Wang, W., Thermodynamic analysis of glycerol partial oxidation for hydrogen production. Fuel Processing Technology 91 (2010): 1401–1408**.**

Wang, X., Li, S., Wang, H., Liu, B., and Ma, X., Thermodynamic Analysis of Glycerin Steam Reforming. Energy & Fuels 22 (2008): 4285–4291.

Wang, X., Li, M., Wang, M., Wang, H., Li, S., Wang, S., and Ma, X., Thermodynamic analysis of glycerol dry reforming for hydrogen and synthesis gas production. Fuel 88 (2009): 2148–2153.

Wen, G., Xu, Y., Ma, H., Xu, Z., Tian, Z., Production of hydrogen by aqueous-phase reforming of glycerol. International Journal of Hydrogen Energy 33 (2008): 6657 – 6666.

Yan, Q., Toghiani, H., Causey, H., Steady state and dynamic performance of proton exchange membrane fuel cells (PEMFCs) under various operating conditions and load changes. Journal of Power Sources 161 (2006): 492–502.

Yang, C., Costamagna, P., Srinivasan, S., Benziger, J., Bocarsly, A.B., Approaches and technical challenges to high temperature operation of proton exchange membrane fuel cells. Journal of Power Sources 103 (2001): 1–9.

Yang, F., and Pitchumani, R., Fuel and Fuel Processing. Fuel Cell Technology. Springer, London, 2006.

Yi, J.S., Nguyen, T.V., Multicomponent transport in porous electrodes of proton exchange membrane fuel cells using the interdigitated gas distributors. Journal of Electrochemical Society 146 (1999): 38–45.

Yoon, S.J., Choi, Y.C., Son, Y., Lee, S.H., Lee, J.G. Gasification of biodiesel by-product with air or oxygen to make syngas. Bioresource Technology 101 (2010): 1227–1232.

Yu, C.Y., Lee, D.W., Park, S.J., Lee, K.Y., Lee, K.H., Study on a catalytic membrane reactor for hydrogen production from ethanol steam reforming. International Journal of Hydrogen Energy 34 (2009): 2947 – 2954.

Zalc, J.M., Loffler, D.G., Fuel processing for PEM fuel cells: transport and kinetic issues of system design. Journal of Power Sources 111 (2002): 58–64.

Zhang, B., Tang, X., Li, Y., Xu, Y., Shen, W., Hydrogen production from steam reforming of ethanol and glycerol over ceria-supported metal catalysts. International Journal of Hydrogen Energy 32 (2007): 2367 – 2373.

Zhang, J., Tang, Y., Song, C., Xia, Z., Li, H., Wang, H., Zhang, J., PEM fuel cell relative humidity (RH) and its effect on performance at high temperatures. Electrochimica Acta 53 (2008): 5315–5321.

Zhang, J., Xie, Z., Zhang, J., Tang, Y., Song, C., Navessin, T., Shi, Z., Song, D., Wang, H., Wilkinson, D.P., Liu, Z., and Holdcroft, S., High temperature PEM fuel cells. Journal of Power Sources 160 (2006): 872–891.

Zhou, T., Liu, H., A 3D model for PEM fuel cells operated on reformate. Journal of Power Sources 138 (2004): 101–110.

APPENDICES

APPENDIX A

PARAMETERS AND CONSTANTS OF HT-PEMFC

The solubility ($C_i^{\text{dissolved}}$) and diffusion coefficient (D_i) can be calculated from the correlation reported by Mamlouk et al. (2011) as follows:

$$D_i = A\exp\left(-\frac{E_a}{RT}\right) \tag{A.1}$$

$$C_i^{dissolved} = B\exp\left(-\frac{\Delta H}{RT}\right) \tag{A.2}$$

A and B are pre-exponential factors (given in Eqs. (A.3) and (A.4)), E_a is the diffusion activation energy, and ΔH is the enthalpy of solution. Both E_a and ΔH change with the concentration of phosphoric acid.

$$B = 1/\begin{pmatrix} 0.0004444022\cdot(100-W)^5 - 0.01678248\cdot(100-W)^4 \\ +0.2476135\cdot(100-W)^3 - 1.714433(100-W)^2 \\ +5.815734(100-W) - 7.662641 \end{pmatrix} \tag{A.3}$$

$$A = 0.00000249927283\exp(1.76593087W) \tag{A.4}$$

The activation energy in phosphoric acid and the enthalpy of solution at different acid weight concentrations (W) can be calculated from the following correlation.

$$E_a = -0.011607142857W^2 + 1.9642142857W - 75.376 \tag{A.5}$$

$$\Delta H = -0.003125W^3 + 0.8371429W^2 - 74.95179W + 2244.786 \tag{A.6}$$

The acid weight concentrations (W) is was obtained from concentrations as mole percent (X) using

$$W = \frac{98X}{0.98X + 18.016 - 0.18016X} \tag{A.7}$$

X is calculated from log (P_{mmHg}) and $1/T$ (valid from 120 to 180 ^{o}C).

$$X = g_1(\log(P))^2 + g_2 \log(P) + g_3 \tag{A.8}$$

Where:

$$g_1 = 107489083.7(1/T)^3 - 3301976.439(1/T)^2 + 30786.6253/T - 99.97517454$$

$$g_2 = -571882856.4(1/T)^3 + 17025276.36(1/T)^2 - 159050.3432/T + 478.3506443$$

$$g_3 = 2563470201(1/T)^3 - 57770551.75(1/T)^2 + 427861.8321/T - 931.0823368$$

A summary of k^a and k^b constants for Eqs.(4.66) and (4.67) is tabled below:

k_0^a	9.6082	k_0^b	26300
k_1^a	0.0002	k_1^b	0.62
k_2^a	−0.0132	k_2^a	−39.7
k_3^a	0.2257	k_3^b	527

APPENDIX B

LIST OF PUBLICATIONS

International publications

1. **Authayanun, S.**, Arpornwichanop, A., Paengjuntuek, W., Assabumrungrat, S. (2010). Thermodynamic study of hydrogen production from crude glycerol autothermal reforming for fuel cell applications. International Journal of Hydrogen Energy, 35, 6617-6623.

2. **Authayanun, S.**, Arpornwichanop, A., Patcharavorachot, Y., Wiyaratn, W. and Assabumrungrat, S. (2011). Hydrogen Production from Glycerol Steam Reforming for Low and High-Temperature PEMFCs. International Journal of Hydrogen Energy, 36, 267-275.

3. **Authayanun, S.**, Mamlouk, M., Arpornwichanop, A. (2012). Maximizing the efficiency of a HT-PEMFC system integrated with glycerol reformer. International Journal of Hydrogen Energy, 37, 6808-6817.

International conferences

1. **Authayanun, S.** and Arpornwichanop, A. (2010). Optimal Condition of Glycerol Steam Reforming for Different Types of PEMFC. XIX International Conference on Chemical Reactors (Chemreactor-19), 5-9 September 2010, Vienna, Austria.

2. **Authayanun, S.,** Mamlouk, M., Scott, K., Arpornwichanop, A. (2012). Design and Analysis of HT-PEMFC Systems with Different Fuel Processors for Stationary Applications. International Conference on Renewable Energies and Power Quality (ICREPQ'12), 28-30 March 2012, Santiago de Compostela, Spain.

National conference

1. **Authayanun, S.** and Arpornwichanop, A. (2010). Analysis of Hydrogen Production from Glycerol Steam Reforming for Low and High-Temperature PEMFC. *Commission on Higher Education Congress III: University Staff Development Consortium (CHE-USDC Congress III)*, 9-11August 2010, Pattaya, Thailand

VITA

Miss Suthida Authayanun was born in Pranakorn Sri Ayuttaya, Thailand, on June 15, 1985. She received the Bachelor Degree in Chemical Engineering from King Mongkut Institute of Technology Ladkrabang in 2007. She began her doctoral degree in June 2007 and received Ph.D. scholarship from the Thailand's Higher Education Commission under the program "Strategic Scholarships for Frontier Research Network for the Joint Ph.D. Program Thai Doctoral degree." During her graduate studies, she spent a period of 6 months in School of Chemical Engineering and Advanced Materials (CEAM), Newcastle University, UK, to undertake some parts of the Ph.D. research.